The Influence of Fibre Processing and Treatments on Hemp Fibre/Epoxy and Hemp Fibre/PLA Composites

THE UNIVERSITY OF
WAIKATO
Te Whare Wānanga o Waikato

A Thesis submitted in
partial fulfilment of the requirements for the degree of Doctor of Philosophy
in Materials and Process Engineering

by

Mohammad Saiful Islam

The University of Waikato, Hamilton, New Zealand

May, 2008

Dedicated

To

My Beloved Wife

Abstract

In recent years, due to growing environmental awareness, considerable attention has been given to the development and production of natural fibre reinforced polymer (both thermoset and thermoplastic) composites. The main objective of this study was to reinforce epoxy and polylactic acid (PLA) with hemp fibre to produce improved composites by optimising the fibre treatment methods, composite processing methods, and fibre/matrix interfacial bonding.

An investigation was conducted to obtain a suitable fibre alkali treatment method to:

(i) remove non-cellulosic fibre components such as lignin (sensitive to ultra violet (UV) radiation) and hemicelluloses (sensitive to moisture) to improve long term composites stability

(ii) roughen fibre surface to obtain mechanical interlocking with matrices

(iii) expose cellulose hydroxyl groups to obtain hydrogen and covalent bonding with matrices

(iv) separate the fibres from their fibre bundles to make the fibre surface available for bonding with matrices

(v) retain tensile strength by keeping fibre damage to a minimum level and

(vi) increase crystalline cellulose by better packing of cellulose chains to enhance the thermal stability of the fibres.

An empirical model was developed for fibre tensile strength (TS) obtained with different treatment conditions (different sodium hydroxide (NaOH) and sodium sulphite (Na_2SO_3) concentrations, treatment temperatures, and digestion times) by a partial factorial design. Upon analysis of the alkali fibre treatments by single fibre tensile testing (SFTT), scanning electron microscopy (SEM), zeta potential measurements, differential thermal analysis/thermogravimetric analysis (DTA/TGA), wide angle X-ray diffraction (WAXRD), lignin analysis and Fourier transform infrared (FTIR) spectroscopy, a treatment consisting of 5 wt% NaOH and 2 wt% Na_2SO_3 concentrations, with a treatment

temperature of 120^{o}C and a digestion time of 60 minutes, was found to give the best combination of the required properties. This alkali treatment produced fibres with an average TS and Young's modulus (YM) of 463 MPa and 33 GPa respectively. The fibres obtained with the optimised alkali treatment were further treated with acetic anhydride and phenyltrimethoxy silane. However, acetylated and silane treated fibres were not found to give overall performance improvement.

Cure kinetics of the neat epoxy (NE) and 40 wt% untreated fibre/epoxy (UTFE) composites were studied and it was found that the addition of fibres into epoxy resin increased the reaction rate and decreased the curing time. An increase in the nucleophilic activity of the amine groups in the presence of fibres is believed to have increased the reaction rate of the fibre/epoxy resin system and hence reduced the activation energies compared to NE.

The highest interfacial shear strength (IFSS) value for alkali treated fibre/epoxy (ATFE) samples was 5.2 MPa which was larger than the highest value of 2.7 MPa for UTFE samples supporting that there was a stronger interface between alkali treated fibre and epoxy resin. The best fibre/epoxy bonding was found for an epoxy to curing agent ratio of 1:1 (E_1C_1) followed by epoxy to curing agent ratios of 1:1.2 ($E_1C_{1.2}$), 1: 0.8 ($E_1C_{0.8}$), and finally for 1:0.6 ($E_1C_{0.6}$).

Long and short fibre reinforced epoxy composites were produced with various processing conditions using vacuum bag and compression moulding. A 65 wt% untreated long fibre/epoxy (UTLFE) composite produced by compression moulding at 70^{o}C with a TS of 165 MPa, YM of 17 GPa, flexural strength of 180 MPa, flexural modulus of 10.1 GPa, impact energy (IE) of 14.5 kJ/m^2, and fracture toughness (K_{Ic}) of 5 MPa.m$^{1/2}$ was found to be the best in contrast to the trend of increased IFSS for ATFE samples. This is considered to be due to stress concentration as a result of increased fibre/fibre contact with the increased fibre content in the ATFE composites compared to the UTFE composites.

Hygrothermal ageing of 65 wt% untreated and alkali treated long and short fibre/epoxy composites (produced by curing at 70^{o}C) showed that long fibre/epoxy composites were more resistant than short fibre/epoxy composites and ATFE composites were more resistant than UTFE composites towards hygrothermal ageing environments as revealed

from diffusion coefficients and tensile, flexural, impact, fracture toughness, SEM, TGA, and WAXRD test results. Accelerated ageing of 65 wt% UTLFE and alkali treated long fibre/epoxy (ATLFE) composites (produced by curing at 70^{o}C) showed that ATLFE composites were more resistant than UTLFE composites towards hygrothermal ageing environments as revealed from tensile, flexural, impact, K_{Ic}, SEM, TGA, WAXRD, FTIR test results.

IFSS obtained with untreated fibre/PLA (UFPLA) and alkali treated fibre/PLA (ATPLA) samples showed that ATPLA samples had greater IFSS than that of UFPLA samples. The increase in the formation of hydrogen bonding and mechanical interlocking of the alkali treated fibres with PLA could be responsible for the increased IFSS for ATPLA system compared to UFPLA system.

Long and short fibre reinforced PLA composites were also produced with various processing conditions using compression moulding. A 32 wt% alkali treated long fibre PLA composite produced by film stacking with a TS of 83 MPa, YM of 11 GPa, flexural strength of 143 MPa, flexural modulus of 6.5 GPa, IE of 9 kJ/m^2, and K_{Ic} of 3 MPa.m$^{1/2}$ was found to be the best. This could be due to the better bonding of the alkali treated fibres with PLA. The mechanical properties of this composite have been found to be the best compared to the available literature.

Hygrothermal and accelerated ageing of 32 wt% untreated and alkali treated long fibre/PLA composites ATPLA composites were more resistant than UFPLA composites towards hygrothermal and accelerated ageing environments as revealed from diffusion coefficients and tensile, flexural, impact, K_{Ic}, SEM, differential scanning calorimetry (DSC), WAXRD, and FTIR results. Increased potential hydrogen bond formation and mechanical interlocking of the alkali treated fibres with PLA could be responsible for the increased resistance of the ATPLA composites.

Based on the present study, it can be said that the performance of natural fibre composites largely depend on fibre properties (e.g. length and orientation), matrix properties (e.g. cure kinetics and crystallinity), fibre treatment and processing methods, and composite processing methods.

Acknowledgements

Firstly, I would like to thank my supervisor, Dr. Kim Pickering who has tirelessly guided and supported me every step of the way in my research, and who was never short on valuable advice and direction when it was needed most.

I am also thankful to my co-supervisor Dr. Johan Verbeek for his valuable suggestions and inspirations. I would like to thank Dr. Rob Torrens for his help and suggestions. I would like to express my sincere thanks to my industrial supervisor, Mr. Nic Foreman, director of Hemptech Ltd., who provided the industrial backing and some of the resources for my research that make this work possible. I would also like to thank Technology for Industry Fellowship (TIF) for their financial support of this project. Many thanks to Kinleith Mill and Dr Gerd Matthesius for giving me the opportunity to work in their lab with dynamic sheet former.

I would like to thank Christine Stewart of teaching and learning development unit (TLDU) for her help during the writing of this thesis. I would like to acknowledge Prof. M. A. Islam for his support and help. I would also like to thank Department of Engineering technicians who provided the technical assistance for my research especially Paul Ewert, Indar Singh, Brett Nichols, Yuanzi Zhang, and Helen Turner.

I would also like to thank the other composite group members (especially Delour, Gareth, Moyeen, Paul Betschart, and Anu) for their constant encouragement and valuable suggestions. I would like to convey my sincere thanks to the Department of Engineering Secretary Mary Dalbeth who was always ready to help me with a smile. Thanks to Stella for helping me with taking some SEM pictures. I am also grateful to my friends (Poom, Neamul, Kamrul, Ashraf, Florian) and well-wishers for their constant encouragement which inspired me to complete this research work.

The most important part of my life is my family. I would never have been able to accomplish any of my goals without the support of my parents, brothers, and sisters. They were always there when I needed them. A very special thanks to my wife, Sadia Saif. I will never be able to express all of my gratitude. You had faith in me and what I was doing even when I had lost it. Thank you for all of your help and sacrifice.

Table of Contents

Abstract iii

Acknowledgements vi

Table of Contents vii

List of Tables xii

List of Figures xiv

Chapter One: Introduction 1

1.1 Introduction 1
1.2 Historical Background of Natural Fibre Composites (NFCs) 3
1.3 Natural Fibre Reinforced Thermoset and Thermoplastic Composites 4
1.4 Future Aspects of Natural Fibre Composites 6
1.5 Objective of the Study 7
1.6 Thesis Organisation 8

Chapter Two: Literature Review 9

2.1 Summary 9
2.2 Natural Fibres: Source and Classification 9
2.3 Comparison of Cellulose Fibres 11
2.4 Industrial Hemp Fibre 13
2.4.1 Plant and Bast Fibre Morphology 15
2.4.2 Factors Affecting Fibre Mechanical Properties 17
2.4.3 Growing Conditions 18
2.4.4 Harvesting 18
2.5 Hemp Fibre Constituents 19
2.5.1 Cellulose 19
2.5.2 Hemicelluloses 20
2.5.3 Lignin 20
2.5.4 Pectin 21
2.6 Matrix 21
2.6.1 Thermosets 22
2.6.2 Bio-derived Thermoplastic Matrices 24
2.7 Natural Fibre Reinforced Polymer Composites 25
2.7.1 Factors Affecting the Use of Natural Fibres in Composites 26
2.7.1.1 Wettability and Interfacial Bonding 26
2.7.1.2 Thermal Stability 27
2.7.1.3 Dispersion of the Fibre in the Matrix 27
2.7.1.4 Biodegradability 28
2.7.1.5 Effect of Fibre Orientation 29
2.7.1.6 Influence of Humidity 29
2.7.1.7 Fibre Aspect Ratio 29
2.7.1.8 Fibre Volume Fraction 30

2.8 Chemical Treatment of Fibres 31
2.8.1 Alkali Treatment of the Fibres 31
2.8.1.1 Empirical Model for the Tensile Strength (TS) of Alkali Treated Fibre by Partial Factorial Design 31
2.8.1.2 Selection of the Levels of Treatment Factors 33
2.8.2 Acetylation of the Fibres 35
2.8.3 Silane Treatment of the Fibres 35
2.9 Interfacial Shear Strength (IFSS) of Composites 36
2.10 Cure Kinetics of Hemp/Epoxy Composites (HECs) 38
2.10.1 Non-isothermal or Dynamic Kinetic Models 41
2.10.2 Isothermal Kinetic Model: Autocatalytic Model 42
2.11 Processing of Fibre Reinforced Composites 44
2.11.1 Hand Lay-up 44
2.11.2 Compression Moulding 44
2.11.3 Film Stacking Technique 45
2.11.4 Vacuum Bag 45
2.12 Modelling of Tensile Strength (TS) of Composites 46
2.12.1 Modified Rule of Mixtures (MROM) 47
2.13 Degradation and Environmental Effects 48
2.13.1 Hygrothermal Ageing of the Composites 48
2.13.2 Accelerated Ageing of the Composites 52
2.14 Fibre and Composites Characterisation Methods 54
2.14.1 Wide Angle X-ray Diffraction (WAXRD) 54
2.14.2 Fourier Transform Infrared (FTIR) Spectroscopy 55
2.14.3 Zeta Potential Measurements 55
2.14.4 Thermal Analysis 58
2.14.4.1 Differential Thermal Analysis/Thermogravimetric Analysis (DTA/TGA) 58
2.14.4.2 Differential Scanning Calorimetry (DSC) 59

Chapter Three: Fibre Treatment and Characterisation 60

3.1 Summary 60
3.2 Experimental Details 60
3.2.1 Materials 60
3.2.2 Methods 61
3.2.2.1 Treatment of the Fibres with Alkali 61
3.2.2.2 Treatment of the Fibres with Acetic Anhydride 61
3.2.2.3 Treatment of the Fibres with Silane 61
3.2.2.4 Zeta Potential Measurement 62
3.2.2.5 Scanning Electron Microscopy (SEM) 62
3.2.2.6 Wide Angle X-ray Diffraction (WAXRD) 62
3.2.2.7 Thermal Analysis 63
3.2.2.8 Lignin Analysis of the Fibres 63
3.2.2.9 Fourier Transform Infrared (FTIR) Spectra 63
3.2.2.10 Single Fibre Tensile Testing (SFTT) 63
3.3 Results and Discussion 64
3.3.1 Alkali Treatment and Characterisation of the Fibres 64
3.3.1.1 Empirical Model for the Tensile Strength (TS) of Alkali Treated Fibre by Partial Factorial Design 64

3.3.1.2 The Effects of Alkali Treatment on Tensile Strength (TS) 82
3.3.1.3 The Effects of Alkali Treatment on Young's Modulus (YM) 85
3.3.1.4 The Effects of Fibre Diameter on Tensile Strength (TS) of the Alkali Treated Fibres 86
3.3.1.5 Scanning Electron Microscopic Evaluation of Alkali Treated Fibres 88
3.3.1.6 Zeta Potential 90
3.3.1.7 Wide Angle X-ray Diffraction (WAXRD) 91
3.3.1.8 Differential Thermal Analysis/Thermogravimetric Analysis (DTA/TGA) 93
3.3.1.9 Lignin Analysis 97
3.3.1.10 Fourier Transform Infrared (FTIR) Spectra 98
3.3.2 Characterisation of Acetylated Fibres 99
3.3.2.1 Scanning Electron Microscopy (SEM) 99
3.3.2.2 Zeta Potential 100
3.3.2.3 Thermal Analysis by Differential Thermal Analysis/ Thermogravimetric Analysis (DTA /TGA) 101
3.3.2.4 Wide Angle X-ray Diffraction (WAXRD) 104
3.3.2.5 Fourier Transform Infrared (FTIR) Spectra 105
3.3.3 Characterisation of Silane Treated Fibres 106
3.3.3.1 Scanning Electron Microscopy (SEM) 106
3.3.3.2 Zeta Potential 107
3.3.3.3 Thermal Analysis by Differential Thermal Analysis/ Thermogravimetric Analysis (DTA /TGA) 108
3.3.3.4 Wide Angle X-ray Diffraction (WAXRD) 111
3.3.3.5 Fourier Transform Infrared (FTIR) Spectra 113
3.4 Chapter Conclusion 113

Chapter Four: Hemp/Epoxy Composites (HECs) 115

4.1 Summary 115
4.2 Experimental Details 116
4.2.1 Materials 116
4.2.2 Methods 117
4.2.2.1 Cure Kinetic Study of Neat Epoxy (NE) and Untreated Hemp Fibre/Epoxy (UTFE) Composites Using Differential Scanning Calorimetry (DSC) 117
4.2.2.2 Interfacial Shear Strength (IFSS) Measurement of Hemp Fibre/Epoxy Samples Using Single Fibre Pull-out Testing 117
4.2.2.3 Production of Preform Fibre Mats 119
4.2.2.4 Production of Composites 121
4.2.2.5 Tensile Testing 123
4.2.2.6 Flexural Testing 123
4.2.2.7 Impact Testing 123
4.2.2.8 Fracture Toughness (K_{Ic}) Testing 124
4.2.2.9 Optical Microscopy 124
4.2.2.10 Scanning Electron Microscopy (SEM) 124
4.2.2.11 Thermogravimetric Analysis (TGA) 124
4.2.2.12 Wide Angle X-ray Diffraction (WAXRD) 125
4.2.2.13 Fourier Transform Infrared (FTIR) Spectra 125
4.2.2.14 Hygrothermal Ageing of the Composites 125
4.2.2.15 Accelerated Ageing of the Composites 125

4.3 Results and Discussion 126
4.3.1 Cure Kinetics of NE and Untreated Hemp Fibre/Epoxy (UTFE) Composites 126
4.3.1.1 Activation Energies Obtained Using the Kissinger and Flynn-Wall-Ozawa Models 126
4.3.1.2 Activation Energies Obtained Using the the Autocatalytic Model 129
4.3.2 Interfacial Shear Strength (IFSS) Measurement of Hemp Fibre/Epoxy Samples 134
4.3.3 Effects of Acetylation, Silane Treatment, Alkali Fibre Treatment and Curing Temperature on Composite Tensile Properties 138
4.3.4 Effects of Epoxy to Curing Agent Ratios on Composite Tensile Properties. 143
4.3.5 Effects of Fibre Soaking Time in Resin Bath on Composite Tensile Properties 145
4.3.6 Effects of Curing Temperatures on Composite Tensile Properties 147
4.3.7 Effects of Fibre Orientation (Short Fibres) on Composite Tensile Properties 150
4.3.8 Effects of Fibre Loading on Composite Tensile Properties, Thermogravimetric Analysis (TGA) of the Composites, and Modelling of Tensile Strength (TS) of the Composites 151
4.3.8.1 Effects of Fibre Loading on Composite Tensile Properties 151
4.3.8.2 Thermogravimetric Analysis (TGA) of the Long Fibre Composites 155
4.3.8.3 Modelling of Tensile Strength (TS) of Composites 156
4.3.9 Flexural, Impact, and Fracture Toughness of the Composites 158
Long Fibre Composites 158
Short Fibre Composites 161
4.3.10 Hygrothermal Ageing of the Composites 164
4.3.10.1 Effects of Hygrothermal Ageing on Mechanical Properties 170
4.3.11 Accelerated Ageing of the Composites 182
4.3.11.1 Fourier Transform Infrared (FTIR) Spectra 189
4.3.11.2 Thermogravimetric Analysis (TGA) 190
4.3.11.3 Wide Angle X-ray Diffraction (WAXRD) 190
4.4 Chapter Conclusion 191

Chapter Five: Hemp/PLA Composites (HPCs) 193

5.1 Summary 193
5.2 Experimental Details 194
5.2.1 Materials 194
5.2.2 Methods 194
5.2.2.1 Interfacial Shear Strength (IFSS) Measurement of Hemp Fibre/PLA Samples Using Single Fibre Pull-out Testing 194
5.2.2.2 Fibre Mat Production 194
5.2.2.3 PLA Sheet Production (Neat PLA): 195
5.2.2.4 Fabrication of Composites 195
5.2.2.5 Composite Mechanical Testing 196
5.2.2.6 Hygrothermal Ageing 197
5.2.2.7 Accelerated Ageing 197
5.2.2.8 Scanning Electron Microscopy (SEM) 197
5.2.2.9 Differential Scanning Calorimetry (DSC) Analysis 197

5.2.2.10 WAXRD 198
5.2.2.11 Fourier Transform Infrared (FTIR) Spectra 198
5.3 Results and Discussion 198
5.3.1 Interfacial Shear Strength (IFSS) Measurement of Hemp Fibre/PLA Samples 198
5.3.2 Mechanical Properties 200
5.3.2.1 Tensile Properties 200
5.3.2.2 Flexural Properties 208
5.3.2.3 Impact Energy (IE) 209
5.3.2.4 Fracture Toughness (K_{Ic}) 210
5.3.3 Crystallinity 211
5.3.3.1 Differential Scanning Calorimetry (DSC) Analysis 211
5.3.3.2 Wide Angle X-ray Diffraction (WAXRD) Analysis 213
5.3.4 Hygrothermal Ageing 214
5.3.4.1 Effects of Hygrothermal Ageing on Mechanical Properties 218
5.3.4.2 Effects of Hygrothermal Ageing on Crystallinity 224
5.3.5 Accelerated Ageing 227
5.3.5.1 Fourier Transform Infrared (FTIR) Spectra Analysis 234
5.3.5.2 Wide Angle X-ray Diffraction (WAXRD) Analysis 235
5.3.5.3 Differential Scanning Calorimetry (DSC) Analysis 236
5.4 Chapter Conclusion 237

Chapter Six: Conclusions 239

6.1 Fibre Treatment and Characterisation 239
6.2 Hemp/Epoxy Composites (HECs) 240
6.3 Hemp/PLA Composites (HPCs) 244

Chapter Seven: Recommendations and Future Work 246

References 248

Appendices 263

Publication List of this Work 263
Glossary of acronyms and Symbols 265

List of Tables

Table 1.1 The use of natural fibres as serial parts in the automotive industry (1997-2001). 6
Table 2.1 Properties of glass and natural fibres. 11
Table 2.2 The prices of some fibres. 12
Table 2.3 Commercially available fibre sources and their production. 12
Table 2.4 Physical characteristics of bast fibres. 12
Table 2.5 Percentage chemical composition of cellulose fibres. 13
Table 3.1 Experimental parameters for the selection of level of treatment factors. 65
Table 3.2 Actual factors and settings for alkali treatment of untreated fibres for the experimental design. 66
Table 3.3 A half fraction coded matrix for four factors at two levels. 67
Table 3.4 Experimental data for alkali treatment of untreated hemp fibres. 68
Table 3.5 Effects of the factors and interactions on fibre TS. 69
Table 3.6 Experimental verification of predicted/estimated fibre TS and treatment parameters. 74
Table 3.7 Experimental data for alkali treatment of untreated hemp fibres. 75
Table 3.8 Effects of the factors and interactions on fibre TS. 76
Table 3.9 Experimental verification of predicted/estimated fibre strength and treatment parameters. 80
Table 3.10 Summary of the single fibre tensile test results for alkali treated hemp fibres. 82
Table 3.11 $\zeta_{plateau}$ and IEP of untreated and alkali treated fibres. 90
Table 3.12 The crystallographic planes at various intensity (WAXRD counts) and 2θ-angles, and the crystallinity indices, *CrI* of untreated and alkali treated hemp fibres. 92
Table 3.13 The peak onset, peak and peak finishing temperatures of the endotherm and both exotherms for the untreated and alkali treated fibres obtained from DTA thermograms. 94
Table 3.14 Activation energies and frequency factors obtained by Broido method for untreated and alkali treated fibres. 96
Table 3.15 Cellulose, lignin, and ash contents of the untreated and alkali treated hemp fibres. 97
Table 3.16 FTIR wavenumbers (cm^{-1}) of untreated and alkali treated fibres. 99
Table 3.17 $\zeta_{plateau}$ and IEP of acetylated fibres compared to alkali treated fibres. 101
Table 3.18 The peak onset, peak, peak finishing temperatures and nature of peaks for the acetylated fibres compared to alkali treated fibres obtained from the DTA thermograms. 102
Table 3.19 Activation energies and frequency factors obtained by Broido method for acetylated fibres compared to alkali treated fibres. 104
Table 3.20 The crystallographic planes at various intensity (WAXRD counts) and 2θ-angles, and the crystallinity indices of acetylated fibres compared to alkali treated fibres. 105

Table 3.21 $\zeta_{plateau}$ and IEP of silane treated fibres compared to alkali treated fibres. 108
Table 3.22 The peak onset, peak, peak finishing temperatures and nature of peaks for the silane treated fibres compared to the alkali treated fibres obtained from the DTA thermograms. 109
Table 3.23 Activation energies and frequency factors obtained by Broido method for silane treated fibres compared to alkali treated fibres. 111
Table 3.24 The crystallographic planes at various intensity (WAXRD counts) and 2θ-angles, and the crystallinity indices of silane treated fibres compared to alkali treated fibres. 112
Table 4.1 Duration of the pressure maintained at each curing temperature. 122
Table 4.2 Heat of reaction for NE and composites at five different heating rates. 127
Table 4.3 Comparison of activation energies obtained by different models. 128
Table 4.4 Curing time, ΔH_t, and α of NE and composites at four different curing temperatures.....130
Table 4.5 Autocatalytic model parameters for NE and composites. 130
Table 4.6 Curing time of NE and composites at four different epoxy to curing agent ratios cured at 25^{o}C.....133
Table 4.7 Diffusion case selection parameter n at three different temperatures. 169
Table 4.8 Diffusion coefficients (D) for NE, UTFE and ATFE composites at three different temperatures. 169
Table 4.9 Tensile properties of hygrothermally aged short and long fibre/epoxy composites at three different temperatures. 178
Table 5.1 Thermal characteristics of PLA and its composites obtained from DSC. 212
Table 5.2 Diffusion case selection parameter n. 218
Table 5.3 Diffusion coefficients for NE, untreated long aligned (FSt) and alkali treated long aligned (FSt) composites at two different temperatures. 218
Table 5.4 Tensile properties of untreated long aligned (FSt) and alkali treated long aligned (FSt) composites after hygrothermal ageing at two different temperatures. 220
Table 5.5 Thermal characteristics of hygrothermally aged PLA and its composites obtained from DSC. 225

List of Figures

Figure 2.1 Overview of natural fibres. 10
Figure 2.2 Classification of natural fibre that can be used as reinforcements in polymers. 10
Figure 2.3 Female hemp plant. 15
Figure 2.4 Cross section of a hemp stem. 16
Figure 2.5 Composition of hemp stem. 17
Figure 2.6 Chemical structure of DGEBA. 23
Figure 2.7 Testing for optimum treatment condition for the TS of hemp fibres. 33
Figure 2.8 2,2 – bis [4 - (2′,3′ –epoxy propoxy) phenyl] propane (DGEBA). 38
Figure 2.9 Higher molecular weight homologues of epoxy resins. 39
Figure 2.10 Curing of epoxy resin with primary and secondary amines 40
Figure 2.11 Schematic representation of parallel and series models. 47
Figure 2.12 Oxidation reactions initiated by UV-radiation. 53
Figure 2.13 Electrokinetic, ε and zeta potentials, ζ of surfaces with different thicknesses of the double layer. 56
Figure 3.1 Single fibre tensile test specimen. 64
Figure 3.2 TS versus NaOH concentration (at 180^{o}C for 60 minutes with 2 wt% Na_2SO_3) plot for the level selection range of alkali fibre treatment. The curved line in the figure indicates principal trend of data points and do not represent any data fitting. 65
Figure 3.3 TS versus digestion time (at 180^{o}C with 5 wt% NaOH and 2 wt% Na_2SO_3) plot for the level selection range of alkali fibre treatment. The curved line in the figure indicates principal trend of data points and do not represent any data fitting. 65
Figure 3.4 TS versus temperature (for 60 minutes with 5 wt% NaOH and 2 wt% Na_2SO_3) plot for the level selection range of alkali fibre treatment. The curved line in the figure indicates principal trend of data points and do not represent any data fitting. 66
Figure 3.5 Plot of the average TS (responses) for each effect (factor and interaction). 70
Figure 3.6 Average TS for the interaction of concentrations of NaOH and Na_2SO_3. 71
Figure 3.7 Average TS for the interaction of concentration of NaOH and Time. 71
Figure 3.8 Average TS for the interaction of concentration of Na_2SO_3 and Time. 71
Figure 3.9 Pareto chart for the half effects of each factor and interaction. 72
Figure 3.10 Plot of the average TS (responses) for each effect (factor and interaction). .. 76
Figure 3.11 Average TS for the interaction of concentration of NaOH and Na_2SO_3. 77
Figure 3.12 Average TS for the interaction of concentration of NaOH and Time. 78
Figure 3.13 Average TS for the interaction of concentration of Na_2SO_3 and Time. 78
Figure 3.14 Pareto chart for the half effects (Δ/2) of each factor and interaction. 79
Figure 3.15 Effect of treatment temperature and digestion time on the TS of 5 wt% NaOH treated hemp fibres. 83
Figure 3.16 Effect of treatment temperature and digestion time on the TS of 10 wt% NaOH treated hemp fibres. 83
Figure 3.17 Effect of NaOH concentration and digestion time on the TS of hemp fibres. 83
Figure 3.18 Effect of treatment temperature and digestion time on the YM of 10 wt% NaOH treated hemp fibres. 85
Figure 3.19 Effect of treatment temperature and digestion time on the YM of 5 wt% NaOH treated hemp fibres. 86

Figure 3.20 Effect of NaOH concentration and digestion time on the YM of hemp fibres. 86
Figure 3.21 Influence of fibre diameter on the TS of P_2E_1 alkali treated hemp fibres. 87
Figure 3.22 Influence of fibre diameter on the TS of P_2E_4 alkali treated hemp fibres. 87
Figure 3.23 Influence of fibre diameter on the TS of P_2E_7 alkali treated hemp fibres. 87
Figure 3.24 SEM of untreated hemp fibre. 89
Figure 3.25 SEM of P_2E_1 alkali treated hemp fibre. 89
Figure 3.26 SEM of P_2E_4 alkali treated hemp fibre. 89
Figure 3.27 SEM of P_2E_7 alkali treated hemp fibre. 89
Figure 3.28 pH dependence of zeta potential of untreated and alkali treated fibres. 90
Figure 3.29 WAXRD pattern of untreated and alkali treated fibres. 91
Figure 3.30 DTA curves for untreated and alkali treated fibres. 93
Figure 3.31 TGA curves for untreated and alkali treated fibres. 93
Figure 3.32 Plots of ln[ln(1/y)] versus $T^{-1}\times10^3$ K^{-1} for the second stage of thermal degradation for untreated and alkali treated fibres. 95
Figure 3.33 Plots of ln[ln(1/y)] versus $T^{-1}\times10^3$ K^{-1} for the third stage of thermal degradation for untreated and alkali treated fibres. 96
Figure 3.34 FTIR-spectra of untreated and alkali treated fibres. 98
Figure 3.35 SEM of acetylated hemp fibre. 100
Figure 3.36 pH dependence of zeta potential of acetylated fibres compared to alkali treated fibres. 100
Figure 3.37 DTA curves for acetylated fibres compared to alkali treated fibres. 101
Figure 3.38 TGA curves for acetylated fibres compared to alkali treated fibres. 102
Figure 3.39 Plots of ln[ln(1/y)] versus $T^{-1}\times10^3$ K^{-1} for the second stage of thermal degradation (first exothermic peak) for acetylated fibres compared to alkali treated fibres. 103
Figure 3.40 Plots of ln[ln(1/y)] versus $T^{-1}\times10^3$ K^{-1} for the third stage of thermal degradation (second exothermic peak) for acetylated fibres compared to alkali treated fibres. 103
Figure 3.41 WAXRD pattern of acetylated fibres compared to alkali treated fibres. 104
Figure 3.42 FTIR spectra of acetylated fibres compared to alkali treated fibres. 106
Figure 3.43 SEM of silane treated hemp fibre surface. 107
Figure 3.44 pH dependence of zeta potential of silane treated fibres compared to alkali treated fibres. 107
Figure 3.45 DTA curves for sialne treated fibres compared to alkali treated fibres. 108
Figure 3.46 TGA curves for silane treated fibres compared to alkali treated fibres. 109
Figure 3.47 Plots of ln[ln(1/y)] versus $T^{-1}\times10^3$ K^{-1} for the second stage of thermal degradation (first exothermic peak) for silane treated fibres compared to alkali treated fibres. 110
Figure 3.48 Plots of ln[ln(1/y)] versus $T^{-1}\times10^3$ K^{-1} for the third stage of thermal degradation (second exothermic peak) for silane treated fibres compared to alkali treated fibres. 111
Figure 3.49 WAXRD pattern of silane treated fibres compared to alkali treated (P_2E_4) fibres. 112
Figure 3.50 FTIR spectra of silane treated fibres compared to alkali treated fibres. 113
Figure 4.1 Test specimen for single fibre pull-out tests. 118
Figure 4.2 Single fibre embedded in epoxy resin. 119
Figure 4.3 Hand carding machine used to produce aligned long fibre mats. 119
Figure 4.4 Dynamic sheet former used to produce aligned short fibre mats. 120

Figure 4.5 Aligned alkali treated fibre mat produced by dynamic sheet forming (DSF). 120
Figure 4.6 Specimen configuration for SENB. 124
Figure 4.7 Heat flow measured by DSC during cure of NE at five different heating rates (*Heat flow normalised to show relative peak sizes). 127
Figure 4.8 Heat flow measured by DSC during cure of composites at five different heating rates (*Heat flow normalised to show relative peak sizes). 127
Figure 4.9 Activation energies obtained by the Kissinger model for NE and composites. 128
Figure 4.10 Activation energies obtained by Flynn-Wall-Ozawa method for NE and composites. 129
Figure 4.11 Conversion rate versus conversion graphs for NE at four different isothermal temperatures. The solid lines are a trend expected from the Autocatalytic Model (Equation (2.11)) 131
Figure 4.12 Arrhenius plot for the reaction constant k_1. 132
Figure 4.13 Arrhenius plot for the reaction constant k_2. 132
Figure 4.14 Typical load versus displacement curve for pull-out tests of hemp/epoxy sample. 134
Figure 4.15 Debonding force versus embedded length plots for UTFE samples at various epoxy resin to curing agent ratios. 135
Figure 4.16 Debonding force versus embedded length plots for ATFE samples at various epoxy resin to curing agent ratios. 135
Figure 4.17 IFSS of UTFE samples found at eight different embedded length and four different epoxy resin to curing agent ratios. The solid lines indicate principal trends of data points and do not represent any data fitting. 136
Figure 4.18 IFSS of ATFE samples found at eight different embedded length and four different epoxy resin to curing agent ratios. The solid lines indicate principal trends of data points and do not represent any data fitting. 136
Figure 4.19 Tensile properties of UTFE, AcFE, STFE, and ATFE composites compared to NE cured at 25^{o}C. Error bars each corresponds to one standard deviation. 138
Figure 4.20 Optical micrograph of UTFE composites cured at 25^{o}C 139
Figure 4.21 Optical micrograph of AcFE composites cured at 25^{o}C. 139
Figure 4.22 Optical micrograph of STFE composites cured at 25^{o}C. 140
Figure 4.23 Optical micrograph of ATFE composites cured at 25^{o}C 140
Figure 4.24 SEM micrograph of the fracture surface of STFE composites. 142
Figure 4.25 Tensile properties of UTFE and ATFE composites compared to NE cured at 25^{o}C and 120^{o}C. Error bars each corresponds to one standard deviation. 142
Figure 4.26 Optical micrograph of ATFE composites cured at 120^{o}C 143
Figure 4.27 Tensile properties of 30 and 40 wt% UTFE and ATFE composites produced at four different epoxy to curing agent ratios. Error bars each corresponds to one standard deviation. 144
Figure 4.28 Optical micrograph of ATFE composites produced by aligned mat obtained by hand carding machine. 145
Figure 4.29 Tensile properties of untreated and alkali treated composites produced by soaking the fibre mats for 10 and 60 minutes. Error bars each corresponds to one standard deviation. 146
Figure 4.30 Poor wetting of fibre in ATFE composites produced by soaking for 10 minutes in the resin bath. 146
Figure 4.31 Good wetting of fibre in ATFE composites produced by soaking for 60 minutes in the resin bath. 147

Figure 4.32 Tensile properties of UTFE and ATFE composites produced at three different curing temperatures. Error bars each corresponds to one standard deviation. 148
Figure 4.33 SEM micrographs of fracture surfaces of tensile tested specimens with 40 wt% alkali treated fibres produced at (a) 120^{o}C and (b) 70^{o}C curing temperatures. 149
Figure 4.34 Tensile properties of random and aligned short fibre composites produced with untreated and alkali treated fibres. Error bars each corresponds to one standard deviation. 150
Figure 4.35 The variation in tensile properties with fibre loading for UTLFE and ATLFE composites. Error bars each corresponds to one standard deviation. 151
Figure 4.36 SEM pictures of fracture surfaces of 65 wt% (a) UTLFE and (b) ATLFE composites. 152
Figure 4.37 The variation in tensile properties with fibre loading for UTSFE and ATSFE composites. Error bars each corresponds to one standard deviation. 153
Figure 4.38 SEM pictures of fracture surfaces of 65 wt% (a) UTSFE and (b) ATSFE composites. 154
Figure 4.39 TGA traces for UTLFE and ATLFE composites. 155
Figure 4.40 Tensile strength versus fibre volume fraction of composites (solid lines for theoretical model values and symbols for experimentally obtained values for UTLFE and UTSFE composites). 156
Figure 4.41 Tensile strength versus fibre volume fraction of composites (solid lines for theoretical model values and symbols for experimentally obtained values for ATLFE and ATSFE composites). 157
Figure 4.42 Flexural strength of UTLFE and ATLFE composites compared to NE. Error bars each corresponds to one standard deviation. 159
Figure 4.43 Flexural modulus of UTLFE and ATLFE composites compared to NE. Error bars each corresponds to one standard deviation. 159
Figure 4.44 IE of UTLFE and ATLFE composites compared to NE. Error bars each corresponds to one standard deviation. 160
Figure 4.45 K_{Ic} of 65 wt% UTLFE and ATLFE composites compared to NE. Error bars each corresponds to one standard deviation. 160
Figure 4.46 Optical micrographs showing major crack of fracture toughness specimens of (a) ATLFE and (b) UTLFE composites. 161
Figure 4.47 Flexural strength and flexural modulus of 65 wt% UTSFE and ATSFE composites compared to NE. Error bars each corresponds to one standard deviation. 162
Figure 4.48 IE of UTSFE and ATSFE composites compared to NE. Error bars each corresponds to one standard deviation. 163
Figure 4.49 K_{Ic} of 65 wt% UTSFE and ATSFE composites compared to NE. Error bars each corresponds to one standard deviation. 163
Figure 4.50 Optical micrographs of (a) UTLFE and (b) ATLFE composite surfaces after hygrothermal ageing at 70^{o}C. 164
Figure 4.51 Thickness swelling of the NE and long and short fibre/epoxy composites after hygrothermal ageing. 165
Figure 4.52 Moisture absorption behaviour of NE at 25, 50, and 70^{o}C. 166
Figure 4.53 Moisture absorption behaviour of 65 wt% UTLFE composites at 25, 50, and 70^{o}C. 166
Figure 4.54 Moisture absorption behaviour of 65 wt% ATLFE composites at 25, 50, and 70^{o}C. 166

Figure 4.55 Moisture absorption behaviour of 65 wt% UTSFE composites at 25, 50, and 70°C. 167
Figure 4.56 Moisture absorption behaviour of 65 wt% ATSFE composites at 25, 50, and 70°C. 167
Figure 4.57 SEM micrographs of (a) UTLFE and (b) ATLFE composites surfaces after hygrothermal ageing at 70°C. 168
Figure 4.58 Diffusion case fitting plots for ATLFE composites at 25 and 50 and 70°C. 168
Figure 4.59 Diffusion case fitting plots for UTSFE composites at 25 and 50 and 70°C. 169
Figure 4.60 Effect of hygrothermal ageing on the TS of NE, UTLFE and ATLFE composites at three different temperatures. Error bars each corresponds to one standard deviation. 170
Figure 4.61 Effect of hygrothermal ageing on the YM of NE, UTLFE and ATLFE composites at three different temperatures. Error bars each corresponds to one standard deviation. 171
Figure 4.62 (a) UTLFE and (b) ATLFE composite fracture surfaces after hygrothermal ageing at 70°C. 172
Figure 4.63 Effect of hygrothermal ageing on the FS of UTLFE and ATLFE composites compared to NE at three different temperatures. Error bars each corresponds to one standard deviation. 173
Figure 4.64 Effect of hygrothermal ageing on the flexural strength of UTLFE and ATLFE composites compared to NE at three different temperatures. Error bars each corresponds to one standard deviation. 173
Figure 4.65 Effect of hygrothermal ageing on the flexural modulus of UTLFE and ATLFE composites compared to NE at three different temperatures. Error bars each corresponds to one standard deviation. 174
Figure 4.66 Effect of hygrothermal ageing on the flexural strain of UTLFE and ATLFE composites compared to NE at three different temperatures. Error bars each corresponds to one standard deviation. 174
Figure 4.67 Effect of hygrothermal ageing on the IE of UTLFE and ATLFE composites compared to NE at three different temperatures. Error bars each corresponds to one standard deviation. 175
Figure 4.68 Effect of hygrothermal ageing on the K_{Ic} of UTLFE and ATLFE composites compared to NE at three different temperatures. Error bars each corresponds to one standard deviation. 175
Figure 4.69 TGA traces for UTLFE and ATLFE composites after hygrothermal ageing at 70°C. 176
Figure 4.70 WAXRD pattern for UTLFE and ATLFE composites before and after hygrothermal ageing at 70°C. 177
Figure 4.71 Effect of hygrothermal ageing on the TS of UTSFE and ATSFE composites compared to NE at three different temperatures. Error bars each corresponds to one standard deviation. 178
Figure 4.72 Effect of hygrothermal ageing on the YM of UTSFE and ATSFE composites compared to NE at three different temperatures. Error bars each corresponds to one standard deviation. 179
Figure 4.73 Effect of hygrothermal ageing on the FS of UTSFE and ATSFE composites compared to NE at three different temperatures. Error bars each corresponds to one standard deviation. 179
Figure 4.74 Effect of hygrothermal ageing on the flexural strength of UTSFE and ATSFE composites compared to NE at three different temperatures. Error bars each corresponds to one standard deviation. 180

Figure 4.75 Effect of hygrothermal ageing on the flexural modulus of UTSFE and ATSFE composites compared to NE at three different temperatures. Error bars each corresponds to one standard deviation. 180
Figure 4.76 Effect of hygrothermal ageing on the flexural strain of UTSFE and ATSFE composites compared to NE at three different temperatures. Error bars each corresponds to one standard deviation. 180
Figure 4.77 Effect of hygrothermal ageing on the IE of UTSFE and ATSFE composites compared to NE at three different temperatures. Error bars each corresponds to one standard deviation. 181
Figure 4.78 Effect of hygrothermal ageing on the K_{Ic} of UTSFE and ATSFE composites compared to NE at three different temperatures. Error bars each corresponds to one standard deviation. 182
Figure 4.79 Visual change during weathering of UTLFE and ATLFE composites. 182
Figure 4.80 SEM of UTLFE composites showing tearing of the fibres after accelerated ageing of 1000 hours. 183
Figure 4.81 Percentage weight gain of NE, UTLFE and ATLFE composites. 184
Figure 4.82 Effect of accelerated ageing on the TS of UTLFE and ATLFE composites compared to NE. Error bars each corresponds to one standard deviation. 185
Figure 4.83 Effect of accelerated ageing on the YM of UTLFE and ATLFE composites compared to NE. Error bars each corresponds to one standard deviation. 185
Figure 4.84 Effect of accelerated ageing on the FS of UTLFE and ATLFE composites compared to NE. Error bars each corresponds to one standard deviation. 185
Figure 4.85 Effect of accelerated ageing on the flexural strength of UTLFE and ATLFE composites compared to NE. Error bars each corresponds to one standard deviation. 186
Figure 4.86 Effect of accelerated ageing on the flexural modulus of UTLFE and ATLFE composites compared to NE. Error bars each corresponds to one standard deviation. 186
Figure 4.87 Effect of accelerated ageing on the flexural strain of UTLFE and ATLFE composites compared to NE. Error bars each corresponds to one standard deviation. 186
Figure 4.88 Effect of accelerated ageing on the IE of UTLFE and ATLFE composites compared to NE. Error bars each corresponds to one standard deviation. 187
Figure 4.89 Effect of accelerated ageing on the K_{Ic} of UTLFE and ATLFE composites compared to NE. Error bars each corresponds to one standard deviation. 187
Figure 4.90 (a) UTLFE and (b) ATLFE composites fracture surfaces after 1000 hours accelerated ageing. 188
Figure 4.91 Micrograph of NE surface after weathering for 1000 hours. 189
Figure 4.92 FTIR spectra of UTLFE composites of before (control) and after 1000 hours accelerated ageing. 189
Figure 4.93 TGA of UTLFE and ATLFE composites after accelerated ageing of 1000 hours. 190
Figure 4.94 WAXRD pattern for UTLFE and ATLFE composites before and after accelerated ageing of 1000 hours. 191
Figure 5.1 Debonding force versus embedded length for UFPLA and ATPLA samples. The solid lines indicate principal trends of data points and do not represent any data fitting. 198
Figure 5.2 IFSS of UFPLA and ATPLA samples, obtained for eight different embedded fibre lengths. The solid lines indicate principal trends of data points and do not represent any data fitting. 199

Figure 5.3 TS of untreated short aligned, alkali treated short aligned, and untreated short random composites compared to neat PLA. Error bars each corresponds to one standard deviation. 200
Figure 5.4 YM of untreated short aligned, alkali treated short aligned, and untreated short random composites compared to neat PLA. Error bars each corresponds to one standard deviation. 201
Figure 5.5 SEM pictures of the fracture surface of (a) alkali treated short aligned and (b) untreated short random composites. 202
Figure 5.6 FS of untreated short aligned, alkali treated short aligned, and untreated short random composites compared to neat PLA. Error bars each corresponds to one standard deviation. 203
Figure 5.7 TS of alkali treated long aligned (DCM), and untreated short random (DCM) composites compared to neat PLA. Error bars each corresponds to one standard deviation. 204
Figure 5.8 Optical micrograph of the surface of (a) alkali treated long aligned (DCM) and (b) untreated short random (DCM) composites. 204
Figure 5.9 YM of alkali treated long aligned (DCM) and untreated short random (DCM) composites compared to neat PLA. Error bars each corresponds to one standard deviation. 204
Figure 5.10 FS of alkali treated long aligned (DCM) and untreated short random (DCM) composites compared to neat PLA. Error bars each corresponds to one standard deviation. 205
Figure 5.11 TS of untreated long aligned (FSt) and alkali treated long aligned (FSt) composites compared to neat PLA. Error bars each corresponds to one standard deviation. 205
Figure 5.12 YM of untreated long aligned (FSt) and alkali treated long aligned (FSt) composites compared to neat PLA. Error bars each corresponds to one standard deviation. 206
Figure 5.13 FS of untreated long aligned (FSt) and alkali treated long aligned (FSt) composites compared to neat PLA. Error bars each corresponds to one standard deviation. 206
Figure 5.14 SEM micrographs of fracture surfaces of (a) untreated long aligned (FSt) and (b) alkali treated long aligned (FSt) composites. 207
Figure 5.15 Flexural strength of untreated long aligned (FSt) and alkali treated long aligned (FSt) composites compared to neat PLA. Error bars each corresponds to one standard deviation. 208
Figure 5.16 Flexural modulus of untreated long aligned (FSt) and alkali treated long aligned (FSt) composites compared to neat PLA. Error bars each corresponds to one standard deviation. 209
Figure 5.17 IE of untreated long aligned (FSt) and alkali treated long aligned (FSt) composites compared to neat PLA. Error bars each corresponds to one standard deviation. 209
Figure 5.18 K_{Ic} of untreated long aligned (FSt) and alkali treated long aligned (FSt) composites compared to neat PLA. Error bars each corresponds to one standard deviation. 210
Figure 5.19 Optical micrographs showing major crack of fracture toughness specimens of (a) untreated long aligned (FSt) and (b) alkali treated long aligned (FSt) composites. 211
Figure 5.20 DSC trace for PLA only sample displaying the glass transition temperature, cold crystallisation, and melting. 211

Figure 5.21 DSC thermograms of untreated long aligned (FSt) and alkali treated long aligned (FSt) composites compared to neat PLA. 212
Figure 5.22 WAXRD pattern for the raw materials used. 213
Figure 5.23 WAXRD curves for untreated long aligned (FSt) and alkali treated long aligned (FSt) composites. 214
Figure 5.24 (a) Untreated long aligned (FSt) and (b) alkali treated long aligned (FSt) composite surfaces after hygrothermal ageing at 50^{o}C. 215
Figure 5.25 Thickness swelling of the composites compared to neat PLA after hygrothermal ageing. 215
Figure 5.26 Moisture absorption behaviour of neat PLA at 25 and 50^{o}C. 216
Figure 5.27 Moisture absorption behaviour of 32 wt% untreated long aligned (FSt) composites at 25 and 50^{o}C....216
Figure 5.28 Moisture absorption behaviour of 32 wt% alkali treated long aligned (FSt) composites at 25 and 50^{o}C....216
Figure 5.29 Diffusion case fitting plots for 32 wt% alkali treated long aligned (FSt) composites at 25 and 50^{o}C....217
Figure 5.30 Effect of hygrothermal ageing on the TS of neat PLA, untreated long aligned (FSt) and alkali treated long aligned (FSt) composites at different temperatures. Error bars each corresponds to one standard deviation. 219
Figure 5.31 Effect of hygrothermal ageing on the YM of neat PLA, untreated long aligned (FSt) and alkali treated long aligned (FSt) composites at different temperatures. Error bars each corresponds to one standard deviation....219
Figure 5.32 (a) untreated long aligned (FSt) and (b) alkali treated long aligned (FSt) composite fracture surfaces after hygrothermal ageing at 50^{o}C. 220
Figure 5.33 Effect of hygrothermal ageing on the FS of neat PLA, untreated long aligned (FSt) and alkali treated long aligned (FSt) composites at different temperatures. Error bars each corresponds to one standard deviation. 221
Figure 5.34 Effect of hygrothermal ageing on the flexural strength of neat PLA, untreated long aligned (FSt) and alkali treated long aligned (FSt) composites at different temperatures. Error bars each corresponds to one standard deviation....222
Figure 5.35 Effect of hygrothermal ageing on the flexural modulus of neat PLA, untreated long aligned (FSt) and alkali treated long aligned (FSt) composites at different temperatures. Error bars each corresponds to one standard deviation.....222
Figure 5.36 Effect of hygrothermal ageing on the flexural strain of neat PLA, untreated long aligned (FSt) and alkali treated long aligned (FSt) composites at different temperatures. Error bars each corresponds to one standard deviation....223
Figure 5.37 Effect of hygrothermal ageing on the IE of neat PLA, untreated long aligned (FSt) and alkali treated long aligned (FSt) composites at different temperatures. Error bars each corresponds to one standard deviation. 223
Figure 5.38 Effect of hygrothermal ageing on the K_{Ic} of neat PLA, untreated long aligned (FSt) and alkali treated long aligned (FSt) composites at different temperatures. Error bars each corresponds to one standard deviation. 224
Figure 5.39 DSC traces for untreated long aligned (FSt) and alkali treated long aligned (FSt) composites after hygrothermal ageing at 50^{o}C....225
Figure 5.40 WAXRD pattern for untreated long aligned (FSt) and alkali treated long aligned (FSt) composites after hygrothermal ageing at 50^{o}C. 226
Figure 5.41 Visual change during ageing of untreated long aligned (FSt) and alkali treated long aligned (FSt) composites. 227
Figure 5.42 (a) Untreated long aligned (FSt) and (b) alkali treated long aligned (FSt) composite surfaces after 1000 hours accelerated ageing. 228

Figure 5.43 Percentage weight gain of neat PLA, untreated long aligned (FSt) and alkali treated long aligned (FSt) composites. 229
Figure 5.44 Effect of accelerated ageing on the TS of neat PLA, untreated long aligned (FSt) and alkali treated long aligned (FSt) composites. Error bars each corresponds to one standard deviation. 230
Figure 5.45 Effect of accelerated ageing on the YM of neat PLA, untreated long aligned (FSt) and alkali treated long aligned (FSt) composites. Error bars each corresponds to one standard deviation. 230
Figure 5.46 Effect of accelerated ageing on the FS of neat PLA, untreated long aligned (FSt) and alkali treated long aligned (FSt) composites. Error bars each corresponds to one standard deviation. 230
Figure 5.47 Effect of accelerated ageing on the flexural strength of neat PLA, untreated long aligned (FSt) and alkali treated long aligned (FSt) composites. Error bars each corresponds to one standard deviation. 231
Figure 5.48 Effect of accelerated ageing on the flexural modulus of neat PLA, untreated long aligned (FSt) and alkali treated long aligned (FSt) composites. Error bars each corresponds to one standard deviation. 231
Figure 5.49 Effect of accelerated ageing on the flexural strain of neat PLA, untreated long aligned (FSt) and alkali treated long aligned (FSt) composites. Error bars each corresponds to one standard deviation. 231
Figure 5.50 Effect of accelerated ageing on the IE of neat PLA, untreated long aligned (FSt) and alkali treated long aligned (FSt) composites. Error bars each corresponds to one standard deviation. 232
Figure 5.51 Effect of accelerated ageing on the K_{Ic} of neat PLA, untreated long aligned (FSt) and alkali treated long aligned (FSt) composites. Error bars each corresponds to one standard deviation. 232
Figure 5.52 (a) Untreated long aligned (FSt) and (b) alkali treated long aligned (FSt) composite fracture surfaces after 1000 hours accelerated ageing. 233
Figure 5.53 SEM micrograph of neat PLA surface after weathering for 750 hours. 234
Figure 5.54 FTIR spectra of untreated long aligned (FSt) composites....235
Figure 5.55 WAXRD pattern for untreated long aligned (FSt) and alkali treated long aligned (FSt) composites after accelerated ageing of 1000 hours. 236
Figure 5.56 DSC traces for untreated long aligned (FSt) and alkali treated long aligned (FSt) composites after accelerated ageing of 1000 hours. 237

The Influence of Fibre Processing and Treatments on Hemp Fibre/Epoxy and Hemp Fibre/PLA Composites

THE UNIVERSITY OF
WAIKATO
Te Whare Wānanga o Waikato

A Thesis submitted in
partial fulfilment of the requirements for the degree of Doctor of Philosophy
in Materials and Process Engineering

by

Mohammad Saiful Islam

The University of Waikato, Hamilton, New Zealand

May, 2008

Dedicated

To

My Beloved Wife

Abstract

In recent years, due to growing environmental awareness, considerable attention has been given to the development and production of natural fibre reinforced polymer (both thermoset and thermoplastic) composites. The main objective of this study was to reinforce epoxy and polylactic acid (PLA) with hemp fibre to produce improved composites by optimising the fibre treatment methods, composite processing methods, and fibre/matrix interfacial bonding.

An investigation was conducted to obtain a suitable fibre alkali treatment method to:

(i) remove non-cellulosic fibre components such as lignin (sensitive to ultra violet (UV) radiation) and hemicelluloses (sensitive to moisture) to improve long term composites stability

(ii) roughen fibre surface to obtain mechanical interlocking with matrices

(iii) expose cellulose hydroxyl groups to obtain hydrogen and covalent bonding with matrices

(iv) separate the fibres from their fibre bundles to make the fibre surface available for bonding with matrices

(v) retain tensile strength by keeping fibre damage to a minimum level and

(vi) increase crystalline cellulose by better packing of cellulose chains to enhance the thermal stability of the fibres.

An empirical model was developed for fibre tensile strength (TS) obtained with different treatment conditions (different sodium hydroxide (NaOH) and sodium sulphite (Na_2SO_3) concentrations, treatment temperatures, and digestion times) by a partial factorial design. Upon analysis of the alkali fibre treatments by single fibre tensile testing (SFTT), scanning electron microscopy (SEM), zeta potential measurements, differential thermal analysis/thermogravimetric analysis (DTA/TGA), wide angle X-ray diffraction (WAXRD), lignin analysis and Fourier transform infrared (FTIR) spectroscopy, a treatment consisting of 5 wt% NaOH and 2 wt% Na_2SO_3 concentrations, with a treatment

temperature of 120^{o}C and a digestion time of 60 minutes, was found to give the best combination of the required properties. This alkali treatment produced fibres with an average TS and Young's modulus (YM) of 463 MPa and 33 GPa respectively. The fibres obtained with the optimised alkali treatment were further treated with acetic anhydride and phenyltrimethoxy silane. However, acetylated and silane treated fibres were not found to give overall performance improvement.

Cure kinetics of the neat epoxy (NE) and 40 wt% untreated fibre/epoxy (UTFE) composites were studied and it was found that the addition of fibres into epoxy resin increased the reaction rate and decreased the curing time. An increase in the nucleophilic activity of the amine groups in the presence of fibres is believed to have increased the reaction rate of the fibre/epoxy resin system and hence reduced the activation energies compared to NE.

The highest interfacial shear strength (IFSS) value for alkali treated fibre/epoxy (ATFE) samples was 5.2 MPa which was larger than the highest value of 2.7 MPa for UTFE samples supporting that there was a stronger interface between alkali treated fibre and epoxy resin. The best fibre/epoxy bonding was found for an epoxy to curing agent ratio of 1:1 (E_1C_1) followed by epoxy to curing agent ratios of 1:1.2 ($E_1C_{1.2}$), 1: 0.8 ($E_1C_{0.8}$), and finally for 1:0.6 ($E_1C_{0.6}$).

Long and short fibre reinforced epoxy composites were produced with various processing conditions using vacuum bag and compression moulding. A 65 wt% untreated long fibre/epoxy (UTLFE) composite produced by compression moulding at 70^{o}C with a TS of 165 MPa, YM of 17 GPa, flexural strength of 180 MPa, flexural modulus of 10.1 GPa, impact energy (IE) of 14.5 kJ/m^2, and fracture toughness (K_{Ic}) of 5 MPa.m$^{1/2}$ was found to be the best in contrast to the trend of increased IFSS for ATFE samples. This is considered to be due to stress concentration as a result of increased fibre/fibre contact with the increased fibre content in the ATFE composites compared to the UTFE composites.

Hygrothermal ageing of 65 wt% untreated and alkali treated long and short fibre/epoxy composites (produced by curing at 70^{o}C) showed that long fibre/epoxy composites were more resistant than short fibre/epoxy composites and ATFE composites were more resistant than UTFE composites towards hygrothermal ageing environments as revealed

from diffusion coefficients and tensile, flexural, impact, fracture toughness, SEM, TGA, and WAXRD test results. Accelerated ageing of 65 wt% UTLFE and alkali treated long fibre/epoxy (ATLFE) composites (produced by curing at 70^{o}C) showed that ATLFE composites were more resistant than UTLFE composites towards hygrothermal ageing environments as revealed from tensile, flexural, impact, K_{Ic}, SEM, TGA, WAXRD, FTIR test results.

IFSS obtained with untreated fibre/PLA (UFPLA) and alkali treated fibre/PLA (ATPLA) samples showed that ATPLA samples had greater IFSS than that of UFPLA samples. The increase in the formation of hydrogen bonding and mechanical interlocking of the alkali treated fibres with PLA could be responsible for the increased IFSS for ATPLA system compared to UFPLA system.

Long and short fibre reinforced PLA composites were also produced with various processing conditions using compression moulding. A 32 wt% alkali treated long fibre PLA composite produced by film stacking with a TS of 83 MPa, YM of 11 GPa, flexural strength of 143 MPa, flexural modulus of 6.5 GPa, IE of 9 kJ/m^2, and K_{Ic} of 3 MPa.m$^{1/2}$ was found to be the best. This could be due to the better bonding of the alkali treated fibres with PLA. The mechanical properties of this composite have been found to be the best compared to the available literature.

Hygrothermal and accelerated ageing of 32 wt% untreated and alkali treated long fibre/PLA composites ATPLA composites were more resistant than UFPLA composites towards hygrothermal and accelerated ageing environments as revealed from diffusion coefficients and tensile, flexural, impact, K_{Ic}, SEM, differential scanning calorimetry (DSC), WAXRD, and FTIR results. Increased potential hydrogen bond formation and mechanical interlocking of the alkali treated fibres with PLA could be responsible for the increased resistance of the ATPLA composites.

Based on the present study, it can be said that the performance of natural fibre composites largely depend on fibre properties (e.g. length and orientation), matrix properties (e.g. cure kinetics and crystallinity), fibre treatment and processing methods, and composite processing methods.

Acknowledgements

Firstly, I would like to thank my supervisor, Dr. Kim Pickering who has tirelessly guided and supported me every step of the way in my research, and who was never short on valuable advice and direction when it was needed most.

I am also thankful to my co-supervisor Dr. Johan Verbeek for his valuable suggestions and inspirations. I would like to thank Dr. Rob Torrens for his help and suggestions. I would like to express my sincere thanks to my industrial supervisor, Mr. Nic Foreman, director of Hemptech Ltd., who provided the industrial backing and some of the resources for my research that make this work possible. I would also like to thank Technology for Industry Fellowship (TIF) for their financial support of this project. Many thanks to Kinleith Mill and Dr Gerd Matthesius for giving me the opportunity to work in their lab with dynamic sheet former.

I would like to thank Christine Stewart of teaching and learning development unit (TLDU) for her help during the writing of this thesis. I would like to acknowledge Prof. M. A. Islam for his support and help. I would also like to thank Department of Engineering technicians who provided the technical assistance for my research especially Paul Ewert, Indar Singh, Brett Nichols, Yuanzi Zhang, and Helen Turner.

I would also like to thank the other composite group members (especially Delour, Gareth, Moyeen, Paul Betschart, and Anu) for their constant encouragement and valuable suggestions. I would like to convey my sincere thanks to the Department of Engineering Secretary Mary Dalbeth who was always ready to help me with a smile. Thanks to Stella for helping me with taking some SEM pictures. I am also grateful to my friends (Poom, Neamul, Kamrul, Ashraf, Florian) and well-wishers for their constant encouragement which inspired me to complete this research work.

The most important part of my life is my family. I would never have been able to accomplish any of my goals without the support of my parents, brothers, and sisters. They were always there when I needed them. A very special thanks to my wife, Sadia Saif. I will never be able to express all of my gratitude. You had faith in me and what I was doing even when I had lost it. Thank you for all of your help and sacrifice.

Table of Contents

Abstract iii

Acknowledgements vi

Table of Contents vii

List of Tables xii

List of Figures xiv

Chapter One: Introduction 1

1.1 Introduction 1
1.2 Historical Background of Natural Fibre Composites (NFCs) 3
1.3 Natural Fibre Reinforced Thermoset and Thermoplastic Composites 4
1.4 Future Aspects of Natural Fibre Composites 6
1.5 Objective of the Study 7
1.6 Thesis Organisation 8

Chapter Two: Literature Review 9

2.1 Summary 9
2.2 Natural Fibres: Source and Classification 9
2.3 Comparison of Cellulose Fibres 11
2.4 Industrial Hemp Fibre 13
2.4.1 Plant and Bast Fibre Morphology 15
2.4.2 Factors Affecting Fibre Mechanical Properties 17
2.4.3 Growing Conditions 18
2.4.4 Harvesting 18
2.5 Hemp Fibre Constituents 19
2.5.1 Cellulose 19
2.5.2 Hemicelluloses 20
2.5.3 Lignin 20
2.5.4 Pectin 21
2.6 Matrix 21
2.6.1 Thermosets 22
2.6.2 Bio-derived Thermoplastic Matrices 24
2.7 Natural Fibre Reinforced Polymer Composites 25
2.7.1 Factors Affecting the Use of Natural Fibres in Composites 26
2.7.1.1 Wettability and Interfacial Bonding 26
2.7.1.2 Thermal Stability 27
2.7.1.3 Dispersion of the Fibre in the Matrix 27
2.7.1.4 Biodegradability 28
2.7.1.5 Effect of Fibre Orientation 29
2.7.1.6 Influence of Humidity 29
2.7.1.7 Fibre Aspect Ratio 29
2.7.1.8 Fibre Volume Fraction 30

2.8 Chemical Treatment of Fibres 31
2.8.1 Alkali Treatment of the Fibres 31
2.8.1.1 Empirical Model for the Tensile Strength (TS) of Alkali Treated Fibre by Partial Factorial Design 31
2.8.1.2 Selection of the Levels of Treatment Factors 33
2.8.2 Acetylation of the Fibres 35
2.8.3 Silane Treatment of the Fibres 35
2.9 Interfacial Shear Strength (IFSS) of Composites 36
2.10 Cure Kinetics of Hemp/Epoxy Composites (HECs) 38
2.10.1 Non-isothermal or Dynamic Kinetic Models 41
2.10.2 Isothermal Kinetic Model: Autocatalytic Model 42
2.11 Processing of Fibre Reinforced Composites 44
2.11.1 Hand Lay-up 44
2.11.2 Compression Moulding 44
2.11.3 Film Stacking Technique 45
2.11.4 Vacuum Bag 45
2.12 Modelling of Tensile Strength (TS) of Composites 46
2.12.1 Modified Rule of Mixtures (MROM) 47
2.13 Degradation and Environmental Effects 48
2.13.1 Hygrothermal Ageing of the Composites 48
2.13.2 Accelerated Ageing of the Composites 52
2.14 Fibre and Composites Characterisation Methods 54
2.14.1 Wide Angle X-ray Diffraction (WAXRD) 54
2.14.2 Fourier Transform Infrared (FTIR) Spectroscopy 55
2.14.3 Zeta Potential Measurements 55
2.14.4 Thermal Analysis 58
2.14.4.1 Differential Thermal Analysis/Thermogravimetric Analysis (DTA/TGA) 58
2.14.4.2 Differential Scanning Calorimetry (DSC) 59

Chapter Three: Fibre Treatment and Characterisation 60

3.1 Summary 60
3.2 Experimental Details 60
3.2.1 Materials 60
3.2.2 Methods 61
3.2.2.1 Treatment of the Fibres with Alkali 61
3.2.2.2 Treatment of the Fibres with Acetic Anhydride 61
3.2.2.3 Treatment of the Fibres with Silane 61
3.2.2.4 Zeta Potential Measurement 62
3.2.2.5 Scanning Electron Microscopy (SEM) 62
3.2.2.6 Wide Angle X-ray Diffraction (WAXRD) 62
3.2.2.7 Thermal Analysis 63
3.2.2.8 Lignin Analysis of the Fibres 63
3.2.2.9 Fourier Transform Infrared (FTIR) Spectra 63
3.2.2.10 Single Fibre Tensile Testing (SFTT) 63
3.3 Results and Discussion 64
3.3.1 Alkali Treatment and Characterisation of the Fibres 64
3.3.1.1 Empirical Model for the Tensile Strength (TS) of Alkali Treated Fibre by Partial Factorial Design 64

3.3.1.2 The Effects of Alkali Treatment on Tensile Strength (TS) 82
3.3.1.3 The Effects of Alkali Treatment on Young's Modulus (YM) 85
3.3.1.4 The Effects of Fibre Diameter on Tensile Strength (TS) of the Alkali Treated Fibres 86
3.3.1.5 Scanning Electron Microscopic Evaluation of Alkali Treated Fibres 88
3.3.1.6 Zeta Potential 90
3.3.1.7 Wide Angle X-ray Diffraction (WAXRD) 91
3.3.1.8 Differential Thermal Analysis/Thermogravimetric Analysis (DTA/TGA) 93
3.3.1.9 Lignin Analysis 97
3.3.1.10 Fourier Transform Infrared (FTIR) Spectra 98
3.3.2 Characterisation of Acetylated Fibres 99
3.3.2.1 Scanning Electron Microscopy (SEM) 99
3.3.2.2 Zeta Potential 100
3.3.2.3 Thermal Analysis by Differential Thermal Analysis/ Thermogravimetric Analysis (DTA /TGA) 101
3.3.2.4 Wide Angle X-ray Diffraction (WAXRD) 104
3.3.2.5 Fourier Transform Infrared (FTIR) Spectra 105
3.3.3 Characterisation of Silane Treated Fibres 106
3.3.3.1 Scanning Electron Microscopy (SEM) 106
3.3.3.2 Zeta Potential 107
3.3.3.3 Thermal Analysis by Differential Thermal Analysis/ Thermogravimetric Analysis (DTA /TGA) 108
3.3.3.4 Wide Angle X-ray Diffraction (WAXRD) 111
3.3.3.5 Fourier Transform Infrared (FTIR) Spectra 113
3.4 Chapter Conclusion 113

Chapter Four: Hemp/Epoxy Composites (HECs) 115

4.1 Summary 115
4.2 Experimental Details 116
4.2.1 Materials 116
4.2.2 Methods 117
4.2.2.1 Cure Kinetic Study of Neat Epoxy (NE) and Untreated Hemp Fibre/Epoxy (UTFE) Composites Using Differential Scanning Calorimetry (DSC) 117
4.2.2.2 Interfacial Shear Strength (IFSS) Measurement of Hemp Fibre/Epoxy Samples Using Single Fibre Pull-out Testing 117
4.2.2.3 Production of Preform Fibre Mats 119
4.2.2.4 Production of Composites 121
4.2.2.5 Tensile Testing 123
4.2.2.6 Flexural Testing 123
4.2.2.7 Impact Testing 123
4.2.2.8 Fracture Toughness (K_{Ic}) Testing 124
4.2.2.9 Optical Microscopy 124
4.2.2.10 Scanning Electron Microscopy (SEM) 124
4.2.2.11 Thermogravimetric Analysis (TGA) 124
4.2.2.12 Wide Angle X-ray Diffraction (WAXRD) 125
4.2.2.13 Fourier Transform Infrared (FTIR) Spectra 125
4.2.2.14 Hygrothermal Ageing of the Composites 125
4.2.2.15 Accelerated Ageing of the Composites 125

4.3 Results and Discussion 126
4.3.1 Cure Kinetics of NE and Untreated Hemp Fibre/Epoxy (UTFE) Composites 126
4.3.1.1 Activation Energies Obtained Using the Kissinger and Flynn-Wall-Ozawa Models 126
4.3.1.2 Activation Energies Obtained Using the the Autocatalytic Model 129
4.3.2 Interfacial Shear Strength (IFSS) Measurement of Hemp Fibre/Epoxy Samples 134
4.3.3 Effects of Acetylation, Silane Treatment, Alkali Fibre Treatment and Curing Temperature on Composite Tensile Properties 138
4.3.4 Effects of Epoxy to Curing Agent Ratios on Composite Tensile Properties. 143
4.3.5 Effects of Fibre Soaking Time in Resin Bath on Composite Tensile Properties 145
4.3.6 Effects of Curing Temperatures on Composite Tensile Properties 147
4.3.7 Effects of Fibre Orientation (Short Fibres) on Composite Tensile Properties 150
4.3.8 Effects of Fibre Loading on Composite Tensile Properties, Thermogravimetric Analysis (TGA) of the Composites, and Modelling of Tensile Strength (TS) of the Composites 151
4.3.8.1 Effects of Fibre Loading on Composite Tensile Properties 151
4.3.8.2 Thermogravimetric Analysis (TGA) of the Long Fibre Composites 155
4.3.8.3 Modelling of Tensile Strength (TS) of Composites 156
4.3.9 Flexural, Impact, and Fracture Toughness of the Composites 158
Long Fibre Composites 158
Short Fibre Composites 161
4.3.10 Hygrothermal Ageing of the Composites 164
4.3.10.1 Effects of Hygrothermal Ageing on Mechanical Properties 170
4.3.11 Accelerated Ageing of the Composites 182
4.3.11.1 Fourier Transform Infrared (FTIR) Spectra 189
4.3.11.2 Thermogravimetric Analysis (TGA) 190
4.3.11.3 Wide Angle X-ray Diffraction (WAXRD) 190
4.4 Chapter Conclusion 191

Chapter Five: Hemp/PLA Composites (HPCs) 193

5.1 Summary 193
5.2 Experimental Details 194
5.2.1 Materials 194
5.2.2 Methods 194
5.2.2.1 Interfacial Shear Strength (IFSS) Measurement of Hemp Fibre/PLA Samples Using Single Fibre Pull-out Testing 194
5.2.2.2 Fibre Mat Production 194
5.2.2.3 PLA Sheet Production (Neat PLA): 195
5.2.2.4 Fabrication of Composites 195
5.2.2.5 Composite Mechanical Testing 196
5.2.2.6 Hygrothermal Ageing 197
5.2.2.7 Accelerated Ageing 197
5.2.2.8 Scanning Electron Microscopy (SEM) 197
5.2.2.9 Differential Scanning Calorimetry (DSC) Analysis 197

5.2.2.10 WAXRD 198
5.2.2.11 Fourier Transform Infrared (FTIR) Spectra 198
5.3 Results and Discussion 198
5.3.1 Interfacial Shear Strength (IFSS) Measurement of Hemp Fibre/PLA Samples 198
5.3.2 Mechanical Properties 200
5.3.2.1 Tensile Properties 200
5.3.2.2 Flexural Properties 208
5.3.2.3 Impact Energy (IE) 209
5.3.2.4 Fracture Toughness (K_{Ic}) 210
5.3.3 Crystallinity 211
5.3.3.1 Differential Scanning Calorimetry (DSC) Analysis 211
5.3.3.2 Wide Angle X-ray Diffraction (WAXRD) Analysis 213
5.3.4 Hygrothermal Ageing 214
5.3.4.1 Effects of Hygrothermal Ageing on Mechanical Properties 218
5.3.4.2 Effects of Hygrothermal Ageing on Crystallinity 224
5.3.5 Accelerated Ageing 227
5.3.5.1 Fourier Transform Infrared (FTIR) Spectra Analysis 234
5.3.5.2 Wide Angle X-ray Diffraction (WAXRD) Analysis 235
5.3.5.3 Differential Scanning Calorimetry (DSC) Analysis 236
5.4 Chapter Conclusion 237

Chapter Six: Conclusions 239

6.1 Fibre Treatment and Characterisation 239
6.2 Hemp/Epoxy Composites (HECs) 240
6.3 Hemp/PLA Composites (HPCs) 244

Chapter Seven: Recommendations and Future Work 246

References 248

Appendices 263

Publication List of this Work 263
Glossary of acronyms and Symbols 265

List of Tables

Table 1.1 The use of natural fibres as serial parts in the automotive industry (1997-2001). 6
Table 2.1 Properties of glass and natural fibres. 11
Table 2.2 The prices of some fibres. 12
Table 2.3 Commercially available fibre sources and their production. 12
Table 2.4 Physical characteristics of bast fibres. 12
Table 2.5 Percentage chemical composition of cellulose fibres. 13
Table 3.1 Experimental parameters for the selection of level of treatment factors. 65
Table 3.2 Actual factors and settings for alkali treatment of untreated fibres for the experimental design. 66
Table 3.3 A half fraction coded matrix for four factors at two levels. 67
Table 3.4 Experimental data for alkali treatment of untreated hemp fibres. 68
Table 3.5 Effects of the factors and interactions on fibre TS. 69
Table 3.6 Experimental verification of predicted/estimated fibre TS and treatment parameters. 74
Table 3.7 Experimental data for alkali treatment of untreated hemp fibres. 75
Table 3.8 Effects of the factors and interactions on fibre TS. 76
Table 3.9 Experimental verification of predicted/estimated fibre strength and treatment parameters. 80
Table 3.10 Summary of the single fibre tensile test results for alkali treated hemp fibres. 82
Table 3.11 $\zeta_{plateau}$ and IEP of untreated and alkali treated fibres. 90
Table 3.12 The crystallographic planes at various intensity (WAXRD counts) and 2θ-angles, and the crystallinity indices, *CrI* of untreated and alkali treated hemp fibres. 92
Table 3.13 The peak onset, peak and peak finishing temperatures of the endotherm and both exotherms for the untreated and alkali treated fibres obtained from DTA thermograms. 94
Table 3.14 Activation energies and frequency factors obtained by Broido method for untreated and alkali treated fibres. 96
Table 3.15 Cellulose, lignin, and ash contents of the untreated and alkali treated hemp fibres. 97
Table 3.16 FTIR wavenumbers (cm^{-1}) of untreated and alkali treated fibres. 99
Table 3.17 $\zeta_{plateau}$ and IEP of acetylated fibres compared to alkali treated fibres. 101
Table 3.18 The peak onset, peak, peak finishing temperatures and nature of peaks for the acetylated fibres compared to alkali treated fibres obtained from the DTA thermograms. 102
Table 3.19 Activation energies and frequency factors obtained by Broido method for acetylated fibres compared to alkali treated fibres. 104
Table 3.20 The crystallographic planes at various intensity (WAXRD counts) and 2θ-angles, and the crystallinity indices of acetylated fibres compared to alkali treated fibres. 105

Table 3.21 $\zeta_{plateau}$ and IEP of silane treated fibres compared to alkali treated fibres. 108
Table 3.22 The peak onset, peak, peak finishing temperatures and nature of peaks for the silane treated fibres compared to the alkali treated fibres obtained from the DTA thermograms. 109
Table 3.23 Activation energies and frequency factors obtained by Broido method for silane treated fibres compared to alkali treated fibres. 111
Table 3.24 The crystallographic planes at various intensity (WAXRD counts) and 2θ-angles, and the crystallinity indices of silane treated fibres compared to alkali treated fibres. 112
Table 4.1 Duration of the pressure maintained at each curing temperature. 122
Table 4.2 Heat of reaction for NE and composites at five different heating rates. 127
Table 4.3 Comparison of activation energies obtained by different models. 128
Table 4.4 Curing time, ΔH_t, and α of NE and composites at four different curing temperatures.....130
Table 4.5 Autocatalytic model parameters for NE and composites. 130
Table 4.6 Curing time of NE and composites at four different epoxy to curing agent ratios cured at 25^{o}C.....133
Table 4.7 Diffusion case selection parameter n at three different temperatures. 169
Table 4.8 Diffusion coefficients (D) for NE, UTFE and ATFE composites at three different temperatures. 169
Table 4.9 Tensile properties of hygrothermally aged short and long fibre/epoxy composites at three different temperatures. 178
Table 5.1 Thermal characteristics of PLA and its composites obtained from DSC. 212
Table 5.2 Diffusion case selection parameter n. 218
Table 5.3 Diffusion coefficients for NE, untreated long aligned (FSt) and alkali treated long aligned (FSt) composites at two different temperatures. 218
Table 5.4 Tensile properties of untreated long aligned (FSt) and alkali treated long aligned (FSt) composites after hygrothermal ageing at two different temperatures. 220
Table 5.5 Thermal characteristics of hygrothermally aged PLA and its composites obtained from DSC. 225

List of Figures

Figure 2.1 Overview of natural fibres. 10
Figure 2.2 Classification of natural fibre that can be used as reinforcements in polymers. 10
Figure 2.3 Female hemp plant. 15
Figure 2.4 Cross section of a hemp stem. 16
Figure 2.5 Composition of hemp stem. 17
Figure 2.6 Chemical structure of DGEBA. 23
Figure 2.7 Testing for optimum treatment condition for the TS of hemp fibres. 33
Figure 2.8 2,2 – bis [4 - (2′,3′ –epoxy propoxy) phenyl] propane (DGEBA). 38
Figure 2.9 Higher molecular weight homologues of epoxy resins. 39
Figure 2.10 Curing of epoxy resin with primary and secondary amines 40
Figure 2.11 Schematic representation of parallel and series models. 47
Figure 2.12 Oxidation reactions initiated by UV-radiation. 53
Figure 2.13 Electrokinetic, ε and zeta potentials, ζ of surfaces with different thicknesses of the double layer. 56
Figure 3.1 Single fibre tensile test specimen. 64
Figure 3.2 TS versus NaOH concentration (at 180^{o}C for 60 minutes with 2 wt% Na_2SO_3) plot for the level selection range of alkali fibre treatment. The curved line in the figure indicates principal trend of data points and do not represent any data fitting. 65
Figure 3.3 TS versus digestion time (at 180^{o}C with 5 wt% NaOH and 2 wt% Na_2SO_3) plot for the level selection range of alkali fibre treatment. The curved line in the figure indicates principal trend of data points and do not represent any data fitting. 65
Figure 3.4 TS versus temperature (for 60 minutes with 5 wt% NaOH and 2 wt% Na_2SO_3) plot for the level selection range of alkali fibre treatment. The curved line in the figure indicates principal trend of data points and do not represent any data fitting. 66
Figure 3.5 Plot of the average TS (responses) for each effect (factor and interaction). 70
Figure 3.6 Average TS for the interaction of concentrations of NaOH and Na_2SO_3. 71
Figure 3.7 Average TS for the interaction of concentration of NaOH and Time. 71
Figure 3.8 Average TS for the interaction of concentration of Na_2SO_3 and Time. 71
Figure 3.9 Pareto chart for the half effects of each factor and interaction. 72
Figure 3.10 Plot of the average TS (responses) for each effect (factor and interaction). .. 76
Figure 3.11 Average TS for the interaction of concentration of NaOH and Na_2SO_3. 77
Figure 3.12 Average TS for the interaction of concentration of NaOH and Time. 78
Figure 3.13 Average TS for the interaction of concentration of Na_2SO_3 and Time. 78
Figure 3.14 Pareto chart for the half effects (Δ/2) of each factor and interaction. 79
Figure 3.15 Effect of treatment temperature and digestion time on the TS of 5 wt% NaOH treated hemp fibres. 83
Figure 3.16 Effect of treatment temperature and digestion time on the TS of 10 wt% NaOH treated hemp fibres. 83
Figure 3.17 Effect of NaOH concentration and digestion time on the TS of hemp fibres. 83
Figure 3.18 Effect of treatment temperature and digestion time on the YM of 10 wt% NaOH treated hemp fibres. 85
Figure 3.19 Effect of treatment temperature and digestion time on the YM of 5 wt% NaOH treated hemp fibres. 86

Figure 3.20 Effect of NaOH concentration and digestion time on the YM of hemp fibres. 86
Figure 3.21 Influence of fibre diameter on the TS of P_2E_1 alkali treated hemp fibres. 87
Figure 3.22 Influence of fibre diameter on the TS of P_2E_4 alkali treated hemp fibres. 87
Figure 3.23 Influence of fibre diameter on the TS of P_2E_7 alkali treated hemp fibres. 87
Figure 3.24 SEM of untreated hemp fibre. 89
Figure 3.25 SEM of P_2E_1 alkali treated hemp fibre. 89
Figure 3.26 SEM of P_2E_4 alkali treated hemp fibre. 89
Figure 3.27 SEM of P_2E_7 alkali treated hemp fibre. 89
Figure 3.28 pH dependence of zeta potential of untreated and alkali treated fibres. 90
Figure 3.29 WAXRD pattern of untreated and alkali treated fibres. 91
Figure 3.30 DTA curves for untreated and alkali treated fibres. 93
Figure 3.31 TGA curves for untreated and alkali treated fibres. 93
Figure 3.32 Plots of ln[ln(1/y)] versus $T^{-1}\times10^3$ K^{-1} for the second stage of thermal degradation for untreated and alkali treated fibres. 95
Figure 3.33 Plots of ln[ln(1/y)] versus $T^{-1}\times10^3$ K^{-1} for the third stage of thermal degradation for untreated and alkali treated fibres. 96
Figure 3.34 FTIR-spectra of untreated and alkali treated fibres. 98
Figure 3.35 SEM of acetylated hemp fibre. 100
Figure 3.36 pH dependence of zeta potential of acetylated fibres compared to alkali treated fibres. 100
Figure 3.37 DTA curves for acetylated fibres compared to alkali treated fibres. 101
Figure 3.38 TGA curves for acetylated fibres compared to alkali treated fibres. 102
Figure 3.39 Plots of ln[ln(1/y)] versus $T^{-1}\times10^3$ K^{-1} for the second stage of thermal degradation (first exothermic peak) for acetylated fibres compared to alkali treated fibres. 103
Figure 3.40 Plots of ln[ln(1/y)] versus $T^{-1}\times10^3$ K^{-1} for the third stage of thermal degradation (second exothermic peak) for acetylated fibres compared to alkali treated fibres. 103
Figure 3.41 WAXRD pattern of acetylated fibres compared to alkali treated fibres. 104
Figure 3.42 FTIR spectra of acetylated fibres compared to alkali treated fibres. 106
Figure 3.43 SEM of silane treated hemp fibre surface. 107
Figure 3.44 pH dependence of zeta potential of silane treated fibres compared to alkali treated fibres. 107
Figure 3.45 DTA curves for sialne treated fibres compared to alkali treated fibres. 108
Figure 3.46 TGA curves for silane treated fibres compared to alkali treated fibres. 109
Figure 3.47 Plots of ln[ln(1/y)] versus $T^{-1}\times10^3$ K^{-1} for the second stage of thermal degradation (first exothermic peak) for silane treated fibres compared to alkali treated fibres. 110
Figure 3.48 Plots of ln[ln(1/y)] versus $T^{-1}\times10^3$ K^{-1} for the third stage of thermal degradation (second exothermic peak) for silane treated fibres compared to alkali treated fibres. 111
Figure 3.49 WAXRD pattern of silane treated fibres compared to alkali treated (P_2E_4) fibres. 112
Figure 3.50 FTIR spectra of silane treated fibres compared to alkali treated fibres. 113
Figure 4.1 Test specimen for single fibre pull-out tests. 118
Figure 4.2 Single fibre embedded in epoxy resin. 119
Figure 4.3 Hand carding machine used to produce aligned long fibre mats. 119
Figure 4.4 Dynamic sheet former used to produce aligned short fibre mats. 120

Figure 4.5 Aligned alkali treated fibre mat produced by dynamic sheet forming (DSF). 120
Figure 4.6 Specimen configuration for SENB. 124
Figure 4.7 Heat flow measured by DSC during cure of NE at five different heating rates (*Heat flow normalised to show relative peak sizes). 127
Figure 4.8 Heat flow measured by DSC during cure of composites at five different heating rates (*Heat flow normalised to show relative peak sizes). 127
Figure 4.9 Activation energies obtained by the Kissinger model for NE and composites. 128
Figure 4.10 Activation energies obtained by Flynn-Wall-Ozawa method for NE and composites. 129
Figure 4.11 Conversion rate versus conversion graphs for NE at four different isothermal temperatures. The solid lines are a trend expected from the Autocatalytic Model (Equation (2.11)) 131
Figure 4.12 Arrhenius plot for the reaction constant k_1. 132
Figure 4.13 Arrhenius plot for the reaction constant k_2. 132
Figure 4.14 Typical load versus displacement curve for pull-out tests of hemp/epoxy sample. 134
Figure 4.15 Debonding force versus embedded length plots for UTFE samples at various epoxy resin to curing agent ratios. 135
Figure 4.16 Debonding force versus embedded length plots for ATFE samples at various epoxy resin to curing agent ratios. 135
Figure 4.17 IFSS of UTFE samples found at eight different embedded length and four different epoxy resin to curing agent ratios. The solid lines indicate principal trends of data points and do not represent any data fitting. 136
Figure 4.18 IFSS of ATFE samples found at eight different embedded length and four different epoxy resin to curing agent ratios. The solid lines indicate principal trends of data points and do not represent any data fitting. 136
Figure 4.19 Tensile properties of UTFE, AcFE, STFE, and ATFE composites compared to NE cured at 25^{o}C. Error bars each corresponds to one standard deviation. 138
Figure 4.20 Optical micrograph of UTFE composites cured at 25^{o}C 139
Figure 4.21 Optical micrograph of AcFE composites cured at 25^{o}C. 139
Figure 4.22 Optical micrograph of STFE composites cured at 25^{o}C. 140
Figure 4.23 Optical micrograph of ATFE composites cured at 25^{o}C 140
Figure 4.24 SEM micrograph of the fracture surface of STFE composites. 142
Figure 4.25 Tensile properties of UTFE and ATFE composites compared to NE cured at 25^{o}C and 120^{o}C. Error bars each corresponds to one standard deviation. 142
Figure 4.26 Optical micrograph of ATFE composites cured at 120^{o}C 143
Figure 4.27 Tensile properties of 30 and 40 wt% UTFE and ATFE composites produced at four different epoxy to curing agent ratios. Error bars each corresponds to one standard deviation. 144
Figure 4.28 Optical micrograph of ATFE composites produced by aligned mat obtained by hand carding machine. 145
Figure 4.29 Tensile properties of untreated and alkali treated composites produced by soaking the fibre mats for 10 and 60 minutes. Error bars each corresponds to one standard deviation. 146
Figure 4.30 Poor wetting of fibre in ATFE composites produced by soaking for 10 minutes in the resin bath. 146
Figure 4.31 Good wetting of fibre in ATFE composites produced by soaking for 60 minutes in the resin bath. 147

Figure 4.32 Tensile properties of UTFE and ATFE composites produced at three different curing temperatures. Error bars each corresponds to one standard deviation. 148
Figure 4.33 SEM micrographs of fracture surfaces of tensile tested specimens with 40 wt% alkali treated fibres produced at (a) 120^{o}C and (b) 70^{o}C curing temperatures. 149
Figure 4.34 Tensile properties of random and aligned short fibre composites produced with untreated and alkali treated fibres. Error bars each corresponds to one standard deviation. 150
Figure 4.35 The variation in tensile properties with fibre loading for UTLFE and ATLFE composites. Error bars each corresponds to one standard deviation. 151
Figure 4.36 SEM pictures of fracture surfaces of 65 wt% (a) UTLFE and (b) ATLFE composites. 152
Figure 4.37 The variation in tensile properties with fibre loading for UTSFE and ATSFE composites. Error bars each corresponds to one standard deviation. 153
Figure 4.38 SEM pictures of fracture surfaces of 65 wt% (a) UTSFE and (b) ATSFE composites. 154
Figure 4.39 TGA traces for UTLFE and ATLFE composites. 155
Figure 4.40 Tensile strength versus fibre volume fraction of composites (solid lines for theoretical model values and symbols for experimentally obtained values for UTLFE and UTSFE composites). 156
Figure 4.41 Tensile strength versus fibre volume fraction of composites (solid lines for theoretical model values and symbols for experimentally obtained values for ATLFE and ATSFE composites). 157
Figure 4.42 Flexural strength of UTLFE and ATLFE composites compared to NE. Error bars each corresponds to one standard deviation. 159
Figure 4.43 Flexural modulus of UTLFE and ATLFE composites compared to NE. Error bars each corresponds to one standard deviation. 159
Figure 4.44 IE of UTLFE and ATLFE composites compared to NE. Error bars each corresponds to one standard deviation. 160
Figure 4.45 K_{Ic} of 65 wt% UTLFE and ATLFE composites compared to NE. Error bars each corresponds to one standard deviation. 160
Figure 4.46 Optical micrographs showing major crack of fracture toughness specimens of (a) ATLFE and (b) UTLFE composites. 161
Figure 4.47 Flexural strength and flexural modulus of 65 wt% UTSFE and ATSFE composites compared to NE. Error bars each corresponds to one standard deviation. 162
Figure 4.48 IE of UTSFE and ATSFE composites compared to NE. Error bars each corresponds to one standard deviation. 163
Figure 4.49 K_{Ic} of 65 wt% UTSFE and ATSFE composites compared to NE. Error bars each corresponds to one standard deviation. 163
Figure 4.50 Optical micrographs of (a) UTLFE and (b) ATLFE composite surfaces after hygrothermal ageing at 70^{o}C. 164
Figure 4.51 Thickness swelling of the NE and long and short fibre/epoxy composites after hygrothermal ageing. 165
Figure 4.52 Moisture absorption behaviour of NE at 25, 50, and 70^{o}C. 166
Figure 4.53 Moisture absorption behaviour of 65 wt% UTLFE composites at 25, 50, and 70^{o}C. 166
Figure 4.54 Moisture absorption behaviour of 65 wt% ATLFE composites at 25, 50, and 70^{o}C. 166

Figure 4.55 Moisture absorption behaviour of 65 wt% UTSFE composites at 25, 50, and 70°C. 167
Figure 4.56 Moisture absorption behaviour of 65 wt% ATSFE composites at 25, 50, and 70°C. 167
Figure 4.57 SEM micrographs of (a) UTLFE and (b) ATLFE composites surfaces after hygrothermal ageing at 70°C. 168
Figure 4.58 Diffusion case fitting plots for ATLFE composites at 25 and 50 and 70°C. 168
Figure 4.59 Diffusion case fitting plots for UTSFE composites at 25 and 50 and 70°C. 169
Figure 4.60 Effect of hygrothermal ageing on the TS of NE, UTLFE and ATLFE composites at three different temperatures. Error bars each corresponds to one standard deviation. 170
Figure 4.61 Effect of hygrothermal ageing on the YM of NE, UTLFE and ATLFE composites at three different temperatures. Error bars each corresponds to one standard deviation. 171
Figure 4.62 (a) UTLFE and (b) ATLFE composite fracture surfaces after hygrothermal ageing at 70°C. 172
Figure 4.63 Effect of hygrothermal ageing on the FS of UTLFE and ATLFE composites compared to NE at three different temperatures. Error bars each corresponds to one standard deviation. 173
Figure 4.64 Effect of hygrothermal ageing on the flexural strength of UTLFE and ATLFE composites compared to NE at three different temperatures. Error bars each corresponds to one standard deviation. 173
Figure 4.65 Effect of hygrothermal ageing on the flexural modulus of UTLFE and ATLFE composites compared to NE at three different temperatures. Error bars each corresponds to one standard deviation. 174
Figure 4.66 Effect of hygrothermal ageing on the flexural strain of UTLFE and ATLFE composites compared to NE at three different temperatures. Error bars each corresponds to one standard deviation. 174
Figure 4.67 Effect of hygrothermal ageing on the IE of UTLFE and ATLFE composites compared to NE at three different temperatures. Error bars each corresponds to one standard deviation. 175
Figure 4.68 Effect of hygrothermal ageing on the K_{Ic} of UTLFE and ATLFE composites compared to NE at three different temperatures. Error bars each corresponds to one standard deviation. 175
Figure 4.69 TGA traces for UTLFE and ATLFE composites after hygrothermal ageing at 70°C. 176
Figure 4.70 WAXRD pattern for UTLFE and ATLFE composites before and after hygrothermal ageing at 70°C. 177
Figure 4.71 Effect of hygrothermal ageing on the TS of UTSFE and ATSFE composites compared to NE at three different temperatures. Error bars each corresponds to one standard deviation. 178
Figure 4.72 Effect of hygrothermal ageing on the YM of UTSFE and ATSFE composites compared to NE at three different temperatures. Error bars each corresponds to one standard deviation. 179
Figure 4.73 Effect of hygrothermal ageing on the FS of UTSFE and ATSFE composites compared to NE at three different temperatures. Error bars each corresponds to one standard deviation. 179
Figure 4.74 Effect of hygrothermal ageing on the flexural strength of UTSFE and ATSFE composites compared to NE at three different temperatures. Error bars each corresponds to one standard deviation. 180

Figure 4.75 Effect of hygrothermal ageing on the flexural modulus of UTSFE and ATSFE composites compared to NE at three different temperatures. Error bars each corresponds to one standard deviation. 180
Figure 4.76 Effect of hygrothermal ageing on the flexural strain of UTSFE and ATSFE composites compared to NE at three different temperatures. Error bars each corresponds to one standard deviation. 180
Figure 4.77 Effect of hygrothermal ageing on the IE of UTSFE and ATSFE composites compared to NE at three different temperatures. Error bars each corresponds to one standard deviation. 181
Figure 4.78 Effect of hygrothermal ageing on the K_{Ic} of UTSFE and ATSFE composites compared to NE at three different temperatures. Error bars each corresponds to one standard deviation. 182
Figure 4.79 Visual change during weathering of UTLFE and ATLFE composites. 182
Figure 4.80 SEM of UTLFE composites showing tearing of the fibres after accelerated ageing of 1000 hours. 183
Figure 4.81 Percentage weight gain of NE, UTLFE and ATLFE composites. 184
Figure 4.82 Effect of accelerated ageing on the TS of UTLFE and ATLFE composites compared to NE. Error bars each corresponds to one standard deviation. 185
Figure 4.83 Effect of accelerated ageing on the YM of UTLFE and ATLFE composites compared to NE. Error bars each corresponds to one standard deviation. 185
Figure 4.84 Effect of accelerated ageing on the FS of UTLFE and ATLFE composites compared to NE. Error bars each corresponds to one standard deviation. 185
Figure 4.85 Effect of accelerated ageing on the flexural strength of UTLFE and ATLFE composites compared to NE. Error bars each corresponds to one standard deviation. 186
Figure 4.86 Effect of accelerated ageing on the flexural modulus of UTLFE and ATLFE composites compared to NE. Error bars each corresponds to one standard deviation. 186
Figure 4.87 Effect of accelerated ageing on the flexural strain of UTLFE and ATLFE composites compared to NE. Error bars each corresponds to one standard deviation. 186
Figure 4.88 Effect of accelerated ageing on the IE of UTLFE and ATLFE composites compared to NE. Error bars each corresponds to one standard deviation. 187
Figure 4.89 Effect of accelerated ageing on the K_{Ic} of UTLFE and ATLFE composites compared to NE. Error bars each corresponds to one standard deviation. 187
Figure 4.90 (a) UTLFE and (b) ATLFE composites fracture surfaces after 1000 hours accelerated ageing. 188
Figure 4.91 Micrograph of NE surface after weathering for 1000 hours. 189
Figure 4.92 FTIR spectra of UTLFE composites of before (control) and after 1000 hours accelerated ageing. 189
Figure 4.93 TGA of UTLFE and ATLFE composites after accelerated ageing of 1000 hours. 190
Figure 4.94 WAXRD pattern for UTLFE and ATLFE composites before and after accelerated ageing of 1000 hours. 191
Figure 5.1 Debonding force versus embedded length for UFPLA and ATPLA samples. The solid lines indicate principal trends of data points and do not represent any data fitting. 198
Figure 5.2 IFSS of UFPLA and ATPLA samples, obtained for eight different embedded fibre lengths. The solid lines indicate principal trends of data points and do not represent any data fitting. 199

Figure 5.3 TS of untreated short aligned, alkali treated short aligned, and untreated short random composites compared to neat PLA. Error bars each corresponds to one standard deviation. 200
Figure 5.4 YM of untreated short aligned, alkali treated short aligned, and untreated short random composites compared to neat PLA. Error bars each corresponds to one standard deviation. 201
Figure 5.5 SEM pictures of the fracture surface of (a) alkali treated short aligned and (b) untreated short random composites. 202
Figure 5.6 FS of untreated short aligned, alkali treated short aligned, and untreated short random composites compared to neat PLA. Error bars each corresponds to one standard deviation. 203
Figure 5.7 TS of alkali treated long aligned (DCM), and untreated short random (DCM) composites compared to neat PLA. Error bars each corresponds to one standard deviation. 204
Figure 5.8 Optical micrograph of the surface of (a) alkali treated long aligned (DCM) and (b) untreated short random (DCM) composites. 204
Figure 5.9 YM of alkali treated long aligned (DCM) and untreated short random (DCM) composites compared to neat PLA. Error bars each corresponds to one standard deviation. 204
Figure 5.10 FS of alkali treated long aligned (DCM) and untreated short random (DCM) composites compared to neat PLA. Error bars each corresponds to one standard deviation. 205
Figure 5.11 TS of untreated long aligned (FSt) and alkali treated long aligned (FSt) composites compared to neat PLA. Error bars each corresponds to one standard deviation. 205
Figure 5.12 YM of untreated long aligned (FSt) and alkali treated long aligned (FSt) composites compared to neat PLA. Error bars each corresponds to one standard deviation. 206
Figure 5.13 FS of untreated long aligned (FSt) and alkali treated long aligned (FSt) composites compared to neat PLA. Error bars each corresponds to one standard deviation. 206
Figure 5.14 SEM micrographs of fracture surfaces of (a) untreated long aligned (FSt) and (b) alkali treated long aligned (FSt) composites. 207
Figure 5.15 Flexural strength of untreated long aligned (FSt) and alkali treated long aligned (FSt) composites compared to neat PLA. Error bars each corresponds to one standard deviation. 208
Figure 5.16 Flexural modulus of untreated long aligned (FSt) and alkali treated long aligned (FSt) composites compared to neat PLA. Error bars each corresponds to one standard deviation. 209
Figure 5.17 IE of untreated long aligned (FSt) and alkali treated long aligned (FSt) composites compared to neat PLA. Error bars each corresponds to one standard deviation. 209
Figure 5.18 K_{Ic} of untreated long aligned (FSt) and alkali treated long aligned (FSt) composites compared to neat PLA. Error bars each corresponds to one standard deviation. 210
Figure 5.19 Optical micrographs showing major crack of fracture toughness specimens of (a) untreated long aligned (FSt) and (b) alkali treated long aligned (FSt) composites. 211
Figure 5.20 DSC trace for PLA only sample displaying the glass transition temperature, cold crystallisation, and melting. 211

Figure 5.21 DSC thermograms of untreated long aligned (FSt) and alkali treated long aligned (FSt) composites compared to neat PLA. 212
Figure 5.22 WAXRD pattern for the raw materials used. 213
Figure 5.23 WAXRD curves for untreated long aligned (FSt) and alkali treated long aligned (FSt) composites. 214
Figure 5.24 (a) Untreated long aligned (FSt) and (b) alkali treated long aligned (FSt) composite surfaces after hygrothermal ageing at 50^{o}C. 215
Figure 5.25 Thickness swelling of the composites compared to neat PLA after hygrothermal ageing. 215
Figure 5.26 Moisture absorption behaviour of neat PLA at 25 and 50^{o}C. 216
Figure 5.27 Moisture absorption behaviour of 32 wt% untreated long aligned (FSt) composites at 25 and 50^{o}C....216
Figure 5.28 Moisture absorption behaviour of 32 wt% alkali treated long aligned (FSt) composites at 25 and 50^{o}C....216
Figure 5.29 Diffusion case fitting plots for 32 wt% alkali treated long aligned (FSt) composites at 25 and 50^{o}C....217
Figure 5.30 Effect of hygrothermal ageing on the TS of neat PLA, untreated long aligned (FSt) and alkali treated long aligned (FSt) composites at different temperatures. Error bars each corresponds to one standard deviation. 219
Figure 5.31 Effect of hygrothermal ageing on the YM of neat PLA, untreated long aligned (FSt) and alkali treated long aligned (FSt) composites at different temperatures. Error bars each corresponds to one standard deviation....219
Figure 5.32 (a) untreated long aligned (FSt) and (b) alkali treated long aligned (FSt) composite fracture surfaces after hygrothermal ageing at 50^{o}C. 220
Figure 5.33 Effect of hygrothermal ageing on the FS of neat PLA, untreated long aligned (FSt) and alkali treated long aligned (FSt) composites at different temperatures. Error bars each corresponds to one standard deviation. 221
Figure 5.34 Effect of hygrothermal ageing on the flexural strength of neat PLA, untreated long aligned (FSt) and alkali treated long aligned (FSt) composites at different temperatures. Error bars each corresponds to one standard deviation....222
Figure 5.35 Effect of hygrothermal ageing on the flexural modulus of neat PLA, untreated long aligned (FSt) and alkali treated long aligned (FSt) composites at different temperatures. Error bars each corresponds to one standard deviation.....222
Figure 5.36 Effect of hygrothermal ageing on the flexural strain of neat PLA, untreated long aligned (FSt) and alkali treated long aligned (FSt) composites at different temperatures. Error bars each corresponds to one standard deviation....223
Figure 5.37 Effect of hygrothermal ageing on the IE of neat PLA, untreated long aligned (FSt) and alkali treated long aligned (FSt) composites at different temperatures. Error bars each corresponds to one standard deviation. 223
Figure 5.38 Effect of hygrothermal ageing on the K_{Ic} of neat PLA, untreated long aligned (FSt) and alkali treated long aligned (FSt) composites at different temperatures. Error bars each corresponds to one standard deviation. 224
Figure 5.39 DSC traces for untreated long aligned (FSt) and alkali treated long aligned (FSt) composites after hygrothermal ageing at 50^{o}C....225
Figure 5.40 WAXRD pattern for untreated long aligned (FSt) and alkali treated long aligned (FSt) composites after hygrothermal ageing at 50^{o}C. 226
Figure 5.41 Visual change during ageing of untreated long aligned (FSt) and alkali treated long aligned (FSt) composites. 227
Figure 5.42 (a) Untreated long aligned (FSt) and (b) alkali treated long aligned (FSt) composite surfaces after 1000 hours accelerated ageing. 228

Figure 5.43 Percentage weight gain of neat PLA, untreated long aligned (FSt) and alkali treated long aligned (FSt) composites. 229
Figure 5.44 Effect of accelerated ageing on the TS of neat PLA, untreated long aligned (FSt) and alkali treated long aligned (FSt) composites. Error bars each corresponds to one standard deviation. 230
Figure 5.45 Effect of accelerated ageing on the YM of neat PLA, untreated long aligned (FSt) and alkali treated long aligned (FSt) composites. Error bars each corresponds to one standard deviation. 230
Figure 5.46 Effect of accelerated ageing on the FS of neat PLA, untreated long aligned (FSt) and alkali treated long aligned (FSt) composites. Error bars each corresponds to one standard deviation. 230
Figure 5.47 Effect of accelerated ageing on the flexural strength of neat PLA, untreated long aligned (FSt) and alkali treated long aligned (FSt) composites. Error bars each corresponds to one standard deviation. 231
Figure 5.48 Effect of accelerated ageing on the flexural modulus of neat PLA, untreated long aligned (FSt) and alkali treated long aligned (FSt) composites. Error bars each corresponds to one standard deviation. 231
Figure 5.49 Effect of accelerated ageing on the flexural strain of neat PLA, untreated long aligned (FSt) and alkali treated long aligned (FSt) composites. Error bars each corresponds to one standard deviation. 231
Figure 5.50 Effect of accelerated ageing on the IE of neat PLA, untreated long aligned (FSt) and alkali treated long aligned (FSt) composites. Error bars each corresponds to one standard deviation. 232
Figure 5.51 Effect of accelerated ageing on the K_{Ic} of neat PLA, untreated long aligned (FSt) and alkali treated long aligned (FSt) composites. Error bars each corresponds to one standard deviation. 232
Figure 5.52 (a) Untreated long aligned (FSt) and (b) alkali treated long aligned (FSt) composite fracture surfaces after 1000 hours accelerated ageing. 233
Figure 5.53 SEM micrograph of neat PLA surface after weathering for 750 hours. 234
Figure 5.54 FTIR spectra of untreated long aligned (FSt) composites....235
Figure 5.55 WAXRD pattern for untreated long aligned (FSt) and alkali treated long aligned (FSt) composites after accelerated ageing of 1000 hours. 236
Figure 5.56 DSC traces for untreated long aligned (FSt) and alkali treated long aligned (FSt) composites after accelerated ageing of 1000 hours. 237

Chapter One

Introduction

1.1 Introduction

A composite is a material that has two or more distinct constituents or phases, where one or more of the phases are dispersed in another continuous phase called the matrix. The matrix can be a ceramic, metal or polymer. Generally, ceramic matrices are stiff, brittle, and survive the highest temperatures, metal matrices are strong and intermediate in stiffness, and polymer matrices are low in strength and stiffness but low in density and easily formed. The reinforcing phase of a composite can be either fibrous or particulate, the difference being that a particle has almost equal dimensions in all directions, whilst a fibre has a much greater length than its cross-section. Both of these reinforcements have been used to produce composites. However, fibrous reinforcements have drawn much attention in recent times due to their high tensile strength (TS) and Young's modulus (YM), low density, and ability to give useful properties to the end products. In fibre reinforced composite materials, fibres are used to carry the loads while the matrices are used to bind the fibres together, transfer the stresses from one fibre to the next and keep them in the desired location and orientation; the matrices also protect the fibres from abrasion and environmental damage upon exposure to elevated temperature and humidity. Many fibre reinforced polymer matrix composite (PMC) materials offer a combination of strength and stiffness that are comparable to, or even better than, some traditional metallic materials.

Fibres can be divided into two major classes, namely synthetic and natural. Though synthetic fibres are strong and stiff, recently, due to increasing environmental awareness, depletion of petroleum resources, disposal problems after use, and the introduction of new rules and regulations by legislative authorities, the production and use of traditional composite materials made with synthetic fibres like glass, aramid and carbon with matrices of polyester, polyurethane, or phenolics, have been criticised [1]. On the other

hand, usage of natural fibres like hemp, flax, jute, and sisal in composites production are drawing increasing attention due to their low cost, low density, recyclability, and biodegradability. Both conventional thermoset (e.g. epoxy, polyester, phenolics) and thermoplastic (e.g. polypropylene (PP), polyethylene (PE), polystyrene) matrices are used with natural fibre in composites production. Meanwhile, bio-derived matrix materials like polylactic acid (PLA), polycaprolactone, and polyhydroxy butyrate (PHB) seek to remedy the issues regarding raw material sources as well as disposal at the end of the product life cycle.

Besides the properties of fibre and matrix, the interface between the two constituents also plays an important role in composite materials. The interface has to be sufficiently strong for the load to be transferred from the matrix to the reinforcing fibres if the composite is to be stronger than its unreinforced matrix. As far as toughness is concerned, the interfacial strength has to be such that it can allow toughening mechanisms like debonding and pull-out to occur.

Fibre length and orientation of the reinforcing fibres are particularly important in contributing to the enhancement in mechanical properties. Though fibre breakage and fibre damage are very common due to mechanical shearing and mixing actions, short fibres can be processed with ease by using extrusion and injection moulding. Also, for shorter length and random or less controlled orientation, composites produced with short fibre exhibit relatively poor mechanical properties and are currently not suitable for use in most structural components.

More controlled orientation of long or continuous fibres leads to composites with higher mechanical properties. The high degree of orientation of long fibres can be achieved by creating yarns through textile processing. The yarns need to have sufficient level of twist to obtain good mechanical strengths. However, the extent of permeability of resins into the yarns decreases with the increasing degree of twist resulting in weak mechanical strength of the composites [2]. Moreover, the yarn production involves high cost. Therefore, simple carding process can be used to obtain good orientation in fibres with large fibre separation and almost no twist that enables the fibres to permeate into the resins with ease resulting in good mechanical properties of the composites. Long fibre reinforced thermoset composites can be processed with hand lay-up, vacuum bag, and filament winding techniques, which are suitable for short production runs and are

expensive. However, both thermoplastic and thermoset composites of intricate shape can be processed by compression moulding into articles.

1.2 Historical Background of Natural Fibre Composites (NFCs)

The production and use of composite materials can be traced back to early human existence. Composites produced with natural plant matter and its constituents like stem and fibre were used to make shelter, tools, clothes, and weapons. In ancient Egyptian times, some 3000 years ago, straw was used to reinforce clay bricks to build walls. These composites were produced by placing the structural elements on top of one another to produce the desired design.

Later on, natural fibre composites (NFCs) lost much of their interest, due to the introduction of more durable construction materials like metals and ceramics. The history of modern composites can be considered to begin in 1937 (when salesmen from the Owens Corning Fibreglass Company began to sell fibreglass to interested parties around the United States). The pace of composites development accelerated during the World War II, when the United States Government became concerned that the supplies of metals for aircraft might not be available and instructed the engineers to try to determine the current best practices in composites production [3]. However, the spur to the rapid development of large scale production of composite materials began in the early 1960s, due to the development of carbon fibres in the UK and boron fibres in the USA. These fibres used to reinforce both thermoset and thermoplastic polymer matrices for use in automotive applications [4].

Over the last few years, natural fibres have attracted attention as substitutes for synthetic fibres in composites production largely due to increased emphasis on sustainability. These natural fibres are low in cost and density, and high in specific strength. They are renewable, nonabrasive, and their specific properties are comparable with the most commonly used reinforcing glass fibres.

1.3 Natural Fibre Reinforced Thermoset and Thermoplastic Composites

Glass is the most common of all reinforcing fibres for use in polymer (thermoset and thermoplastic) matrix composites. The major advantage of glass fibre includes low price, high TS, high chemical resistance and relative ease of processing. However, it suffers with many disadvantages. It has low YM, relatively high specific gravity among other conventional fibres, sensitivity to abrasion with handling, relatively low fatigue resistance, and high hardness which causes excessive wear on moulding dies and cutting tools [5]. The biggest problem with glass and other conventional fibres is that they are not biodegradable or easily recyclable and their disposal is difficult. Alternative synthetic fibres such as aramid and carbon are limited to applications in industries such as aerospace and ballistics, where cost of the product is less important than maximising the performance (high strength, stiffness and low density) to an extremely higher level.

The use of natural fibres as reinforcement in PMCs to replace conventional fibres like glass is currently receiving increasing attention because of the growing environmental awareness and advantages (low cost, low density, high specific properties, abundant availability) they possess. The annual agricultural crop fibres (e.g. hemp, flax) have higher mechanical strength as compared to commonly used wood based fibres (e.g. wood flour, wood fibre) and the PMCs produced using these fibres as reinforcements can result in significant property improvements. Recent research on the use of annual growth agricultural crop lignocellulosic fibres suggests that they have the potential to be used as reinforcement both in thermoset and thermoplastic matrices. Of these fibres, hemp is the least used fibre in the production of PMCs and yet according to Hughes [6], it has the best mechanical and thermal properties. However, there are a number of problems associated with incorporating natural fibre into polymer matrices namely: (i) poor compatibility of a hydrophilic fibre and a hydrophobic matrix that results in poor mechanical properties of the composites, (ii) high sensitivity of natural fibre towards moisture that results in composite dimensional instability and loss in mechanical properties through swelling [7], and (iii) relatively poor thermal stability.

Thermoset resins (e.g. epoxy, polyester, phenolic, and polyurethane) are used for NFCs in applications where higher performance is required. These thermoset polymers contain

reactive functional groups that aid the development of an interface with the natural fibres. Thermoset composites have superior thermal stability and lower water absorption compared to thermoplastic composites. Epoxy and phenolic are known to have the ability to form covalent bonds with plant cell walls through -OH groups [8]. Moreover, composites manufacture can be achieved using low viscosity epoxy that cure at room temperature and the polymerisation of epoxy (curing reaction) is carried out by addition reaction without evolution of volatiles which is a desirable property to prepare void-free products. Therefore, although epoxy resins are relatively expensive than polyesters, they have good potential for the development of NFCs [9].

Thermoplastic composites are recyclable, have low processing costs and the ability to be moulded into complex parts when compared to thermoset composites. Composites based on petroleum originated thermoplastic matrices such as PP and PE are very common today and are being extensively used in automotive applications, building materials, and household products. However, growing environmental awareness is forcing the industries to find more environmentally friendly materials for their products. Therefore, materials derived from natural resources of plant origin (e.g. cellulose and starch), synthetic polymers from natural monomers (e.g. PLA), and polymers from microbial fermentation (e.g. PHB) are being assessed by researchers [10-14] for use as potential matrices in bio-degradable and ecologically friendly composites. The study of PLA and especially of natural fibre/PLA composites is very limited [15, 16]. However, Bodros *et al.* [17] showed that the TS and YM of PLA/flax composites are higher than PP/flax composites and that the specific TS and modulus of flax/PLA composite are very close to glass/polyester composites.

For natural fibres to be able to compete with synthetic fibres, improvement of the mechanical and thermal properties of the composites is necessary. This can be achieved by obtaining better adhesion between fibre and matrix and also by using better composite processing conditions.

1.4 Future Aspects of Natural Fibre Composites

About seventy years ago, natural fibres such as hemp and flax were used mostly in textile and paper industries. Currently, the market for natural fibres has expanded to the extent that most European car producers now use natural fibres for interior components because of their low density, acceptable mechanical properties, low wear on tools, and low processing costs. Applications of natural fibres as reinforcement in automotives can be seen in Table 1.1 [18].

Table 1.1 The use of natural fibres as serial parts in the automotive industry (1997-2001).

Manufacturers/Customers	Model/Application (dependent on model)
Audi	TT, A2, A3, A4 Avant (1997), A4 Variant (1997), A6, A8 (1997), Roadster, Coupe/Seat back, side and back door panels, parcel tray, boot lining, rear flap lining, rear storage panel, spare tyre lining
BMW	3, 5 and 7 Series and others/Door inserts/door panels, headliner panel, boot lining, seat back
Citroen	C4 (2001)/Door inserts
Daimler Chrysler	A-Klasse, C-Klasse, E-Klasse, S-Klasse/Door inserts, Windshield/dashboard, business table, column cover
Fiat	Punto, Brava, Marea, Alfa Romeo 146, 156, Sportwagon
Ford	Mondeo CD 162 (1997), Cougar (1998), Mondeo (2000), Focus/Door insets, B-column cover, Parcel tray, in the future also motor protection (cover undershield)
MAN	Bus (1997)/Headliner panel
Mitsubishi	Miscellaneous models (since 1997)
Nissan	Miscellaneous models
Opel	Astra, Vectra, Zafira/Headliner panel, door inserts, column cover, instrument panel, rear shelf panel
Peugeot	New model 406
Renault	Clio, Twingo
Rover	Rover 2000 and others/Insulation, rear storage panel
Saab	Coupe (1998)/Door inserts
SEAT	Door inserts, seat backs
Toyota	Miscellaneous models
Volkswagen	Golf A4, Golf 4 Variant (1998), Passat Variant, Bora/Door inserts, seat backs, rear flap lining, parcel tray
Volvo	C70, V70, Coupe (1998)Door inserts, parcel tray

The market for natural fibres has been growing at an increasing rate, especially for automotive applications [18]. For instance, the German automotive industry increased its usage of natural fibres from 4,000 tons in 1996 to 18,000 tons in 2003. From 1996 to 2002, there was almost a linear increase in quantities used, with yearly growth rates of

between 10 and 20% [19]. It has been projected that the usage of natural fibre by the European automotive industry may increase to more than 100,000 tons by 2010.

Compared to Europe, the Asian markets have also been using natural fibres for many years. For example, jute is a common reinforcement for composites in India. Jute fibre with polyester resins are used in buildings, elevators, pipes, and panels [20].

It is apparent that considerable opportunities may be opening up for injection moulded components based on short natural fibre reinforced polymer granules. However, this technology has limited commercial production and marketing. This technology can be equally suitable with hemp, flax or jute, with a view of targeting a new range of hard interior components. According to Ellison and McNaught [21], the same injection moulding technology may bring wider opportunities in the plastics market for items such as computer, audio and television casings. NFCs can also be very cost effective materials for applications in building and construction (e.g. walls, ceiling, partition, window and door frames), storage devices (e.g. bio-gas containers, post boxes), furniture (chairs, stools, tables), electronic devices (outer casing of mobile phones), automobile and railway coach interior parts (inner fenders and bumpers), toys and other miscellaneous applications (helmets, suitcases).

1.5 Objective of the Study

The principal reasons for using natural fibres are their economical feasibility, enhanced sustainability and good specific mechanical properties. The advantage of using long fibres is in their ability to make composites of high mechanical properties while short fibres (e.g. wood fibre), are very difficult to make composites with comparable mechanical properties. The objective of the current work is to produce hemp/epoxy composites (HECs) and hemp/PLA composites (HPCs) of high quality for potential use in elaborate engineering applications. In this study, hemp fibre will be used to reinforce two matrix systems, epoxy and PLA. In order to remove lignin, hemicelluloses and pectin from the fibre surface to improve long term stability of the composites, alkali treatment of the fibres will be carried out in the production of both HECs and HPCs. As fibre surface treatment plays an important role in the composites performance, the hemp fibre surface will also be treated with acetic anhydride and organosilane for the production of HECs.

The principal objective of this thesis is to assess the viability of several processing techniques to produce HECs and HPCs. Based on the critical literature review, the study has been broken down into the following objectives:

(1) Treatment of the fibres with alkali and derivation of an empirical model by fractional factorial design for the TS of alkali treated fibre, and characterisation of the fibre surface treatments (alkali, acetic anhydride and organosilane) by TS of single fibre, wide angle X-ray diffraction (WAXRD), Fourier transform infrared (FTIR), scanning electron microscopy (SEM), thermogravimetric/differential thermal analysis (TGA/DTA), and zeta potential.

(2) Investigation of the influence of alkali fibre treatment on the interfacial shear strength (IFSS) of HECs and HPCs, and an assessment of the cure kinetics and variation of the epoxy to curing agent ratio on the IFSS of HECs.

(3) The use of different methods for the production of HECs and HPCs and the investigation of mechanical, thermal, morphological, and physical properties of the produced composites.

(4) Determination of the influence of the fibre surface treatment on the end use properties (accelerated ageing and water absorption behaviour) of the HECs and HPCs.

1.6 Thesis Organisation

This thesis contains seven chapters. An introduction to investigate the rationale of the present study (influence of fibre processing and treatments on hemp fibre/epoxy and hemp fibre/PLA composites) and its objectives are described in Chapter 1. A comprehensive literature review related to the present work is included in Chapter 2. Details of the relevant test methods, experimental procedures, results and discussion, and conclusions are incorporated within individual chapters from Chapter 3 to 5. Chapter 3 deals with industrial hemp fibre treatment and characterisation. Chapter 4 covers the influence of fibre treatment and processing on industrial hemp fibre/epoxy composites. Chapter 5 shows the influence of fibre treatment and processing on hemp fibre/PLA composites. Chapter 6 provides a conclusion of the results described in Chapter 3 to 5. Finally, Chapter 7 includes some recommendations and future work based on the current study.

Chapter Two

Literature Review

2.1 Summary

This chapter describes

- the source and classification of natural fibres, and a comparison of cellulose fibres
- the properties of industrial hemp fibre and its constituents
- the nature of matrix, its types and role in composites
- the major factors affecting the performance of composites
- the fibre treatments and characterisations to modify fibre/matrix interface as it plays an important role in the mechanical properties of the composites
- the cure kinetics of hemp/epoxy composites, the interfacial shear strength (IFSS) of the composites, the strength predictions of the composites, and the processing methods of the composites
- the degradation behaviour of composites (by hygrothermal and accelerated ageing) mentioning some previous work in these fields.

2.2 Natural Fibres: Source and Classification

Natural fibres can be sourced from plants, animals and minerals. An overview of natural fibres is presented in Figure 2.1 [22]. Generally, plant or vegetable fibres are used to reinforce polymer matrices and a classification of vegetable fibres is

given in Figure 2.2 [23]. Plant fibres are a renewable resource and have the ability to be recycled. The plant fibres leave little residue if they are burned for disposal, returning less carbon dioxide (CO_2) to the atmosphere than is removed during the plant's growth.

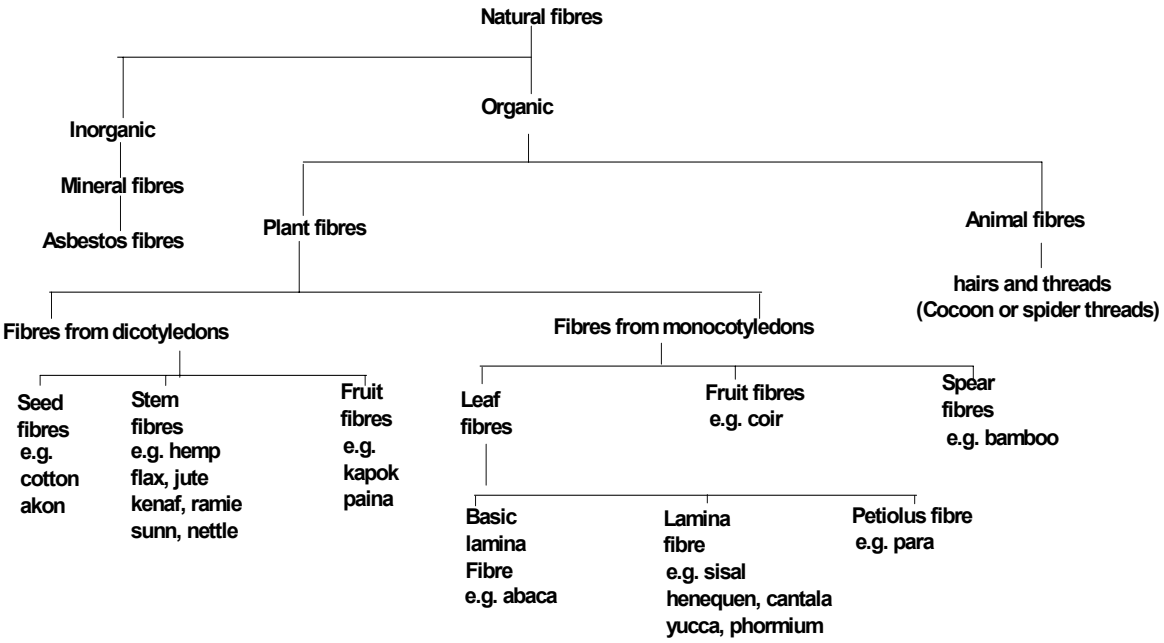

Figure 2.1 Overview of natural fibres.

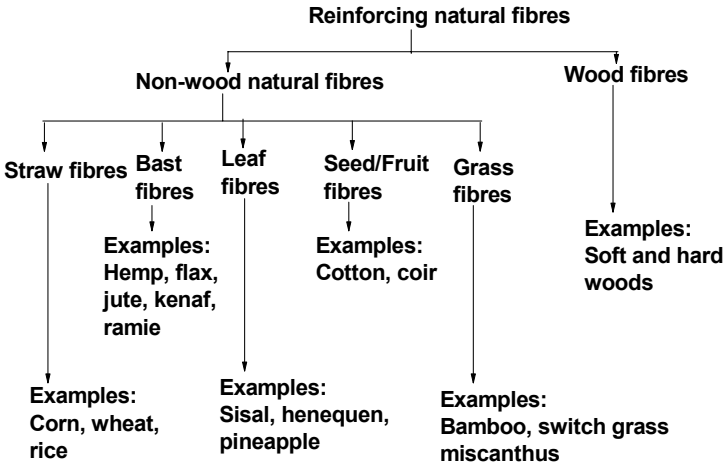

Figure 2.2 Classification of natural fibre that can be used as reinforcements in polymers.

The leading driver for substituting natural fibres for glass is that they can be grown with lower cost than glass. The price of glass fibre is around US $1.96 per

kg and has a density of 2.5 g/cc. On the other hand, natural fibre costs US $ 0.2-0.5 per kg and has a density of 1.2-1.5 g/cc. As can be seen from Table 2.1 [22], the TS of natural fibres is substantially lower than that of glass fibres though the modulus is of the same order of magnitude. However, when the specific modulus of natural fibres (modulus per unit specific gravity) is considered, the natural fibres show values that are comparable to or even better than glass fibres. Material cost savings, due to the use of natural fibres and high fibre filling levels, coupled with the advantage of being non-abrasive to the mixing and moulding equipment make natural fibres an exciting prospect. These benefits mean natural fibres could be used in many applications, including building, automotive, household appliances, and other applications.

Table 2.1 Properties of glass and natural fibres.

Properties	Fibre						
	E-glass fibre	Hemp	Flax	Jute	Sisal	Coir	Ramie
Density, g/cc	2.55	1.48	1.4	1.46	1.33	1.25	1.5
TS, MPa	2400	550-900	800-1500	400-800	600-700	220	500
YM, GPa	73	70	60-80	10-30	38	6	44
Specific modulus	29	47	26-46	7-21	29	5	2
FS (%)	3	1.6	1.2-1.6	1.8	2-3	15-25	2
Moisture absorption (%)	-	8	7	12	11	10	12-17

2.3 Comparison of Cellulose Fibres

Chemical composition, surface characteristics, structural defects, strength, stiffness, and costs are some of the important parameters in selecting natural cellulose fibres for use in polymer composites. The prices of natural fibres fluctuates considerably depending on a number of factors like supply, demand, quality, and exchange rate [23]. Table 2.2 [24] shows a comparison of prices for commonly used fibres.

Table 2.2 The prices of some fibres.

Fibre	Price (USD/kg)
Jute	0.4-0.7
Hemp	0.5-1.5
Flax	0.4-0.8
Sisal	0.6-1.0
Wood	0.2-0.4
Glass	1.5-2.5
Carbon	10-100

Wood is the most abundantly used natural cellulose fibre because of its extensive use in pulp and paper industries. However, for better strength and stiffness cellulose fibres like hemp, flax, jute, kenaf and sisal are becoming increasingly important in composites production. Commercially available cellulose fibres and their sources are listed in Table 2.3 [25].

Table 2.3 Commercially available fibre sources and their production.

Fibre source	Species	World production (10^3 tonnes)	Origin
Wood	(>10,000 species)	1,750,000	Stem
Bamboo	(>1250 species)	10,000	Stem
Cotton lint	Gossypium sp.	18,450	Fruit
Jute	Corchorus sp.	2,300	Stem
Kenaf	Hibiscas cannabinus	830	Stem
Flax	Linum usitatissimum	830	Stem
Sisal	Agave sislana	378	Leaf
Roselle	Hibiscus sabdariffa	250	Stem
Hemp	Cannabis sativa	214	Stem
Coir	Cocos nucifera	100	Fruit
Ramie	Boehmeria nivea	100	Stem
Abaca	Musa textilis	70	Leaf
Sunn hemp	Crotolaria juncea L.	70	Stem

Hemp, flax, jute and kenaf are called bast fibres, as they develop in the inner bark (phloem) of the stem of dicotyledonous plants. Some physical characteristics of bast fibres are given in Table 2.4 [22].

Table 2.4 Physical characteristics of bast fibres.

Fibre	Length of textile fibre (mm)	Length of ultimate fibre (mm)	Diameter (μm)	Weight per length	Density (g/cc)
Hemp	1000-3000	5-55	16-50	3.20	1.4
Flax	300-900	13-60	12-30	1.7-17.8	1.4
Jute	150-360	0.8-6	5-25	13.27	1.4
Sisal	600-1000	0.8-8	100-400	9-400	1.2-1.45
Ramie	1500	40-250	16-125	4.6-6.4	1.4
Kenaf	900-1800	1.5-11	14-33	50	-

Hemp, flax, and jute have similar morphologies and can have similar functions in composite materials. Cellulose, hemicelluloses, and lignin are the basic components of natural fibres and govern the physical properties of fibres. Gassan and Bledzki [24] reported that cellulose, lignin, hemicelluloses, and pectin cell walls differ in their composition and structure depending on the climatic conditions and age. The chemical composition of some cellulose fibres are given in Table 2.5 [22].

Table 2.5 Percentage chemical composition of cellulose fibres.

Fibre	Cellulos-e	Hemicellul-oses	Lignin	Pectin	Water solubles	Fat and wax	Moistu-re
Hemp	67.00	16.10	3.30	0.80	2.10	0.70	10.00
Flax	64.10	16.70	2.00	1.80	3.90	1.50	10.00
Jute	64.40	12.00	11.90	0.20	1.10	0.50	10.00
Sisal	65.80	12.00	9.90	0.80	1.20	0.30	10.00
Ramie	68.60	13.10	0.60	1.90	5.50	0.30	10.00
Sunn	67.80	16.60	3.50	0.30	1.40	0.40	10.00
Abaca	63.20	19.60	5.10	0.50	1.40	0.20	10.00

The chemical constituent of plant fibres is important, since it can affect their ultimate utilisation. Robson [25] reported that the chemical constituents of plant fibres have specialised functions in the cell wall. Cellulosic microfibrils form crystalline regions and impart enormous strength and stiffness, cellulose and hemicelluloses form semi-crystalline and amorphous regions which provide necessary flexibility while the amorphous regions of lignin give rigidity and a degree of hydrophobia [22].

2.4 Industrial Hemp Fibre

Industrial hemp (cannabis sativa L.) is one of the oldest crops known to humans, and there is evidence of its use by ancient and modern civilizations. Many hemp fibre products (dating back to around 600-800 BC) have been discovered—commonly in the forms of rope, canvas and cordage. The earliest discovered article was a 10,000 year old piece of hemp fabric found in Taiwan [26]. Due to the similar leaf shape, hemp is frequently confused with marijuana. Although both plants are from the same species, cannabis, industrial hemp can be grown with little or none of the psychoactive properties of marijuana by utilizing low-THC (delta-9-tetrahydrocannabinol) varieties.

Hemp is a bast fibre plant similar to flax, kenaf, jute and ramie. Long slender primary fibres on the outer portion of the stalk characterise bast fibre plants. The primary hemp fibre is attached to the core fibre by pectin—a glue-like soluble gelatinous carbohydrate. This fibre can be used for production of composites—ropes, textiles specialty pulp and paper. The fibre from the wood-like core can be used for animal bedding, garden mulch, fuel and an assortment of building materials. The seed contains between 25-35% oil by weight, which is rich in essential fatty acids considered to be necessary to maintain health [27] and cannabinoids for medical, spiritual and recreational purposes.

The commercial production of hemp originated in Central Asia [28] but has been cultivated from the Equator to the polar circle [29]. Chinese writings state that the emperor Shen Nung first taught the people of China to cultivate hemp and produce cloth around 2,800 BC. They are the earliest known civilization to use hemp (in the Sung dynasty around 500 AD). The Spaniards brought hemp to the Western Hemisphere in 1545. In 1645 it was introduced to the USA by the Puritans in New England as a fibre source for household spinning and weaving. At the end of the 18th century, Australia and New Zealand were considered as ideal places by England to grow hemp, reducing their dependency on Russian hemp.

The start of hemp's decline was in the early 1800s when cheaper alternative fibres such as jute and sisal became more readily available from India, Bangladesh and China. Hemp's popularity was also affected by technological breakthroughs in the late 1800s such as the cotton gin. Around this time, methods for creating paper from trees allowed new products that were cheaper or more desirable than hemp to be produced [30]. The rise of the petrochemical industries at the start of the 20th century brought further competition while the final nail in hemp's coffin came in 1937 when the United States Government's Marijuana Tax Act was introduced. The act required the registration and licensing of all hemp growers with the federal government in an effort to restrict production of marijuana. Many other countries followed the USA's lead and made hemp production and possession illegal. Production restrictions were slightly lifted to support the war effort from 1943-1945. However, it was not until 1992 that a number of countries

started officially passing legislation allowing restricted cultivation of low-THC industrial hemp.

Since 1961, industrial hemp cultivation has been illicit in New Zealand due to the introduction of the Misuse of Drugs Act. It was not until late 2001, that a new bill was passed to allow the cultivation of industrial hemp under licence with levels of no more than 0.3% THC. Where hemp has become legal again a dramatic increase in industrial hemp growth has occurred. Therefore, now is the right time for New Zealand to get the benefits from the rising popularity of hemp.

2.4.1 Plant and Bast Fibre Morphology

Industrial hemp is an annual plant and normally dioecious, meaning the species has separate male and female plants. A female hemp plant can be seen in Figure 2.3. However, monoecious varieties (male and female parts on the same plant) can also be grown through breeding and selection. Hemp is sensitive to day length and the plant matures as days get shorter. Its growing season is from the middle of April to the middle of September and it can be grown as a fibre, seed, or dual purpose crop.

Figure 2.3 Female hemp plant.

The cross-section of hemp is almost orbicular at the bottom and angular at the top. The stalk is generally 4-10 mm thick and 1.5-2.5 m high. The interior of the stalk is hollow, surrounded by woody cores called hurds, Figure 2.4. The hurd fibres are very thin walled, weak, brittle, and comparatively shorter than bast fibre and therefore are not considered for composite production. Outside the cambium layer where cells grow and differentiate is the phloem or parenchyma layer, which contains the valuable long cells known as bast fibre.

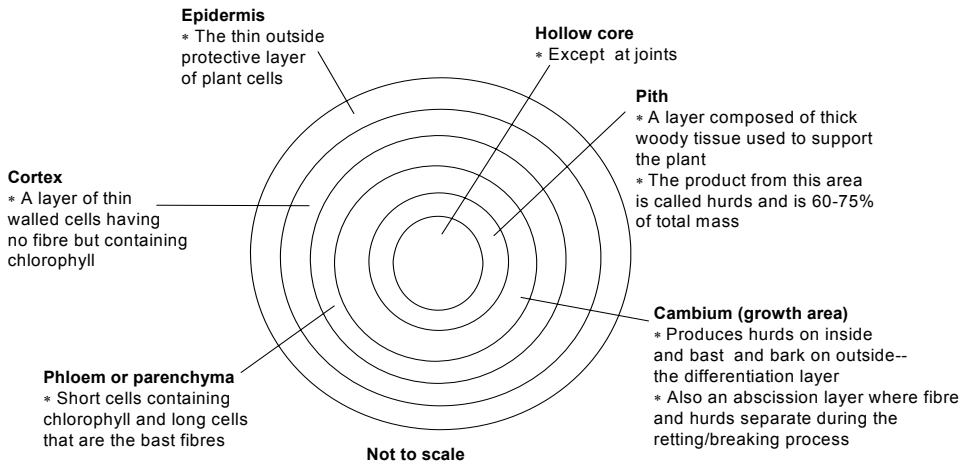

Figure 2.4 Cross section of a hemp stem.

Hemp seeds are smooth and about one-eighth to one-fourth of an inch long. The seeds usually contain from 29 to 34% oil. The oil is similar in composition to drying oils such as linseed and tung and consists primarily of three fatty acids: linoleic (54-60%), linolenic (15-20%), and oleic (11-13%). Both the fibre and seed can be used in a wide range of applications.

Industrial hemp can be grown in a variety of soils, but it does best in loose, well-drained loam soils with high fertility and abundant organic matter. Plants require plentiful moisture throughout the growing season, especially during the first 6 weeks [31]. Hemp also needs substantial amounts of nutrients to produce high yields.

Hemp diseases are not widespread and occur sporadically. They are usually caused by seed- and soil-borne fungi which can be controlled by seed treatment before planting or by rotation [31]. Under favourable conditions, hemp is very

competitive with weeds, so herbicides are generally unnecessary in hemp fibre production. The hemp fibres can be considered as composites as they consist of cellulose microfibrils wound in amorphous materials like lignin and hemicellulose. The primary cell of the fibre cell wall is located on the outside of the fibre and is relatively thin consisting of pectin, lignin and cellulose. The secondary cell wall is composed of two or three layers that make up most of the fibre diameter, and consists of highly crystalline cellulose microfibrils and amorphous celluloses [32]. The technical fibre is simply a smaller part of a bast fibre bundle. The elementary fibre, also called ultimate or single fibre, is one cell of the bast fibres. The principle of the different levels of fibres in the plant is described in Figure 2.5 [15].

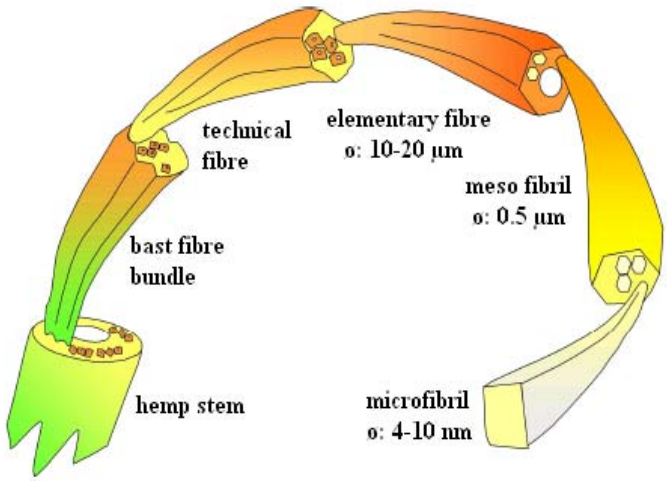

Figure 2.5 Composition of hemp stem.

2.4.2 Factors Affecting Fibre Mechanical Properties

Several structural aspects like crystallinity and amorphousness, orientation of molecular chains, and imperfections (e.g. pits and nodes) affect the mechanical strength of hemp fibres like other natural fibres. The variation in chemical composition and structural imperfections develops in hemp fibres due to growth conditions and harvest procedures. Therefore, a large variation in mechanical strength occurs in fibres and differs between different parts of a plant as well as from one plant to another.

There are other factors that may also affect the fibre properties including, maturity of the plants, fibre separation process, type of soil and the climate under which they were grown. The crystalline structure of cellulose makes the fibres stiff and strong in tension but also susceptible to kink band formation under compressive loading which significantly reduces fibre strength [33].

2.4.3 Growing Conditions

Hemp is a high yield commercial fibre crop that flourishes in areas with moderately cool climates. It can be grown on a wide range of soils, but tends to grow best on soil that is well drained, high in organic matter and non-acidic. The plants are distinctly male or female and they generally flower between June and October. Hemp requires limited pesticides as it grows quickly, attracting few pests. Hemp's extensive root system is very beneficial, as it is effective in preventing erosion, aiding in the removal of toxins and improving the soil structure by aerating the soil for future crops. Another remarkable environmental benefit of growing hemp is that it consumes carbon dioxide and it is an ideal rotation crop. Hemp grows successfully at a density of up to 150 plants per square meter and reaches a height of between two and five meters in a three-month growing season.

2.4.4 Harvesting

Hemp crops are harvested at different times; for example, harvesting stalks for high quality primary fibre occurs as soon as the crop flowers, and harvesting for seed production and stalks occur 4–6 weeks after flowering, when male plants begin to shed their pollen [34]. Harvesting hemp for paper pulp and textiles occurs as the female plant is in flower and before seed formation, utilising specialised cutting equipment.

The moisture content at the time of harvest is about 54%. For storage of dry hemp, the moisture content must be less than 15% to avoid fibre decay by micro-organisms. The crop is cut, and then the stalks are allowed to rett in the field to loosen the fibres. During this process, most of the nutrients extracted by the plant

are returned to the soil as the leaves decompose. The stalks are turned and then baled with hay harvesting equipment.

Hemp grown for fibre is harvested at early to mid flowering stage using specialised equipment. Hepworth *et al.* [35] reported that early harvesting of hemp is beneficial, resulting in stiffer composites. This is because of the fibre bundles in the tissue which are stuck to the epidermis and these tissue strips result in a single large fibre. If hemp is harvested late in the season for bast fibre production, drying conditions are often poor, with subsequent loss of fibre yield and quality in the drying swath.

2.5 Hemp Fibre Constituents

The constituents of hemp fibre vary with origin, area of production, variety, and maturity of the plant. The major constituents of fully developed hemp fibre cell walls are cellulose, hemicelluloses, lignin, and pectin. The pectins occur in most mature plant cell walls with the exception of hurd fibres, wherein extensive secondary cell wall thickening replaces almost all of the pectin with lignin.

2.5.1 Cellulose

The long thin crystalline microfibrils in the secondary cell wall are made of cellulose. It is the reinforcing material and is responsible for the high mechanical strength of fibres. It consists of a linear polymer of D-anhydroglucose units where two adjacent glucose units are linked together by β-1,4-glycosidic linkages with elimination of one water molecule between their -OH groups at carbon atoms 1 and 4. Chemically, cellulose is defined as a highly crystalline segment alternating with regions of non-crystalline or amorphous cellulose [32, 36].

The glucose monomers in cellulose form hydrogen bonds both within its own chain (intramolecular) forming fibrils and with neighbouring chains (intermolecular), forming microfibrils. These hydrogen bonds lead to formation of a linear crystalline structure with high rigidity and strength. The amorphous cellulose regions have a lower frequency of intermolecular hydrogen bonding, thus exposing reactive intermolecular -OH groups to be bonded with water

molecules. Amorphous cellulose can therefore be considered as hydrophilic in nature due to their tendency to bond with water. On the other hand, very few accessible intermolecular –OH are available in crystalline cellulose and it is far less hydrophilic than amorphous cellulose. Crystalline microfibrils have tightly packed cellulose chains within the fibrils, with accessible –OH groups present on the surface of the structure. Only very strong acids and alkalis can penetrate and modify the crystalline lattice of cellulose.

2.5.2 Hemicelluloses

Hemicelluloses in hemp fibres are polysaccharides (excluding pectin) bonded together in relatively short and highly branched chains. Hemicelluloses differ from cellulose in three different ways. Firstly, unlike cellulose (containing only 1,4-β-D-glucopyranose units) they contain several different sugar units. Secondly, they exhibit a considerable degree of chain branching, whereas cellulose is a linear polymer. Thirdly, the degree of polymerization of native cellulose is ten to hundred times higher than that of hemicelluloses. Unlike cellulose, the constituents of hemicelluloses differ from plant to plant. Hemicelluloses contain substituents like acetyl (-$COCH_3$) groups and glucoronic acid. By attaching ferulic acid and p-coumaric residues, hemicelluloses can form covalent bonds to lignin [37]. Due to this linking ability of hemicelluloses, degradation of it leads to disintegration of the fibres into cellulose microfibrils resulting in lower fibre bundle strength [38].

Mainly the acid residues attached to hemicelluloses make it highly hydrophilic and increase the fibres' water uptake, which increases the risk of microbiological fibre degradation. It has been found that hemicelluloses thermally degrade more at lower temperatures (150-180°C) than cellulose (200-230°C) [39].

2.5.3 Lignin

Together with cellulose, lignin is the most abundant and important polymeric organic substance in the plant world. Lignin increases the compression strength of plant fibres by gluing the fibres together to form a stiff structure, making it possible for trees of 100 meters to remain upright. Lignin is essentially a

disordered, polyaromatic, and cross-linked polymer arising from the free radical polymerisation of two or three monomers structurally related to phenylpropane [40]. Free radical coupling of the lignin monomers gives rise to a very condensed, reticulated, and cross-linked structure. The lignin matrix is therefore analogous to a thermoset polymer in conventional polymer terminology. The dissolution of lignin using chemicals aids fibre separation. When exposed to ultraviolet light, lignin undergoes photochemical degradation [41]. Since hemp belongs to the angiosperm phylum, it contains hardwood lignin of coniferyl alcohol, sinapyl alcohol and a minor content of p-coumaryl alcohol [32]. It was shown by treatment of hemp with P. radiata Cel that degradation of lignin and pectin (presumably) reduces the fibre bundle TS slightly [32]. Therefore lignin seems to act like a matrix material within the fibres, making stress transfer on a micro-fibril scale and single fibre scale possible.

2.5.4 Pectin

Pectin is a complex branched structure of acidic structural polysaccharides, found in fruits and bast fibres. The majority of the structure consists of homopolymeric partially methylated poly-α-(1-4)-D-galacturonic acid residues, but there are substantial 'hairy' non-gelling areas of alternating α-(1-2)-L-rhamnosyl-α-(1-4)-D-galacturonosyl sections containing branch-points with mostly neutral side chains (1-20 residues) of mainly L-arabinose and D-galactose (rhamnogalacturonan I). Pectin is the most hydrophilic compound in plant fibres due to the carboxylic acid groups and is easily degraded by defibration with fungi [32]. Tests on hemp fibres (single fibres as well as fibre bundles) show that treatment with pectinase enzymes can result in pectin degradation which might lead to a slight reduction in fibre strength [32]. Pectin along with lignin and hemicelluloses present in natural fibres can be hydrolysed at elevated temperatures.

2.6 Matrix

The matrix plays an important role in the performance of fibre reinforced polymer composites. Both thermosets and thermoplastics (including bio-derived ones) are attractive as matrix materials in the production of composites.

2.6.1 Thermosets

Much of the early work used thermosetting resins as matrix material for composite production. Products like tufnol which is made from cotton fibres and epoxy resin, have been available for some time, having good stiffness and strength [25]. In the last few years there has been renewed interest in these products for use in automotive applications [42]. To achieve reinforcing effects in composites it is necessary to have good adhesion between the fibres and resins. Epoxy and phenolic thermosetting resins are known to be able to form covalent cross-links with plant cell walls via -OH groups [8]. Composite manufacture can be achieved using low viscosity epoxy and phenolic resins that cure at room temperature. In addition epoxy resin does not produce volatile products during curing which is most desirable in production of void free composites. Therefore, although epoxy resins are relatively more expensive than polyester, they have potential for the development of high added value plant fibre composites, where long fibres at a high content are required.

The functional group in epoxy resins is called the oxirane, a three-membered strained ring containing oxygen. Epoxy resins, depending on their backbone structure, may be low or high viscosity liquids or solids. In low viscosity resin, it is possible to achieve a good wetting of fibres by the resin without using high temperature or pressure. The impregnation of fibres with high viscosity resins is done by using high temperature and pressure.

A wide range of starting materials can be used for the preparation of epoxy resins thereby providing a variety of resins with controllable high performance characteristics. These resins generally are prepared by reacting to a polyfunctional amine or phenol with epichlorohydrin in the presence of a strong base. The commerically available diglycidyl ether of bisphenol-A (DGEBA), Figure 2.6, is characterised by epoxy equivalent weight, which can be determined either by titration or quantitative infrared spectroscopy. The presence of glycidyl units in these resins enhances the processability but reduces thermal resistance.

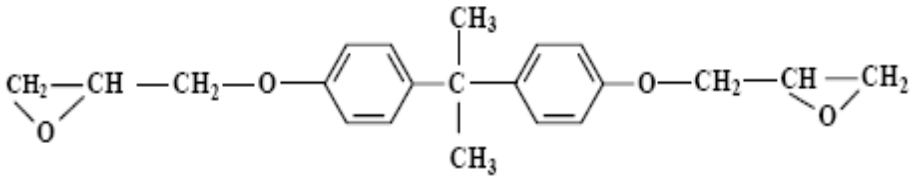

Figure 2.6 Chemical structure of DGEBA.

The most widely used curing agents for epoxy resins are primary and secondary amines. The overall reaction rate of an amine with an epoxide is influenced by the steric hindrance and the electron withdrawing or electron donating groups present in the amine [43].

During curing, epoxy resins can undergo three basic reactions.

1. Epoxy groups are rearranged and form direct linkages between themselves.

2. Aromatic and aliphatic -OHs link up to the epoxy groups.

3. Cross-linking takes place with the curing agent through various radical groups.

The advantages of epoxy resins are low polymerisation shrinkages unlike polyesters during cure, good mechanical strength, excellent resistance to chemicals and solvents, and excellent adhesion to fibres. The epoxy molecule also contains two ring groups at its centre, which are able to absorb both mechanical and thermal stresses better than linear groups, giving epoxy resin very good stiffness, toughness and heat resistance.

The primary disadvantages of the epoxy resins are that they require long curing times and, in general, their mould release characteristics are poor. The epoxy resins are characterised by their high adhesive strengths. This property is attributed to the polarity of aliphatic -OH groups and ether groups that exist in both the initial resin and cured system. The polarity associated with these groups promotes electromagnetic bonding forces between epoxy molecules and the polar fibres.

2.6.2 Bio-derived Thermoplastic Matrices

Cellulose fibres (e.g. hemp, flax, jute) are widely used with conventional thermoplastic polymers (e.g. PP, PE) as reinforcement in composite production to improve mechanical properties. In fact, the history of composites from renewable resources is far longer than conventional polymers. The study and utilization of natural polymers is an ancient science. Typical examples, such as paper, silk, skin, and bone arts, can easily be found in museum around the world. In the biblical Book of Exodus, Moses's mother built the ark from rushes, pitch and slime- a kind of fibre reinforced composite, according to the current classification of material. During the opium war more than 1000 years ago, the Chinese built their castles to defend against invaders using a kind of mineral particle reinforced composite made from gluten rice, sugar, calcium carbonate and sand [44].

However, the availability of petroleum at a lower cost and the bio-chemical inertness of petroleum based products have proven disastrous for the market of natural polymers. It is only about last two decades when the significance of eco-friendly materials has been realized. Now polymers from renewable resources have started drawing an increasing amount of attention. The two main reasons for that are environmental concerns [45], and the realization that the petroleum resources are limited.

Generally, polymers from renewable resources can be classified into three groups: (1) natural polymers such as starch, protein, and cellulose (2) synthetic polymers from natural monomers, such as PLA and (3) polymers from microbial fermentation, such as polyhydroxy butyrate (PHB). Like numerous other petroleum based polymers, many properties of polymers from renewable resources can be improved through composite production [44].

The development of synthetic polymers like PLA using monomers from natural resources has been a driving force for the development of biodegradable polymers from renewable resources. Therefore, in today's world PLA is the most promising among bio-derivable polymers [44]. PLA can be processed (e.g. compression moulding, pultrusion, extrusion and injection moulding) like petroleum based polyolefins and its mechanical property is better than the widely used polymer PP

[46]. On degradation PLA does not emit any carbon dioxide to the environment like other biodegradable materials from renewable resources. The degradation occurs by hydrolysis to lactic acid, which is metabolized by micro-organisms to water and carbon dioxide. If PLA is comprised together with other biomass, the biodegradation occurs within a couple of weeks and the material can fully disappear within a month [47]. Chemically, it is a linear aliphatic polyester of lactic acid which can be obtained by fermentation of renewable agricultural materials like corn, sugarcane and sugar beets. Lactic acid is converted to a cyclic lactide dimer which is then polymerised to PLA through a ring opening reaction.

The major applications of PLA products are in household wastes as plastic bags, barriers for sanitary products and diapers, planting, and disposable cups and plates. However, a number of authors reported the possibilities of developing fully bio-degradable composite products by using biodegradable polymers as matrix and natural fibres as reinforcements [48, 49]. Keller *et al.* [50] reported that PLA should produce fibre reinforced composites with high mechanical properties for light weight construction materials. Oksman *et al.* [51] observed that PLA had good potential as a polymer matrix in flax fibre reinforcement for composites production. They reported that the composite strength produced with PLA/flax was about 50% better than that of PP/flax composites. Due to the increasing commercial interest for natural fibre reinforced polymer composites for use in automotive applications and building constructions as well as demands for environmentally friendly materials, the development of fully biodegradable composites for many applications could be an interesting area of research.

2.7 Natural Fibre Reinforced Polymer Composites

Natural fibre reinforced polymer composites are hybrid with their properties, with characteristics of both natural fibres and polymers. Incorporation of natural fibres into polymer is now a standard technology to improve the mechanical properties of polymers. Mechanical properties like TS and YM are enhanced in the end

products (composites) as the fibres in the composites determine the TS and YM of the materials [52].

2.7.1 Factors Affecting the Use of Natural Fibres in Composites

Natural fibres are very attractive reinforcement materials for composites, as they are readily available, renewable, cost effective, and have good specific properties. However, the processing and properties of composite materials depend on the properties and proportions of the matrix and the reinforcement as discussed below:

2.7.1.1 Wettability and Interfacial Bonding

Interfacial bonding largely depends on the adhesion between the reinforcement and the matrix. The adhesion plays an important role to transfer the stress from the matrix to the fibre and thus contributes towards the properties of the composites. Poor surface adhesion due to insufficient wetting is the principal reason for the formation of a weak or ineffective interface between the fibre and the matrix. Most thermoplastics (e.g. PP and PE) are generally non-polar (hydrophobic) in nature, which makes them incompatible with polar (hydrophilic) natural fibres and thus results in an inefficient fibre matrix bonding. On the other hand, thermosets like epoxy and phenolic are known to be able to form covalent cross-links with plant cell walls via -OH groups [8]. However, due to the presence of unstable non-cellulosic components like hemiclluloses and lignin, untreated natural fibre have performed well below their potential abilities. Therefore, to increase long term stability of the composites, surface treatment of untreated fibre is necessary. Sometimes, to improve the composite properties by increasing the utilisation of the mechanical properties of reinforcing fibres in the composites, bonding between fibres and matrix are improved by using various fibre and matrix treatments. When the fibre and matrix are brought into close contact, a number of different bonding mechanisms may occur (namely, mechanical interlocking, electrostatic bonding, chemical bonding, and reaction or interdiffusion bonding). It is noted that more than one bonding mechanism may be operative at the same

time for a given system and the bonding mechanism may change during the various production stage or during service [4].

2.7.1.2 Thermal Stability

Natural fibres have low thermal stability that results in the exclusion of some manufacturing processes, and also limits the use of the composites to low temperature applications. The low thermal stability increases the possibility of cellulosic degradation and possibility of emissions of volatile materials that could adversely affect the composite properties. Processing temperatures are thus limited to about 200^{o}C, although it is possible to use higher temperature for short periods of time. This apparently limits the type of thermoplastics that can be used with natural fibres [53].

2.7.1.3 Dispersion of the Fibre in the Matrix

The incorporation of natural fibres into polymeric matrices is often associated with poor dispersion of the fibres, due to the large differences in polarity as well as strong hydrogen bonds between adjacent molecules of the fibres. Good distribution of fibres within the matrix is necessary in order to obtain satisfactory properties of the composites. A good distribution implies that the fibres are fully separated from one another, and each fibre is fully surrounded by the matrix. Insufficient fibre dispersion can lead to clumping and agglomeration of the fibres, resulting in an inhomogeneous mixture of matrix-rich and fibre-rich areas. This segregation is undesirable as the matrix rich areas are weak while fibre rich areas are susceptible to microcracking. Micro cracks are responsible for inferior mechanical properties of composites. It is therefore, necessary for the composites to be homogeneous in fibre and matrix distribution to ensure good mechanical properties.

Strong intermolecular hydrogen bonding between fibres and the fibre length are the two main factors that affect the extent of fibre distribution and dispersion in a composite. To separate the fibres from their fibre bundles it is necessary to dissolve the pectins and lignins joining the individual fibres together. Fibre separation can easily be performed by digesting the fibre with strong alkali [54].

Fibre separation also occurs during compounding with the thermoplastic matrix. Several factors contribute to this fibre attrition, such as the shearing forces generated in the compounding equipment, residence time, temperature, and viscosity of the mix [53].

The use of a surface active agent such as stearic acid or pre-treating the fibre with acetic anhydride can also improve composite properties, as fibre clumping is not as severe a problem with treated fibres as it is with untreated fibre [55]. The length of the fibres used in the composites is a critical factor during processing by the compounding equipments where shear forces generated. Excess length leads to entanglements, resulting in clumping and reduction in composite strength. If the fibres are very short, the stress transfer area will be too small to effective reinforcement. As fibre lengths reduce during composites processing by shear, the compression moulding is generally recommended [56] as this is a process with the least amount of shear produced during processing. To produce efficient composites with well dispersed fibres, it is necessary to make careful selection of the initial fibre lengths, processing aids, techniques, and conditions.

2.7.1.4 Biodegradability

Natural fibres degrade easily when exposed to nature. Some methods for degradation include biological, chemical, mechanical, thermal, photochemical and aqueous. The biodegradability of natural fibre is often put forward as a positive advantage justifying the use of these fibres. However, for many outdoor applications it is necessary for the composites to be serviceable for several years. In order to increase their service life it is necessary to control this natural degradation. One way of preventing or slowing down the natural degradation process is by modifying the cell wall chemistry. Undesirable natural fibre properties such as dimensional instabilities, flammability, biodegradability, and chemical degradation can be eliminated or slowed down in this manner [57]. Chemical treatments can reduce the water uptake in the fibres, and can therefore reduce the amount of fibre swelling and biological degradation by blocking the available –OH group on the fibre surface [58]. It is reported in the literature that encasing in thermoplastic reduced water uptake [58].

2.7.1.5 Effect of Fibre Orientation

Natural fibre reinforced composites are made with random and oriented fibres. Composites made with oriented fibre in the test direction are generally stronger and stiffer than randomly oriented fibre. Both the failure strain (FS) and the maximum stress of fracture decrease with increasing angle of the fibre orientation axis with the test direction. The composite TS decreases by four times when the angle between the fibre orientation axis with the test direction increases by about 26^{o} while the composites YM decreases by only two times [39].

2.7.1.6 Influence of Humidity

Water on the fibre surface and on the matrix like PLA, can act like a separating agent between the fibre and matrix during the formation of the fibre/matrix interface. Therefore, fibre and matrix drying is necessary prior to processing. On top of that evaporation of the water during composites processing over $100^{o}C$ leads to the formation of voids, the most undesirable phenomenon of composite production. Thus, reduces the mechanical properties of composites. Gassan *et al.* [59] reported an increase of TS of 10% and YM of 20% for jute/epoxy composites when they dried the fibre to minimise the humidity content of jute fibre from 10 to 1 prior to the composites processing. The hydrophilic fibres also absorb moisture during the service life of composites. Moisture absorption leads to fibre swelling which causes micro-cracking of the composites, resulting in degradation of mechanical properties. Joseph *et al.* [7] showed that moisture absorption of NFCs can be reduced significantly by improving the interfacial bonding through chemical treatment of the fibres and/or matrices.

2.7.1.7 Fibre Aspect Ratio

The fibre length to diameter ratio or fibre aspect ratio, is a critical parameter in a composite material. For each short fibre composite system, there is a critical fibre aspect ratio, which may be defined as the minimum fibre aspect ratio in which the maximum allowable fibre stress can be achieved for a given load [60]. Along with the fibre and matrix properties, the critical fibre length also depends on the quality of the fibre/matrix interface. To attain maximum reinforcement, the fibre aspect

ratio of any composite system should be above its critical value to ensure maximum stress transfer to the fibres before the composite fails. If the fibre aspect ratio is lower than its critical value, insufficient stress will be transferred and reinforcement of the fibre will be insufficient (i.e. the fibres are not loaded to their maximum stress values) [60]. By contrast, if the fibre aspect ratio is too high, the fibres may get entangled during mixing resulting in poor fibre dispersion. An aspect ratio in the range of 100-200 after composite processing is recommended for high performance short fibre composites [60].

2.7.1.8 Fibre Volume Fraction

The mechanical properties of composites are strongly influenced by the content of the reinforcing fibre. Composites properties change with variations in fibre content, particularly TS and YM can be predicted using failure prediction models such as the "modified rule of mixtures (MROM)".

$$M_c = V_m M_m^* + V_f M_f K_1 K_2 \tag{2.1}$$

where, M_c is the TS or YM of the composite, M_f is the TS or YM of the fibre, V_m is the volume fraction of the matrix, V_f is the volume fraction of the fibre, K_1 is the orientation factor, K_2 is a factor dependent on the stress transfer between the matrix and the fibres, and M_m^* is the tensile contribution of the polymer matrix at the FS of the fibres or the YM of the polymer matrix. The mechanical properties of short fibre composites are more difficult to predict than continuous fibre composites. This is due to the complexity of determining parameters such as fibre dispersion, orientation and geometry of the fibres within the composites, fibre and matrix volume fractions, and the IFSS between the fibre and the matrix [36].

At low fibre volume fractions, a decrease in TS is usually observed. This is due to the introduction of flaws created by the fibre ends. These flaws act as stress risers, and cause the bonds between the fibre and matrix to break. At higher volume fractions, the matrix is sufficiently restrained and the stress is more evenly

distributed. This results in the reinforcing effect outweighing the effects of the stress concentrations [58].

As the fibre volume fraction is further increased, the tensile properties gradually increase until they surpass those of the matrix. The corresponding fibre volume fraction at which the strength properties of the composite cease to decline and start to increase is known as the critical fibre volume fraction. At high fibre volume fractions, the TS of the composites start to decrease due to insufficient filling of the matrix material. Nishino *et al.* [61] produced a kenaf/poly-L-lactic acid composite, and found that strength increases linearly with an increase of fibre volume fraction of up to about 70 vol%, after which there was a reduction in strength. Fu *et al.* [62] reported another explanation for the decrease in composite mechanical properties at high volume fractions. During extrusion and injection moulding of short fibre reinforced polymers, fibre damage takes place as a result of fibre polymer interaction, and fibre contact with the surface of the processing equipment. At high volume fractions, there is an increase in fibre-fibre interaction and fibre equipment contact, resulting in reduction of fibre length and fibre efficiency. High fibre contents therefore lead to reduction in the mean fibre length, and if the mean fibre length is very different than the critical fibre length, the reinforcement efficiency is reduced.

2.8 Chemical Treatment of Fibres

2.8.1 Alkali Treatment of the Fibres

2.8.1.1 Empirical Model for the Tensile Strength (TS) of Alkali Treated Fibre by Partial Factorial Design

Experimental design deals with conducting a series of tests in which changes are made purposefully to input variables (factors) of a process in order to observe the corresponding changes of the outputs (responses). The process is defined as some combination of equipment, materials, methods, and some other resources which when used together transforms inputs into outputs. Thus, experimental design is a scientific approach which enables the researcher a better understanding of a

process, and to determine which input variables are most influential on the outputs and where to set those influential input variables so that the outputs can be optimized. Though the concept of experimental design has been used for a long time in science, industry only started using around 1940 [63]. In recent years, however, due to its great success in Japan, this method has gained great popularity [63].

In the treatment of fibres, a number of factors could affect the fibre strength. A large number of experiments are necessary to optimise the parameters. The experimental design could be an effective tool in optimising the parameters of fibre treatment processes.

The major constituent of natural fibre is crystalline cellulose. It also contains hemicelluloses, lignin and waxy substances [64]. However, lignin and hemicelluloses can degrade over time [65]. Therefore, to increase the long-term stability of NFCs and to improve interfacial bonding, researchers have attempted various surface treatments. These include alkali treatment [66-69], anhydride modification [70], organosilane treatment [71], and the use of various coupling agents [72, 73] of which, alkali treatment has been found to be the most feasible [74]. Meanwhile, several researchers have reported improvement in properties of natural fibres at different alkali concentration, and digestion time and temperature.

Bledzki *et al.* [75] applied a NaOH concentration of 22% at temperatures 4, 10, and 20^{o}C on hemp fibre and a NaOH concentration of 29% on flax fibres while Wang and Postle [76] applied 1.9% NaOH solution with Na_2SO_3 and Na_2CO_3 at two different temperature (95 and 120^{o}C) with a digestion time of 45 and 50 minutes to remove surface impurities from Australian hemp fibres. Geethamma *et al.* [77] used a 5% NaOH solution to remove surface impurities from oil palm and short coir fibres. Alkali treatment of fibres has also been seen to increase the percentage crystallinity [65] and molecular alignment of cellulose and thus has the potential to improve fibre strength by removing amorphous noncellulosic substances.

From the available literature, it was observed that different researchers used combinations of different concentrations of NaOH, digestion time, and

temperature to treat natural fibres. Moreover, sodium sulfite (Na_2SO_3) is also used with alkali during the production of pulp to soften the lignin in pulp and paper industry [78]. Thus, the fibre treatment method can be presented as shown in Figure 2.7:

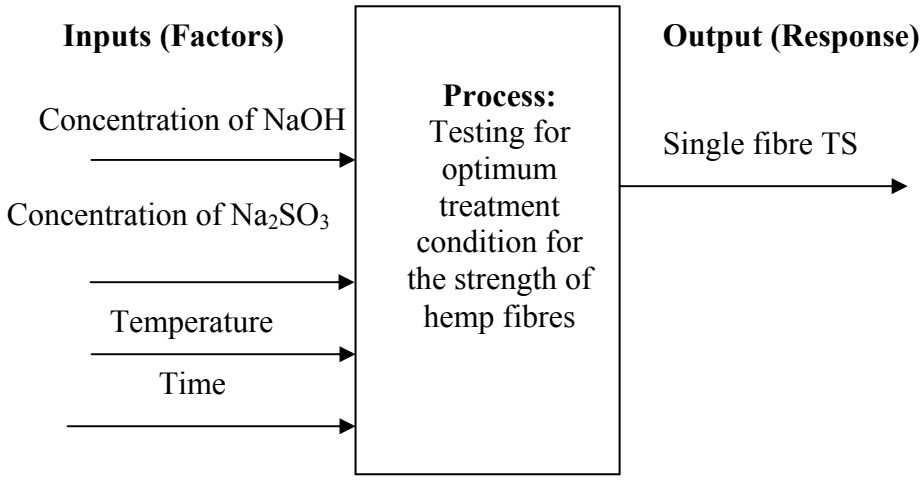

Figure 2.7 Testing for optimum treatment condition for the TS of hemp fibres.

It is clear from Figure 2.7 that an extensive study is necessary to develop an optimum alkali fibre treatment method. The present study aims at performing an experimental design to obtain an optimum fibre treatment and to derive a regression equation to predict the fibre strength.

2.8.1.2 Selection of the Levels of Treatment Factors

Four variables (concentration of NaOH, concentration of Na_2SO_3, time and temperature) were selected for treatment of the Retted UK hemp (untreated) fibre by using a statistically designed experiment. The purpose of conducting this designed experiment was to determine which of the four factors (concentration of NaOH, concentration of Na_2SO_3, time and temperature) are influential in optimizing fibre strength.

To study four factors, each at four levels, a full factorial design would consist of $4^4 = 256$ runs. The obvious disadvantage of this design is the cost, time, and resources needed. In order to reduce the number of runs necessary, a fractional factorial design was conducted. Each of the four variables was investigated at two

levels to observe if the fibre strength changed as the independent variable moved from one level to another. Since only a straight line can be fitted through two points, it would only be possible to estimate the linear effect of each variable with a two-level experiment. To use more than two levels for each variable would require too many runs and hence very time consuming.

The selection of the two levels to be used for each variable is very important. When the levels are too close, the change in fibre strength might be found so small that it might remain undetected in the experiment. When the levels are too far, the estimated change in the fibre strength might again be negligible, if the levels are located on either side of a maximum or minimum [79].

In the present work, regions of experiments were identified (from physical intuition) which would lead to useless results such as combinations of low concentrations of alkali with low temperatures and short digestion times (e.g. 5 wt% NaOH at 30^{o}C for 30 min) which would insufficiently digest non-cellulose components as well as concentrations of high alkali with high temperatures and long digestion times (e.g. 20 wt% NaOH at 180^{o}C for 360 min) which would damage the fibre.

Alkali fibre treatments using NaOH improve adhesion characteristics of natural fibres by removing lignin, pectin, and hemicelluloses; which then provide the fibre surface with a rough texture, the rough and clean fibre surface facilitates mechanical interlocking and improves wetting ability with the matrix [80]. NaOH also assists separation of the elementary fibre as well as exposure of active OH groups for hydrogen and covalent bonding with the matrix [81]. The Bledzki *et al.* [75] investigated the influence of alkali treatment of hemp fibres on the properties of unidirectional epoxy resin model composites and reported an increase in flexural modulus of up to about 100% and flexural strength of up to about 50% for unidirectional hemp-epoxy composites. Gassan and Bledzki [68] reported that treating the fibre surface with 26 wt% NaOH for 20 minutes at 20°C improves the mechanical properties of unidirectional jute/epoxy composite up to 60% when compared to untreated fibre composite, at a fibre content of 40 vol%. Prasad *et al.* [69] studied the alkali treatment of coir fibre with 5 wt% NaOH for 72-96 hours at

28°C. The alkali treatment of the coir fibre improved the flexural strength of the polyester resin composites by 40%.

2.8.2 Acetylation of the Fibres

Fibre treatment with acetic anhydride is an effective method of reducing the hydrophilic characteristics of natural fibres [24]. Acetic anhydride is a compatibiliser that lowers the surface energy of the fibre to make it non-polar and more similar to the thermoplastic matrix [82]. Acetylation has been shown to reduce swelling of wood in water [83]. Reduction of about 50 and 65% moisture uptake of acetylated jute and pine fibres, respectively has been reported in literature [24]. Hill *et al.* [84] noted that acetylation of coir fibre resulted in a slight increase in TS, YM, and impact energy (IE) of coir/polyester composites compared to unmodified coir/polyester composites. Rong *et al.* [85, 86] showed that the TS of acetylated sisal/epoxy composite was slightly higher than the untreated sisal epoxy composites.

2.8.3 Silane Treatment of the Fibres

More recently, organic-inorganic silane coupling agents have been used to couple cellulose fibres to thermoplastic like PP though they have been used for over 50 years to couple glass fibres with polymeric matrices [87]. Yan *et al.* [88] showed the influence of silane treatment of fibre on the performance of sisal textile reinforced vinylester composites. Sisal fibre was treated with 3-aminopropyltriethoxy silane and γ-methacryloxypropyl trimethoxy silane solution in acetone with a concentration of 6 wt% for 24 hours. A small increase in TS (about 3%) and tensile modulus (about 14%) of the composites was observed compared to untreated fibre composites. The flexural strength and flexural modulus of silane treated fibre composites were found to increase by 15% and 30%, respectively compared to untreated composites. However, silane treatment of the fibres did not influence the IE. Mäder and Gliesche [89] treated flax and ramie with 3 wt% aqueous γ-aminopropyl triethoxy silane solution at 80^{o}C. They observed a reduction in the flexural strength and an increase in flexural modulus of flax/epoxy composites, and did not observe any remarkable increase in the flexural strength on ramie/epoxy composites as compared to untreated fibre

composites. However, they observed an increase of about 20% in the flexural modulus of ramie/epoxy composites.

2.9 Interfacial Shear Strength (IFSS) of Composites

In a composite material, fibre ensures the strength, the matrix helps to keep the desired location, and the interface, as a key element of the composite, transfers the load from the matrix to the fibres, and is responsible for the reinforcing effect. Thus, the processing behaviour and the mechanical properties of fibre reinforced polymer composites are influenced by the properties of both the bulk materials and the interface. However, the interface is the key region that determines the characteristics of fibre reinforced composites to some extent. Several test methods (e.g. single fibre pull-out, fragmentation, microindentation, and push out) have been developed to characterise the interface and improve understanding of the adhesion between fibre and matrix resin [90, 91]. Of the methods, single-fibre pull-out test is the most commonly used method because of its ease of application and versatility. Perhaps, it is the oldest direct measurement technique which was developed in the early stages of composite research when the fibres were large and easy to handle [92]. The test is involved with pulling a single fibre out of a block of resin and has gained a large degree of popularity since the 1980s and is used with many fibre-matrix combinations [93].

In single fibre pull-out test, the debonding process generally starts at the fibre entry point and gradually extends along the fibre until the debonding of the fibre ends [94]. The main advantage of this test is that the debonding force and embedded length are monitored during the pull-out process and the maximum pull-out force is converted to an apparent IFSS according to the following Kelly/Tyson equation [95]:

$$\tau = \frac{F_{\max}}{2\pi r l} \tag{2.2}$$

where, F_{max} is the maximum debonding force, r is the radius and l is the embedded length of the fibre.

Another advantage of this method is that since the matrix is in compression during this test, the strength of the matrix is not a significant factor allowing brittle matrices like epoxy resin and PLA to be used [96].

The whole procedure of pull-out test involves the assumption that the interfacial loading is a shear mode, the shear stress along the fibre is homogeneous and the friction between debonded fibre and matrix is negligible [97]. This can be true in the case of a ductile matrix. However, for ideal elastic fibre and matrix behaviour and a brittle interface fracture, strong stress field inhomogeneities are developed at the entry and end of the fibre [98]. Thus, the apparent shear stress obtained using Equation (2.2) decreases with increasing fibre length for elastic fibre and matrix behaviour, whereas it is independent from the fibre embedded length for a very ductile matrix.

There is an ample literature available with synthetic fibre/polymer matrix system to measure IFSS by single fibre pull-out tests [99-101]. However, very limited work has been reported so far to measure IFSS for natural fibres especially by this technique. Herrera-Franco *et al.* [102] used different surface treatments to treat henequen fibres and measured IFSS of henequen/PE fibre systems by single fibre pull-out test to use as an indicator of the fibre-matrix adhesion improvement. They reported an increase of IFSS with different surface treatments. Arbelaiz *et al.* [103] also used different surface treatment to modify flax fibres and carried out single fibre pull-out test of flax/PP systems to calculate apparent IFSS. They observed that IFSS values were higher for alkali treated and maleated polypropylene (MAPP) treated fibre/PP systems. The aim of this study is to investigate the effects of alkali fibre treatment of hemp fibre on the IFSS of hemp/epoxy and hemp/PLA composites obtained by single fibre pull-out test.

2.10 Cure Kinetics of Hemp/Epoxy Composites (HECs)

Thermosetting epoxies possess many desirable properties such as high TS and modulus, excellent chemical and solvent resistance, dimensional and thermal stability, good creep resistance, and excellent fatigue properties [5]. These characteristics make them ideal candidates as matrices for many important applications including adhesives, electronic encapsulants, and matrix for high performance fibre reinforced composites [5]. The physical properties of thermosetting system including epoxy resins are dependent on the extent of cure, which depends on the curing conditions, the time and temperature of cure. Therefore, the kinetic study of a curing reaction is important in order to obtain epoxy resins with controlled physical properties, and for establishing optimum curing conditions. Although epoxy resins can be cured with different group of curing agents, most studies performed to date have been with amine curing agents [104-106].

Epoxy resins are characterised by the presence of a three membered ring containing two carbons and an oxygen (epoxy group or epoxide or oxirane ring). Schlack reported the first liquid diepoxide, Figure 2.8, as the reaction product of bisphenol-A with an excess of epichlorohydrin [107].

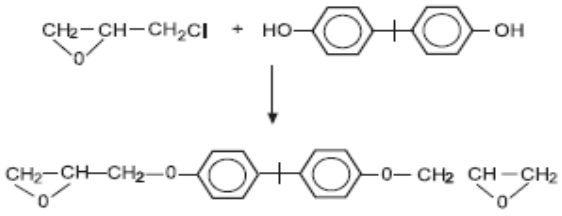

Figure 2.8 2,2 – bis [4 - (2′,3′ –epoxy propoxy) phenyl] propane (DGEBA).

This resin is commonly called as DGEBA. The higher molecular weight homologs are represented by the structure showed in Figure 2.9.

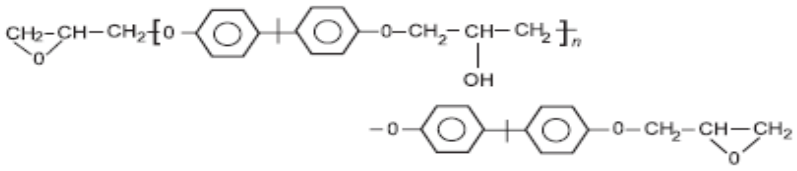

Figure 2.9 Higher molecular weight homologues of epoxy resins.

n is the number of repeating unit and its value in liquid resins is less than 2.5 and may be as high as 18 in high melting point solid resins. DGEBA, Figure 2.8, is used extensively in industry due to its fluidity, ease of processing, and good physical properties of the cured resin. As the value of n increases, the fluidity of resin decreases and, therefore, in the composites industry the general-purpose epoxy resins have a maximum degree of polymerisation up to four only [9].

The choice of curing agent depends on processing method, curing conditions, i.e. curing temperature and time, physical and chemical properties desired, toxicological and environmental limitations, and cost. A variety of curing agents containing active hydrogen atom such as aliphatic and aromatic amines, polyamide amines, polyamides, anhydrides, dicyandiamide, isocyanate, polysulphides, mercaptans, melamine-formaldehyde, and urea formaldehyde have been used [9].

For curing epoxy resins, aliphatic amines are the most widely used. These are highly reactive, low molecular weight curing agents that result in tightly cross-linked network [9]. Generally, the curing of amine with DGEBA involves three main reactions: a primary amine group addition to the epoxy ring, a secondary amine group addition, Figure 2.10, and etherification.

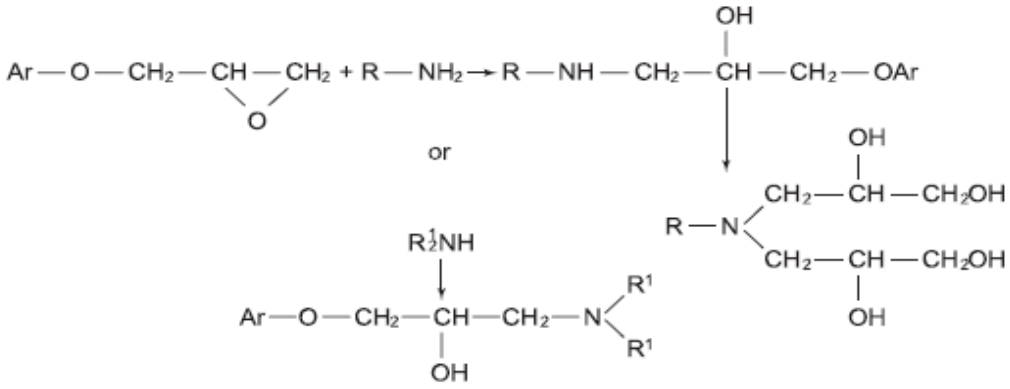

Figure 2.10 Curing of epoxy resin with primary and secondary amines

This is an autocatalytic process as the hydroxylic molecules are formed as one of the reaction products, partly protonating the oxygen atom of the epoxy group, facilitating the ring opening reaction. As a result, the reaction kinetics determines the structure of the epoxy network that forms. On the other hand, a change in the structure of the epoxy network on addition of other polymers, might also influence the reaction kinetics. The addition of natural cellulose fibres to epoxy resins is thus expected to alter the cure kinetics. While the cure kinetics of various neat epoxy (NE) resins and epoxy resins with other fillers have been extensively studied mostly by using differential scanning calorimetry (DSC) [108-111], the cure kinetics of epoxy resins with natural fibres has not yet been studied.

The basic assumption for the application of DSC to the cure of epoxy resin is that the measured heat flow (dH/dt) is proportional to the reaction rate (dα/dt). All kinetic model start with the basic rate equation of the form:

$$\frac{d\alpha}{dt} = k(T) f(\alpha) \tag{2.3}$$

where, $\frac{d\alpha}{dt}$ is the rate of conversion, $k(T)$ is the reaction rate constant and $f(\alpha)$ is a kinetic model function that depends on the conversion. An integrated form of the above equation often appears as

$$g(\alpha) = \int_0^{\alpha} \frac{d\alpha}{f(\alpha)} = k(T)t \tag{2.4}$$

where, $g(\alpha)$ is the integrated form of the conversion dependence function.

The rate constant $k(T)$ depends on temperature and has the Arrhenius form:

$$k(T) = A\exp(-\frac{E_a}{RT}) \tag{2.5}$$

where, A is the pre-exponential factor, E_a is the activation energy, and R is the gas constant, and T is the absolute temperature.

Techniques using DSC can use two basic approaches: an isothermal approach where a single cure temperature is used at a given cure cycle and a dynamic approach where the rate of heating is kept constant for a given cure cycle. The isothermal cure method monitors the conversion and the rate of conversion continuously, as the uncured resin is curing isothermally, over the entire course of the reaction.

Both in dynamic and isothermal techniques, it is assumed that the rate of conversion $\frac{d\alpha}{dt}$ is directly proportional to the rate of heat flow, φ generated in the curing reactions according to the equation:

$$\frac{d\alpha}{dt} = \frac{\varphi}{\Delta H} = (\frac{1}{\Delta H})(\frac{dH}{dt}) \tag{2.6}$$

where, ΔH is the enthalpy of the curing reaction. The conversion at time t (α_t) is taken to be the heat evolved at time t (ΔH_t) divided by the total heat of reaction (ΔH_{tot}):

$$\alpha_t = (\frac{\Delta H_t}{\Delta H_{tot}}) \tag{2.7}$$

2.10.1 Non-isothermal or Dynamic Kinetic Models

The dynamic kinetic models proposed by Kissinger [112, 113] and Ozawa-Flynn-Wall [114, 115] are based on multiple-heating-rates. These models assume that the conversion value is constant at the exothermic peak temperature in a DSC

analysis, and is independent of the heating rate [116, 117]. According to Kissinger [112], the activation energy can be calculated from maximum reaction rate (where, $d(\frac{d\alpha}{dt})/dt$ is zero under the condition of constant heating rate) from the following relation:

$$\frac{d[\ln(q/T_m^2)]}{d(1/T_m)} = -\frac{E_a}{R} \tag{2.8}$$

where, T_m is the exothermic peak temperature, q is the constant heating rate, and R is the universal gas constant (8.314 kJ mol^{-1} K^{-1}). Therefore, a plot of $\ln(q/T_m^2)$ versus $1/T_m$ gives the activation energy without a specific assumption of the conversion dependent function. It is simplistic to assume a single reaction occurring during the curing process given the complexity of the reaction.

Based on Doyle's approximation [118] for the integral of p(E/RT) (a p-function defined by Doyle) an alternative kinetic model was developed by Flynn-Wall-Ozawa [114, 115] for the calculation of activation energy. They expressed the function $g(\alpha)$ as

$$\log q = \log[\frac{AE_a}{g(\alpha)R}] - 2.315 - \frac{0.4567E_a}{RT_m} \tag{2.9}$$

where, T_m is the exothermic peak temperature and A is the frequency factor.

Using the above equation the activation energy E_a can be calculated from a plot of $\log q$ versus $1/T_m$.

2.10.2 Isothermal Kinetic Model: Autocatalytic Model

The autocatalytic model is a phenomenological approach. It assumes that at least one of the reaction products is involved in the propagating reaction, and thus is characterised by an accelerating isothermal conversion rate, which typically reaches its maximum between 20 and 40% conversion. For the determination of the cure kinetics by means of this autocatalytic, the isothermal cure reactions of

NE and epoxy with fibre was carried out at four different temperatures (25, 50, 70, and 120^{o}C). The kinetics of autocatalysed reactions are described by the following equation [119]:

$$\frac{d\alpha}{dt} = k'\alpha^{m}(1-\alpha)^{n} \tag{2.10}$$

where m and n are the reaction orders and k' is the specific reaction rate constant. According to this model, the rate is zero or very small initially and attains a maximum value at some intermediate conversion, typically between 20–40% conversion [120]. The initial rate of autocatalytic reactions may not be necessarily zero, as there is a possibility that reactants can be converted into products via alternative paths, only one of which is autocatalytic. To take into account these autocatalytic characteristics, a generalised expression can be used as follows:

$$\frac{d\alpha}{dt} = (k_1 + k_2\alpha^{m})(1-\alpha)^{n} \tag{2.11}$$

Such a model has also been successfully applied to autocatalytic polymerisation reactions [119, 121]. In this case, the influence of the reaction products on the conversion rate is given by the term $k_2\alpha^{m}$.

In this work, cure kinetics were studied by using two dynamic kinetic models (Kissinger [112] and Flynn-Wall-Ozawa [114, 115, 122] models were used because of their wide applicability and the kinetic parameters can be quantified without prior knowledge of reaction mechanism) and one isothermal model (the phenomenological model developed by Kamal [119]). Both dynamic and isothermal models were used to investigate the cure kinetics of an epoxy system containing DGEBA and aliphatic amine as curing agent. The effects of addition of 40 wt% untreated fibre in the same epoxy resin (DGEBA) curing agent (aliphatic amine) system on the cure kinetics were also studied.

2.11 Processing of Fibre Reinforced Composites

There is an extensive range of well established processing methods available for fibre reinforced composites. These vary from simple labour intensive methods suitable for one-offs to automated methods for rapidly producing large numbers of complex components. The method of production depends on the factors such as cost, shape of component, number of components and required performance.

2.11.1 Hand Lay-up

In hand lay-up, the reinforcement is put down to line a mould, previously treated with a release agent to prevent sticking and perhaps a gel coat to give a decorative and protective surface. The reinforcement can be in many forms including woven rovings and chopped strand mat. The liquid thermosetting resin is mixed with a curing agent and applied with a brush or roller taking care to work it into the reinforcement. The most commonly employed resins are polyesters and curing is usually performed at room temperature. A prime consideration is the viscosity and the working time of the resin.

Hand lay-up requires little capital equipment but is labour intensive. It is particularly suited for one-offs or short production runs and can be used for large components such as hulls of boats and swimming pools. The main disadvantages of this method are the low reinforcement content of about 30 vol% and the difficulty in removing all of the trapped air, hence the mechanical properties are not good.

2.11.2 Compression Moulding

Compression moulding is the most common method of processing thermosets and thermoplastics. It is used to produce large and relatively flat composite parts with good mechanical properties. Compression moulding basically involves the hot pressing of randomly oriented or aligned fibre mats, either chopped or in continuous form, with a thermoset or a thermoplastic material.

In the case of thermosets, a fibre mat soaked in thermoset resin is placed onto the bottom half of a compression mould cavity which can be pre-heated to the desired cure temperature. Then the top half of the mould is lowered at a constant rate until the desired process pressure is reached to cure the composite. Once the composite has been cured, it is cooled and removed from the mould.

In the case of thermoplastics, the compression moulding operation begins with the placement of a fibre-mat and thermoplastic sheets onto the bottom half of a pre-heated mould cavity. The top half of the mould is lowered at a constant rate until the desired process pressure is reached, thus causing the melting and consolidation of the composite. Once the composite has been consolidated, it is cooled and removed from the mould.

2.11.3 Film Stacking Technique

Film stacking is a technique with which thermoplastic composites can be prepared [123]. Film stacking is very similar to compression moulding. The only difference of film stacking with compression moulding is that, in film stacking thermoplastic matrix in the form of film (instead of in the form of sheet) is used. Thus, in film stacking fibre tows arranged in sheet form are sandwiched between matrix polymer films. This assembly is then placed within a press where temperature transforms the film into a polymer melt. Pressure is then applied and forces the melt to impregnate the fibre tow. Appropriate process conditions must be used in order to sufficiently reduce the matrix viscosity without thermally degrading the actual composite or de-align the fibrous reinforcement. Insufficient heat input and/or pressure will typically result in un-wetted fibre and a high void content within the final material. Therefore, careful selection of process parameters such as pressure and heat are required to achieve composites with good mechanical properties.

2.11.4 Vacuum Bag

In this method the heated pre-impregnated reinforcement, which is sealed to the mould by a flexible sheet or membrane, is forced in to the mould as air is removed. The mould may be male or female and the vacuum is maintained until the curing process has reached completion.

2.12 Modelling of Tensile Strength (TS) of Composites

A simple way of predicting the TS of unidirectional, continuous fibre-reinforced polymer composites in the axial direction is to use the "rule of mixtures (ROM)" [124, 125]. According to this model, the equation for TS is as follows:

$$\sigma_c = \sigma_f V_f + \sigma_m V_m \quad \text{(ROM)} \tag{2.12}$$

where σ_c is the TS of the composite, σ_f is the mean TS of the fibre, and σ_m is the TS of the polymer matrix and V_f and V_m are the volume fractions of the fibre and matrix, respectively.

Equation (2.12) is also known as the Parallel model and it assumes that iso-strain conditions exist for both polymer matrix and fibre. A basic concept in the ROM is the evaluation of each contribution of the fibre and matrix based on their strengths, and calculation of the ultimate strength of the composite as the sum of contributions according to their relative volumetric properties. The traditional way of predicting transverse TS is to use the series model of the ROM which can be expressed as follows:

$$\sigma_c = \frac{\sigma_m \sigma_f}{\sigma_m V_f + \sigma_f V_m} \quad \text{(Series Model)} \tag{2.13}$$

The schematic representations of parallel and series models are given in Figure 2.11.

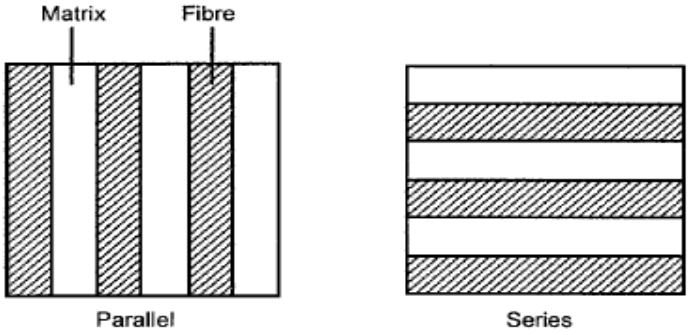

Figure 2.11 Schematic representation of parallel and series models.

The Parallel model can be regarded as an upper bound and the Series Model represents the lower bound for the TS of achievable strength [124].

However, the ultimate TS of a composite is affected by not only the fibre and matrix fractions and strengths but also the microgeometry of the composite components, and interfacial bonding. It is very important how the two phases are mixed and interconnected to form a composite of continuous phase. It is assumed in the ROM that the fibres in composites are perfectly oriented along the direction of tensile load, and are also uniformly distributed. In reality, there are some misalignments and non-homogeneity in the distribution of fibres even in a unidirectional composite. Thus, the ROM often overestimates the ultimate TS of unidirectional fibre (both long and short) composites [125, 126]. Moreover, the ROM indicates that the strength of a composite increases linearly with an increase in the fibre volume fraction which is not true as the strength of a real composite deviates from the ROM in a non-linear fashion and usually begins to decrease at or above a fibre volume fraction of 80% [125].

2.12.1 Modified Rule of Mixtures (MROM)

The ROM model has been further modified to account for the influence of fibre orientation and fibre/matrix interfacial strength on the TS of the composites [124, 125]. According to this model:

$$\sigma_c = \sigma_m^* V_m + \sigma_f V_f K_1 K_2 \tag{2.14}$$

where, σ_c, σ_f, are the TS of the composite and fibre, respectively; σ_m^* is the TS of the polymer matrix at the failure strain (FS) of the composite; V_f and V_m are the volume fractions of the fibre and matrix, respectively; K_1 is an orientation factor, and K_2 is a factor dependent on the stress transfer between the matrix and the fibres. K_1 has a value of unity for axially aligned fibre composites, yields a value of 0.375 for planar random configuration, and it has the value of 0.2 for a three dimensional randomly oriented fibre composites, K_2 has the value of unity for continuous fibre composites with a perfect interface [127].

2.13 Degradation and Environmental Effects

Natural fibres are widely used for reinforcing polymers. There are many applications of natural fibre composites in everyday life (discussed earlier in section 1.4). However, the main disadvantage of natural fibres is their hydrophilic nature. They also have poor environmental and dimensional stability that prevent a wider use of natural fibre composites. The possibility for using these materials in outdoor applications makes it necessary to analyse their mechanical behaviour under the influence of weathering action [128]

2.13.1 Hygrothermal Ageing of the Composites

Natural fibres such as hemp, flax, jute and kenaf have received considerable attention as an environmentally friendly alternative for the use of glass fibres in engineering composites [128]. These plant fibres have a number of techno-ecological advantages over traditional glass fibres since they are renewable, can be incinerated with high energy recovery and CO_2 neutral life cycle, show less concern with safety and health (e.g. skin irritation) and give less abrasive wear to processing equipments such as extruders and moulds. In addition they exhibit excellent mechanical properties especially when their low density and price are taken into account [129, 130]. Although natural fibres have a number of ecological advantages over glass fibres they also possess some disadvantages such as higher moisture absorption which brings about dimensional changes, leading to

microcracking, poor thermal stability which may lead to thermal degradation during processing [53, 131], poor wettability, and insufficient adhesion between untreated fibres and the polymeric matrix lead to debonding with age [132-134].

On the moisture effect, the mechanical properties of natural fibre reinforced composites can be reduced to great extent under moist conditions [135, 136]. This is a serious concern as there are potential outdoor applications such as decking and railing [137, 138], where moisture absorption can have significant influence for these materials. The interfacial bonds between the natural fibres (which contain -OH, carboxyl (-COOH), and other polar groups) and the relatively hydrophobic polymer matrices would be weakened with higher water uptake. The weakened interface causes the reduction in the mechanical properties of the composites.

The change in dimension of natural fibres with moisture gain is attributed to the interaction of the cell-wall polymers containing -OH, -COOH, and other polar groups with water molecules via hydrogen bond formation [139]. The hemicelluloses and amorphous regions of the cellulose are generally responsible for the moisture absorption properties of fibres. Therefore, alkali treatment is generally done to remove hemicelluloses from natural fibres because along with being largely hydrophilic they are non-load carrying as well. The study of the water absorption behaviour of composites is necessary in order to estimate not only the consequences that the water absorption of fibres may have on the composite properties, but also how this water uptake can be minimized. The way in which composite materials absorb water depends upon many factors, such as temperature, fibre volume fraction, orientation of the reinforcing fibres, fibres permeability, exposed area of the surface, diffusivity, and reaction between water and matrix [140, 141].

Moisture absorption in composite materials can be conducted by several different mechanisms. The main process consists of diffusion water molecules inside the microgaps between polymer chains. The other common mechanisms are capillary transport into the gaps and flaws at the interfaces between fibres and polymer, due to the incomplete wettability and impregnation; and transport by microcracks in the matrix, formed during compounding process [142, 143]. In spite of the fact

that all three mechanisms are active jointly during moisture exposure of the composite materials, the overall effect can be modelled conveniently using the diffusional mechanism only.

There are three different categories of diffusion behaviour [143]. Case I, or Fickian diffusion, in which the rate of diffusion is much less than that of the polymer segment mobility. The equilibrium inside the polymer is rapidly reached and it is maintained with independence of time. Case II, in which penetrant mobility is much greater than other relaxation processes. This diffusion is characterised by the development of a boundary between the swollen outer part and the inner core of the polymer. The boundary advances at a constant velocity and the core diminishes in size until an equilibrium penetrant concentration is reached in the whole polymer. Non-Fickian or anomalous diffusion occurs when the penetrant mobility and the polymer segment relaxation are comparable. It is then an intermediate behaviour between case I and case II diffusion.

These three cases of diffusion can be distinguished theoretically by the shape of the sorption curve represented by

$$\frac{M_t}{M_\infty} = kt^n \tag{2.15}$$

where M_t is the moisture content at time t; M_∞ is the moisture content at the equilibrium; and k and n are constants.

The value of coefficient n shows different behaviour between cases; for Fickian diffusion n = ½, while for case II n = 1. For anomalous diffusion, n shows an intermediate value ($1/2<n<1$). Moisture absorption in natural fibre reinforced composites usually follows case I or Fickian behaviour. Loos and Springer [144] investigated the moisture absorption behaviour of several resins used for making PMCs. They reported that the materials exhibited Fickian diffusion behaviour at higher temperatures. The characteristics of Fickian diffusion have been summarized as (a) the absorption curves are linear in the initial stages and (b) above the linear portion both absorption and desorption curves are concave to the abscissa [145].

Equation (2.15) can be written in the following logarithmic form,

$$\log(\frac{M_t}{M_\infty}) = \log k + n \log t \tag{2.16}$$

The analysis of the diffusion mechanism and kinetics can be performed on the basis of Fick's theory and adjusting the experimental values in Equation (2.16).

The diffusion coefficient, D is the most important parameter of the Fick's theory, as this shows the ability of solvent to penetrate into the composite structure. For small time ($\frac{M_t}{M_\infty} \leq 0.5$), the following equation can be used [146].

$$(\frac{M_t}{M_\infty})^2 = \frac{16D}{\pi}\frac{t}{L^2} \tag{2.17}$$

where L is the thickness of the sample.

The diffusion processes are activated by an increase in temperature most likely due to the increased mobility of the molecules in the process. In case of Fickian diffusion, the diffusion coefficient follows an exponential Arrhenius type relation with temperature expressed by

$$D = D_0 \exp(-\frac{E_a}{RT}) \tag{2.18}$$

where D_0 is the permeability index, E_a is the activation energy of the diffusion process, R is the universal gas constant and T is the absolute temperature.

As mentioned before, apart from diffusion, two other minor mechanisms are active in moisture exposure of composite materials. The capillary mechanism involves the flow of water molecules into the interface between fibres and matrix. It is particularly important when the interfacial adhesion is weak, and the debonding of fibres and matrix has started. On the other hand, transport by microcracks includes the flow and storage of water in the cracks, pores or small channels in the composite structure. These imperfections can be originated during the processing of the materials or due to environmental and service effects. The

objective of this study is to relate kinetics and characteristics of the water absorption in hemp fibre/epoxy and hemp fibre/PLA composites. Water uptake leads to the degradation of the fibres and the fibre-matrix interface resulting in a loss of mechanical performance. Therefore, the effects of hygrothermal ageing on mechanical properties of the composites will also be studied.

2.13.2 Accelerated Ageing of the Composites

NFCs offer many advantages over conventional structural materials. They have high strength and modulus to weight ratios, fatigue and corrosion resistant, tailorable and require low maintenance. However, because of their unknown long term properties when exposed to a combination of in-service loads and environments, designers are still reluctant to use NFCs in primary load bearing structures [147]. The effect of exposure to moisture, heat, and ultra-violet (UV) radiation, and more importantly a combination of these parameters may degrade the material's stiffness and strength.

The photodegradation of natural fibres like wood is attributed to the degradation of its components namely cellulose, hemicelluloses, and lignin according to Dence [148]. Lignin and hemicelluloses are more prone to degradation than cellulose by various means [149]. Lignin degrades upon exposure to UV-light and hemicelluloses degrade upon moisture absorption and biological means [150]. The UV-degradation process is known to be triggered by the formation of free radicals and probably starts with the oxidation of phenolic -OHs [151]. Moreover, singlet oxygen that can be formed by oxygen quenching of photoexcited lignin plays a role in the degradation of lignocellulosic natural fibres like wood [151]. The formed singlet oxygen is a source of peroxides [152], which can initiate the auto-oxidation of carbohydrates and cleavage of lignin [153, 154]. The oxidative reactions initiated by UV-radiation can be represented as in Figure 2.12 [64].

Initiation

$$RH \xrightarrow{h\nu} R^{\bullet}$$

Propagation

$$R^{\bullet} + O_2 \rightarrow ROO^{\bullet}$$

$$ROO^{\bullet} + R'H \rightarrow ROOH + R'^{\bullet}$$

Branching

$$ROOH \xrightarrow{h\nu} RO^{\bullet} + {}^{\bullet}OH$$

$$2ROOH \rightarrow ROO^{\bullet} + RO^{\bullet} + H_2O$$

Figure 2.12 Oxidation reactions initiated by UV-radiation.

In PLA the active oxygen species initiate the degradation reaction by attacking neighbouring polymer chain and the degradation process extends into the polymer matrices through the diffusion of these reactive oxygen species [155].

Photodegradation leads to a discoloration of epoxy resin and to a deterioration of its physical properties [156]. The main photooxidative pathway of the epoxy resin involves the abstraction of the hydrogen atom on the secondary carbon atom situated in the α position to the ether bond [157]. It has been shown that the photoinitiating species essentially derive from the phenoxy part, whereas the propagation principally depends on the amine concentration and on the electron density at the nitrogen atom [158].

Ideally, composite materials and their structures that are intended for long term use, should be tested in real time and with realistic in-service environments. Often this is not viable because the time involved would significantly delay product development and accelerated ageing techniques are required [147]. During accelerated weathering, measured variables can include exposure time, exposure to UV irradiation over a specific wavelength range, and exposure to moisture as number of cycles or time. It is recommended that the performance of the materials after weathering be reported after a specific radiant exposure, the time integral of irradiance [159].

The use of NFCs in non-structural (e.g. siding, roofing), or structural (e.g. decking) materials has resulted in concern about the durability of these products when exposed to environments [160]. Durability of the composites upon exposure to UV-light is of particular concern as UV-light can cause the changes in the surface chemistry of the composites commonly known as photodegradation [161, 162]. The degradation ranges from mere surface discoloration affecting the aesthetic appeal in indoor applications to extensive loss of mechanical properties [163, 164]. Moreover, the combination of light, moisture, and temperature in outdoor applications can completely destroy the lignocellulosic network, limiting the performance of unprotected wood in outdoor applications[165].

2.14 Fibre and Composites Characterisation Methods

2.14.1 Wide Angle X-ray Diffraction (WAXRD)

WAXRD is a well established method for determining the crystallinity of partially crystalline materials [166, 167]. Hermans and Weidinger [166] conducted the first quantitative investigation into the crystallinity of cellulose fibres by means of WAXRD. WAXRD patterns of crystalline cellulose show reflections superimposed on a diffuse background, and the ratio of the sum of the relative integrated intensities and the total intensity provides a measure of the degree of crystallinity. WAXRD has been widely applied to study the crystallinity of pulp and cellulose fibres [168-170]. Mwaikambo and Ansell [171] measured the crystallinity index of hemp, kapok, sisal, and flax fibres by using WAXRD method. They showed that the increase in crsytallinity index obtained by WAXRD was, in fact, an increase in the order of the crystalline packing rather than an increase in the intrinsic crystallinity. Mathew *et al.* [11] studied the crystallinity of PLA by using WAXRD method and showed that heat treatment of PLA increased its crystallinity.

2.14.2 Fourier Transform Infrared (FTIR) Spectroscopy

FTIR is a powerful tool for identifying types of chemical bonds in a molecule by producing an infrared absorption spectrum that is like a molecular "fingerprint". FTIR is most useful for identifying chemicals that are either organic or inorganic. It can be utilised to quantitate some components of an unknown mixture. It can be applied to the analysis of solids, liquids, and gasses. The term FTIR refers to a fairly recent development in the manner in which the data is collected and converted from an interference pattern to a spectrum. FTIR is perhaps the most powerful tool for identifying types of chemical bonds (functional groups). The wavelength of light absorbed is characteristic of the chemical bond as can be seen in this annotated spectrum. By interpreting the infrared absorption spectrum, the chemical bonds in a molecule can be determined. FTIR spectra of pure compounds are generally so unique that they are like the molecular "fingerprint" [172].

FTIR spectroscopy has been shown to be a useful tool for investigating the fine structural characterisation of cellulose and its chemical modification [173-175]. Sahoo *et al.* [176] modified jute fibre chemically and demonstrated the difference between unbleached and bleached pulp from the difference in peaks in IR-spectra. By FTIR study Ray and Sarkar [177] found an increased amount of -OH groups in jute fibres due to chemical changes upon alkali treatment. From FTIR spectra Mwaikambo and Ansell [171] showed that kapok was the most reactive followed by jute, sisal, and then hemp fibre. Wong *et al.* [178] used FTIR spectroscopy to monitor hydrogen bonding in polyhydroxy butyrate-flax composites.

2.14.3 Zeta Potential Measurements

Electrokinetic properties can describe the electrical potential adjacent to a solid surface, if this is moved in respect to the surrounding liquid phase [179]. It is described by the zeta potential (ζ), this is the potential at the border line between the stationary and mobile liquid phase. It depends on the chemical properties of the fibre surface as well as the liquid phase. This is on the one hand, the chemical nature of dissociable surface groups (the adsorption of ions like hydroxyl groups)

at the solid surface and on the other hand, the ionic strength and the pH value of the liquid phase [180, 181].

When a solid is immersed in a liquid, Figure 2.13 [182], an electrochemical (or Nernst) potential (ε) is developed between the body of the solid and the body of the liquid; this potential is proportional to the ionic activity or to the loss of ions at the surface in contact with the liquid. The ions formed on the surface AB of the solid attract oppositely charged ions from the liquid and so form two different layers of which the outer layer becomes more diffuse. If the solid and its surface is moved, the ABCD portion of this diffuse layer moves with it. In effect, CD then defines the boundary and thus the effective volume of the solid, as far as flow is concerned. The two differently charged layers which lie between this boundary CD and the surface of the solid AB are known as double (or Stern-Gouy) layer [182].

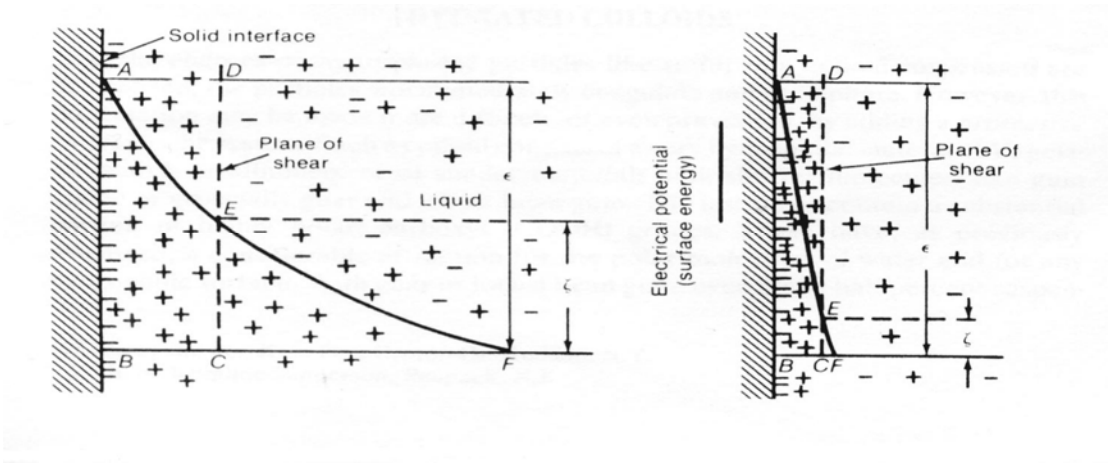

Figure 2.13 Electrokinetic, ε and zeta potentials, ζ of surfaces with different thicknesses of the double layer.

In this double layer the potential decrease from the surface potential to the equilibrium in the bulk phase. The general features and properties of the electric double layer at the solid/liquid boundary in an aqueous medium are described by several researchers [183-185]. Since the surface potential cannot be measured directly, use is generally made of the experimentally accessible zeta potential (ζ). When investigating solid surfaces like fibres, the zeta potential is calculated from the measured streaming potential.

It can be assumed that the surface potential is mainly responsible for different kind of sloid liquid interactions. Natural cellulose fibres exhibit a highly polar surface due to the presence of hydroxyl and carboxyl groups. These groups enable the formation of hydrogen and some times covalent bonds in the interface of the reinforced composite materials. Hydroxyl groups are mainly part of celluloses. Carboxyl groups are the part of unstable hemicelluloses and often removed by various surface treatments like alkali treatment. The surface treatment also removes some lignin, pectin, and waxy substances along with hemicelluloses and thus exposes cellulose hydroxyl groups. The high polarity of the cellulose fibres is the reason for their hydrophilic behaviour. The adsorption of water or electrolyte solutions causes an interfibrillar swelling of the surface layers and therefore the size of the active surface is increased. However, the nature of dissociable groups should not change. The swelling itself causes a reduction of the ζ, because of the shift of the shear plane into the liquid phase and can therefore be used for characterisation of the accessibility of the dissociated groups by means of measured pH-ζ functions [186].

ζ has become a useful parameter to monitor changes in electrochemical behaviour. The ζ is generally measured as a function of pH, showing a plateau in the basic region where all the acid groups are dissociated or a maximum number of hydroxyl group or other anions are adsorbed. Reducing the pH causes the association of acid groups and dissociation of alkaline groups, as well as desorption of anions and adsorption of cations, so that a situation of charge equilibrium is reached. This point is known as the isoelectric point (IEP), at which ζ is zero. If it is independent of the ionic strength of the electrolyte then it is the point of zero charge. The IEP can be used to determine surface chemistry by comparing shifts in the IEP after reaction. For example, a shift to lower pH for a wood fibre indicates that more sites, such as hydroxyl groups, are available for bonding. The plateau region can indicate whether a material is hydrophilic or hydrophobic [186].

According to Aranberri-Askargorta *et al.* [187] the performed ζ measurements clearly reflect differences in the degree of hydrophilicity of the natural fibres. On the basis of the experimental value of zeta potential Bismarck *et al.* [188] showed

that the retting of green flax fibres reduced the hydrophilicity of the fibres as retted fibres contained a relatively high amount of wax on their surfaces. From the ζ measurements of the untreated and treated fibres Pothan *et al.* [189] reported that chemical modification alters the polarity of the already acidic cellulose fibres.

2.14.4 Thermal Analysis

Thermal analysis comprises a group of techniques in which a physical property of a substance is measured as a function of temperature, while the substance is subjected to a controlled temperature programme. It is an important analytical method in understanding the structure-property relationship and industrial production of different polymeric materials, especially fibre reinforced composites. Moreover, it is a useful technique to determine the thermal stability of the materials. In addition, it is possible to quantify the amount of moisture and volatiles present that can cause deformation in composites.

2.14.4.1 Differential Thermal Analysis/Thermogravimetric Analysis (DTA/TGA)

In DTA, the temperature difference that develops between a sample and an inert reference material is measured, when both are subjected to identical heat treatments. DTA involves heating or cooling a test sample and an inert reference under identical conditions, while recording any temperature difference between the sample and reference. This differential temperature is then plotted against time, or against temperature. Changes in the sample which lead to the absorption or evolution of heat can be detected relative to the inert reference. TGA indicates a number of stages of thermal breakdown and weight loss of the material in each stage.

Both DTA and TGA can be used to study the thermal behaviour of natural fibre and its composites [190, 191]. Several researchers [192, 193] studied the influence of chemical treatment and of cellulose on its thermal degradation by using DTA. Rana *et al.* [194] carried out TGA analysis to study the thermal behaviour of acetylated jute fibre and to compare it with the control and found that acetylated jute had better thermal stability than the control.

2.14.4.2 Differential Scanning Calorimetry (DSC)

In DSC, the heat flow rate is associated with a thermal event that can be measured as a function of time and temperature. It relies on differences in energy required to maintain the sample and reference at an identical temperature. DSC can be used to study the thermal behaviour, crystallinity, and cure kinetics of natural fibres and natural fibre reinforced composites [74, 195, 196].

Chapter Three

Fibre Treatment and Characterisation

3.1 Summary

This chapter describes the materials, methods and results for the:

- treatment of hemp fibre with alkali to obtain an optimum alkali treatment method and development of an empirical model for the tensile strengths of various alkali treated fibres by fractional factorial design
- comparison of untreated and alkali treated hemp fibre by single fibre tensile testing as well as SEM, zeta potential, DTA/TGA, WAXRD, FTIR and lignin analysis
- effect of alkali treatments on fibre diameter, tensile strength (TS) and Young's modulus (YM)
- treatment of the optimised alkali treated fibre by silane and acetic anhydride, and comparison of silane treated and acetylated fibres in terms of SEM, zeta potential, DTA/TGA, WAXRD, and FTIR analysis.

3.2 Experimental Details

3.2.1 Materials

Retted hemp bast fibre was supplied by Hemcore, UK. Analytical grade Na_2SO_3, 98% NaOH pellets, 99% acetic anhydride, and 94% phenyltrimethoxy silane were used for the treatment of the fibres.

3.2.2 Methods

3.2.2.1 Treatment of the Fibres with Alkali

The pieces of the woody cores presented in the retted hemp bast fibre were removed manually. After weighing, fibres were placed into stainless steel canisters of 1L capacity. Pre-weighed NaOH and Na_2SO_3 solution was then poured into the canisters such that the fibre to Na_2SO_3 and NaOH solution ratio was 1:2:10 by weight. The canisters were then placed into a small lab-scale pulp digester at a required digestion temperature and time for alkali treatment of the fibres. Fibres were washed in a pulp and paper fibre washer for about 45 minutes after the alkali treatment to remove chemical residues until a fibre pH of 7 was obtained. Fibres were then dried in an oven for 48 hours at 70^{o}C.

3.2.2.2 Treatment of the Fibres with Acetic Anhydride

Alkali treated fibres were dried at 80^{o}C for 24 hours prior to the treatment. They were then placed in a sufficient amount of acetic anhydride to cover the fibre before removal and transfer to a beaker for heat treatment in a pre-heated oven at 120^{o}C for 3 hours. They were then left in the air stream to evaporate the solvent and further placed in a pre-heated oven at 100^{o}C for 6 hours. Fibres were washed in a pulp and paper fibre washer for about 45 minutes after the acetylation to remove chemical residues until a fibre pH of 7 was obtained. Fibres were then dried in an oven for 48 hours at 70^{o}C.

3.2.2.3 Treatment of the Fibres with Silane

Alkali treated fibres were dried at 80^{o}C for 24 hours prior to the treatment. Then they were vacuum impregnated with a 5 wt% solution of phenyltrimethoxy silane in methanol for about an hour and then they were left in the solution at ambient temperature for 24 hours. The fibres were then separated from the solution and the solvent was allowed to evaporate by using air stream at room temperature for 6 hours. Subsequently, they were heat treated in a pre-heated oven at 100^{o}C for 6 hours. Fibres were washed in a pulp and paper fibre washer for about 45 minutes after the silane treatment to remove chemical residues until a fibre pH of 7 was obtained. Fibres were then dried in an oven for 48 hours at 70^{o}C.

3.2.2.4 Zeta Potential Measurement

The zeta potential of untreated and alkali treated fibres was determined in a 1.00×10^{-3} M potassium chloride (KCl) electrolyte solution at room temperature using a Mutek SZP 06 System based on the streaming potential method. The pH of the electrolyte solution was varied from 11 to 3. The pH of 11 was obtained using 0.1M potassium hydroxide (KOH) solution and then decreased incrementally using 0.1M hydrochloric acid (HCl) solution.

3.2.2.5 Scanning Electron Microscopy (SEM)

The morphology of the untreated and alkali treated fibres was studied using a Hitachi S-4000 Field Emission SEM operated at 5 kV. Carbon tape was used to mount the samples on aluminum stubs. The samples were then sputter coated with platinum and palladium to make them conductive prior to SEM observation.

3.2.2.6 Wide Angle X-ray Diffraction (WAXRD)

0.5 g of fibre was compressed into a tablet using a hydraulic press at 20 MPa pressure. A Philips X-ray diffractometer, employing CuKα (λ = 1.54) radiation and a graphite monochromator with a current of 40 mA and a voltage of 40 mV was used with a diffraction intensity in the range of 6 to 60^{o} (2θ-angle range). WAXRD analysis of the acetylated and silane treated fibres were carried out after doing alkali treatment of those fibres.

The percentage crystallinity index (*CrI*) was determined using the Segal empirical method [197] according to the following equation:

$$CrI = \frac{I_{002} - I_{am}}{I_{002}} \times 100 \qquad (3.1)$$

where, I_{002} is the maximum intensity of the 002 lattice reflection (the highest peak for native cellulose) of the cellulose crystallographic form at 2θ = 22.5^{o} [198] and I_{am} is the intensity of diffraction of the amorphous material at 2θ = 18.5^{o}.

3.2.2.7 Thermal Analysis

DTA and TGA were carried out using an SDT 2960 Simultaneous DTA-TGA analyzer. All the measurements were taken whilst maintaining a static air flow of 150 mL/min with a constant heating rate of 10^{o}C/min in an open alumina crucible. The weight of the specimens was around 10 mg, with a scanned temperature range of 25 to 600^{o}C.

3.2.2.8 Lignin Analysis of the Fibres

The lignin analysis was carried out at the Environmental Chemistry Laboratory at Landcare Research New Zealand Limited, in accordance with the terms of International Accreditation New Zealand.

3.2.2.9 Fourier Transform Infrared (FTIR) Spectra

Infrared spectra were obtained using an FTIR Digilab FTS-40 spectrometer. Untreated and alkali treated fibres were ground into small particles in liquid nitrogen and mixed and compressed with potassium bromide (KBr) into a thin disc using a hydraulic press at 8 MPa pressure.

3.2.2.10 Single Fibre Tensile Testing (SFTT)

Alkali treated single hemp fibres were tensile tested according to American Society for testing and materials (ASTM) D3379-75 standard test method for TS and YM for high-modulus single filament materials. Fibres were separated by hand and attached to cardboard mounting-cards with 10 mm holes punched into them to give a gauge length of 10 mm. Polyvinyl acetate (PVA) glue was used to hold the fibres in place. A sketch of SFTT specimen can be seen from Figure 3.1.

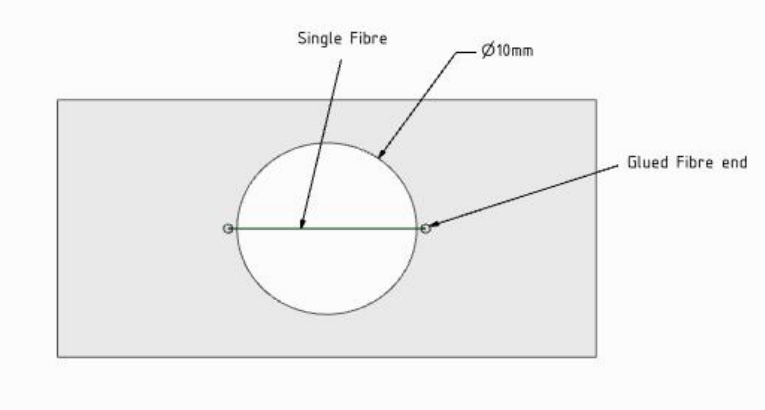

Figure 3.1 Single fibre tensile test specimen.

The fibres were then placed under an optical microscope and inspected with a calibrated eyepiece at 200× magnification to determine the average diameter of each fibre. The mounted fibres were then placed in the grips of an Instron-4204 tensile testing machine, and a hot-wire cutter was used to cut the supporting sides of the mounting cards. Tensile testing of the fibres was carried out to failure at a rate of 0.5 mm/min using a 10 N-load cell. For the partial factorial design of the alkali treatments, five repeates of each treatment were carried out. 25 replicates were used and thus average TSs and Young's moduli were obtained using the results from 125 specimens.

3.3 Results and Discussion

3.3.1 Alkali Treatment and Characterisation of the Fibres

3.3.1.1 Empirical Model for the Tensile Strength (TS) of Alkali Treated Fibre by Partial Factorial Design

Selection of the Levels of Treatment Factors

In order to select the level of NaOH concentration, digestion time, and temperature experiments had been conducted under the following conditions as described in Table 3.1, and the effects of the concentration of NaOH, digestion time, and temperature on the TS of the fibres are presented in Figures 3.2, 3.3, and 3.4, respectively.

Table 3.1 Experimental parameters for the selection of level of treatment factors.

Level Selection	NaOH Conc. (wt%)	Digestion Time (min)	Treatment Temp. (^{0}C)	Na_2SO_3 Conc. (wt%)	Corresponding Figure
Concentration of NaOH	5, 6, 10, 20	60	180	2	Figure 3.2
Digestion time	5	30, 35, 120, 360	180	2	Figure 3.3
Treatment Temperature	15	60	30, 35, 120, 180	2	Figure 3.4

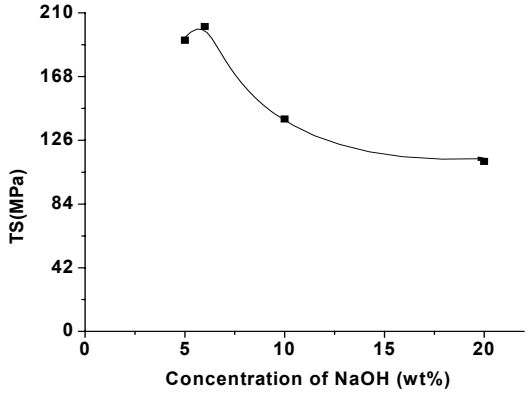

Figure 3.2 TS versus NaOH concentration (at 180^{o}C for 60 minutes with 2 wt% Na_2SO_3) plot for the level selection range of alkali fibre treatment. The curved line in the figure indicates principal trend of data points and do not represent any data fitting.

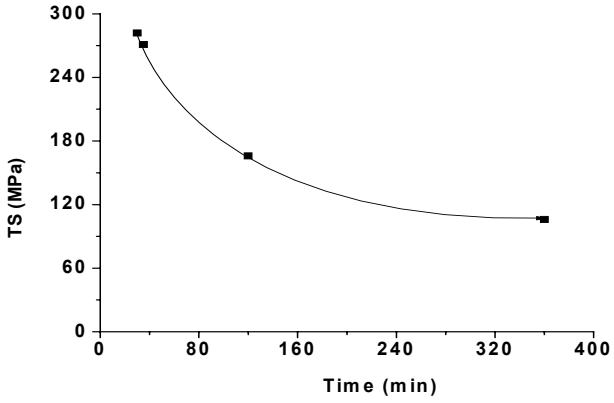

Figure 3.3 TS versus digestion time (at 180^{o}C with 5 wt% NaOH and 2 wt% Na_2SO_3) plot for the level selection range of alkali fibre treatment. The curved line in the figure indicates principal trend of data points and do not represent any data fitting.

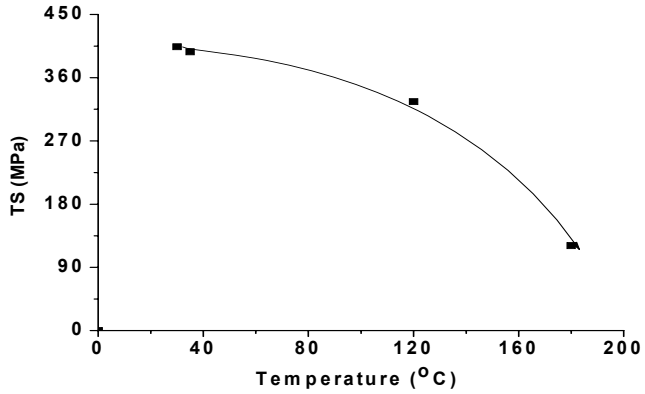

Figure 3.4 TS versus temperature (for 60 minutes with 5 wt% NaOH and 2 wt% Na_2SO_3) plot for the level selection range of alkali fibre treatment. The curved line in the figure indicates principal trend of data points and do not represent any data fitting.

As can be seen from Figures 3.2 to 3.4 if the levels are too close (say 5 and 6 wt% NaOH in Figure 3.2, 30 and 35 minutes in Figure 3.3, and 30 and 35°C in Figure 3.4), the change in fibre strengths are so small that they might remain masked within experimental errors. It is obvious from the results, however, the linear approximation of the TS over the whole range of NaOH concentration, digestion time and digestion temperature under study would result in large inaccuracy. Therefore, in order to make linear approximations, it is reasonable to select neither a very small range nor a very big one. This leads to splitting the experimental design into two parts as follows: The first part consists of the NaOH concentration level at 15 and 20 wt%, and the second part at 5 and 10 wt%. The factors and settings for alkali treatment of untreated hemp fibres for the experimental design (split into two parts) are shown in Table 3.2.

Table 3.2 Actual factors and settings for alkali treatment of untreated fibres for the experimental design.

Actual Factors↓ **Level→**	**Part 1**		**Part 2**	
	Low	**High**	**Low**	**High**
f_1 - Concentration of NaOH (wt%)	15	20	5	10
f_2 - Concentration of Na_2SO_3 (wt%)	0	2	0	2
f_3 - Time (min)	120	360	30	60
f_4 - Temperature (°C)	30	60	120	180

In experimental design in order to ease the data treatment procedure, the actual values of the factors are replaced by the coded value. The coding (and decoding in reverse) is done according to the following relations:

$$f_j = \frac{x_j d_j}{2} + \overline{f_j} \text{ or } x_j = \frac{2(f_j - \overline{f_j})}{d_j} \quad (3.2)$$

where, f_j = actual value for factor j, x_j = coded value for factor j, d_j = range for the actual value of j, and $\overline{f_j}$ = actual average for factor j. The indices j = 1, 2, 3, and 4 stand respectively for concentration of NaOH, concentration of Na_2SO_3, digestion time, and temperature.

The design matrix of testing 4 factors in a half fraction of 8 run combinations is given in Table 3.3. The design procedure is described in detail in reference [199].

Table 3.3 A half fraction coded matrix for four factors at two levels.

Run No.	x_1	x_2	x_3	$x_4 (x_1 x_2 x_3)$	$x_1 x_2$ $(x_3 x_4)$	$x_1 x_3$ $(x_2 x_4)$	$x_2 x_3$ $(x_1 x_4)$
1	-1	-1	-1	+1	+1	+1	-1
2	-1	-1	+1	+1	-1	-1	+1
3	-1	+1	-1	-1	+1	-1	+1
4	-1	+1	+1	-1	-1	+1	-1
5	+1	-1	-1	-1	-1	+1	+1
6	+1	-1	+1	-1	+1	-1	-1
7	+1	+1	-1	+1	-1	-1	-1
8	+1	+1	+1	+1	+1	+1	+1

From Table 3.3 it can be seen that factor x_4 is aliasing with the $x_1\ x_2\ x_3$, while $x_1\ x_2$ is aliasing with $x_3\ x_4$, $x_1\ x_3$ is aliasing with $x_2\ x_4$ and $x_2\ x_3$ is aliasing with $x_1\ x_4$. Thus, if any 2-factor interaction column has a significant effect, it might be due to one or both of the aliased effects for that column. Since x_1x_2 was aliased with x_3x_4, analysis for these columns would give the same interaction values. The practical implication of x_1x_2 is aliased with x_3x_4 is that it is unable to determine if the interaction calculated for column x_1x_2 is due to x_1x_2, x_3x_4, or due to some combination of the two. Fortunately for industrial experiments, the effects of interactions are usually small relative to the effect of factors, thus providing justification of using the fractional factorial design [199]. In addition to that, not all fractional factorial designs result in the loss of all interaction parameters. It is,

however, unusual for an interaction to be important without one or both of the constituent factors being important.

Part 1

An 8-run fractional factorial design was conducted with 5 replicates of each run. The results are summarised in Table 3.4.

Table 3.4 Experimental data for alkali treatment of untreated hemp fibres.

Run No.	NaOH Conc. (wt%)	Na_2SO_3 Conc. (wt%)	Time (min)	Temp. (^oC)	Exp. Value of the Replicate Fibre TS (MPa)	Avg. Exp. TS (MPa)	STD (MPa)
1	15	0	120	30	440, 331, 470, 384, 375	400	61.49
2	15	0	360	60	258, 308, 427, 341, 422	351	73.17
3	15	2	120	60	312, 477, 411, 370, 402	394	60.29
4	15	2	360	30	239, 248, 201, 376, 252	263	66.21
5	20	0	120	60	309, 216, 231, 272, 179	241	50.38
6	20	0	360	30	208, 93, 114, 165, 139	144	44.89
7	20	2	120	30	279, 208, 298, 332, 222	268	52.04
8	20	2	360	60	211, 96, 127, 141, 104	136	45.70

In order to determine the important and trivial factors as well as interactions, two approaches could be applied as described in the literatures, namely (1) a graphical approach [199] and (2) analysis of variances (ANOVA)/sample variances [200]. In this study the graphical approach was used as described below.

The Graphical Approach

The purpose of the graphical approach was to derive a prediction equation, which could be used to (a) estimate the untested combinations (b) predict a target value, and (c) complete sensitivity analysis and tolerance design. The detailed procedure involved with the following analyses steps.

Step (1): As can be seen from Table 3.4 run numbers 1 and 3 are the highest desirable fibre TSs. For the design in Table 3.4, NaOH concentration was at the low setting of 15 wt% for run number 1 to 4. At that concentration there were twenty TS readings. The average of these twenty readings was found to be 352 MPa. Similarly, when the NaOH concentration was at the higher setting of 20 wt%, the average readings was found to be 197 MPa. The difference (average at the high minus average at the low) between these two averages was found at -155 MPa. This difference was defined as the effect of NaOH concentration factor. On average, it was estimated that changing the NaOH concentration from 15 to 20

wt% during alkali fibre treatment, decreased the single fibre TS by 155 MPa. Analysis of the time column, Table 3.4, gave an average of 326 MPa when the time was set at 120 minutes (low) and 223 MPa when the time was set at 360 minutes (high). The estimated effect for time was found at -102 MPa. Comparing the effect of NaOH concentration with the effect of time indicated that the NaOH concentration factor appeared to be about 1.5 times more important than time in effecting single fibre TS over the tested levels. The detail procedure of calculations of responses effects and half effects can be found in the literature [199]. The average fibre TSs (response), effects, and half effects for the applicable factors (x_1 to x_4) and interactions (x_1x_2, x_1x_3, and x_2x_3) were calculated at each level for each column and are given in Table 3.5.

Table 3.5 Effects of the factors and interactions on fibre TS.

Coded Factors/Interactions	Avg TS at Low (Mpa)	Avg TS at High (MPa)	Effect , Δ (MPa)	Half Effect, Δ/2 (MPa)
x_1 (NaOH Conc.)	352	197	-155	-77.5
x_2 (Na_2SO_3 Conc.)	284	265	-19	-9.5
x_3 (Time)	326	223	-102	-51.0
x_4 (Temperature)	269	280	12	6.0
x_1x_2	260	289	28	14.0
x_1x_3	281	268	-12	-6.0
x_2x_3	289	260	-29	-14.5

Step (2): Figure 3.5 is the graphical presentation of the average TS for each factor and interaction. It reveals the relative importance of all of the effects (factors and interactions).

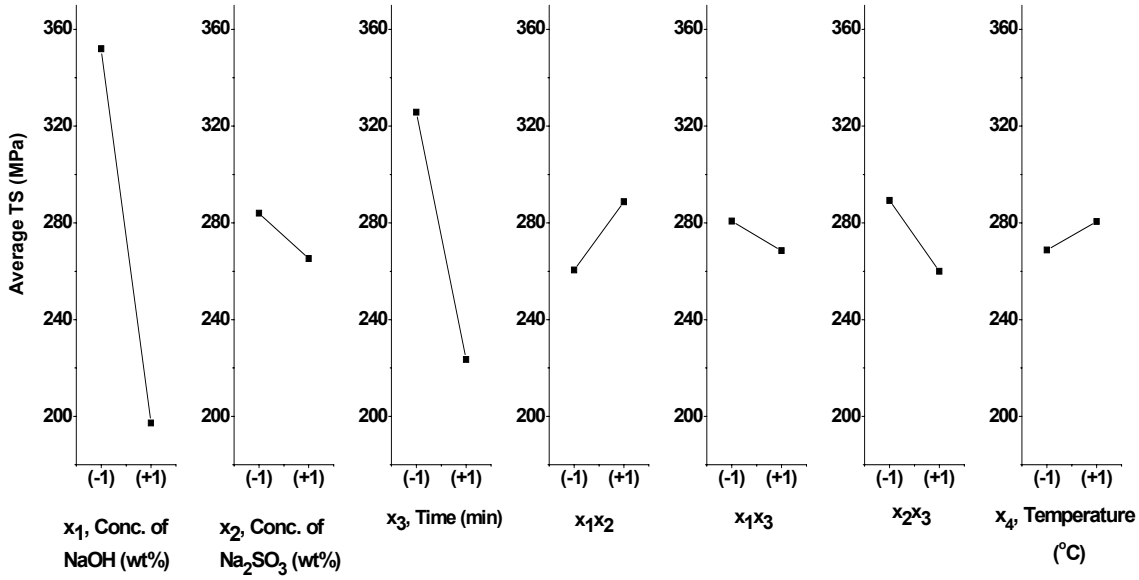

Figure 3.5 Plot of the average TS (responses) for each effect (factor and interaction).

Figures 3.6, 3.7, and 3.8 show the graphical representation of the interactions of concentration of NaOH with concentration of Na_2SO_3 (x_1x_2), concentration of NaOH with time (x_1x_3), and concentration of Na_2SO_3 with time (x_2x_3), respectively. Figure 3.6 shows that the effect of NaOH concentration at both Na_2SO_3 concentrations is negative. The Na_2SO_3 concentration lines intersect each other within the range of two NaOH concentration levels under investigation. The point of intersection is almost at the end of the two NaOH concentration levels and therefore, the interaction parameter between NaOH concentrations and Na_2SO_3 concentrations at the levels under investigation could be insignificant. Similarly, from Figure 3.7, (it can be seen that) the time lines do not intersect each other within the range of two NaOH concentration levels under investigation and from Figure 3.8, (it can be seen that) the time lines do not intersect each other within the range of two Na_2SO_3 concentration levels under investigation. Therefore, the interaction parameter between NaOH concentrations and times, Figure 3.7, and Na_2SO_3 concentrations and times, Figure 3.8, at the levels under investigation could be insignificant.

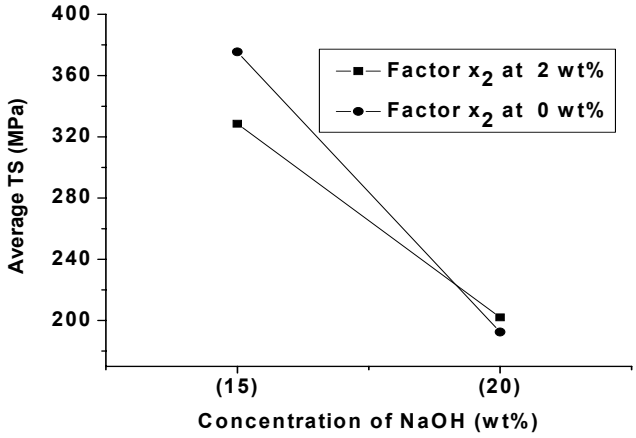

Figure 3.6 Average TS for the interaction of concentrations of NaOH and Na_2SO_3.

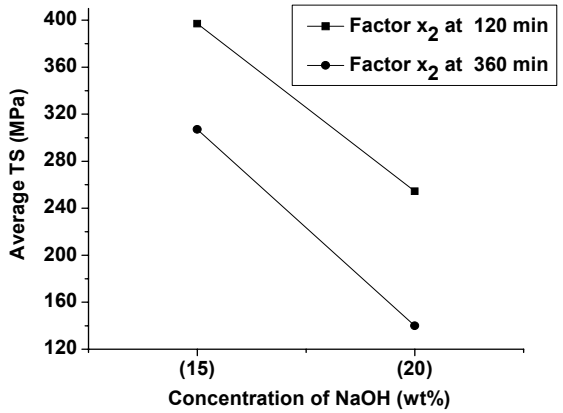

Figure 3.7 Average TS for the interaction of concentration of NaOH and Time.

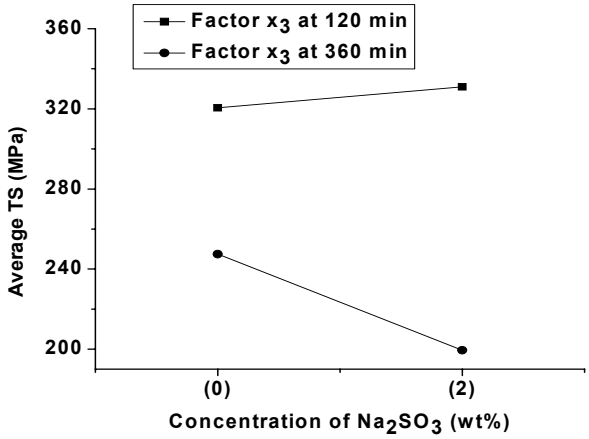

Figure 3.8 Average TS for the interaction of concentration of Na_2SO_3 and Time.

Step (3): From the half effect the following prediction equation can be derived as described in literature [199]:

$$\hat{y} = \bar{y} + (\Delta_{x_1}/2)x_1 + (\Delta_{x_2}/2)x_2 + (\Delta_{x_3}/2)x_3 + (\Delta_{x_4}/2)x_4 + (\Delta_{x_1x_2}/2)x_1x_2 + (\Delta_{x_1x_3}/2)x_1x_3 + (\Delta_{x_2x_3}/2)x_2x_3 \quad (3.3)$$

here $\bar{y}$ is the average TS of all the eight runs, $\Delta_{x_1}/2$ is the half effect for the NaOH concentration, $\Delta_{x_2}/2$ is the half effect for Na_2SO_3 concentration, $\Delta_{x_3}/2$ is the half effect for digestion time, $\Delta_{x_4}/2$ is the half effect for treatment temperature, $\Delta_{x_1x_2}/2$ is the half effect for the interaction between NaOH and Na_2SO_3 concentration, $(\Delta_{x_1x_3}/2)$ is the half effect for the interaction between NaOH concentration and digestion time, and $(\Delta_{x_2x_3}/2)$ is the half effect for the interaction between Na_2SO_3 concentration and digestion time.

By putting the values of half effects Equation (3.3) gets the form:

$$\hat{y} = 275 - 77.5x_1 - 9.5x_2 - 51x_3 + 6x_4 + 14x_1x_2 - 6x_1x_3 - 14.5x_2x_3 \quad (3.4)$$

Step (4): The Pareto chart generated from the absolute value (average TS) of half effects for each factor and interaction is shown in Figure 3.9.

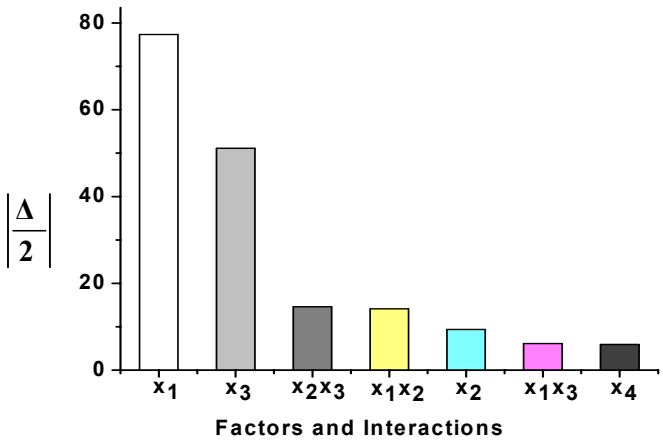

Figure 3.9 Pareto chart for the half effects of each factor and interaction.

Step (5): On the basis of the above Pareto chart, it was decided that the factors x_1 and x_3 were important.

Step (6): Therefore, from the above analysis the following prediction equation can be derived:

$$\hat{y} = 275 - 77.5x_1 - 51x_3 \qquad (3.5)$$

Although the coded factors x_2 and x_4 are missing in the equation, and also all the interaction terms are ignored, this equation is valid for coded-factor ranges x_i ε (-1, 1) for i = 1, 2, 3, 4 i.e. for real factor ranges f_1 () ε (15, 20), f_2 () ε (0, 2), f_3 (min) ε (120, 360), and f_4 (^{o}C) ε (30, 60).

This prediction equation could be used to (a) estimate the untested combinations in this fractional factorial design, (b) predict a target value, and (c) complete sensitivity analysis and tolerance design.

(a) The Estimation of Tensile Strength (TS) for Untested Combination of Treatment Factors

The prediction Equation (3.5) could be used to estimate the TS of fibre for an untested combination of factors. For example, the TS of fibres can be predicted which are treated under the following conditions: f_1 = 16, f_2 = 1.5, f_3 = 200 min and f_4 = 40^{o}C. The value of the actual factors is converted into coded values as defined by the Equation (3.2). Thus for the present case: x_1 = -0.6, x_2 = 0.5, x_3 = -0.33, and x_4 = -0.33. Using the coded values, the TS of the fibre estimated by the Equation (3.5) is 338 MPa.

(b) The Prediction of the Combination of Factors for a Target Value of Fibre Tensile Strength (TS)

The prediction Equation (3.5) could be used to select a number of combination of the factors for a given target value of the TS of the fibre. For example, say the target value is 370 MPa. The following experimental combination was taken to get the target value by using Equation (3.5). The coded values are: x_1 = -1 (taken), x_2 = -1 (any value taken), x_3 = -0.35 (calculated by using Equation (3.5)), and x_4 =

-1 (any value taken) and the corresponding real values are: $f_1 = 15$, $f_2 = 0$, $f_3 = 198$ min, and $f_4 = 30^oC$.

(c) Sensitivity Analysis and Tolerance Design [201, 202]

Experimental Verification

Experiments were conducted under the conditions as described in (a) and (b). The experimentally obtained fibre TS is shown in Table 3.6. The deviation of the experimental value from the predicted is calculated by the following equation: Percent (%) deviation = ((Experimental averaged value – predicted value)/predicted value)×100.

Table 3.6 Experimental verification of predicted/estimated fibre TS and treatment parameters.

NaOH Conc. (wt%)	Na_2SO_3 Conc. (wt%)	Time (min)	Temp. (^oC)	Exp. Fibre TS (MPa)	Avg Exp. Fibre TS (MPa)	Predicted Fibre TS (MPa)	Deviation (%)	Tolerance Limit (MPa)	Is the Limit Acceptable?
16	1.5	200	40	351, 297, 217, 402, 342	322	337.9	4.8	±32	Yes
15	0	198	30	501, 422, 436, 296, 378	407	370	10	±17	No

Here, the tolerance limit of experimental parameters in (a): $\Delta f_1 = \pm 0.5$, and $\Delta f_3 = \pm 40$ min corresponding to coded value of $\Delta x_1 = \pm 0.2$, and $\Delta x_3 = \pm 0.33$, respectively.

Such deviation in experimental condition would lead to a change in $y_{predicted}$ of Equation (3.5) as: $y + \Delta y = 275 - 77.5(x_1 + \Delta x_1) - 51(x_3 + \Delta x_3)$

$$|\Delta y|_{\max} = |77.5 \times \Delta x_1| + |51 \times \Delta x_3| = |77.5 \times 0.2| + |51 \times 0.33| = |32|$$

So, the predicted value varies from the experimental value (averaged) by ±32 MPa roughly. As the experimental value deviated from the predicted value, Table 3.6, within the permissible limit of ±32 MPa, the model was accepted.

The tolerance limit of experimental parameter in (b): $\Delta f_1 = \pm 0.00$, and $\Delta f_3 = \pm 39$ min corresponding to the coded values of $\Delta x_1 = \pm 0.00$, and $\Delta x_3 = \pm 0.325$, respectively.

Such deviation in experimental condition would lead to a change in $y_{predicted}$ of Equation (3.5) as: $y + \Delta y = 275 - 77.5(x_1 + \Delta x_1) - 51(x_3 + \Delta x_3)$

$$|\Delta y|_{\max} = |77.5 \times \Delta x_1| + |51 \times \Delta x_3| = |77.5 \times 0.00| + |51 \times 0.325| = |17|$$

So, the predicted value varies from the experimental value (averaged) by ±17 MPa roughly. Although the experimental value deviated from the predicted value, Table 3.6, above the permissible limit of ±17 MPa, the deviation of experimental value was only 10% above of the predicted value which could be within the margin of experimental error. Therefore, the model was accepted.

Step (8): As the objective was to maximize the TS, the best settings of the factors appeared to be x_1 and x_3 at low that means concentration of NaOH was at 15 wt% and digestion time was at 120 min. The predicted maximum TS would be 403 MPa. On the other hand, the predicted minimum TS at 20 wt% NaOH concentration and 360 minutes digestion time would be 146 MPa.

Part 2

An 8-run fractional factorial design was conducted with 5 replicates of each run. The results are summarised in Table 3.7.

Table 3.7 Experimental data for alkali treatment of untreated hemp fibres.

Run No.	NaOH Conc. (wt%)	Na_2SO_3 Conc. (wt%)	Time (min.)	Temp. (^oC)	Exp. Value of the Replicate Fibre TS (MPa)	Avg Fibre TS (MPa)	STD (MPa)
1	5	0	30	120	572, 510, 400, 542, 385	482	84.58
2	5	0	60	180	375, 181, 245, 148, 206	231	87.96
3	5	2	30	180	285, 205, 363, 390, 167	282	96.68
4	5	2	60	120	366, 401, 578, 509,460	463	84.56
5	10	0	30	180	278, 168, 139, 231, 110	185	68.55
6	10	0	60	120	359, 397, 183, 393, 206	308	104.61
7	10	2	30	120	450, 634, 624, 398, 499	521	104.92
8	10	2	60	180	95, 177, 103, 90, 234	140	63.44

In order to determine important and trivial factors as well as interactions, a graphical approach was used and is described below.

The Graphical Approach [199]

Step (1): As can be seen from Table 3.7 run numbers 1 and 7 are the highest desirable fibre TSs. The average TS (response), effects, and half effects for the applicable factors (x_1 to x_4) and interactions (x_1x_2, x_1x_3, and x_2x_3) are given in Table 3.8.

Table 3.8 Effects of the factors and interactions on fibre TS.

Factors/Interactions	Avg Fibre TS at Low (MPa)	Avg Fibre TS at High (MPa)	Effect, Δ (MPa)	Half Effect, Δ/2 (MPa)
x_1	364.50	288.5	-76.0	-38.0
x_2	301.50	351.5	50.0	25.0
x_3	367.50	285.5	-82.0	-41.0
x_4	443.50	209.5	-234.0	-117.0
x_1x_2	309.50	343.5	34.0	17.0
x_1x_3	350.0	303.0	-47.0	-23.5
x_2x_3	335.50	317.5	-18.0	-9.0

Step (2): Figure 3.10 is the graphical presentation of the average TSs. It reveals the relative importance of all of the effects (factors and interactions).

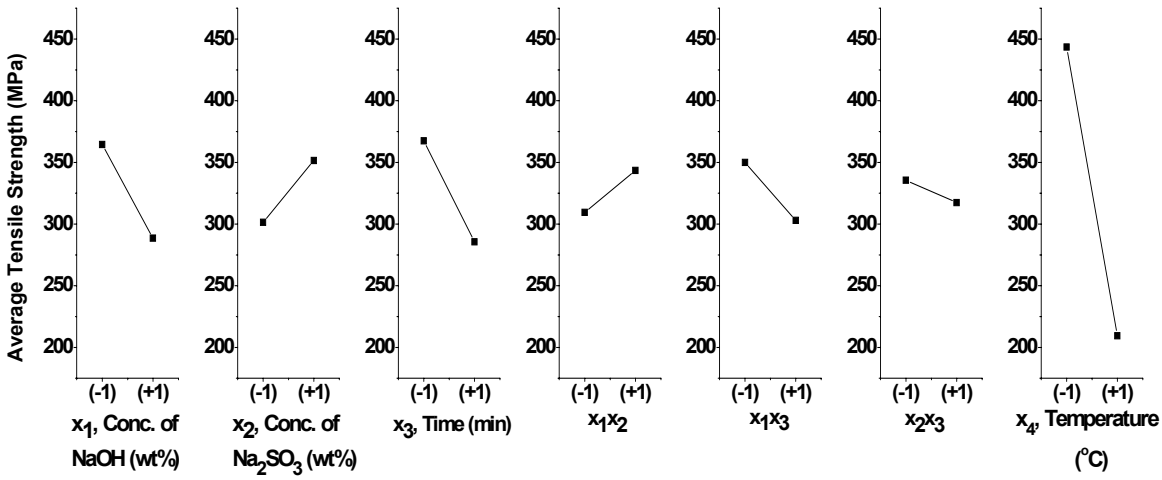

Figure 3.10 Plot of the average TS (responses) for each effect (factor and interaction).

Figures 3.11, 3.12, and 3.13 show the graphical representation of the interactions of concentration of NaOH with concentration of Na_2SO_3 [x_1x_2], concentration of NaOH with time [x_1x_3], and concentration of Na_2SO_3 with time [x_2x_3], respectively. Figure 3.11 shows that the effect of NaOH concentration at all the two Na_2SO_3 concentrations is negative. The Na_2SO_3 concentration lines do not intersect with each other within the range of two NaOH concentration levels under investigation. Therefore, the interaction parameter between NaOH concentrations and Na_2SO_3 concentrations at the levels under investigation could be insignificant. Similarly, from Figure 3.12, (it can be seen that) the time lines do not intersect each other within the range of two NaOH concentration levels under investigation and from Figure 3.13, (it can be seen that) the time lines do not intersect each other within the range of two Na_2SO_3 concentration levels under investigation. Therefore, the interaction parameter between NaOH concentrations and times, Figure 3.12, and Na_2SO_3 concentrations and times, Figure 3.13, at the levels under investigation could be insignificant.

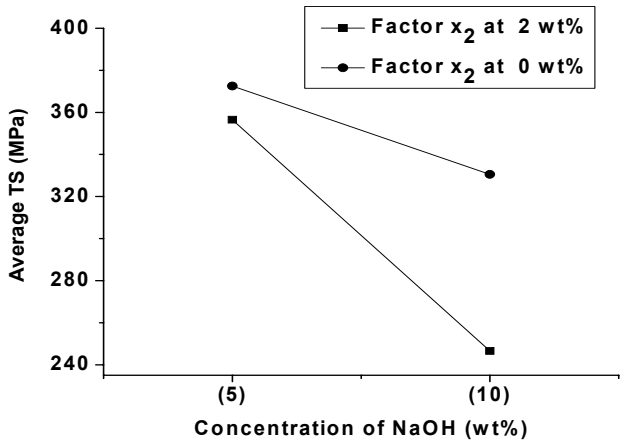

Figure 3.11 Average TS for the interaction of concentration of NaOH and Na_2SO_3.

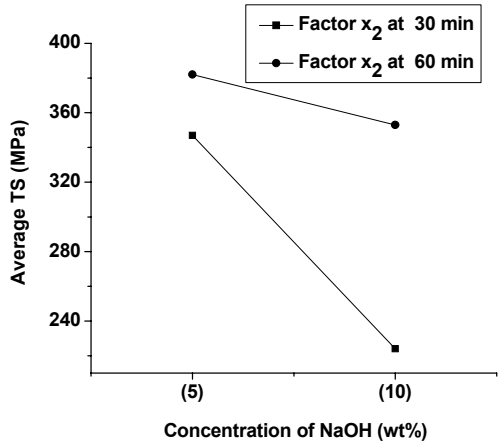

Figure 3.12 Average TS for the interaction of concentration of NaOH and Time.

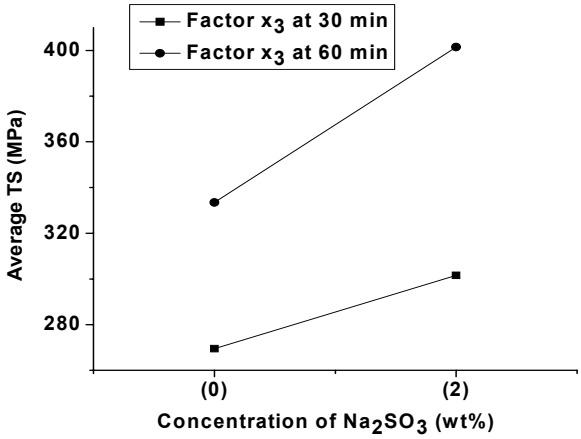

Figure 3.13 Average TS for the interaction of concentration of Na_2SO_3 and Time.

Step (3): From the half effect, the following prediction equation can be derived by using Equation (3.3).

$$\hat{y} = 326.5 - 38x_1 + 25x_2 - 41x_3 - 117x_4 + 17x_1x_2 - 23.5x_1x_3 - 9x_2x_3 \quad (3.6)$$

Step (4): The Pareto chart generated from the absolute value (average TS) of half effects for each factor and interaction is shown in Figure 3.14.

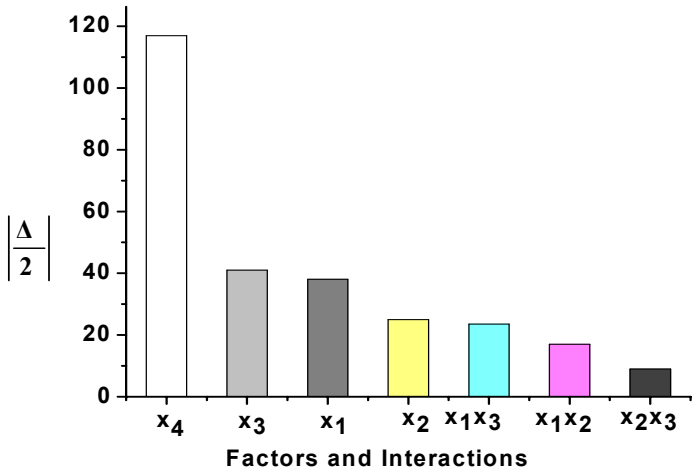

Figure 3.14 Pareto chart for the half effects (Δ/2) of each factor and interaction.

Step (5): On the basis of the above Pareto chart, it was decided that the factors x_1, x_2, x_3, and x_4 were important.

Step (6): Therefore, from the above analysis the following prediction equation can be derived:

$$\hat{y} = 326.5 - 38x_1 + 25x_2 - 41x_3 - 117x_4 \qquad (3.7)$$

Although the interaction terms are ignored, this equation is valid for coded-factor ranges x_i ε (-1, 1) for i = 1, 2, 3, 4 i.e. for real factor ranges f_1 (wt%) ε (5, 10), f_2 (wt%) ε (0, 2), f_3 (min) ε (30, 60), and f_4 (^{o}C) ε (120, 180).

This prediction equation was used to (a) estimate the untested combinations in this fractional factorial design (b) predict a target value and (c) complete sensitivity analysis and tolerance design.

(a) The Estimation of Untested Combination

The TS of the fibre under the following conditions: f_1 = 6 wt%, f_2 = 1.0 wt%, f_3 = 50 min, and f_4 = 140^{o}C was estimated. The value of the real factors was converted into coded values as defined by the Equation (3.2). Thus for the present case: x_1 = -0.6, x_2 = 0.0, x_3 = 0.33, and x_4 = -0.33. Using the coded values, the TS of the fibre

was estimated using the Equation (3.7). For this case the estimated fibre strength was 374 MPa.

(b) The Prediction of the Combination of Factors for a Target Value of Fibre TS

A target value of fibre strength was taken as 450 MPa. The following experimental combination was taken to get the target value by using Equation (3.7). The coded values are: x_1 = -1 (taken), x_2 = +1 (taken), x_3 = -0.48 (calculated by using Equation (3.7)), and x_4 = -1 (taken) and the corresponding real values are: f_1 = 5 wt%, f_2 = 2 wt%, f_3 = 37.8 min, and f_4 = 120°C.

(c) Sensitivity Analysis and Tolerance Design [201, 202]

Experimental Verification

Experiments were conducted under the conditions as described in (a) and (b). The experimentally obtained fibre TS is shown in Table 3.9.

Table 3.9 Experimental verification of predicted/estimated fibre strength and treatment parameters.

NaOH Conc. (wt%)	Na_2SO_3 Conc. (wt%)	Time (min)	Temp. (°C)	Exp. Fibre TS (MPa)	Avg Exp. Fibre TS (MPa)	Predic-ted Fibre TS (MPa)	Deviati-on (%)	Tolera-nce Limit (MPa)	Is the Limit Accep-table?
6	1.5	50	140	409, 311, 277, 361, 467	365	374	5.7	±86	Yes
5	2	1.35	120	306, 488, 349, 539, 431	423	450	6.1	±36	Yes

Here, the tolerance limit of experimental parameters in (a): $\Delta f_1 = \pm 0.5$ wt%, $\Delta f_2 = \pm 0.5$ wt%, $\Delta f_3 = \pm 10$ min and $\Delta f_4 = \pm 10\,^{o}$C corresponding to coded value of $\Delta x_1 = \pm 0.2$, $\Delta x_2 = \pm 0.5$, $\Delta x_3 = \pm 0.67$, and $\Delta x_4 = \pm 0.33$ respectively.

Such deviation in experimental condition would lead to a change in $y_{predicted}$ of Equation (3.7) as:

$$y + \Delta y = 326.5 - 38(x_1 + \Delta x_1) + 25(x_2 + \Delta x_2) - 41(x_3 + \Delta x_3) - 117(x_4 + \Delta x_4)$$

$$|\Delta y|_{\max} = |38 \times \Delta x_1| + |25 \times \Delta x_2| + |41 \times \Delta x_3| + |117 \times \Delta x_4|$$
$$= |38 \times 0.2| + |25 \times 0.5| + |41 \times 0.67| + |117 \times 0.33| = |86|$$

So, the predicted value varies from the experimental value (averaged) by ±86 MPa roughly. As the experimental value deviated from the predicted value, Table 3.9, within the permissible limit of ±86 MPa, the model was accepted.

The tolerance limit of experimental parameter in (b): $\Delta f_1 = \pm 0.00$ wt%, $\Delta f_2 = \pm 1.0$ wt%, $\Delta f_3 = \pm 3.9$ min and $\Delta f_4 = \pm 0.00\,^{o}$C corresponding to coded value of $\Delta x_1 = \pm 0.00$, $\Delta x_2 = \pm 1.0$, $\Delta x_3 = \pm 0.26$, and $\Delta x_4 = \pm 0.00$ respectively.

Such deviation in experimental condition would lead to a change in $y_{predicted}$ of Equation (3.7) as:

$$y + \Delta y = 326.5 - 38(x_1 + \Delta x_1) + 25(x_2 + \Delta x_2) - 41(x_3 + \Delta x_3) - 117(x_4 + \Delta x_4)$$

$$|\Delta y|_{\max} = |38 \times \Delta x_1| + |25 \times \Delta x_2| + |41 \times \Delta x_3| + |117 \times \Delta x_4|$$
$$= |38 \times 0.00| + |25 \times 1.0| + |41 \times 0.26| + |117 \times 0.00| = |36|$$

So, the predicted value varies from the experimental value (averaged) by ±36 MPa roughly. As the experimental value deviated from the predicted value, Table 3.9, within the permissible limit of ±36 MPa, the model was accepted.

Step (7) As the objective was to maximize the TS, the best settings of the factors appeared to be x_1, x_3, and x_4 at low and x_2 at high that means concentration of NaOH was at 5 wt%, digestion time at 30 min, temperature at 120^{o}C and concentration of Na_2SO_3 at 2 wt%. The predicted maximum TS would be: 547.5 MPa. On the other hand, the predicted minimum TS (at 10 wt% NaOH concentration, 60 min digestion time, 180^{o}C treatment temperature, and 0 wt% Na_2SO_3 concentration) would be 155.5 MPa.

The accuracy (at a confidence level of 95%, α = 0.05) of the prediction of TS using the empirical model was quite satisfactory as the experimental TS of alkali treated fibre obtained was almost within the range of tolerance limit of the model.

For better prediction, one could carry out total factorial design or choose higher order regression analysis. Such approach, however, would require more number of experiments (more than twice of the number of the experiments require for the full factorial design compared to fractional factorial design), but the accuracy of the prediction would improve very little [199].

3.3.1.2 The Effects of Alkali Treatment on Tensile Strength (TS)

The results of alkali treated single fibre TS from Tables 3.4 and 3.7 are combined and shown in Table 3.10. It also includes the average Young's moduli and fibre diameters after different alkali treatments. Figures 3.15, 3.16, and 3.17 further illustrate the effects of NaOH concentration, treatment temperature and digestion time on the average fibre TS.

Table 3.10 Summary of the single fibre tensile test results for alkali treated hemp fibres.

Treatment Sample No.	Treatment Variables	TS (MPa)	YM (GPa)	Avg Fibre Diameter (μm)
--	Untreated	526±155	34.2±11.3	32.6±4.9
P_1E_1	15% NaOH, 120 min, 30°C	400±61	31.8±7.1	26.1±5.5
P_1E_2	15% NaOH, 360 min, 60°C	351±73	26.3±5.2	25.7±7.6
P_1E_3	15% NaOH, 2% Na_2SO_3, 120 min, 60°C	394±60	30.6±8.2	25.3±6.9
P_1E_4	15% NaOH, 2% Na_2SO_3, 360 min, 30°C	263±66	25.6±5.7	24.6±3.5
P_1E_5	20% NaOH, 120 min, 60°C	241±50	25.3±6.9	24.5±6.0
P_1E_6	20% NaOH, 360 min, 30°C	144±45	21.3±7.2	22.1±5.6
P_1E_7	20% NaOH, 2% Na_2SO_3, 120 min, 30°C	268±52	25.1±4.5	24.7±5.2
P_1E_8	20% NaOH, 2% Na_2SO_3, 360 min, 60°C	136±46	22.9±7.4	22.6±4.2
P_2E_1	5% NaOH, 30 min, 120°C	482±85	33.9±8.9	26.8±5.7
P_2E_2	5% NaOH, 60 min, 180°C	231±88	25.7±6.3	24.5±4.5
P_2E_3	5% NaOH, 2% Na_2SO_3, 30 min, 180°C	282±96	27.2±5.5	25.3±3.7
P_2E_4	5% NaOH, 2% Na_2SO_3, 60 min, 120°C	463±84	32.8±9.1	25.9±7.3
P_2E_5	10% NaOH, 30 min, 180°C	185±68	22.0±3.2	23.1±7.1
P_2E_6	10% NaOH, 60 min, 120°C	308±105	29.8±3.8	25.6±4.0
P_2E_7	10% NaOH, 2% Na_2SO_3, 30 min, 120°C	521±105	33.2±7.8	26.5±4.8
P_2E_8	10% NaOH, 2% Na_2SO_3, 60 min, 180°C	140±63	21.7±6.9	22.4±6.8

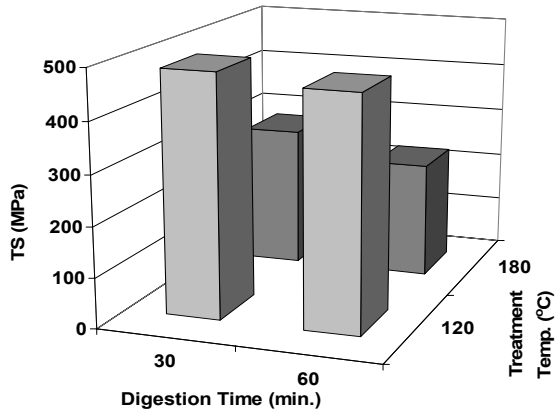

Figure 3.15 Effect of treatment temperature and digestion time on the TS of 5 wt% NaOH treated hemp fibres.

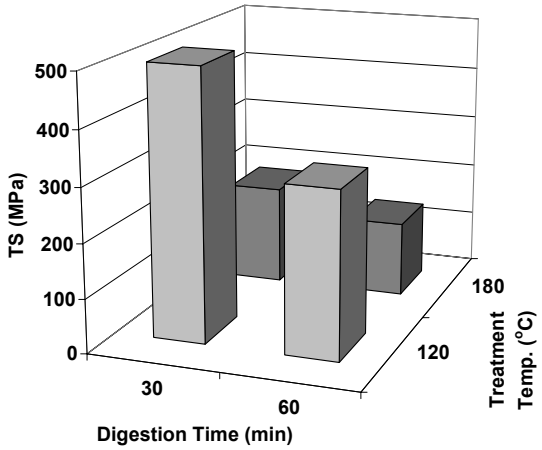

Figure 3.16 Effect of treatment temperature and digestion time on the TS of 10 wt% NaOH treated hemp fibres.

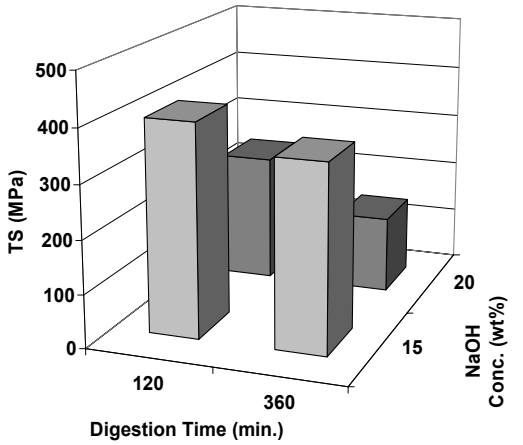

Figure 3.17 Effect of NaOH concentration and digestion time on the TS of hemp fibres.

From these results, it can be seen that the alkali treatment which resulted in the strongest fibre was treatment P_2E_7, closely followed by treatment P_2E_1 and P_2E_4.

These three alkali treatments were probably the mildest of the sixteen treatments used. When compared to the TS of the control (untreated fibre), it can be seen that alkali treatment resulted in almost similar fibre TS from treatment P_2E_7, and decreased fibre TSs from treatments P_2E_1 and P_2E_4. The process variable that most notably affected the fibre strength for 5 and 10 wt% NaOH treatments was the treatment temperature, Equation (3.7). For 5 wt% NaOH treatments, a 45% reduction in TS was observed when the temperature was increased from 120 to 180^{o}C. The reduction in strength was even more pronounced at a NaOH concentration of 10 wt%, and the fibre TS reduction for the temperature increase from 120 to 180^{o}C was about 60%. The large reductions in fibre TS experienced at 180^{o}C were expected, as cellulose starts to degrade at that temperature [32]. The process variable that most notably affected the fibre TS for 15 and 20 wt% NaOH treatments was the NaOH concentration, Equation (3.5). A reduction in fibre TS for the NaOH concentration increase from 15 to 20% was about 59% for the digestion time of 360 minutes and it was about 40% for the digestion time of 120 minutes, Figure 3.17. From the results in Table 3.10, it can also be seen that the alkali treatments reduced the fibre diameter of the treated fibres, and that fibre diameter reductions appeared to be related to the severity of the alkali treatment. This might be caused by the removal of the non-crystalline fibre constituents such as hemicelluloses, lignin, pectin, and cellulose microfibrils to some extent.

Alkali treatment P_2E_7 gave almost similar TS of untreated control fibre. This is likely to have been caused by the removal of non-strength contributing fibre surface components, which consequently would have led to a reduction in the average fibre cross-sectional area**.** The alkali treatment may also have led to a better packing of the cellulose microfibrils, a decrease in the microfibril spiral angle, and an increase in the molecular orientation of the cellulose chains [24]; all of which would have acted not to decrease the TS of the fibre for that particular treatment. For alkali treatment P_2E_1 and P_2E_4, the TS appeared to have decreased to a small extent due to removal of non-strength contributing component during alkali treatment, and due to weakening of the cellulose fibres. For other alkali treatments, the TS was found to be reduced and the reduction was proportional to the degree of harshness of the alkali treatment. The TS reductions indicate that the cellulose had been degraded or the fibre structure disrupted and the fibres had been significantly weakened.

3.3.1.3 The Effects of Alkali Treatment on Young's Modulus (YM)

The Young's moduli of the alkali treated hemp fibres are shown in Table 3.10. The effects of fibre treatment temperature and digestion time on the average fibre YM are further illustrated in Figures 3.18, 3.19, and 3.20. From the results, it can be seen that the average fibre YM of treatment P_2E_1, P_2E_4, and P_2E_7 are slightly lower than that of the control (untreated fibre). For other alkali treatments the reduction of fibre YM compared to the untreated control was notable and it seemed to decrease with the increase of the severity of the alkali treatment processes. Generally, it can be said that the fibre YM decreased with the increase of the removal of surface components such as hemicelluloses, lignin, and pectin. For alkali treatment P_2E_7, it can be seen that the removal of surface components slightly reduced the fibre YM. Lignin, hemicelluloses, and pectin are generally highly cross-linked and branched and keep the fibres in proper orientation and locations, and thus give structural integrity and rigidity in the cellulose fibres. Therefore, the removal of these components from fibre surface could lead to decrease in fibre YM.

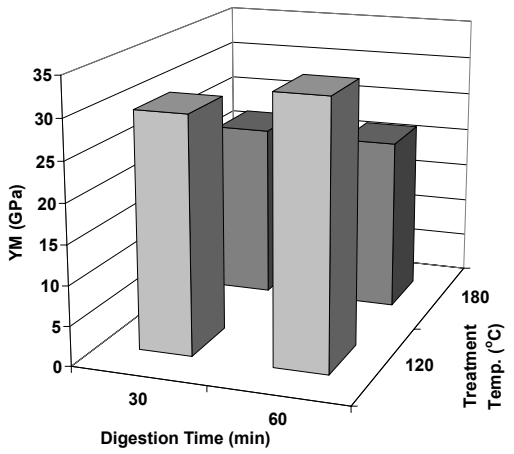

Figure 3.18 Effect of treatment temperature and digestion time on the YM of 10 wt% NaOH treated hemp fibres.

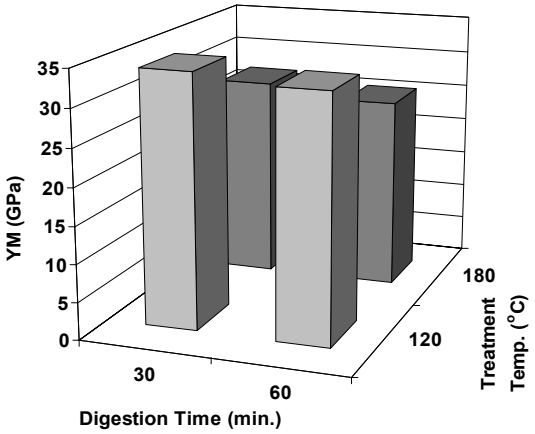

Figure 3.19 Effect of treatment temperature and digestion time on the YM of 5 wt% NaOH treated hemp fibres.

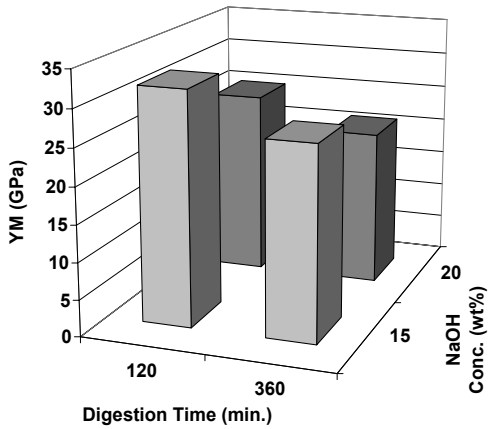

Figure 3.20 Effect of NaOH concentration and digestion time on the YM of hemp fibres.

3.3.1.4 The Effects of Fibre Diameter on Tensile Strength (TS) of the Alkali Treated Fibres

The purpose of this investigation was to determine if hemp fibre diameter had any influence on the fibre TSs. For P_2E_1, P_2E_4 and P_2E_7, Table 3.10, alkali treated hemp fibres, all fibres tested are plotted, Figures 3.21, 3.22, and 3.23, on a TS versus diameter scatter graph.

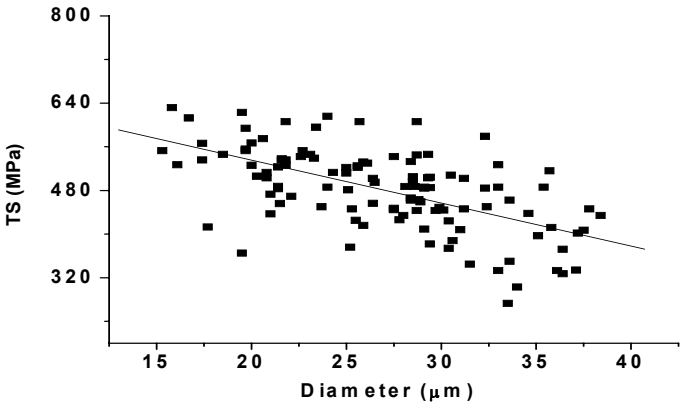

Figure 3.21 Influence of fibre diameter on the TS of P_2E_1 alkali treated hemp fibres.

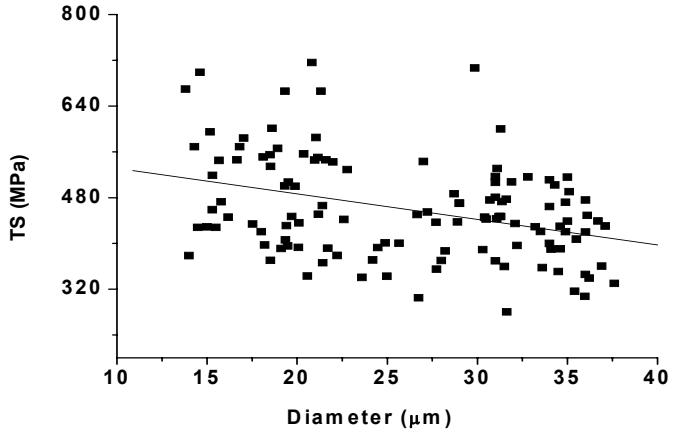

Figure 3.22 Influence of fibre diameter on the TS of P_2E_4 alkali treated hemp fibres.

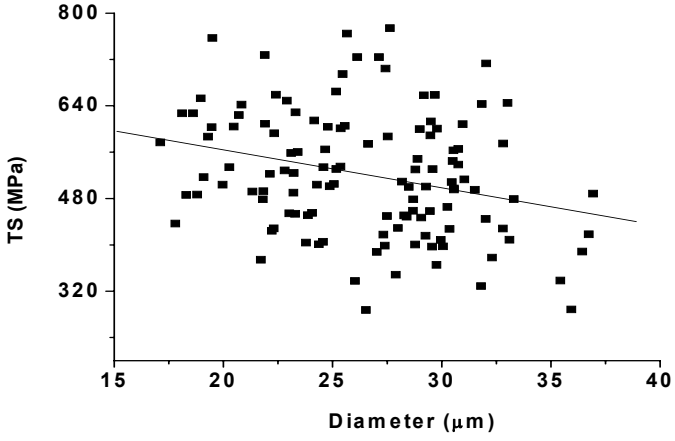

Figure 3.23 Influence of fibre diameter on the TS of P_2E_7 alkali treated hemp fibres.

From the trendlines of the plots in Figures 3.21 to 3.23, it can be seen that there is a general trend for the smaller diameter fibres to have higher TSs when compared to the larger diameter fibres. An explanation for the trend is that comparatively

larger fibres were slightly distorted and had elliptical, rather than circular cross-sectional shapes. It was found that distortion of the fibre cross-sections from circular to elliptical resulted in an increase of about 8% in cross-sectional area for the larger fibre diameters (in the range of about 25-33 μm). Since the TS was calculated with the assumption that the fibre cross sections were circular, the elliptical fibres would have been calculated as having a larger cross-sectional area than in reality. TS was calculated by dividing the tensile load by the fibre cross-sectional area, therefore, fibres with larger than actual cross-sectional areas would then result in lower calculated TSs.

However, it is possible that the reduction in TS with increased diameter could be due to the presence of larger amount of flaws for the higher diameter fibres. Natural fibres are grown with a large amount of flaws and imperfections in their structure. The presence of flaws and imperfections adversely affects the mechanical properties of the fibres [203]. It is reasonable that the number of flaws will increase in proportion with the fibre diameter and contribute to the decrease in fibre TSs [32, 204].

3.3.1.5 Scanning Electron Microscopic Evaluation of Alkali Treated Fibres

The SEM micrographs of untreated and alkali treated (treatment P_2E_1, P_2E_4, and P_2E_7) fibres are shown in Figures 3.24 to 3.27. From the micrographs, the fibre surfaces appeared to be covered with noncellulosic components in the case of untreated fibre, which was removed on alkali treatment to expose clean and rough surfaces which would be expected to be mainly cellulose. The rough surface morphology of the alkali treated fibre is expected to help attaining mechanical interlocking when used in composites and the clean surfaces are expected to provide direct bonding between the fibre cellulose and a matrix such as epoxy resin. Of the three alkali treated fibres, treatment P_2E_4 produced cleaner, and more separated fibres.

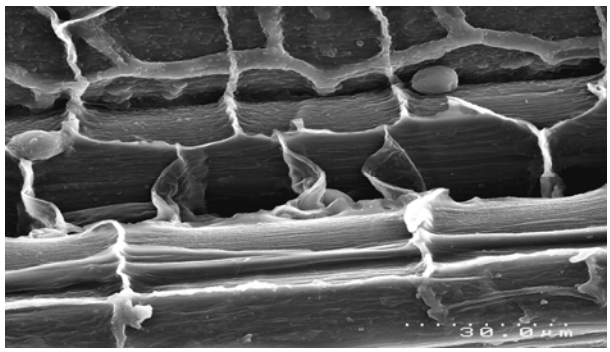

Figure 3.24 SEM of untreated hemp fibre.

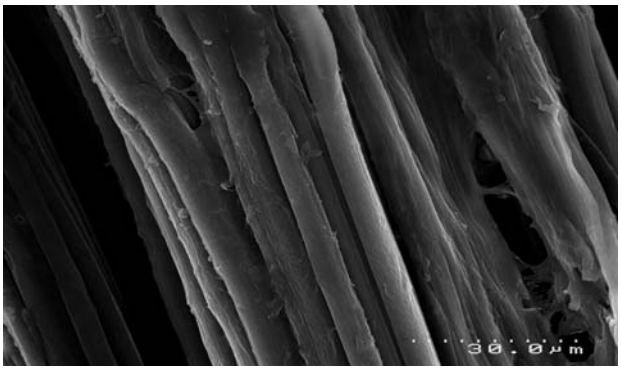

Figure 3.25 SEM of P_2E_1 alkali treated hemp fibre.

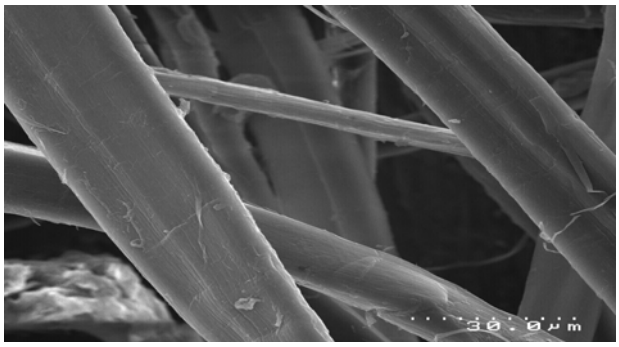

Figure 3.26 SEM of P_2E_4 alkali treated hemp fibre.

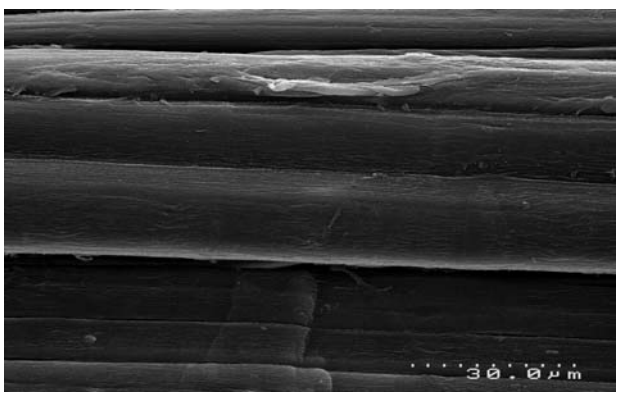

Figure 3.27 SEM of P_2E_7 alkali treated hemp fibre.

3.3.1.6 Zeta Potential

Figure 3.28 shows the pH dependence of zeta potential values of untreated and alkali treated (treatment P_2E_1, P_2E_4, and P_2E_7) fibres. It is evident from this figure that alkali treatment generally reduces the zeta potential. This might be caused by

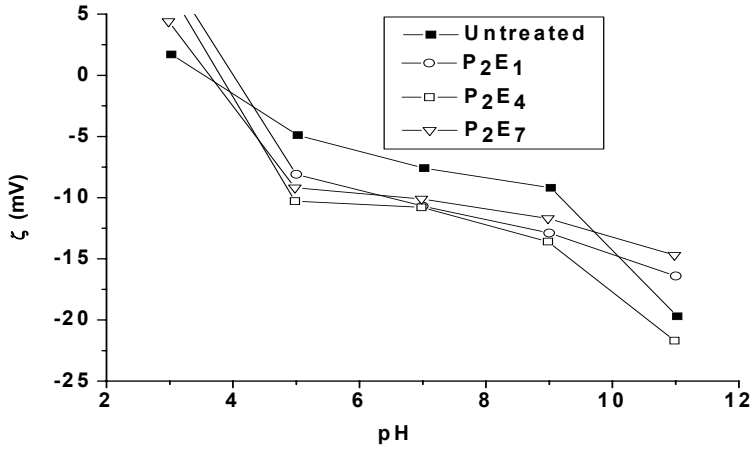

Figure 3.28 pH dependence of zeta potential of untreated and alkali treated fibres.

the increase in the accessibility of the dissociable functional groups in the fibre surface due to the removal of the waxy substances which obscure the fibre surface [182]. Table 3.11 shows the $\zeta_{plateau}$ value and IEP of the untreated and alkali treated (treatment P_2E_1, P_2E_4, and P_2E_7) fibres.

Table 3.11 $\zeta_{plateau}$ and IEP of untreated and alkali treated fibres.

Sample	IEP (pH) (ζ=0)	$\zeta_{plateau}$ (mV)
Untreated	3.5	-7.7
P_2E_1	3.7	-10.5
P_2E_4	3.8	-11.5
P_2E_7	3.6	-10.0

Considerably lower $\zeta_{plateau}$ values were observed for all three alkali fibre treatments compared to that for untreated fibre. The slight increase in the IEP by alkali treated fibres highlights the reduction of the acidity of the fibre surface and an enlargement of the double layer giving further evidence for increased -OH group exposure [188]. The enlargement of the double layer would also decrease the zeta potential of the solution as seen.

Among the three alkali fibre treatments the lowest $\zeta_{plateau}$ value of -11.5 mV and the highest IEP of 3.8 were observed for the fibres of alkali fibre treatment P_2E_4.

The trend of reduced $\zeta_{plateau}$ value and increased IEP were observed with the alkali treated fibres might be due to the exposure of more -OH and -COOH groups upon removal of the non-cellulosic fibre materials such as wax or lignin [205]. So, generally a reduction in $\zeta_{plateau}$ value and an increase in IEP can be seen with the intensity of the alkali treatment as follows: intensity: $P_2E_4 > P_2E_1 > P_2E_7$; $\zeta_{plateau}$: $P_2E_4 < P_2E_1 < P_2E_7$ and IEP: $P_2E_4 > P_2E_1 > P_2E_7$.

3.3.1.7 Wide Angle X-ray Diffraction (WAXRD)

As can be seen in Figure 3.29, the untreated and alkali treated (treatment P_2E_1, P_2E_4, and P_2E_7) fibres exhibit five main peaks at 2θ-angles of 15, 16.5, 22.5, 34.5 and 46.5^o corresponding to ($\bar{1}$ 0 1), ($\bar{1}$ 1 1), (0 0 2), ($\bar{2}$ 3 1) and ($\bar{4}$ 1 2) crystallographic planes of cellulose [206]. For the untreated fibre, the peaks at 15 and 16.5^o are merged, appearing more like one broad peak, which suggests

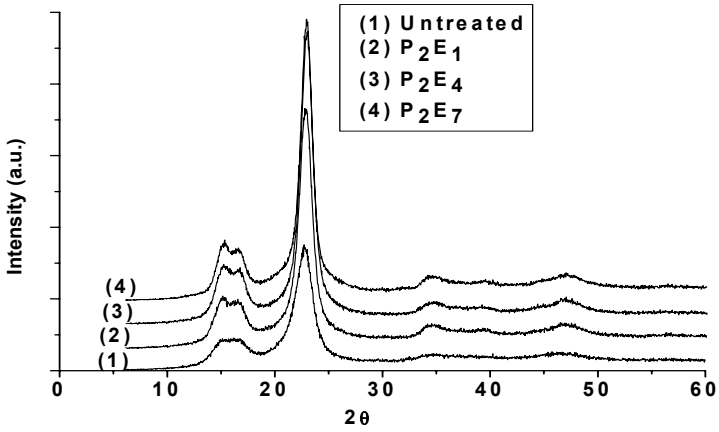

Figure 3.29 WAXRD pattern of untreated and alkali treated fibres.

the presence of a large amount of amorphous materials such as lignin, hemicelluloses and amorphous cellulose [177]. The two peaks are more separate in the case of all the three alkali treated fibres suggesting a higher cellulose content. Assessment of the relative amount of amorphous materials of the cellulosic fibres can be carried out by using a reference point away from the crystalline peaks. Commonly this is taken at a 2θ-angle of 18.5^o [198] As shown in Table 3.12, alkali treatment brings about an increase in the intensity values relating to amorphous materials (at a 2θ-angle of 18.5^o), as well as for all the

intensity values of the crystalline cellulose peaks, suggesting an increase in crystalline and amorphous cellulose. This would be expected simply due to removal of non-cellulosic materials such as waxes, lignin and hemicelluloses, as supported by the separation of the ($\bar{1}$ 0 1) and ($\bar{1}$ 1 1) peaks [207]. The increase of crystalline cellulose content during alkali treatment observed elsewhere, has been explained by removal of non-cellulosic materials enabling better packing of cellulose chains [171]. Harsher treatments have also been seen to reduce

Table 3.12 The crystallographic planes at various intensity (WAXRD counts) and 2θ-angles, and the crystallinity indices, *CrI* of untreated and alkali treated hemp fibres.

Sample	2θ (°)	WAXRD Counts	h k l	*CrI* (%)
Untreated	15	571	--	83.89
	16.5	566	$\bar{1}$ 1 1	
	18.5	370	Amorphous	
	22.5	2298	002	
	34.5	296	$\bar{2}$ 3 1	
	46.5	356	$\bar{4}$ 1 2	
P_2E_1	15	1090	--	91.09
	16.5	957	$\bar{1}$ 1 1	
	18.5	406	Amorphous	
	22.5	4557	002	
	34.5	478	$\bar{2}$ 3 1	
	46.5	475	$\bar{4}$ 1 2	
P_2E_4	15	1146	--	91.94
	16.5	1061	$\bar{1}$ 1 1	
	18.5	390	Amorphous	
	22.5	4842	002	
	34.5	450	$\bar{2}$ 3 1	
	46.5	506	$\bar{4}$ 1 2	
P_2E_7	15	1026	--	90.98
	16.5	922	$\bar{1}$ 1 1	
	18.5	393	Amorphous	
	22.5	4358	002	
	34.5	461	$\bar{2}$ 3 1	
	46.5	516	$\bar{4}$ 1 2	

cellulose crystallinity, due to the increased exposure of -OH groups which could increase the degree of swelling leading to the breakage of hydrogen bonds [177]. Here, the *CrI* was seen to increase, indicating an increase in the ratio of crystalline to amorphous cellulose, suggesting that the removal of non-cellulosic material and increased packing of cellulose chains outweighs any crystalline cellulose degradation that may be occurring for the treated fibres.

3.3.1.8 Differential Thermal Analysis/Thermogravimetric Analysis (DTA/TGA)

The DTA and TGA curves of untreated and alkali treated (treatment P_2E_1, P_2E_4, and P_2E_7) fibres are shown in Figures 3.30 and 3.31 respectively. The DTA curves, Figure 3.30 for untreated and all three alkali treated fibres show an

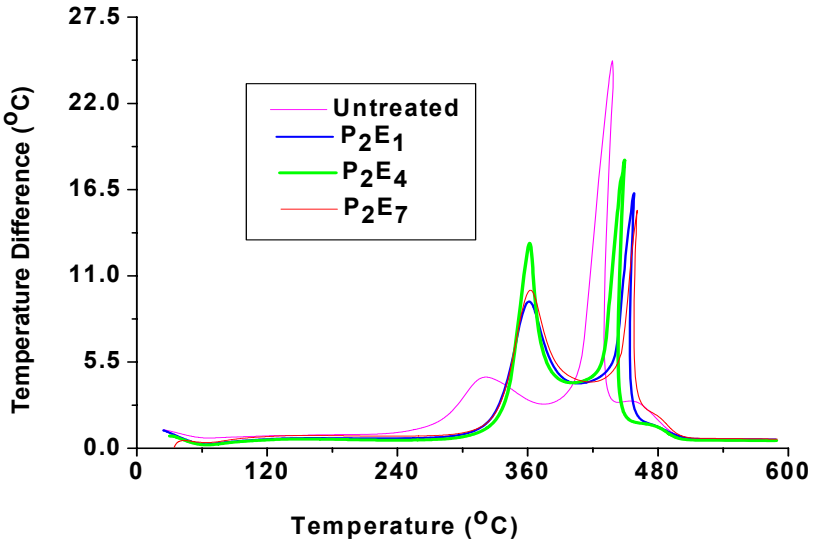

Figure 3.30 DTA curves for untreated and alkali treated fibres.

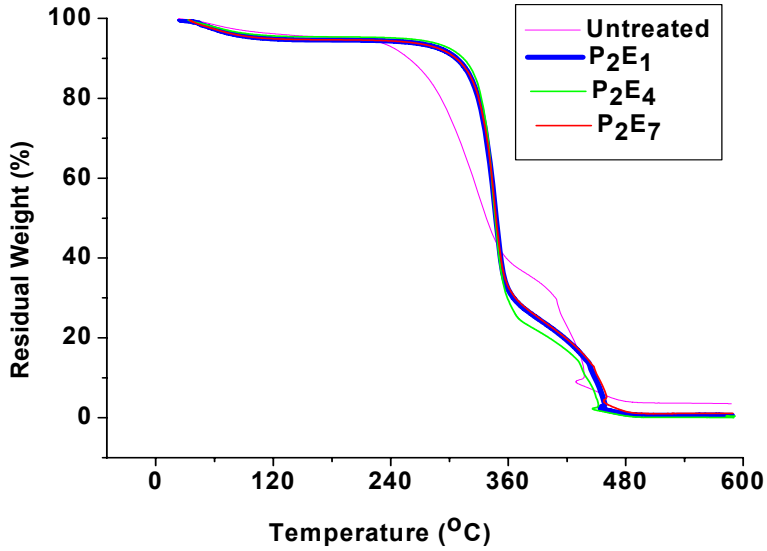

Figure 3.31 TGA curves for untreated and alkali treated fibres.

endotherm around 60°C due to the evolution of adsorbed moisture. At higher temperatures there are two exotherms. The first exotherm has a peak temperature

of about 318°C for untreated fibre and about 363°C for alkali treated fibres and is likely to be caused by the decomposition of cellulose leading to the formation of volatile products [208]. The second exotherm has a peak temperature of 436°C for untreated fibre and around 450 to 460°C for alkali treated fibres and is expected to be due to the oxidation of volatile and charred products. The increase in the first and second exothermic peak temperatures for alkali treated fibres indicates their greater thermal stability. The peak onset, peak, peak finishing temperatures and the nature of peaks for the untreated and alkali treated fibres obtained from DTA thermograms are shown in Table 3.13. The temperature at which percentage weight losses have occurred, Figure 3.31, can be seen to be consistently higher for alkali treated fibres compare to untreated fibres up to about 360°C and after that the converse is true, which may be due to stable lignocellulosic complex formed at higher temperature in the more lignin rich untreated fibres and shielding the fibre from weight loss above 360°C [209].

Table 3.13 The peak onset, peak and peak finishing temperatures of the endotherm and both exotherms for the untreated and alkali treated fibres obtained from DTA thermograms.

Sample	Peak Onset Temperature (°C)	Peak Temperature (°C)	Peak Finishing Temperature (°C)	Nature of Peak
Untreated	23.4	58.1	90.9	Endo
	225.8	318.3	374.8	Exo
	383.2	436.8	445.7	Exo
P_2E_1	28.9	62.3	96.7	Endo
	273.8	363.3	406.7	Exo
	420.3	458.4	472.5	Exo
P_2E_4	37.8	63.9	98.6	Endo
	283.1	363.5	396.8	Exo
	418.8	450.7	462.2	Exo
P_2E_7	30.9	60.2	94.8	Endo
	280.5	363.1	415.1	Exo
	423.5	460.6	469.8	Exo

For various stages of thermal degradation of fibres, the following equation of Broido [210] was used to determine the kinetic parameters:

$$\ln(\ln\frac{1}{y}) = -\frac{E_a}{RT} + \ln(\frac{RZ}{E_a\beta}T_m^2) \tag{3.8}$$

where y is the fraction of non-volatilised material yet to decompose, T_m is the peak temperature, β is the heating rate, Z is the frequency factor, E_a is the activation energy, and R is the universal gas constant. To evaluate E_a and Z (a constant

indicating the number of collisions required for reactions to occur) of untreated and alkali treated fibres the above equation of Broido [210] was used. Using the equation, plots of *ln[ln(1/y)]* versus 1/T (Broido plots) for second (first exothermic peak) and third (second exothermic peak) stages of thermal degradation were obtained for which examples are shown in Figures 3.32 and 3.33. Linear relations were found in each instance and the activation energy and frequency factors were calculated from the slopes and intercepts of these plots, respectively, and are given in Table 3.14. Activation energies (E_a) for the first and second exothermic peak for the untreated and alkali treated fibres show that the alkali treated fibres have greater values of activation energies and frequency

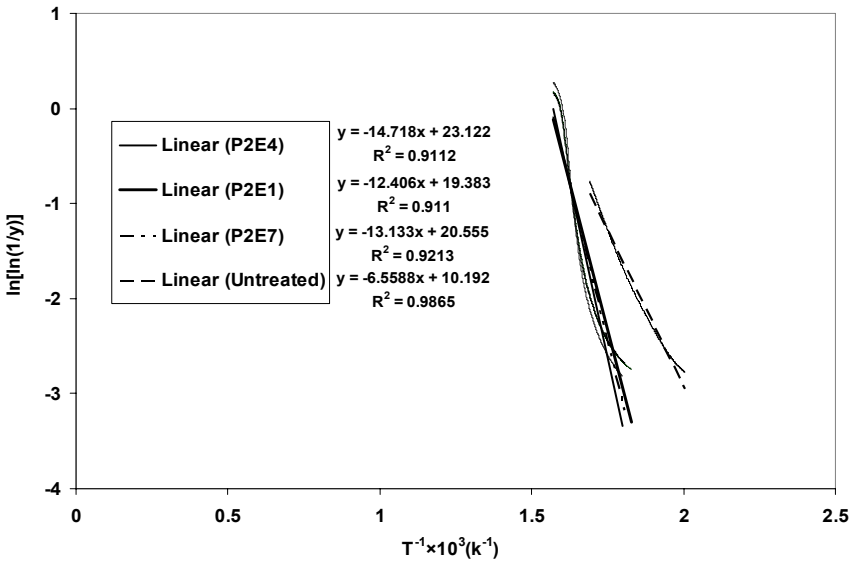

Figure 3.32 Plots of ln[ln(1/y)] versus $T^{-1}\times10^3$ K^{-1} for the second stage of thermal degradation for untreated and alkali treated fibres.

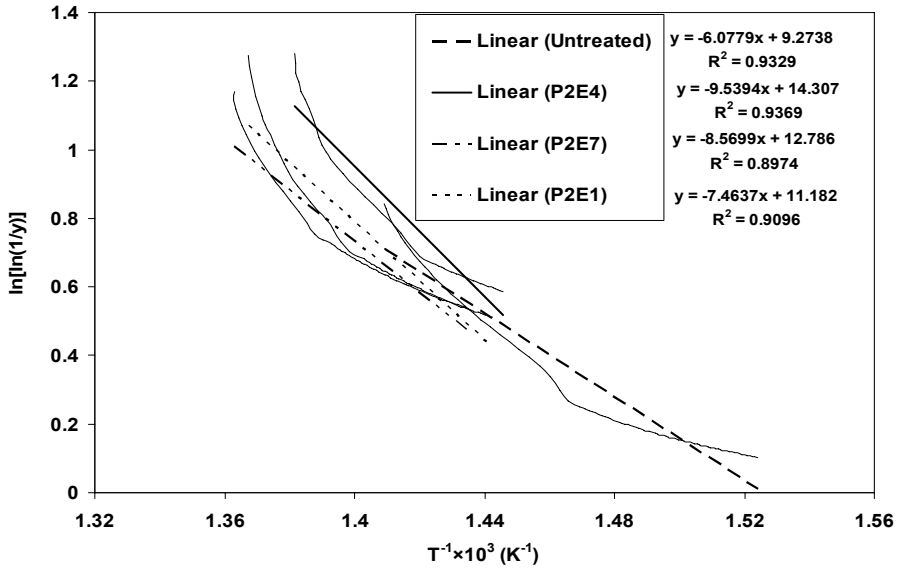

Figure 3.33 Plots of ln[ln(1/y)] versus $T^{-1}\times10^{3}$ K^{-1} for the third stage of thermal degradation for untreated and alkali treated fibres.

factors within the range of their respective first and second exothermic peaks. These greater values may be caused by an increase in crystalline cellulose by better packing of cellulose chains upon alkali treatment of fibres as discussed in section 3.3.1.7. Therefore, it can be inferred that alkali treated fibres appeared with slower reaction rate at their decomposition temperatures as well as shifted their peak temperature to a higher level than the untreated fibres. Removal of non-cellulosic impurities at a greater extent in case of alkali treated fibres compared to untreated fibres initiates less active sites and reduces the rate of thermal

Table 3.14 Activation energies and frequency factors obtained by Broido method for untreated and alkali treated fibres.

Sample	2nd Peak		3rd Peak	
	E_a (kJmol^{-1})	Z(s^{-1})	E_a (kJmol^{-1})	Z(s^{-1})
Untreated	54.53	8.34×10^{1}	50.53	2.14×10^{1}
P_2E_1	103.14	1.33×10^{6}	62.05	1.67×10^{2}
P_2E_4	122.36	6.66×10^{7}	79.31	4.96×10^{3}
P_2E_7	109.19	4.57×10^{6}	62.05	1.66×10^{2}

degradation according to Wielage *et al.* [211], and might be a cause of the increased activation energy and frequency factor. Alkali fibre treatment increased cellulose *CrI* compared to untreated fibres (as can be seen from WAXRD results in section 3.3.1.7) and therefore, might increase the activation energies and frequency factors. Shah *et al.* [212] reported that sodium hydroxide treatment of lignocellulosic fibres leads to the formation of a lignin–cellulose complex which

gives more stability to the fibre. Further, from the results it can be seen that among the three alkali fibre treatments, fibre treatment P_2E_4 appeared with the highest activation energy and frequency factor which could be due to comparatively better crystalline packing order for this alkali treatment (P_2E_4) than the other two alkali treatments (P_2E_1, P_2E_7) as is shown in WAXRD results in section 3.3.1.7.

3.3.1.9 Lignin Analysis

Lignin removal from natural fibres is important for long term usage of natural fibre reinforced polymer composites, as it degrades over time [65]. Lignin is amorphous in nature and forms a three dimensional network structure in natural fibre cell walls. Therefore, complete removal of lignin from fibre is not possible as it causes chain degradation due to rupture of covalent bonds [213]. It can be seen from Table 3.15 that alkali treatment removes lignin from hemp fibres and

Table 3.15 Cellulose, lignin, and ash contents of the untreated and alkali treated hemp fibres.

Sample	Cellulose (%)	Lignin (%)	Ash (%)
Untreated	63.3	4.5	2.6
P_2E_1	95.0	1.1	0.2
P_2E_4	96.7	0.3	0.2
P_2E_7	96.9	0.6	0.2

the alkali treatment that was performed with use of 2 wt% sodium sulfite (Na_2SO_3) along with alkali, removed more lignin than when no Na_2SO_3 was used. Na_2SO_3 is generally used with alkali during the production of pulp to soften the lignin in pulp and paper industry [78]. These results show that the degree of lignin removal depends on each of the process variables; namely NaOH concentration, Na_2SO_3 concentration, treatment temperature, and digestion time. Furthermore, from Table 3.15 it can be seen that alkali fibre treatment P_2E_4 has low lignin content, and alkali fibre treatment P_2E_7 has high cellulose content. Low lignin content with high cellulose content is attributed to low cellulose chain degradation during treatment. However, as shown previously (section 3.3.1.2) alkali fibre treatment P_2E_7 gave higher single fibre TS than that of alkali fibre treatment P_2E_4. The relatively higher single fibre TS of alkali fibre treatment P_2E_7 compared to alkali fibre treatment P_2E_4 may be due to slightly lower cellulose degradation of fibres of alkali fibre treatment P_2E_7. As cellulose is responsible for mechanical

strength of fibres, degradation of it to any extent would decrease the TS of P_2E_4 alkali treated fibres [36]. Again, as shown in section 3.3.1.3 the fibres of alkali fibre treatment P_2E_4 have a slightly lower YM compared to fibres of alkali fibre treatment P_2E_7 which supporting higher removal of lignin and other non-cellulosic surface components (e.g. hemicelluloses, pectin) by alkali fibre treatment P_2E_4 compared to alkali fibre treatment P_2E_7.

3.3.1.10 Fourier Transform Infrared (FTIR) Spectra

Figure 3.34 shows the FTIR spectra of untreated and alkali treated fibres (P_2E_1, P_2E_4, and P_2E_7) for which there is a summary of the most significant peaks in Table 3.16. For the untreated hemp fibres, peaks in the region of 3629-3796 cm^{-1} commonly related to stretching vibrations of -OH groups. These were found to shift slightly to 3619-3795 cm^{-1} for treated fibres, supporting the possibility of increased availability of -OH groups. Removal of hemicelluloses of alkali treated

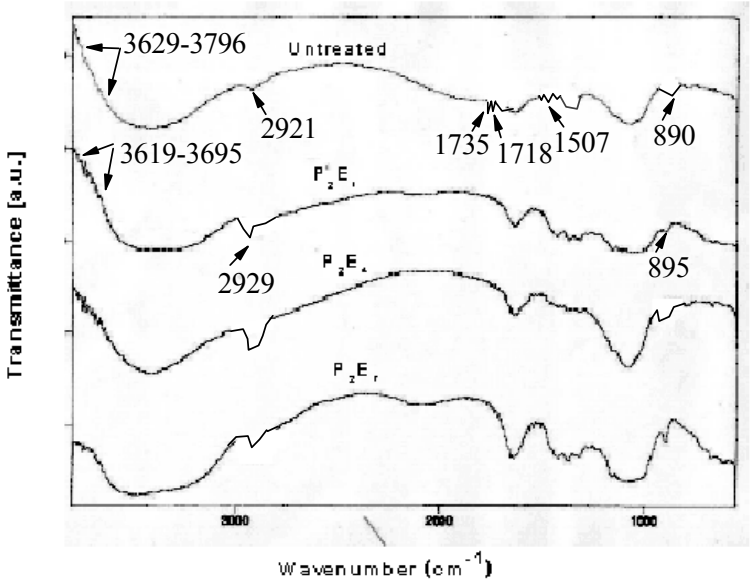

Figure 3.34 FTIR-spectra of untreated and alkali treated fibres.

Table 3.16 FTIR wavenumbers (cm^{-1}) of untreated and alkali treated fibres.

Wavenumber (cm^{-1})		Bond Description
Untreated	**Alkali Treated**	
3629-3796	3619-3795	O-H stretching relating to hydrogen bonding
2921	2929	C-H stretching vibration in cellulose and hemicelluloses
1735, 1718	1719, 1735	C=O stretching of carboxylic acid or ester
1654	1654	C=C stretching
1448-1534	1460, 1518, 1522	C-H bond in aromatic ring present in lignin component
1437	1438	CH_2 bending in lignin
1384	----	C-H bending
1070, 1152	1080	C-C stretching
890	895	C-H stretching for β glycosidic linkage

fibres is suggested by two sharp peaks at 1718 and 1735 cm^{-1} for untreated fibres which are likely to be due to the carbonyl (C=O) stretching vibration of carboxylic acid and ester groups present in hemicelluloses. These are found to be reduced in intensity for alkali treated fibres. Further evidence is provided by the reduction of the peak intensity and peak shift from 2921 cm^{-1} for untreated fibres to 2929 cm^{-1} for alkali treated fibres. Reduction in the peak intensities between 1448-1534 cm^{-1} especially for an intense peak at 1507 cm^{-1} associated with the bending of C-H bond in the aromatic ring present mostly in lignin compounds, suggests the removal of significant amount of lignin by alkali treatment. The peak at 890 cm^{-1} for untreated fibre is characteristic of the β-glycoside linkage between cellulose monosaccharides and undergoes a shift to 895 cm^{-1} with higher intensities for alkali treated fibres. This may be due to the rotation of the glucose residues around the β-glycosidic bonds which indicates the chemical modification of the alkali treated fibres as reported by other authors [207].

3.3.2 Characterisation of Acetylated Fibres

3.3.2.1 Scanning Electron Microscopy (SEM)

Figure 3.35 shows the scanning electron micrograph of acetylated hemp fibres. It can be seen that acetic anhydride treatment reduced the surface roughness of the alkali treated (treatment P_2E_4) fibre, Figure 3.26, to a small extent and made the surface cleaner. For the purpose of comparison, SEM macrograph for untreated fibre can also be seen in Figure 3.24 which was covered with non-cellulosic fibre components.

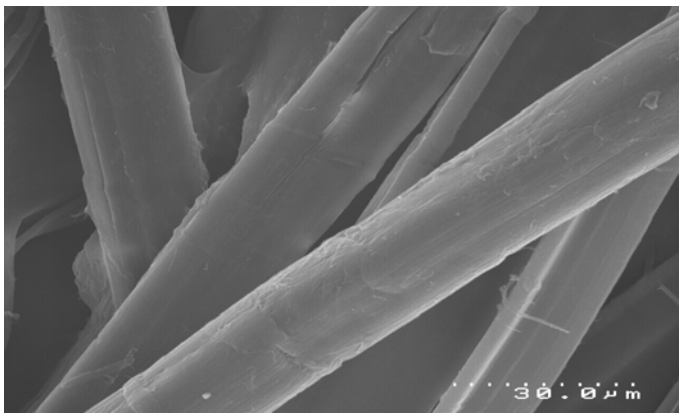

Figure 3.35 SEM of acetylated hemp fibre.

3.3.2.2 Zeta Potential

Figure 3.36 shows the pH dependence of zeta potential values of acetylated fibres compared to alkali treated (treatment P_2E_4) fibres. It is evident from this figure that acetic anhydride of fibres generally increases the zeta potential. This could be caused by the decrease in the accessibility of the dissociable functional groups in the fibre surface due to the substitution of -OH and -COOH groups by non-polar

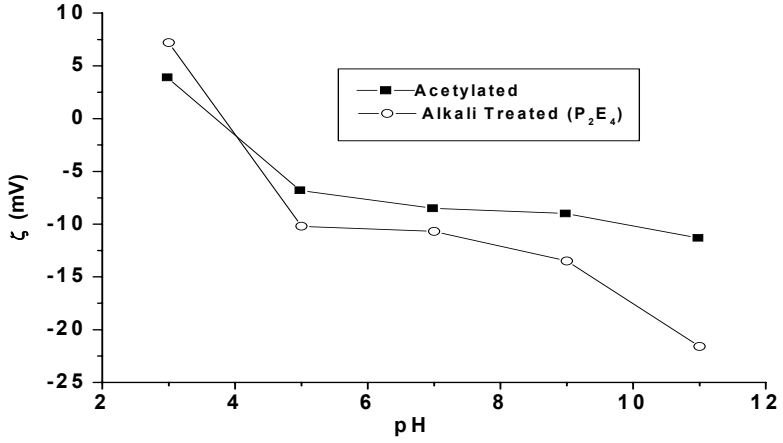

Figure 3.36 pH dependence of zeta potential of acetylated fibres compared to alkali treated fibres.

-$COCH_3$ groups which obscures the fibre surface [182]. The substitution of -OH and -COOH groups by non-polar -$COCH_3$ groups can be further evident from FTIR spectra discussed in section 3.3.2.5. Table 3.17 shows the $\zeta_{plateau}$ value and IEP of the acetylated and alkali treated (treatment P_2E_4) fibres.

A considerably higher $\zeta_{plateau}$ value was observed for acetylated fibre compared to alkali treated fibre. The slight decrease in the IEP by acetic anhydride treatment highlights the increase of the acidity of the fibre surface and a compaction of the double layer giving further evidence for decreased -OH group exposure [188]. The compaction of the double layer would also increase the zeta potential of the solution as seen.

Table 3.17 $\zeta_{plateau}$ and IEP of acetylated fibres compared to alkali treated fibres.

Sample	IEP (pH) (ζ=0)	$\zeta_{plateau}$ (mV)
Acetylated	3.5	-8.6
Alkali treated (P_2E_4)	3.8	-11.5

3.3.2.3 Thermal Analysis by Differential Thermal Analysis/ Thermogravimetric Analysis (DTA /TGA)

The DTA and TGA curves of acetylated fibres compared to alkali treated (treatment P_2E_4) fibres are shown in Figures 3.37 and 3.38 respectively. The DTA curves, Figure 3.37, for acetic anhydride treated and the alkali treated fibres show an endotherm around 60^{o}C due to the evolution of adsorbed moisture. At higher temperatures there are two exotherms. The first exotherm has a peak temperature of about 363^{o}C for both acetylated and alkali treated fibres and is likely to be caused by the decomposition of cellulose leading to the formation of volatile products [208]. The second exotherm has a peak temperature of about 450^{o}C for both acetylated and alkali treated fibres and is expected to be due to the

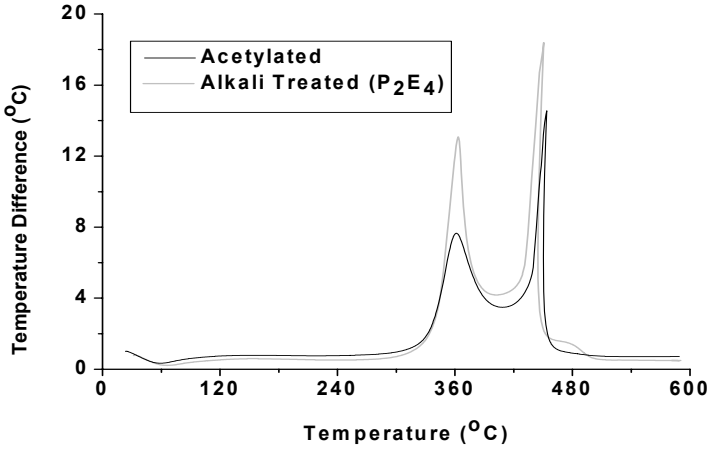

Figure 3.37 DTA curves for acetylated fibres compared to alkali treated fibres.

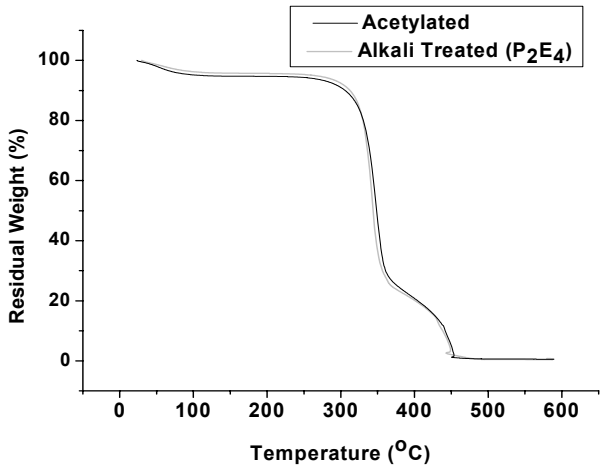

Figure 3.38 TGA curves for acetylated fibres compared to alkali treated fibres.

oxidation of volatile and charred products. The peak onset, peak, peak finishing temperatures and nature of peaks for the acetylated fibres compared to alkali treated fibres obtained from the DTA thermograms are shown in Table 3.18. From the results it can be seen that upon acetylation of alkali treated fibre the onset

Table 3.18 The peak onset, peak, peak finishing temperatures and nature of peaks for the acetylated fibres compared to alkali treated fibres obtained from the DTA thermograms.

Sample	Peak Onset Temperature (^0C)	Peak Temperature (^0C)	Peak Finishing Temperature (^0C)	Nature of Peak
Acetylated	29.2	61.8	89.7	Endo
	271.8	364.0	418.9	Exo
	420.7	453.2	467.2	Exo
Alkali treated (P_2E_4)	37.8	63.9	98.6	Endo
	283.1	363.5	396.8	Exo
	418.8	450.7	462.2	Exo

temperature for the first exothermic peak reduces from 283 to 271^{o}C and the onset temperature of second exothermic peak increases from 418 to 420^{o}C. The temperature at which percentage residual weights have occurred can be seen in Figure 3.38 and is shown to be slightly lower for acetylated fibres at the initial stages of thermal degradation and slightly higher at the later stages of thermal degradation when compared to alkali treated fibres. Therefore, it is clear from the results that acetylated fibres have slightly lower thermal stability at the initial stages and slightly higher thermal stability at the later stages of thermal degradation compared to alkali treated fibres.

The Broido method [210] was used to evaluate the activation energy (E_a) and frequency factor of acetylated fibres compared to alkali treated fibres. Using the Broido equation, plots of ln[ln(1/y)] versus 1/T (Broido plots) for second (first exothermic peak) and third (second exothermic peak) stages of thermal degradation were plotted for which examples are shown in Figures 3.39 and 3.40.

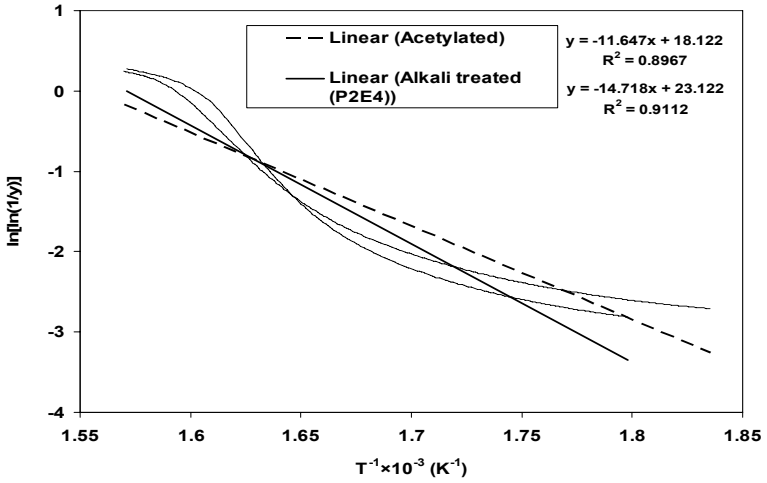

Figure 3.39 Plots of ln[ln(1/y)] versus $T^{-1}\times10^{3}$ K^{-1} for the second stage of thermal degradation (first exothermic peak) for acetylated fibres compared to alkali treated fibres.

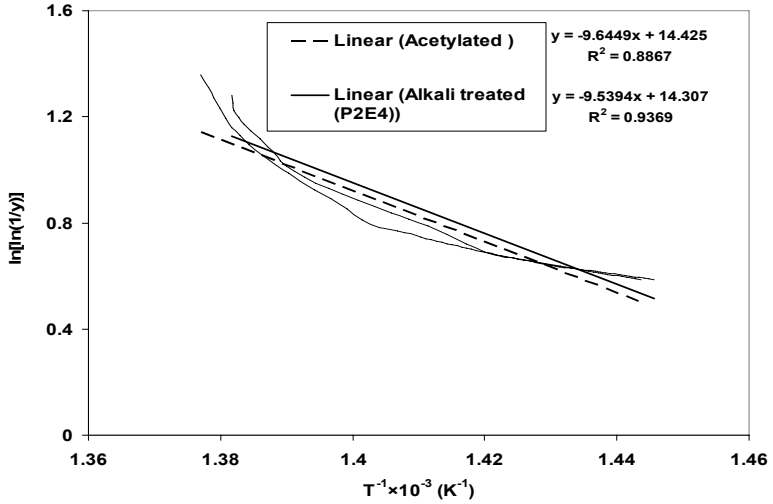

Figure 3.40 Plots of ln[ln(1/y)] versus $T^{-1}\times10^{3}$ K^{-1} for the third stage of thermal degradation (second exothermic peak) for acetylated fibres compared to alkali treated fibres.

The activation energies and frequency factors were calculated from the slopes and intercepts of these plots, respectively, and are given in Table 3.19. From the values of activation energies (E_a) and frequency factors for the first and second

exothermic peak of the fibres show that acetylated fibres appeared with lower values of activation energy (96.83 kJ/mol) and frequency factor (3.54×10^5 s^{-1}) for the first exothermic peak and almost similar activation energy and frequency factor for the second exothermic peak compared to alkali treated fibres. The decrease in activation energy and frequency factor for the first exothermic peaks of acetylated fibres does not conform with the increased cellulose crystallinity of this fibre. However, decrease in activation energy and frequency factor for the first exothermic peaks may be explained by the reduction in molecular regularity of the fibres by the introduction of acetyl groups in the fibre according to Rong *et al.* [86].

Table 3.19 Activation energies and frequency factors obtained by Broido method for acetylated fibres compared to alkali treated fibres.

Sample	2nd Peak		3rd Peak	
	E_a (kJmol^{-1})	Z(s^{-1})	E_a (kJmol^{-1})	Z(s^{-1})
Acetylated	96.83	3.54×10^5	80.19	5.59×10^3
Alkali Treated (P_2E_4)	122.36	6.66×10^7	79.31	4.96×10^3

3.3.2.4 Wide Angle X-ray Diffraction (WAXRD)

Figure 3.41 shows the WAXRD pattern of acetylated fibres compared to alkali treated (P_2E_4) fibres. From the figure it can be seen that acetic anhydride treatment of alkali treated fibre reduces the intensity of both amorphous materials and crystalline cellulose. However, it can be conferred that acetylation reduces the

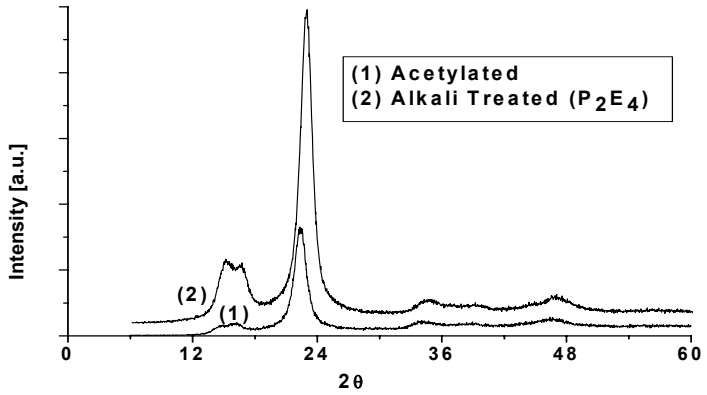

Figure 3.41 WAXRD pattern of acetylated fibres compared to alkali treated fibres.

intensity of amorphous materials comparatively more than crystalline cellulose and resulted in a slight increase in crystallinity index, Table 3.20. Zafeiropoulos *et al.* [4] reported that acetylation increased the crystallinity of fibres due to an increased removal of the fibre amorphous constituents during the treatment. Rong *et al.* [86] also found an increase in the crystallinity upon acetylation of fibres although addition of -$COCH_3$ group in cellulose might reduce molecular regularity. They explained that a small amount of -$COCH_3$ group usually softens the cellulose chains and thus facilitates the ordered rearrangement of the molecules through a chainfold conformation mechanism.

Table 3.20 The crystallographic planes at various intensity (WAXRD counts) and 2θ-angles, and the crystallinity indices of acetylated fibres compared to alkali treated fibres.

Sample	2θ (°)	WAXRD Counts	h k l	*CrI* (%)
Acetylated	15	198	--	92.93
	16.5	191	$\bar{1}$ 1 1	
	18.5	143	Amorphous	
	22.5	2024	002	
	34.5	248	$\bar{2}$ 3 1	
	46.5	317	$\bar{4}$ 1 2	
Alkali Treated (P_2E_4)	15	1146	--	91.94
	16.5	1061	$\bar{1}$ 1 1	
	18.5	390	Amorphous	
	22.5	4842	002	
	34.5	450	$\bar{2}$ 3 1	
	46.5	506	$\bar{4}$ 1 2	

3.3.2.5 Fourier Transform Infrared (FTIR) Spectra

It can be seen from Figure 3.42 that acetic anhydride treatment of hemp fibre led to the appearance or increment of transmittance in the regions 1735 – 1737 and 1162-1229 cm^{-1} [214-216]. The peak at around 1735 – 1737 cm^{-1} is due to the

esterification of the -OH groups that results in an increased stretching vibration of

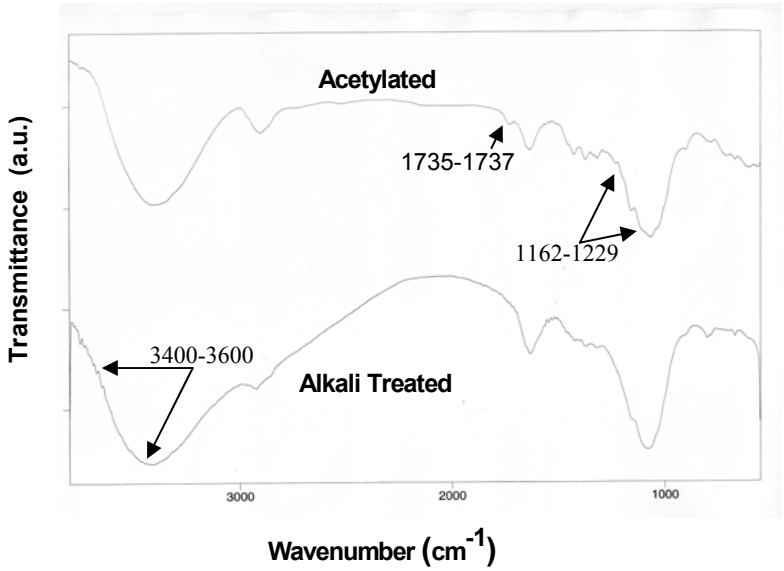

Figure 3.42 FTIR spectra of acetylated fibres compared to alkali treated fibres.

the C=O group present in the ester bonds. The band in the spectrum of untreated fibres, Figure 3.34, at 1735 cm^{-1} is assigned to the C=O stretching vibration of the -COOH and $-COCH_3$ groups of hemicelluloses and are found to be reduced in intensity for alkali treated fibres. The appearance of the peak in acetic anhydride treated fibres with high intensity indicates that the $-COCH_3$ groups are involved in an ester bond with the -OH groups of the fibres. If the $-COCH_3$ groups were in the form of acetic acid, then the stretching of C=O should have appeared below 1720 cm^{-1} in the case of diacids and at about 1760 cm^{-1} in the case of monoacids [216]. The esterification reaction is also confirmed by the appearance of new peaks at 1162-1229 cm^{-1}, attributed to C-O stretching of the ester -COOH group. The strong absorption between 3400 and 3600 cm^{-1} in all of the FTIR spectra is caused by the remaining OH groups of the alkali treated fibre constituents, Figure 3.42. As a result of esterification there is a reduction of this band shown in this Figure.

3.3.3 Characterisation of Silane Treated Fibres

3.3.3.1 Scanning Electron Microscopy (SEM)

Figure 3.43 shows the SEM micrographs of silane treated hemp fibre. It can be seen that silane treatment removed more non-cellulosic components from the

alkali treated (treatment P_2E_4) fibres, Figure 3.26. For the purpose of comparison SEM micrograph for untreated fibre can also be found in Figure 3.24.

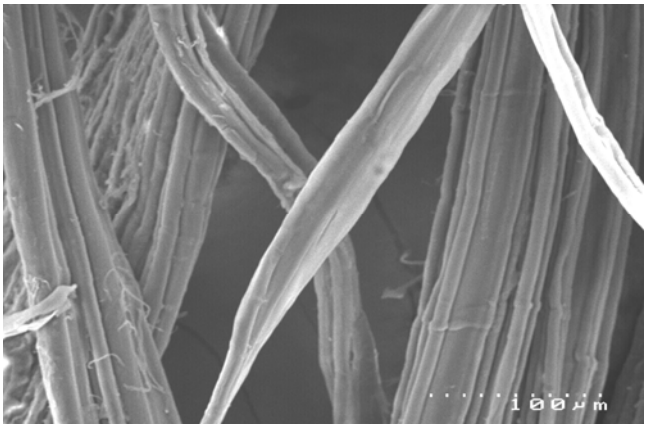

Figure 3.43 SEM of silane treated hemp fibre surface.

3.3.3.2 Zeta Potential

Figure 3.44 shows the pH dependence of zeta potential values of silane treated fibres compared to alkali treated (treatment P_2E_4) fibres. It is evident from this

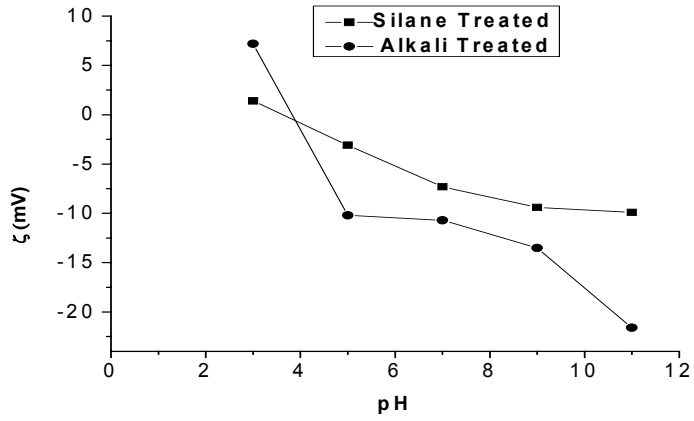

Figure 3.44 pH dependence of zeta potential of silane treated fibres compared to alkali treated fibres.

figure that silane treatment of fibres generally increases the zeta potential. This might be caused by the decrease in the accessibility of the dissociable functional groups in the fibre surface due to the substitution of -OH and -COOH groups by silane group with aromatic ring which obscures the fibre surface [182]. Table 3.21 shows the $\zeta_{plateau}$ value and IEP of the silane treated fibres compared to alkali treated (treatment P_2E_4) fibres.

Table 3.21 $\zeta_{plateau}$ and IEP of silane treated fibres compared to alkali treated fibres.

Sample	IEP (pH) (ζ=0)	$\zeta_{plateau}$ (mV)
Silane Treated	3.5	-9.7
Alkali Treated (P_2E_4)	3.8	-11.5

A considerably higher $\zeta_{plateau}$ value was observed for silane treated fibre compared to alkali treated fibre. The slight decrease in the IEP by silane treatment highlights the increase of the acidity of the fibre surface leading to an compaction of the double layer giving further evidence for decreased -OH group exposure [188]. The compaction of the double layer would also increase the zeta potential of the solution as seen.

3.3.3.3 Thermal Analysis by Differential Thermal Analysis/ Thermogravimetric Analysis (DTA /TGA)

The DTA and TGA curves of silane treated fibres compared to alkali treated (treatment P_2E_4) fibres are shown in Figures 3.45 and 3.46 respectively. The DTA curves, Figure 3.45 for silane and the alkali treated fibres show an endotherm

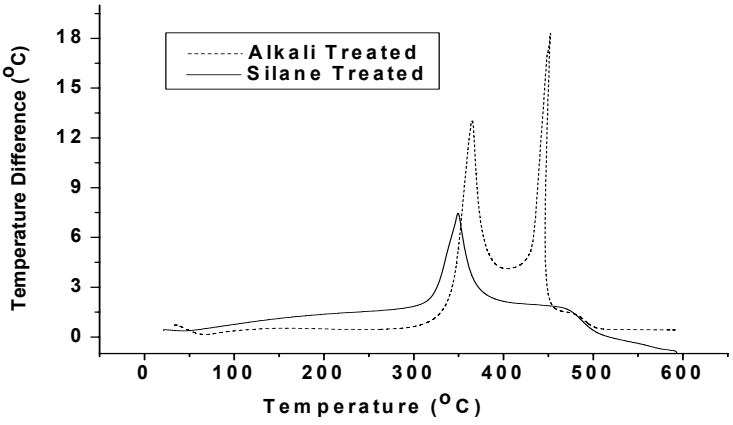

Figure 3.45 DTA curves for sialne treated fibres compared to alkali treated fibres.

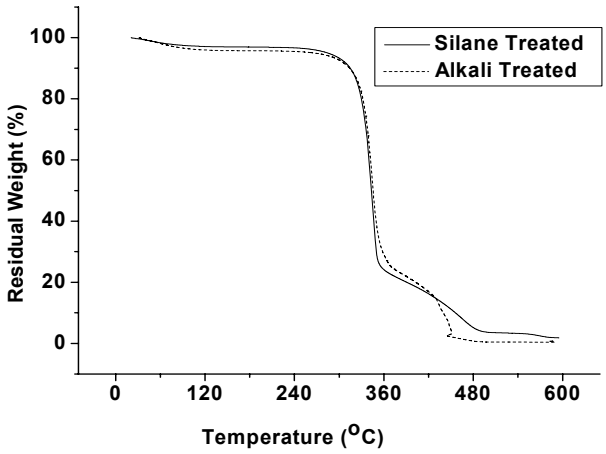

Figure 3.46 TGA curves for silane treated fibres compared to alkali treated fibres.

around 60°C due to the evolution of adsorbed moisture. At higher temperatures there are two exotherms. The first exotherm has a peak temperature of about 352°C for silane treated and about 363°C for alkali treated fibres and is likely to be caused by the decomposition of cellulose leading to the formation of volatile products [208]. The second exotherm has a peak temperature of about 480°C for silane treated and about 450°C for alkali treated fibres and is expected to be due to the oxidation of volatile and charred products. The peak onset, peak, peak finishing temperatures and nature of peaks for the silane treated fibres compared to the alkali treated fibres obtained from the DTA thermograms are shown in Table 3.22. From the results it can be seen that upon silane treatment of alkali treated fibre the onset temperature for the first exothermic peak reduces from

Table 3.22 The peak onset, peak, peak finishing temperatures and nature of peaks for the silane treated fibres compared to the alkali treated fibres obtained from the DTA thermograms.

Sample	Peak Onset Temperature (°C)	Peak Temperature (°C)	Peak Finishing Temperature (°C)	Nature of Peak
Silane Treated	45.6	56.2	85.1	Endo
	250.4	352.7	412.9	Exo
	426.1	479.3	520.6	Exo
Alkali Treated (P_2E_4)	37.8	63.9	98.6	Endo
	283.1	363.5	396.8	Exo
	418.8	450.7	462.2	Exo

283 to 250°C and the onset temperature of second exothermic peak increases from 418 to 426°C. The temperature at which percentage weight losses have occurred can be seen in Figure 3.46 and is shown to be lower for silane treated fibres at the

initial stages of thermal degradation (first exothermic peak or second stages of thermal degradation) and higher at the later stages of thermal degradation (second exothermic peak or third stages of thermal degradation) when compared to alkali treated fibres. Silane treatment appeared to shift the second exothermic peaks towards a higher temperature compared to alkali treated fibres, this may be due to the presence of high molecular weight polysiloxanes in the fibre structure which might be thermally more stable than cellulose. However, for the first exothermic peak the reduction in peak temperature for the silane treated fibres may be due to the degradation of cellulose chains caused by formation of polysiloxane.

The Broido method [210] was used to evaluate the activation energy (E_a) and frequency factor of silane treated fibres compared to alkali treated fibres. Using the Broido equation, plots of *ln[ln(1/y)]* versus *1/T* (Broido plots) for second (first exothermic peak) and third (second exothermic peak) stages of thermal degradation were plotted for which examples are shown in Figures 3.47 and 3.48. The activation energies and frequency factors were calculated from the slopes and intercepts of these plots, respectively, and are given in Table 3.23. From the values of activation energies (E_a) and frequency factors for the first and second exothermic peak of silane treated fibres compared to alkali treated fibres

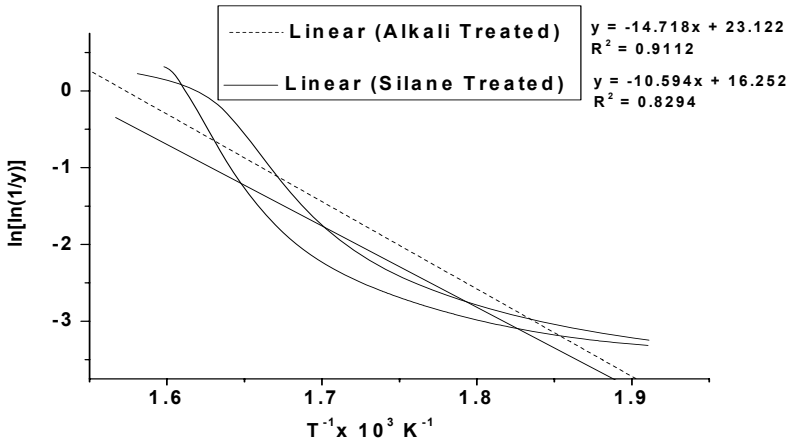

Figure 3.47 Plots of ln[ln(1/y)] versus $T^{-1}\times10^{3}$ K^{-1} for the second stage of thermal degradation (first exothermic peak) for silane treated fibres compared to alkali treated fibres.

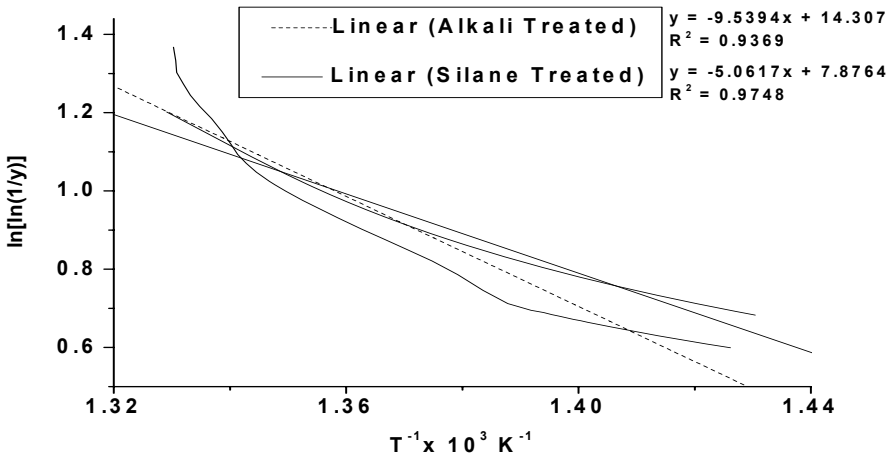

Figure 3.48 Plots of ln[ln(1/y)] versus $T^{-1}\times10^{3}$ K^{-1} for the third stage of thermal degradation (second exothermic peak) for silane treated fibres compared to alkali treated fibres.

Table 3.23 Activation energies and frequency factors obtained by Broido method for silane treated fibres compared to alkali treated fibres.

Sample	2nd Peak		3rd Peak	
	E_a (kJmol^{-1})	Z(s^{-1})	E_a (kJmol^{-1})	Z(s^{-1})
Silane Treated	88.1	1.14×10^{7}	42.1	2.63×10^{3}
Alkali Treated (P_2E_4)	122.36	6.66×10^{7}	79.31	4.96×10^{3}

show that silane treated fibres appeared with lower values of activation energy and frequency factor for both first and second exothermic peaks. The decrease in activation energy and frequency factor for the silane treated fibre for the second stage of thermal degradation compared to the alkali treated fibre is in conformity of the decreased cellulose crystallinity of the silane treated fibres. However**,** decrease in activation energy and frequency factor for the third stages of thermal degradation may be caused by some catalytic action of some free radicals formed by peak broadening. Peak broadening for the third stages of thermal degradation was also reported by Sreekala *et al.* [217].

3.3.3.4 Wide Angle X-ray Diffraction (WAXRD)

Figure 3.49 shows the wide angle x-ray diffraction pattern of silane treated fibres compared to alkali treated (P_2E_4) fibres. It can be seen that silane treatment of

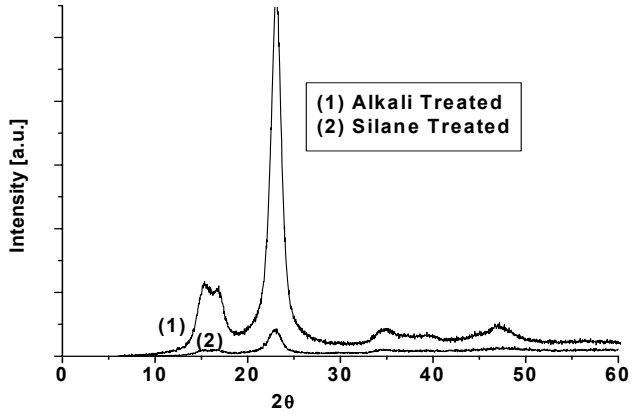

Figure 3.49 WAXRD pattern of silane treated fibres compared to alkali treated (P_2E_4) fibres.

Table 3.24 The crystallographic planes at various intensity (WAXRD counts) and 2θ-angles, and the crystallinity indices of silane treated fibres compared to alkali treated fibres.

Sample	2θ (°)	WAXRD Counts	h k l	*CrI* (%)
Silane Treated	15	81	--	86.53
	16.5	101	$\bar{1}$ 1 1	
	18.5	45	Amorphous	
	22.5	334	002	
	34.5	104	$\bar{2}$ 3 1	
	46.5	132	$\bar{4}$ 1 2	
Alkali Treated (P_2E_4)	15	1146	--	91.94
	16.5	1061	$\bar{1}$ 1 1	
	18.5	390	Amorphous	
	22.5	4842	002	
	34.5	450	$\bar{2}$ 3 1	
	46.5	506	$\bar{4}$ 1 2	

alkali treated fibre reduces the intensity of both amorphous materials and crystalline cellulose to a great extent. Silane treatment reduced the intensity of crystalline cellulose more than the amorphous materials and resulted in a decrease in crystallinity index, Table 3.24. Rong *et al.* [86] also reported a decrease in crystallinity of silane treated fibres. Generally, silane coupling agent reacts with -OH groups forming alkoxysilanes which undergo stages of hydrolysis, condensation, and bond formation. Therefore, in addition to the reaction of silanols with cellulose -OH groups of the fibre surface, formation of large polysiloxane molecules also took place that would destroy the cellulose chains to some extent and resulted in corresponding reduction in crystallinity.

3.3.3.5 Fourier Transform Infrared (FTIR) Spectra

Absorption of the peaks in that region (3400 and 3600 cm^{-1}) for the silane treated fibre was found to reduce as can be seen a narrower peak in Figure 3.50 [218].

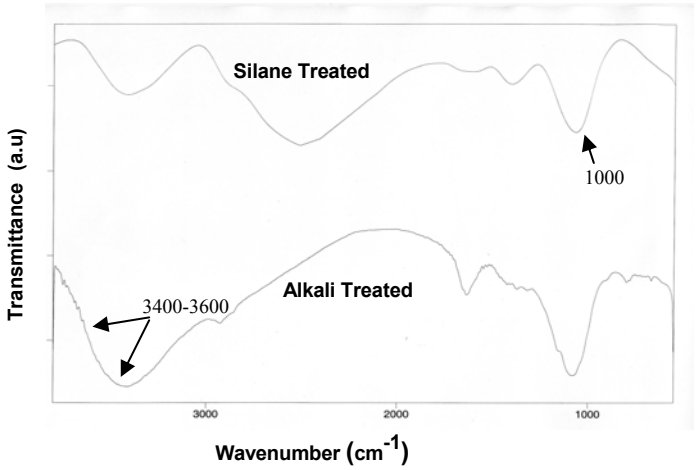

Figure 3.50 FTIR spectra of silane treated fibres compared to alkali treated fibres.

However, the strong and broad absorption between 3400 and 3600 cm^{-1} in the FTIR spectrum of alkali treated fibre is caused by the presence of -OH groups and hydrogen bonding between those groups, Figure 3.50. Moreover, an increase in absorbance can be observed at around 1000 cm^{-1} for the silane treated fibres. This could be attributed to the presence of –Si-O-Si- and –Si-O-C- bonds [219].

3.4 Chapter Conclusion

Treatment of fibres with different NaOH concentrations, Na_2SO_3 concentration, digestion times and temperatures was found to remove fibre surface constituents and as a consequence decreased fibre diameter, fibre TS and YM. Alkali treatment was found to roughen fibre surfaces and increase exposure of –OH groups in the fibre surface to facilitate bonding with epoxy resin and PLA matrices. Alkali treatment of the fibres was also found to lead to higher crystallinity and thermal stability. A graphical method was used to develop an empirical model for the TS of alkali treated fibre by partial factorial design. The empirical prediction equations developed were found to predict TS value of treated fibres within the range of the experimental conditions with almost no error.

An alkali fibre treatment method with 5 wt% NaOH, 2 wt% Na_2SO_3, 120^oC treatment temperature, and 60 minutes digestion time was considered optimum as it was found to give the best combination of fibre tensile strength retention, increased fibre surface roughness and increased exposure of cellulose –OH groups These were necessary to facilitate bonding with the matrices (epoxy resin and PLA). The fibres obtained from the optimised alkali treatment were further treated with acetic anhydride and silane. Acetylation of the alkali treated fibres was found to reduce fibre surface roughness and cellulose –OH groups (as –OH groups were replaced by $–COCH_3$) exposure along with a slight increase in crystallinity. Silane treatment of the alkali treated fibres was found to reduce cellulose –OH groups (-OH groups are replaced with silane groups) exposure, thermal stability and crystallinity.

Chapter Four

Hemp/Epoxy Composites (HECs)

4.1 Summary

This chapter describes the materials, methods and results for the:

- assessment of the cure kinetics for untreated hemp fibre/epoxy (UTFE) composites
- determination of IFSS of untreated and alkali treated hemp fibre in epoxy resin
- production of long and short hemp fibre preform mats
- production of optimised long aligned hemp fibre/epoxy composites in terms of different (a) fibre treatments (b) epoxy to curing agent ratios (c) resin soaking times, and (d) curing temperatures. 40 wt% hemp fibre/epoxy composites were produced for (a) to (d) with an extra set of 30 wt% hemp fibre/epoxy composites produced for (b). Assessment of performance for the produced composites was carried out by tensile testing, SEM and optical microscopy
- comparison of optimised untreated and alkali treated long and short aligned hemp fibre/epoxy composites at three different fibre contents (40, 50, and 65 wt%) in terms of tensile testing and SEM analysis. 40 wt% untreated and alkali treated short random oriented fibre/epoxy composites were also produced using the optimised composite production method and assessed by tensile testing

- comparison of tensile properties obtained experimentally with theoretically calculated values for untreated and alkali treated long and short hemp fibre/epoxy composites

- further characterisation of optimised 65 wt% untreated and alkali treated long and short aligned hemp fibre/epoxy composites in terms of flexural, impact, and fracture toughness as well as TGA and WAXRD analysis

- hygrothermal ageing of optimised 65 wt% untreated and alkali treated long and short aligned hemp fibre/epoxy composites. The aged composites were assessed in terms of tensile, flexural, impact, and fracture toughness as well as SEM, TGA and WAXRD analysis

- accelerated ageing of optimised 65 wt% untreated and alkali treated long aligned hemp fibre/epoxy composites. The aged composites were assessed in terms of tensile, flexural, impact, and fracture toughness well as SEM, FTIR, TGA and WAXRD analysis.

4.2 Experimental Details

4.2.1 Materials

Retted hemp bast fibre (untreated) was supplied by Hemcore, UK. Commercially available DGEBA epoxy resin with an epoxide equivalent weight of 190 (R180) and an aliphatic diamine curing agent with an equivalent weight of 38 (H180) were obtained from Fibreglass International, Australia. The materials were used in the condition in which they were received without any further purification. Analytical grade Na_2SO_3, 98% NaOH pellets, 99% acetic anhydride, and 94% phenyltrimethoxy silane were used for the treatment of the fibres.

4.2.2 Methods

4.2.2.1 Cure Kinetic Study of Neat Epoxy (NE) and Untreated Hemp Fibre/Epoxy (UTFE) Composites Using Differential Scanning Calorimetry (DSC)

Thermal analysis (dynamic and isothermal) of the curing reaction of neat epoxy (NE) and 40 wt% UTFE composite samples was carried out using a DSC 2920 differential scanning calorimeter. An epoxy resin to curing agent ratio of 1:1 was used for both NE and 40 wt% UTFE composite samples. The weight of each specimen was set at approximately 10 mg. For 40 wt% UTFE composite samples, untreated fibres of 1 mm in length were placed in an aluminum pan. The uncured epoxy resin pre-mixed with curing agent was then poured on the fibres, ensuring wetting of the fibres with the mixture. The samples were then enclosed within the aluminum pans and scanned immediately, maintaining a static air flow of 50 mL/min. Dynamic scans of NE and 40 wt% UTFE composite samples were carried out at five different heating rates (2.5, 5, 10, 15, and 20^{o}K/min) with a scanned temperature range from room temperature to 250^{o}C. For isothermal analysis, initially a steady isothermal baseline was established for each of the four selected cure temperatures (25, 50, 70, and 120^{o}C) using two empty aluminum sample pans. Isothermal scans of NE and 40 wt% UTFE composite samples were then carried out such that the curing reactions were considered complete when the isothermal DSC thermograms levelled off to the baseline. Similarly, isothermal scans of NE and 40 wt% UTFE composite samples at three further epoxy to curing agent ratios of 1:0.6, 1:0.8, and 1:1.2 were carried out at 25^{o}C.

4.2.2.2 Interfacial Shear Strength (IFSS) Measurement of Hemp Fibre/Epoxy Samples Using Single Fibre Pull-out Testing

For the measurement of IFSS, single-fibre pull-out test specimens were prepared according to the literature [220] using a silicone rubber block 12 mm long, 10 mm wide, and 3 mm deep. A 6 mm diameter circular hole was punched from the centre of the top face of the block through the depth of the material. Along the 12 mm length side of the block wall a slot was cut from the centre of the length to the edge of the circular hole to a depth of 2 mm according to Figure 4.1. Eight

different embedded lengths from 0.25 mm to 2 mm at 0.25 mm intervals

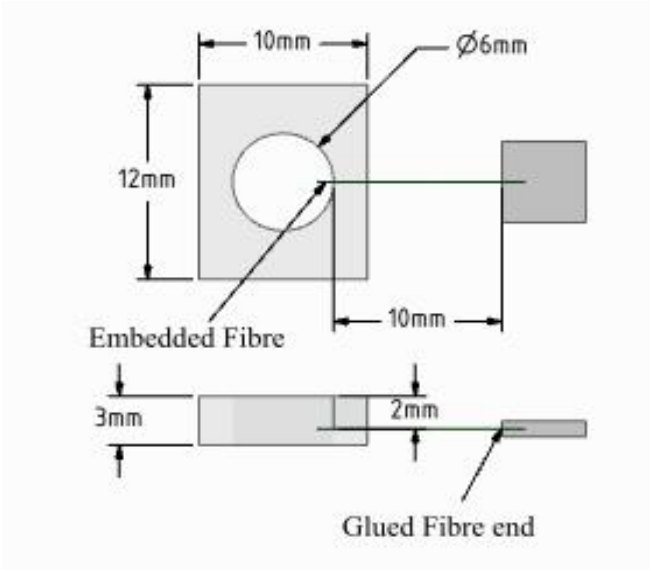

Figure 4.1 Test specimen for single fibre pull-out tests.

were produced by placing dried single fibres into the 2 mm slot with the required length extending into the block for four different ratios of epoxy resin to curing agent (1:0.6, 1:0.8, 1:1 and 1:1.2). The embedded lengths were measured by placing the silicone rubber block under an electron microscope with a calibrated eyepiece at 50× magnification, while a calibrated eyepiece at 200× magnification was used to determine the average diameter of each embedded fibre. The hole at the centre of the block was filled with epoxy resin and cured at room temperature (20±2^{o}C) for 24 hours using a vacuum bag and post cured at 50^{o}C in an oven for 4 hours. Figure 4.2 shows a single fibre embedded in epoxy resin. The free end of the fibre that had been contained within the mould slot was glued to a cardboard using polyvinyl acetate (PVA) glue to give a gauge length of 10 mm. Five specimens were prepared at each embedded length for both untreated fibre/epoxy (UTFE) and alkali treated fibre/epoxy (ATFE) samples and the average debonding force of the five specimens was measured using an Instron tensile tester at a crosshead speed of 0.5 mm/min.

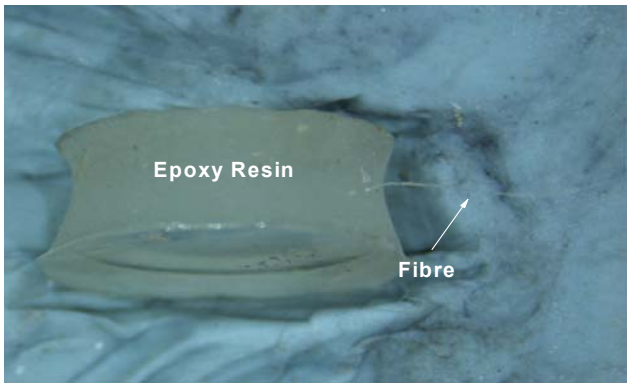

Figure 4.2 Single fibre embedded in epoxy resin.

4.2.2.3 Production of Preform Fibre Mats

Long Fibre Mats

For the production of long fibre/epoxy composites, long fibres were dried at 80^{o}C for 24 hours to produce fibre mats using the following two methods:

(1) 60g of dried fibres were aligned by hackling (by hand) to maintain a thickness of 3.5 mm, and

(2) 60g of dried fibres were aligned using a hand carding machine, Figure 4.3, from Ashford Handicrafts Limited, Ashburton, New Zealand to maintain a thickness of 3.5 mm.

Figure 4.3 Hand carding machine used to produce aligned long fibre mats.

For method 1, long untreated, alkali treated, acetylated and silane treated fibres were used and for method 2, long untreated and alkali treated fibres were used. Fibre treatment methods are described in section 3.2.2.

Short Fibre Mats

For the production of short fibre/epoxy composites, untreated and alkali treated short fibres were dried at 80°C for 24 hours to produce fibre mats using the following two methods:

Aligned Mats by Dynamic Sheet Forming (DSF)

200g of dried fibres were pelletised to lengths of less than 8 mm and then separated with water at 72,000 rpm using a disintegrator. The disintegrated fibres were then used to produce aligned short fibre mats of 3 mm thickness using a Centre Technique De L'Industrie Des Papiers Cartons Et Cellulose Dynamic Vertical Former, Figure 4.4 from Ateliers De Construction Allimand, France which is commonly used for laboratory production of paper. The fibre mats obtained, Figure 4.5, were placed in a dryer at 100°C for 24 hours and then cut to a size (22 cm long and 15 cm wide) to fit in a compression mould.

Figure 4.4 Dynamic sheet former used to produce aligned short fibre mats.

Figure 4.5 Aligned alkali treated fibre mat produced by dynamic sheet forming (DSF).

Random Mats by Hand Lay-up

Random orientation short fibre mats were also produced by placing 60g dried short fibres in a compression mould, pouring water over the fibres and then pressing at room temperature. Planar random orientation mats of uniform thickness of 3.5 mm were produced by this technique.

4.2.2.4 Production of Composites

(a) Untreated, Alkali Treated, Acetylated, and Silane Treated Fibre Composites Produced at Different Curing Temperatures

Untreated, alkali treated, acetylated, and silane treated (treatment methods described in section 3.2.2) long fibre mats produced by hackling were dried in an oven at 80^{o}C for 24 hours and placed in an epoxy resin (epoxy to curing agent ratio of 1:1) bath for about 10 minutes. The resin soaked mats were fabricated into composites with a fibre content of 40 wt% at two different curing temperatures as described below:

Cured at 25^{o}C:

The soaked mat was placed in a mould and pressed for 24 hours at a pressure of 2 MPa and then post cured in an oven at 50^{o}C for four hours.

Cured at 120^{o}C

The soaked mat was placed in a mould pre-heated to 120^{o}C and then pressed at a pressure of 2 MPa and temperature of 120^{o}C for about 5 minutes.

Acetylation and silane treatment of the fibres were carried out after the fibres were alkali treated. Untreated and alkali treated long fibre mats produced using a hand carding machine were dried at 80^{o}C for 24 hours and used for the production of composites using methods b, c, and d as described below.

(b) Composites Produced at Different Epoxy to Curing Agent Ratios

Fibre mats were placed in a mould and epoxy resin was then poured onto the mats and allowed to soak into the fibres for 10 minutes. Four different epoxy resin to curing agent ratios (1:0.6, 1:0.8, 1:1, and 1:1.2) were used. A hand roller was used to remove the excess resin from the fibre mats to maintain 30 and 40 wt% of

fibres in the composites. The epoxy resin soaked fibre mats were placed into a vacuum bag and cured under vacuum for 24 hours at room temperature (25^{o}C) followed by post curing of the composite mats in an oven at 50^{o}C for four hours.

(c) Composites Produced Using Different Fibre Soaking Times in Resin Bath

Fibre mats were placed in an epoxy resin (epoxy to curing agent ratio of 1:1) bath. The mats were soaked in resin for 10 or 60 minutes. The fibre content of the composites was maintained at 40 wt%. The resin soaked mats were then placed into a vacuum bag and cured under vacuum for 24 hours at room temperature (25^{o}C) followed by post curing of the composite mats in an oven at 50^{o}C for four hours.

(d) Composites Produced Using Different Curing Temperatures

Fibre mats were placed in an epoxy resin (epoxy to curing agent ratio of 1:1) bath for about 1 hour. The resin soaked mats were then fabricated into composites by placing in a pre-heated mould at three different curing temperatures and compressed at a constant pressure of 9.4 MPa. The duration of the pressure maintained at each curing temperature was based on completion of curing reaction as observed from thermal analysis results as per section 4.3.1, Table 4.1.

Table 4.1 Duration of the pressure maintained at each curing temperature.

Curing Temperature (^{o}C)	Duration of the Pressure Maintained
25	12 hours
70	20 minutes
120	5 minutes

40 wt% fibre epoxy composites were produced at each of the three curing temperatures.

(e) Short Fibre Composites Produced with Random and Aligned Orientations

Untreated and alkali treated random and aligned short fibre mats were dried in an oven at 80^{o}C for 24 hours and placed in a resin bath for about 1 hour. The resin soaked mats were then placed in a mould pre-heated at 70^{o}C and then pressed at a pressure of 9.4 MPa and temperature of 70^{o}C for about 20 minutes to give a fibre content of 40 wt%.

(f) Composites Produced at Different Fibre Contents

Untreated and alkali treated long and short fibre mats (long and short aligned fibre mats produced using hand carding machine and dynamic sheet former respectively) were dried in an oven at 80^{o}C for 24 hours and placed in a resin bath for about 1 hour. The resin soaked mats were placed in a compression mould pre-heated at 70^{o}C and then pressed at 70^{o}C for about 20 minutes. Three different pressures of 9.4, 10.2, and 12.6 MPa were used to give three different fibre loadings of 40, 50, and 65 wt% respectively.

4.2.2.5 Tensile Testing

Samples were cut into tensile test specimens using a computer numerical controlled (CNC) mill (for production methods (a) to (c) of section 4.2.2.4) which was later changed to a scroll saw which gave a better finish (for production methods (d) to (f) of section 4.2.2.4) in accordance with ASTM D 638-03 Standard Test Method for Tensile Properties of Plastics and placed in a conditioning chamber at 23^{o}C ± 3^{o}C and 50% ± 5% relative humidity for 24 hours. The specimens were then tested using an Instron-4204 tensile testing machine fitted with a 5 kN load cell at a rate of 1 mm/min. An Instron 2630-112 extensometer was used to measure strain. Five to six replicates were used.

4.2.2.6 Flexural Testing

Samples were cut into flexural test specimens using a scroll saw. The flexural (three point bend) test was carried out in accordance with the ASTM D 790-03 Standard Test Methods for Flexural Properties of Unreinforced and Reinforced Plastics and Electrical Insulating Materials by using a Lloyd LR 100 K tensile testing machine fitted with a 5 kN load cell.

4.2.2.7 Impact Testing

Samples were cut into impact test specimens using a scroll saw. Charpy impact testing was carried out in accordance with the International Standard Organization (ISO) 179 Standard Test Method. Dimensions of the samples were 80 mm × 8 mm × 4 mm with a single notch of 0.25 mm (type A). An advanced universal

pendulum impact tester POLYTEST with an impact velocity of 2.9 m/s and a hammer weight of 0.475 kg at 21^{o}C was used.

4.2.2.8 Fracture Toughness (K_{Ic}) Testing

Samples were cut into fracture toughness test specimens using a scroll saw. Single-edge-notch bending (SENB) specimens were obtained in accordance with ASTM D 5045-99 Standard Test Methods for Plane-Strain Fracture Toughness and Strain Energy Release Rate of Plastic Materials.

Figure 4.6 shows the specimen configuration for SENB. The crack length, a, is nominally equal to the thickness, B, and is between 0.45 and 0.55 times the width, W. The ratio W/B is nominally equal to 2. The specimens were then tested using a Lloyd LR 100 K tensile testing machine fitted with a 5 kN load cell operating at a rate of 10 mm/min.

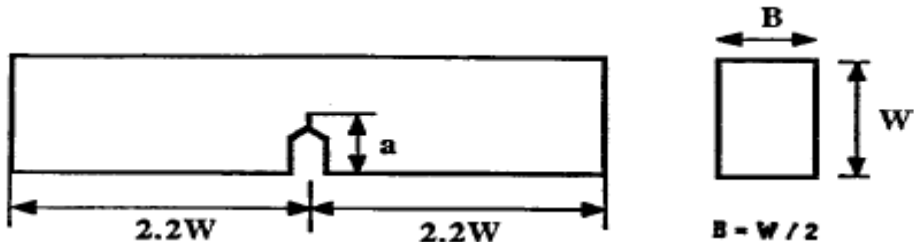

Figure 4.6 Specimen configuration for SENB.

4.2.2.9 Optical Microscopy

To assess the fibre orientation in the mats, fibre distribution and porosity of composites, samples were sectioned through their thickness to examine their cross-section and placed under an optical microscope (Olympus BX 60).

4.2.2.10 Scanning Electron Microscopy (SEM)

The fracture surfaces of the composites were examined using SEM following the method described in section 3.2.2.

4.2.2.11 Thermogravimetric Analysis (TGA)

The TGA of the composites was carried out using the method described in section 3.2.2.

4.2.2.12 Wide Angle X-ray Diffraction (WAXRD)

The WAXRD analysis of the composites was carried out using the method described in section 3.2.2.

4.2.2.13 Fourier Transform Infrared (FTIR) Spectra

The FTIR spectra analysis of the composites was carried out using the method described in section 3.2.2.

4.2.2.14 Hygrothermal Ageing of the Composites

Hygrothermal ageing of the samples was carried out in accordance with ASTM D 570-98: Standard Test Method for Water Absorption of Plastics. The samples were submerged in distilled water at 25, 50, and 70^{o}C and removed from the water at certain periods of time, wiped with a clean dry cloth to remove the surface water, weighed in a high precision balance to assess the weight change and then resubmerged for continued ageing. Weighing of the samples was stopped when further weight gain was found to be insignificant. Tensile, flexural, impact, and fracture toughness testing of the aged samples were carried out in accordance with ASTM standards as described in section 4.2.2.5 to 4.2.2.8 respectively. Five specimens of each batch were tested.

4.2.2.15 Accelerated Ageing of the Composites

Accelerated ageing of the samples was carried out using an accelerated weathering tester (Model QUV/spray with solar eye irradiance control) in accordance with ASTM G 154-00a: Standard Practice for Operating Fluorescence Light Apparatus for UV Exposure of Non-metallic Materials. A fluorescent bulb (UVA) with 0.68 W/m^2 irradiance (at 340 nm) was used with cycles of 1 hour UV irradiation, followed by 1 minute of spray with de-ionized water and a subsequent 2 hours condensation while maintaining a temperature of 50^{o}C. Five specimens from each batch of tensile, flexural, impact, and fracture toughness testing samples were subjected to the ageing process for durations of 250, 500, 750, and 1000 hours.

4.3 Results and Discussion

4.3.1 Cure Kinetics of NE and Untreated Hemp Fibre/Epoxy (UTFE) Composites

To calculate activation energies of neat epoxy (NE) and 40 wt% UTFE composites, two dynamic kinetic models (the Kissinger and the Flynn-Wall-Ozawa Models), and one isothermal kinetic model (the Autocatalytic Model) described in section 2.10 were used.

4.3.1.1 Activation Energies Obtained Using the Kissinger and Flynn-Wall-Ozawa Models

To calculate activation energies using the Kissinger and Flynn-Wall-Ozawa Models, the peak temperature (T_m) for each heating rate and the total heat of reaction (ΔH_{tot}) obtained from DSC for both NE and composites were used. Figures 4.7 and 4.8 show the DSC exotherms obtained at different heating rates for NE and composites respectively. From these figures it can be seen that the exotherm peak was found at increasingly higher temperatures as the heating rate increased. The total heat of reaction (ΔH_{tot}) values for the NE and composites were taken as the average of the heat of reaction (ΔH_0) values obtained at different heating rates as per other researchers [221, 222]. To calculate the heat of reaction (ΔH_0) at each heating rate, the total area under each exotherm was determined. These results along with the peak temperatures of the exotherms are summarised in Table 4.2. It was observed that the ΔH_0 values did not vary greatly with the increase of heating rate for either NE or the composites. A similar lack of variation with NE was observed by Lopez *et al.* [223]. From the results, Table 4.2, it was also observed that the heat of reaction at the same heating rate and the total heat of reaction are lower for the composite samples than for NE which might be due to the enhanced nucleophilic activity of the amine groups of the curing agent in presence of the fibre [224].

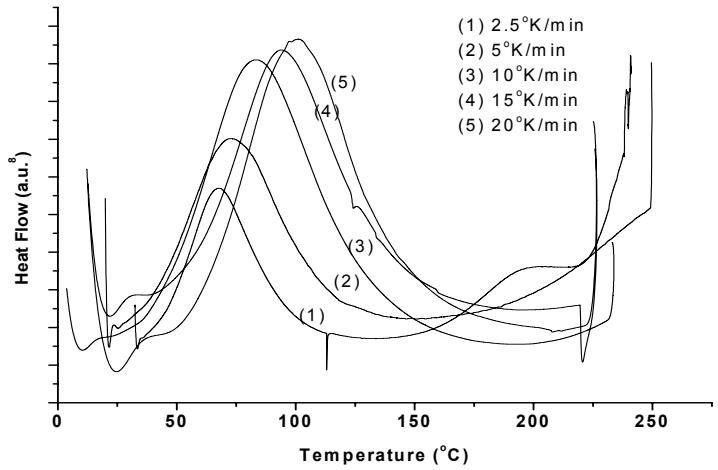

Figure 4.7 Heat flow measured by DSC during cure of NE at five different heating rates (*Heat flow normalised to show relative peak sizes).

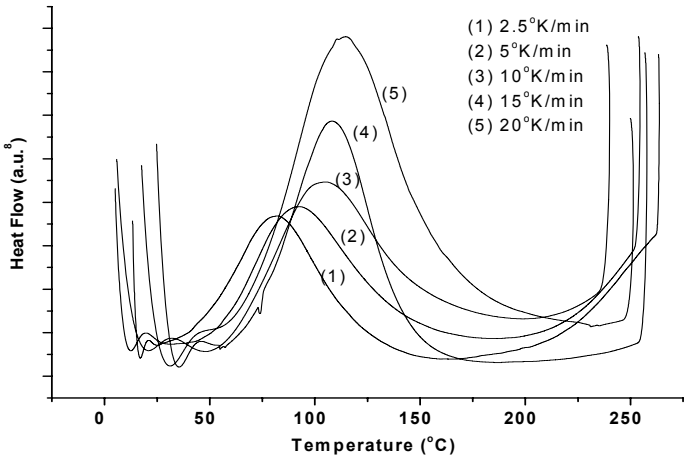

Figure 4.8 Heat flow measured by DSC during cure of composites at five different heating rates (*Heat flow normalised to show relative peak sizes).

Table 4.2 Heat of reaction for NE and composites at five different heating rates.

Heating Rate, q (K min^{-1})	**ΔH_0 (J/g)**		**Peak Temperature, T_m (K)**	
	NE	**Composites**	**NE**	**Composites**
2.5	292.5	120.8	352.6	341.2
5	298.0	124.8	365.5	346.2
10	301.8	126.8	373.4	354.7
15	304.7	128.3	379.1	363.4
20	305.0	133.6	387.6	374.3
Average, ΔH_{tot}	**300.4**	**126.86**		

The exotherms, Figures 4.7 and 4.8, were analysed to obtain activation energies. Based on the Kissinger Model, Equation (2.8), the activation energies E_a were

obtained from the plot of $\ln(q/T_m^2)$ versus $1/T_m$ for NE and composites, Figure 4.9.

A linear relationship was observed here, confirming the validity of the proposed model given in Equation (2.8). The activation energies E_a were calculated from the slopes, yielding values of 56.7 and 50.9 kJ/mol, Table 4.3, for NE and composites respectively. The lower activation energy of the composites compared to that of NE indicates that fibre addition enhances the reaction rate supporting the enhanced nucleophilic activity of amine groups in curing agent. The value for the activation energy of NE agreed reasonably well with the activation energies of similar epoxy/amine systems obtained by other researchers [225].

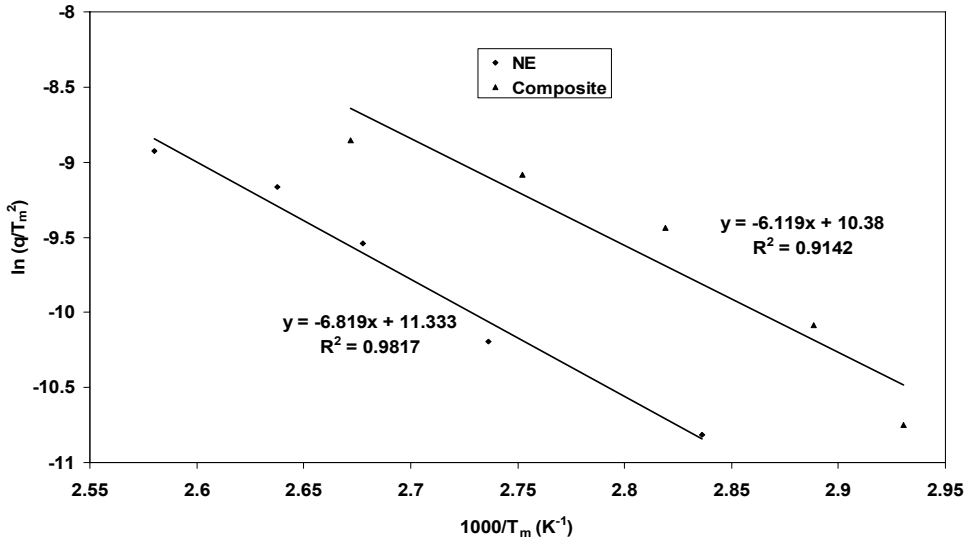

Figure 4.9 Activation energies obtained by the Kissinger model for NE and composites.

Table 4.3 Comparison of activation energies obtained by different models.

Sample	Kissinger Model	Flynn-Wall-Ozawa Model	Autocatalytic Model	
	E_a (kJ/mol)	E_a (kJ/mol)	E_{a1} (kJ/mol)	E_{a2} (kJ/mol)
NE	56.7	58.5	37.2	45.3
Composites	50.9	54.6	36.8	38.3

Based on the Flynn-Wall-Ozawa Model, Equation (2.9), activation energies were calculated from the slopes of the plots of $\log q$ versus $1/T_m$ of NE and composites [226], Figure 4.10. A linear relationship was observed here, confirming the validity of the proposed model given in Equation (2.9). The activation energies thus obtained were 58.5 and 54.6 kJ/mol, Table 4.3, for NE and composites respectively. The lower activation energy for NE compared to that for composites

is in agreement with the trend found for the Kissinger Model although the values are slightly higher than the activation energies obtained by the Kissinger Model. Other researchers have also reported that the activation energies of NE obtained from the Flynn-Wall-Ozawa Model were higher than those for the Kissinger Model [223, 225]. However, the values here support that the activation energy is lower for composites than NE.

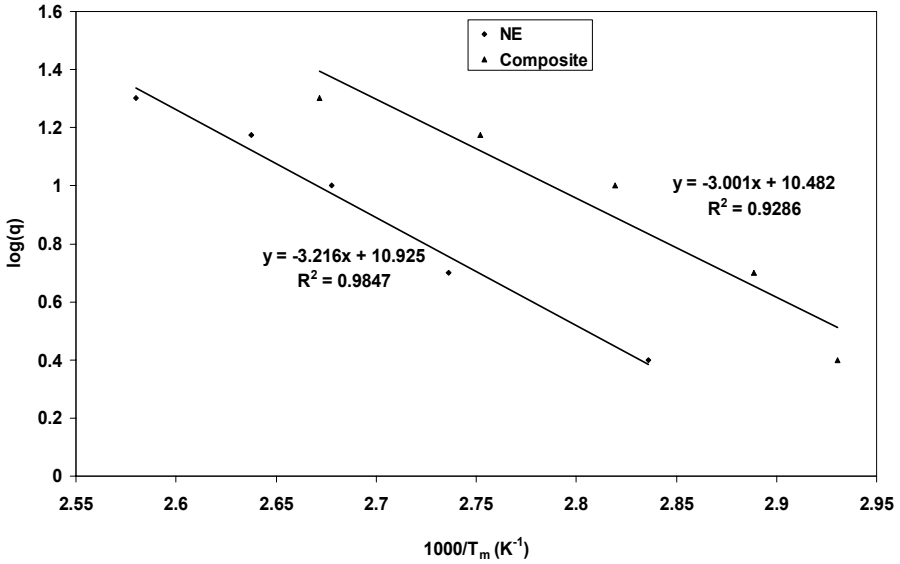

Figure 4.10 Activation energies obtained by Flynn-Wall-Ozawa method for NE and composites.

4.3.1.2 Activation Energies Obtained Using the the Autocatalytic Model

To calculate activation energies of NE and composites using the Autocatalytic Model, Equation (2.11), the kinetic parameters k_1 and k_2 of the model were used as per other researchers [120]. To calculate these kinetic parameters, the time required for cure to occur, the heat of reaction obtained from an isothermal scan at time t (ΔH_t), and the final degree of cure (α_f) collected from isothermal DSC scans which were carried out at four different curing temperatures, Table 4.4, were used.

To calculate the kinetic parameter, k_1 of the Autocatalytic Model for both NE and composite samples, at the start of the cure reaction $(t = 0 \text{ and } \alpha = 0)$, Equation (2.11) can be simplified to:

$$\left[\frac{d\alpha}{dt}\right]_{t=0} = k_1 \tag{4.1}$$

Table 4.4 Curing time, ΔH_t, and α of NE and composites at four different curing temperatures.

Curing Temperature (°C)	Samples	Curing Time (min)	ΔH_t (J/g)	α_f
25	NE	827	140.9	0.47
	Composites	719	65.3	0.51
50	NE	300	172.0	0.57
	Composites	191	77.9	0.61
70	NE	38	229.9	0.77
	Composites	19.5	104.3	0.82
120	NE	6.5	258.7	0.86
	Composites	4.5	114.4	0.90

Thus, the kinetic parameter, k_1 for both NE and composites was determined directly from isothermal reaction rate curves by extrapolating to zero time and is given in Table 4.5. For determination of the kinetic parameter, k_2 and other kinetic parameters m and n of the model (m and n are calculated along with k_1 and k_2 to see if the experimental data obtained in this study are a good fit to the trend that would be expected from the Autocatalytic Model), there are different calculative approaches, which have been applied by other researchers [120, 227]. However, the graphical–analytical method applied by Kenny [228] was applied in the present study to calculate the kinetic parameters k_2, m and n, Table 4.5, due to its ease of use. The detailed calculative approach can be found in the literature [228].

Table 4.5 Autocatalytic model parameters for NE and composites.

Sample	Temperature (°C)	m	n	$k_1 \times 10^3$ (min^{-1})	$k_2 \times 10^3$ (min^{-1})
NE	25	0.83	4.64	3.79	9.1
	50	0.68	3.72	17.91	100.2
	70	0.39	2.52	38.12	291.4
	120	0.35	1.75	126.97	715.7
Composites	25	1.18	3.98	6.30	19.2
	50	0.81	3.27	24.93	159.6
	70	0.67	1.67	43.33	436.2
	120	0.29	0.51	202.35	775.2

For both NE and composites, the values of m and n appear to decrease and the values of k_1 and k_2 appear to increase to some extent with increasing isothermal

temperatures. Other researchers have also reported that the value of m and n decreased and value of k_1 and k_2 increased with increasing temperatures [120, 229].

A good fit to the experimental data of the studied reaction systems (NE and composite samples) was obtained by using the Autocatalytic Model, Equation (2.11), with four kinetic parameters (k_1, k_2, *m, and n*). Figure 4.11 shows plots (experimental values) of reaction rate, $\frac{d\alpha}{dt}$ versus degree of cure (α) for NE at four different isothermal temperatures. The solid lines are for the trends that would be expected from the model. The maximum rate for both NE and composites is observed at conversions around 10-35% for the four different isothermal temperatures, Figure 4.11, as expected for an autocatalytic reaction.

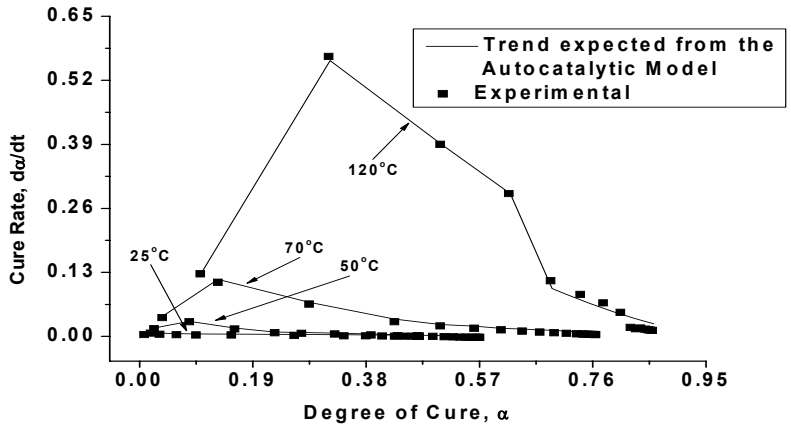

Figure 4.11 Conversion rate versus conversion graphs for NE at four different isothermal temperatures. The solid lines are a trend expected from the Autocatalytic Model (Equation (2.11)).

In the Autocatalytic Model there are two kinetic rate constants as described in section 2.10.2 and therefore, two activation energies, E_{a1} and E_{a2}, can be obtained by using the Arrhenious relation of kinetic parameters k_1 and k_2, Equation (2.5), described in section 2.10. By taking logarithm of Equation (2.5) it yields

$$\ln k = \ln A - \frac{E_a}{RT} \tag{4.2}$$

Using Equation (4.2) the linear plots of lnk_1 versus $1/T$, Figure 4.12, and lnk_2 versus $1/T$, Figure 4.13 were obtained to calculate activation energies E_{a1} and E_{a2} from the slopes of the graphs. The activation energies obtained are given in Table 4.3.

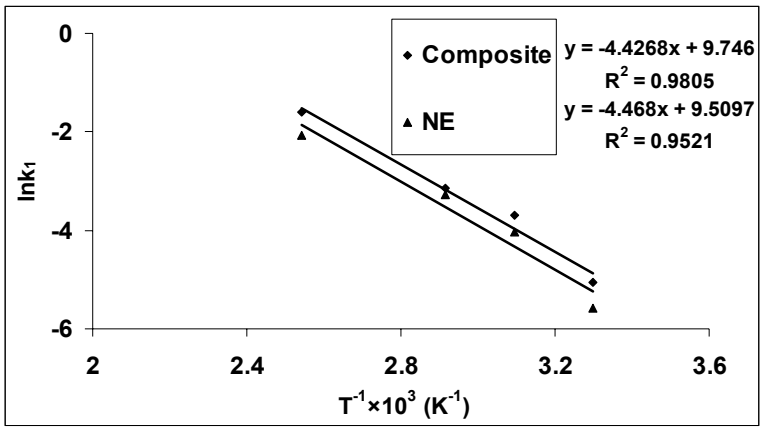

Figure 4.12 Arrhenius plot for the reaction constant k_1.

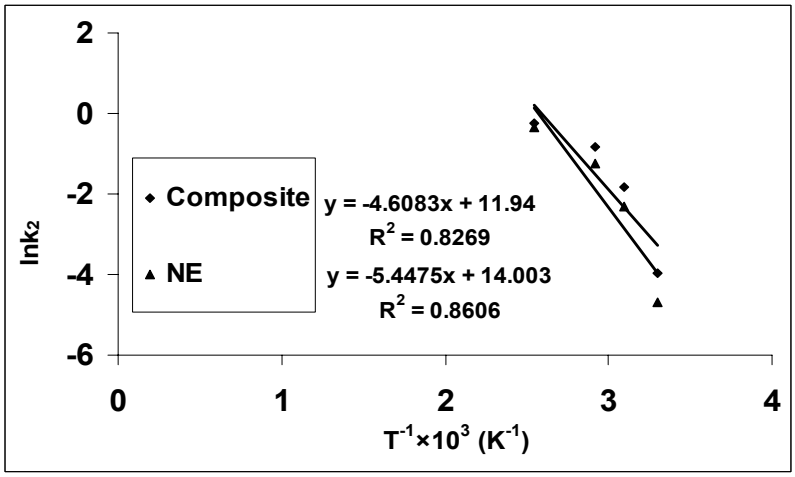

Figure 4.13 Arrhenius plot for the reaction constant k_2.

It can be seen that for this model as for the Kissinger and Flynn-Wall-Ozawa models, the activation energies for the curing of composites exhibited lower values compared to curing of NE, Table 4.3, supporting that the addition of fibre in epoxy enhanced the curing reaction between epoxy resin and amine curing agent. The average activation energies obtained from Kissinger and Flynn-Wall-Ozawa Models were higher than those obtained from the Autocatalytic Model. This might be due to a wide temperature range of 25-120^{o}C used in the study of the Autocatalytic Model. The wide temperature range could lead to a large

variation in reaction constants which would result in a reduction in the slope of the Arrhenius plot and as a consequence a reduction in activation energy.

Isothermal Cure Reactions at Different Epoxy Resin to Curing Agent Ratios

In the previous section, activation energies of NE and composites at an epoxy to curing agent ratio of 1:1 at four different cure temperatures (25, 50, 70 and 120^{o}C) were discussed. In the current study, isothermal scans of NE and composites at four different epoxy to curing agent ratios of 1:0.6, 1:0.8, 1:1, and 1:1.2 at 25^{o}C cure temperature were carried out. Table 4.6 summarises the time required to cure NE and composites at four different epoxy to curing agent ratios cured at 25^{o}C. Both NE and composites had incomplete cure reactions at epoxy to curing agent ratios of 1:0.6 and 1:0.8 which is likely to be due to the deficiency of the availability of the curing agent necessary for the completion of the curing reaction. The cure reactions were complete for both NE and composites at epoxy to curing agent ratios of 1:1 and 1:1.2 and the time required for the curing was found to decrease with the increase of the curing agent as expected. It can also be seen that at the same epoxy to curing agent ratio, the time required to cure NE is greater than that for the composites which might again be caused by the enhanced nucleophilic activity of amine groups in the presence of the cellulosic fibres [224]. In this study, calculation of activation energies at different epoxy to curing agent ratios was not possible due to incomplete curing reactions at epoxy to curing agent ratios of 1:0.6 and 1:0.8 (below their stoicheometric ratio).

Table 4.6 Curing time of NE and composites at four different epoxy to curing agent ratios cured at 25^{o}C.

Epoxy to Curing Agent Ratios	Samples	Curing Time (min)
1:0.6	NE	Incomplete Curing After 1440 min
	Composites	Incomplete Curing After 1440 min
1:0.8	NE	Incomplete Curing After 1440 min
	Composites	Incomplete Curing After 1440 min
1:1	NE	827
	Composite	719
1:1.2	NE	641
	Composite	528

4.3.2 Interfacial Shear Strength (IFSS) Measurement of Hemp Fibre/Epoxy Samples

An example of the load versus displacement curves obtained in the pull-out tests of hemp fibre/epoxy samples is shown in Figure 4.14. From the figure, five stages can be seen [230]. During the first stage, (A to B) system slack is taken up, whilst elastic deformation of the fibre is seen to start at point B of the second stage and continues until point C where the stress field around the embedded fibre is sufficient to initiate crack propagation. Thus, debonding (the third stage) initiates at point C and continues until point D where a sudden drop of load is observed due to the complete debonding (the fourth stage). During the fifth stage, (E to F), pull-out of the fibre occurs. All the hemp fibre-epoxy resin samples showed similar graphs with a sudden drop in the load at point D [231].

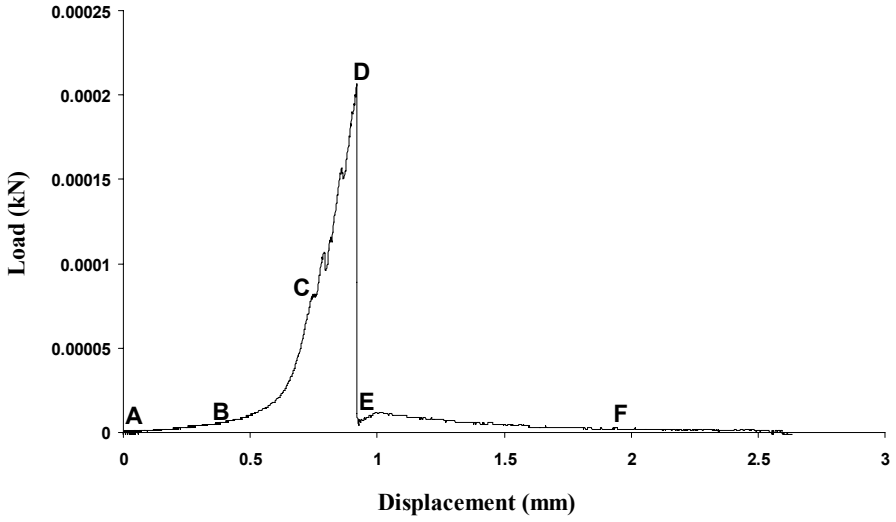

Figure 4.14 Typical load versus displacement curve for pull-out tests of hemp/epoxy sample.

Figures 4.15 and 4.16 show the debonding force for the UTFE and ATFE samples respectively at four different ratios of epoxy resin to curing agent cured at room temperature. Linear relationships between the debonding force and embedded length were obtained for all fibre-epoxy resin samples, though with different slopes. The higher slopes obtained for debonding force versus embedded length (at all ratios of epoxy resin to curing agent) for the ATFE samples compared to the UTFE samples suggested a stronger interface between alkali treated fibre and

epoxy resin. Figures 4.17 and 4.18 show the IFSS calculated by dividing the debonding force by the interfacial area of the UTFE and ATFE samples, Equation (2.2), respectively [232]. The highest IFSS value for ATFE samples was 5.2 MPa which was larger than the highest value of 2.7 MPa for UTFE samples supporting that there was a stronger interface between alkali treated fibre and epoxy resin. Higher interfacial bonding for ATFE samples can be explained by the

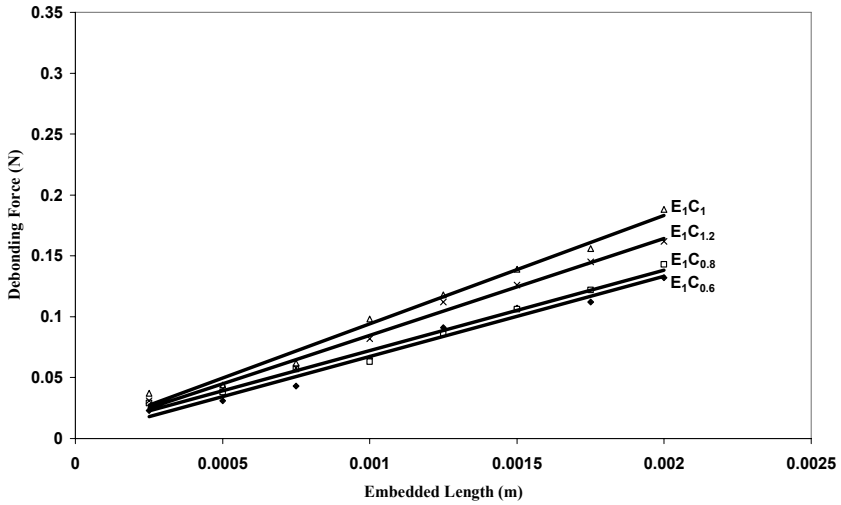

Figure 4.15 Debonding force versus embedded length plots for UTFE samples at various epoxy resin to curing agent ratios.

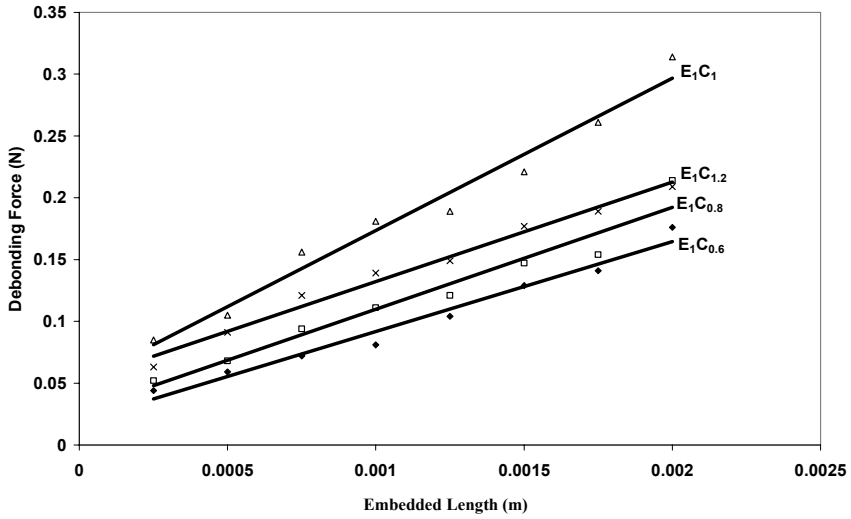

Figure 4.16 Debonding force versus embedded length plots for ATFE samples at various epoxy resin to curing agent ratios.

increase of available –OH groups as observed by FTIR analysis described in section 3.3.1.10 due to alkali treatment. These would be expected to occur due to removal of the non-cellulosic materials covering the cellulose –OH groups and

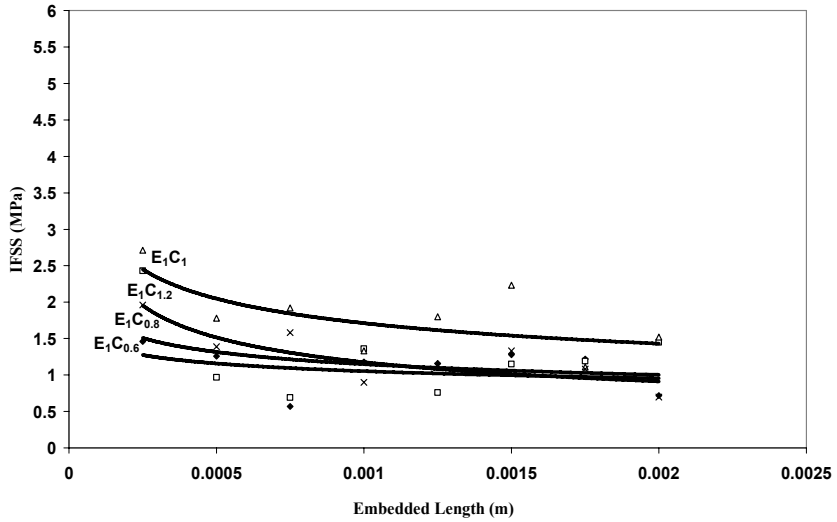

Figure 4.17 IFSS of UTFE samples found at eight different embedded length and four different epoxy resin to curing agent ratios. The solid lines indicate principal trends of data points and do not represent any data fitting.

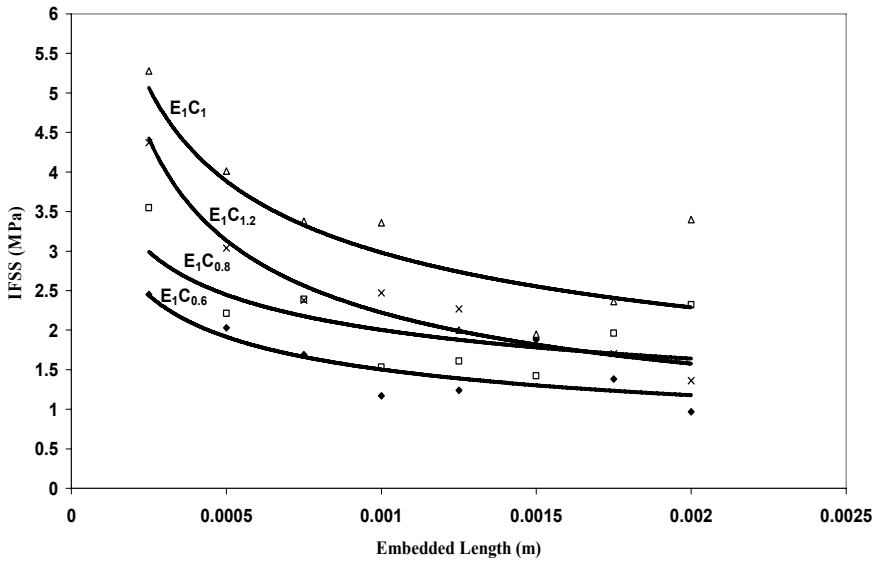

Figure 4.18 IFSS of ATFE samples found at eight different embedded length and four different epoxy resin to curing agent ratios. The solid lines indicate principal trends of data points and do not represent any data fitting.

also due to increased roughness, which would generally increase the surface area of the fibre. Increased exposure of cellulose –OH groups would provide increased

potential for hydrogen and covalent bonding with amine (NH_2) group of the curing agent and epoxide or -OH group of epoxy resin. In addition to increasing –OH groups for bonding, increased surface roughness would also provide for better mechanical interlocking with epoxy resin [4, 8].

From the slopes of the graphs of debonding force versus embedded length, Figures 4.15 and 4.16, it can be determined that for both UTFE and ATFE samples, the best fibre/epoxy bonding is for E_1C_1 followed by $E_1C_{1.2}$ and $E_1C_{0.8}$, and finally for $E_1C_{0.6}$. It had been thought that increasing the curing agent to epoxy resin ratio above its stoicheometry may have allowed for extra active hydrogen groups to form hydrogen bonding with the –OH groups of fibre to provide increased interfacial bonding. However, the fact the E_1C_1 samples were found to have better IFSS than $E_1C_{1.2}$ samples suggests that either matrix integrity has been compromised or reduced wettability has been a factor. The best wettability would be expected to occur for resins with the lowest viscosity for which curing time (as discussed in section 4.3.1) could be used to indicate the relative order; resins with the longest curing time would be expected to have the lowest viscosity. Therefore, the best wettability would be expected to be for $E_1C_{0.6}$ followed by $E_1C_{0.8}$ and E_1C_1, and finally for $E_1C_{1.2}$. Better wetting not increasing the fibre/epoxy bonding in $E_1C_{0.6}$ and $E_1C_{0.8}$ samples, may be due to reduced matrix integrity or reduced interfacial bonding.

IFSS was found to reduce with embedded length for both UTFE and ATFE samples, such that ATFE samples were found to be more variable than UTFE samples, Figures 4.17 and 4.18. This variation of IFSS versus embedded length indicates a brittle interface fracture behaviour as reported by other researchers [97]. A non-constant function arises with pull-out by brittle fracture due to the requirement of a critical crack length, which, once achieved, requires no further increase of stress for a longer embedded fibre length. As previously discussed, the increased access of –OH groups is likely to be contributing to the increase in interfacial strength and therefore increased brittle behaviour of the ATFE samples. The degree of inconsistancy for both UTFE and ATFE samples increased with the increase in the epoxy to curing agent ratios which was expected due to the increase in the degree of cross linking with the increased amount of curing agent in the samples.

4.3.3 Effects of Acetylation, Silane Treatment, Alkali Fibre Treatment and Curing Temperature on Composite Tensile Properties

Figure 4.19 shows the TS of 40 wt% UTFE, acetylated fibre/epoxy (AcFE), silane treated fibre/epoxy (STFE) and ATFE composites compared to neat epoxy (NE). It can be seen that ATFE composites were the only ones with a modest improvement in TS compared to NE. The limited benefit obtained by fibre

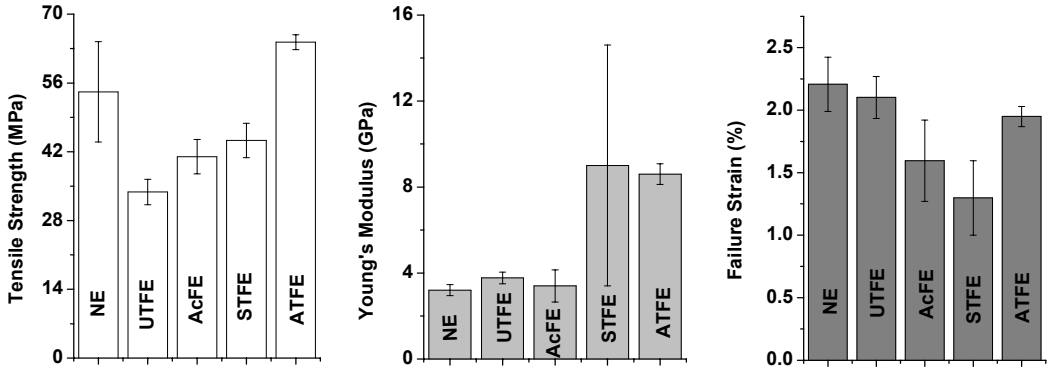

Figure 4.19 Tensile properties of UTFE, AcFE, STFE, and ATFE composites compared to NE cured at 25°C. Error bars each corresponds to one standard deviation.

addition might be due to poor fibre wetting leading to a weak interface. Figures 4.20 to 4.23 show the optical micrographs of UTFE, AcFE, STFE, and ATFE composites respectively. The poor fibre wetting of the UTFE composites is evident by dry fibre (whitish area in the fibres), fibre swelling, and porosity, Figure 4.20. In addition to poor processing conditions (subsequent optimisation was carried out for later experiments), poor fibre wetting of the untreated fibres by epoxy resin may also be caused by the presence of non-cellulosic surface components which cover the –OH groups of the cellulose responsible for the potential bonding with epoxy resin.

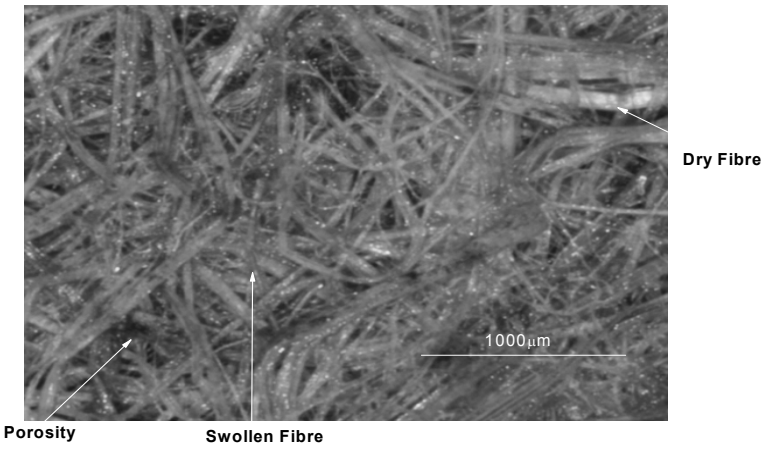

Figure 4.20 Optical micrograph of UTFE composites cured at 25°C.

The poor fibre wetting of the AcFE composites is evident by dry fibre (whitish area in the fibres), fibre swelling, and porosity, Figure 4.21. However, a reduction

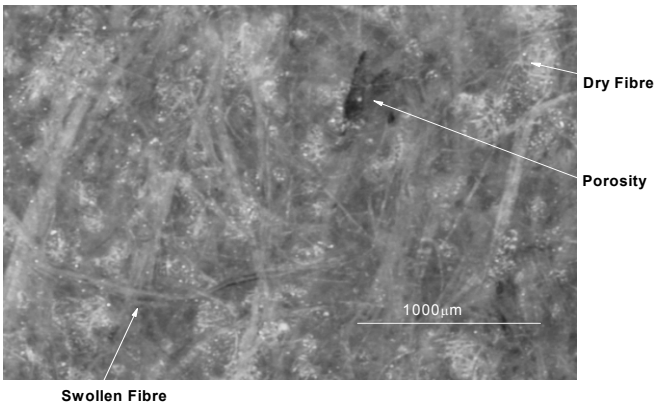

Figure 4.21 Optical micrograph of AcFE composites cured at 25°C.

in fibre swelling can be seen when compared to UTFE composite. To obtain acetylated fibres, the untreated fibres were treated with alkali to remove non-cellulose surface components and make the cellulose -OH groups available for bonding with epoxy. However, acetylation of the fibre would be expected to replace highly polar fibre -OH groups with less polar $-COCH_3$ groups as supported by FTIR analysis in section 3.3.2.5, and reduce the compatibility of the fibre with the resin. This is because the less polar $-COCH_3$ groups may not form covalent bonds with the epoxide or -OH groups of the epoxy resin, or the active hydrogen groups of the curing agent. Thus, acetylation of fibre would also be

expected to result in poor bonding of the fibres with epoxy resin although not as bad as for untreated fibre.

The poor fibre wetting of the STFE composites is also evident by dry fibre (whitish area in the fibres), fibre swelling, and porosity, Figure 4.22. However, STFE composites were found to contain less dry fibre compared to UTFE and AcFE composites. The reduction in dry fibre might be due to the increased wettability of the silane treated fibre with epoxy resin.

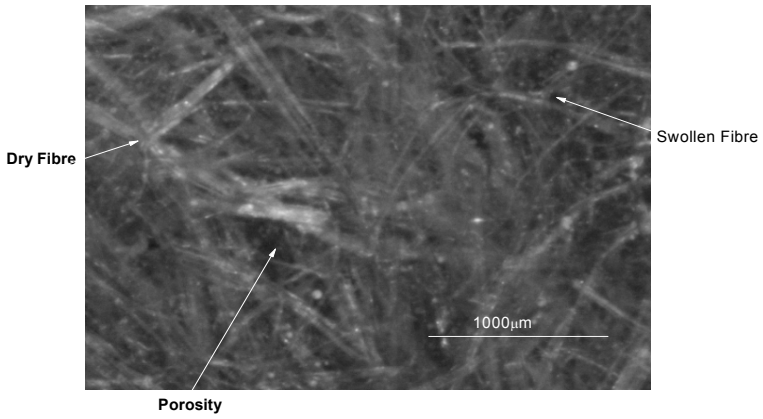

Figure 4.22 Optical micrograph of STFE composites cured at 25^{o}C.

The poor fibre wetting of the ATFE composites is evident by dry fibre (whitish area in the fibres), fibre swelling, and porosity, Figure 4.23. However, ATFE

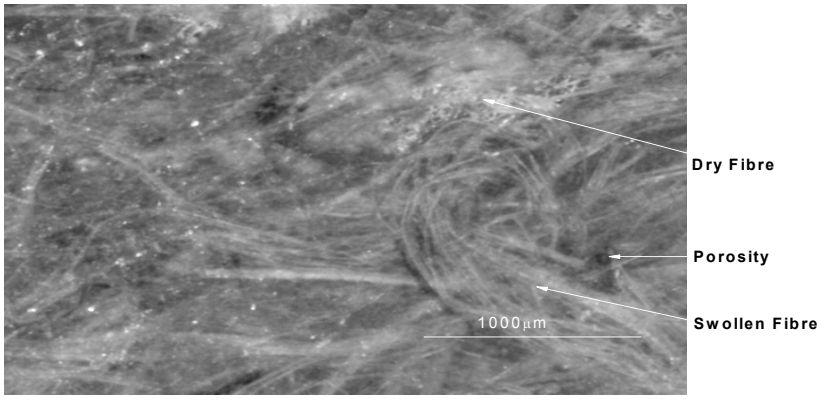

Figure 4.23 Optical micrograph of ATFE composites cured at 25^{o}C.

composites were found to contain less dry fibre, less fibre swelling, and less porosity compared to UTFE, AcFE, and STFE composites. Alkali treatment resulted in an increase in -OH groups on the fibre surface and possibly an increase in exposed surface area due to the removal of non-cellulose fibre components like hemicelluloses, lignin, and pectin as supported by FTIR analysis described in section 3.3.1.10. Therefore, more -OH groups were revealed which would be more compatible with epoxy resin. It is well known that epoxy resin has active groups known as epoxide or -OH groups to produce a network structure with the active hydrogen atoms of an amine curing agent [4]. It is very likely that these epoxide groups and the active hydrogen groups of the hardener can react well with the free -OH groups of the cellulose present in hemp fibres to form very strong covalent bonds in addition to the hydrogen bonds. Alkali treatment of fibres also made the fibre surface rougher, which allows more mechanical interlocking with epoxy resin. Thus, the formation of more hydrogen and covalent bonding, and increased mechanical interlocking of the alkali treated fibres with the epoxy resin, compared to untreated fibres, resulted in an increase in composite tensile strength and stiffness. The reduction in FS of the ATFE composites, compared to UTFE composites, could be due to increased cross linking between fibre and epoxy by the increased exposure of –OH groups in the alkali treated fibres.

From Figures 4.20 to 4.23, it can be seen that the presence of porosity, dry fibre, and swollen fibre in the composites are in the order: UTFE> AcFE > STFE > ATFE which was found to be consistent with increasing TS of the composites. High pressure during the curing process is needed because the low density of the hemp fibre like other natural fibres caused the fibre to float up in the resin and fibre mats to swell before curing [203]. The presence of pores in the composites which is likely to be due to low processing pressure corresponded to inefficient load transfer between the fibre and matrix which resulted in poor TS of the composites [84].

Furthermore, STFE composites showed an increase in YM of about 143% over untreated fibre, 164% over acetylated fibre, and about 4% over ATFE composites. The higher YM and lower FS of the STFE composites compared to the other composites could be attributed to excessive cross-linking of the fibre -OH groups with the highly active silane groups and active hydrogen groups of the amine

curing agent. This theory is supported by the brittle fracture surface of a STFE composite given in Figure 4.24.

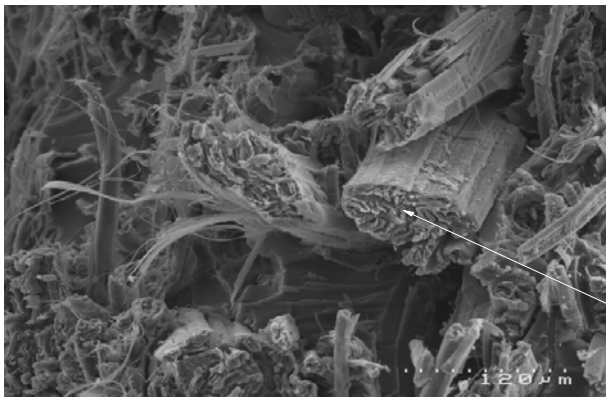

Figure 4.24 SEM micrograph of the fracture surface of STFE composites.

Figure 4.25 shows the effect of curing temperature on the tensile properties of NE and composites. In each case, an increase in TS and YM was observed for NE and

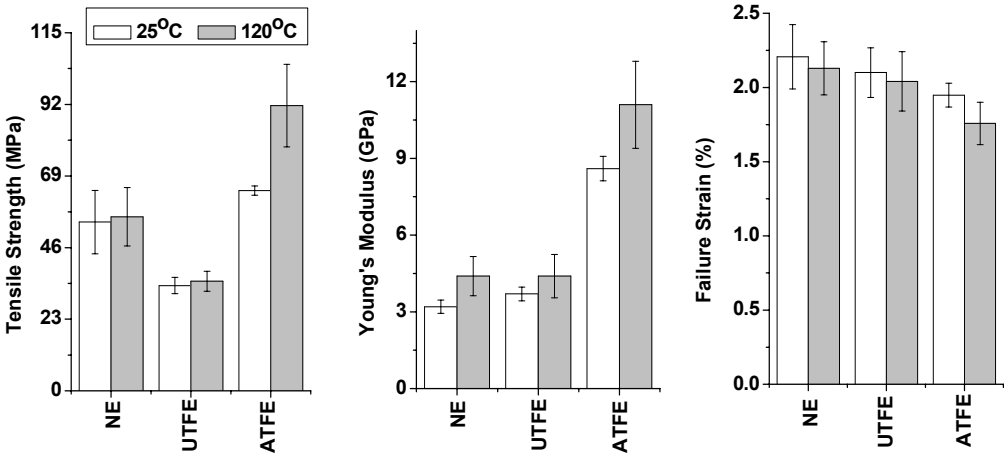

Figure 4.25 Tensile properties of UTFE and ATFE composites compared to NE cured at 25°C and 120°C. Error bars each corresponds to one standard deviation.

composites cured at 120°C compared to the NE and composites cured at 25°C. The increase in TS and YM for the NE could be due to the increased interaction of epoxy resin with the amine curing agent due to the reduction of viscosity of epoxy resin at 120°C compared to 25°C. The increase in TS and YM for the composites at 120°C compared to 25°C may be due to a reduction in viscosity of the epoxy resin that could lead to better wetting of the fibre with epoxy resin at 120°C as

well as better matrix integrity. Better wetting of the fibres with epoxy resin cured at 120°C was supported by the presence of less porosity, less fibre swelling, and absence of dry fibres in the composites cured at 120°C, Figure 4.26, than the composites cured at 25°C, Figure 4.23. A slight decrease in FS could be due to a stronger interface formed by better wetting of the fibres with epoxy resin at 120°C. The ATFE composites showed the greatest improvement in TS and YM when the increased curing temperature was used compared to UTFE composites. The increased TS could be attributed to the reduced porosity due to the increased wetting and the increased YM could be attributed to the better potential for bonding of the alkali treated fibres compared to untreated fibres, Figures 4.23 and 4.26.

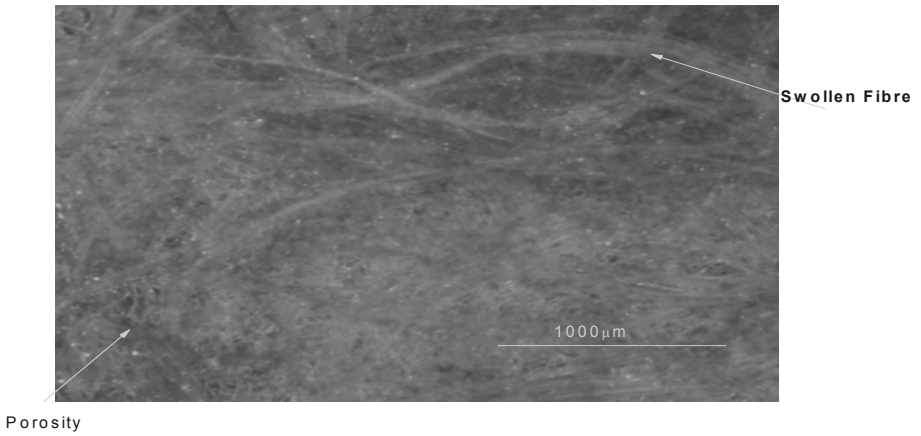

Figure 4.26 Optical micrograph of ATFE composites cured at 120°C.

4.3.4 Effects of Epoxy to Curing Agent Ratios on Composite Tensile Properties

Figure 4.27 shows the tensile properties of 30 and 40 wt% UTFE and ATFE composites produced using four different epoxy to curing agent ratios. From the

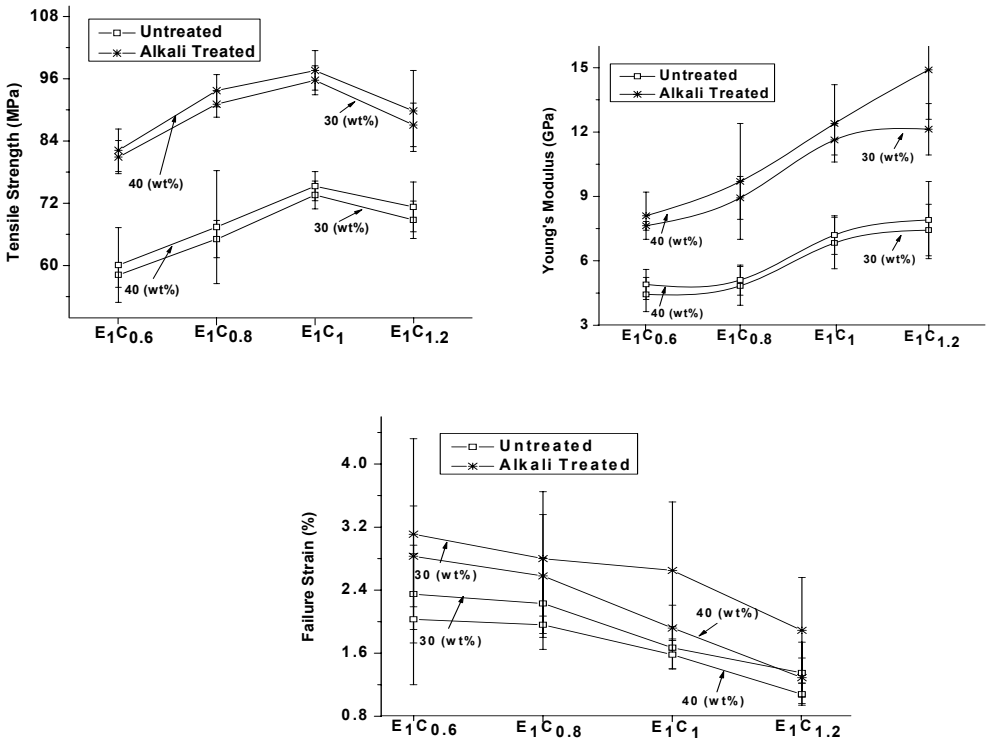

Figure 4.27 Tensile properties of 30 and 40 wt% UTFE and ATFE composites produced at four different epoxy to curing agent ratios. Error bars each corresponds to one standard deviation.

results, it can be seen that the TS and YM increased for both the UTFE and ATFE composites as the ratio of epoxy resin to curing agent was raised from 1:0.6 to 1:1. On the other hand, TS was found to decrease and YM was found to increase when composites were produced with an epoxy to curing agent ratio of 1:1.2. The results are consistent with the IFSS values described in section 4.3.2. The decrease in the FS of the composites with the increase of the epoxy resin to curing agent ratios could be explained by the reduced matrix integrity and its wettability with fibre as discussed in section 4.3.2.

The increase in TS and YM of the composites with the increase in fibre loading appears simply to be due to an increase in reinforcement. The decrease in FS with increased fibre loading may be caused by the increased constraint at higher fibre loading of 40 wt% compared to the fibre loading of 30 wt%.

Composites produced with alkali treated fibres were found to exhibit better tensile properties than those with untreated fibres at both fibre loadings (30 and 40 wt%) and with all tested epoxy to curing agent ratios. This could be due to the increased

bonding of epoxy resin with fibres due to the increased availability of fibre –OH groups and surface roughening upon alkali treatment as discussed in section 4.3.2.

The increase in tensile properties for UTFE and ATFE composites seen when fibre was aligned by hand carding, Figure 4.27, compared to fibre aligned by hackling, Figure 4.19, (section 4.3.3), may be attributed to the better separation and fibre alignment obtained by the carding process [233]. The improved fibre separation led to better wetting of the fibres with resin and resulted in fewer pores in the composites, as can be supported by comparison of Figure 4.28 with Figure 4.23 (section 4.3.3); Figure 4.23 shows much more pororsity due to dry and swelled fibres. However, to reduce the number of pores in the composites to an acceptable level, further improvements in composite processing were necessary.

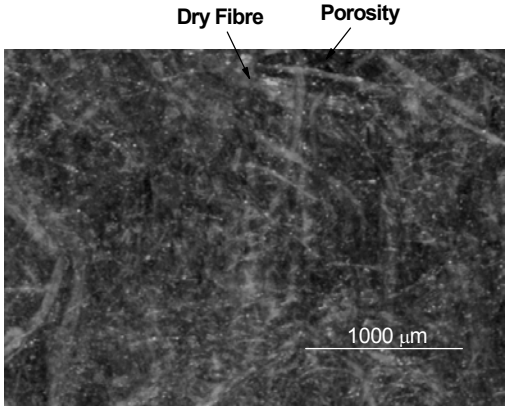

Figure 4.28 Optical micrograph of ATFE composites produced by aligned mat obtained by hand carding machine.

4.3.5 Effects of Fibre Soaking Time in Resin Bath on Composite Tensile Properties

Figure 4.29 shows the tensile properties of UTFE and ATFE composites produced by soaking the fibre mats for 10 and 60 minutes. From the results it can be seen that the tensile properties of both the UTFE and ATFE composites increased with the increase in soaking time to some extent. The increased tensile properties with the soaking time of 60 minutes, compared to that of 10 minutes, are likely to be due to increased fibre wetting during soaking by the epoxy resin leading to better interfacial strength. The increased soaking time also appears to have decreased

porosity in the composites as supported by the optical micrographs of the 10 and 60 minutes soaked composites given in Figures 4.30 and 4.31 respectively; composites produced with 10 minutes soaking time were found to appear with a lot of dry fibres while almost no dry fibres were visible for the composites produced with 60 minutes soaking time.

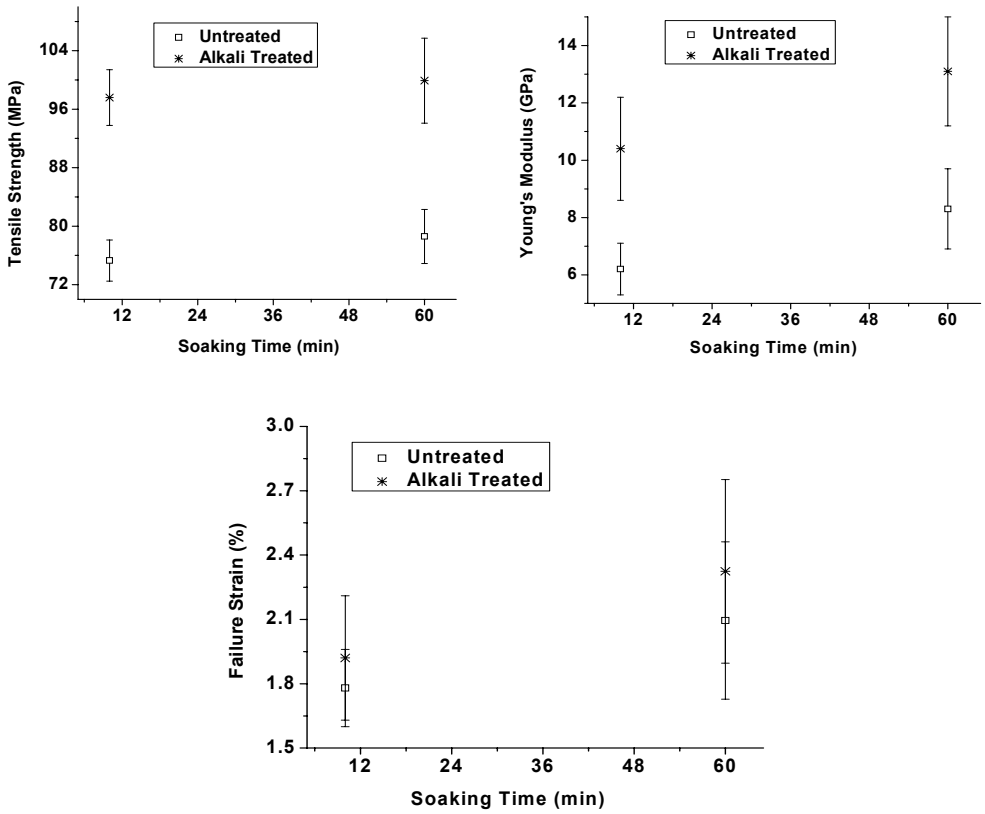

Figure 4.29 Tensile properties of untreated and alkali treated composites produced by soaking the fibre mats for 10 and 60 minutes. Error bars each corresponds to one standard deviation.

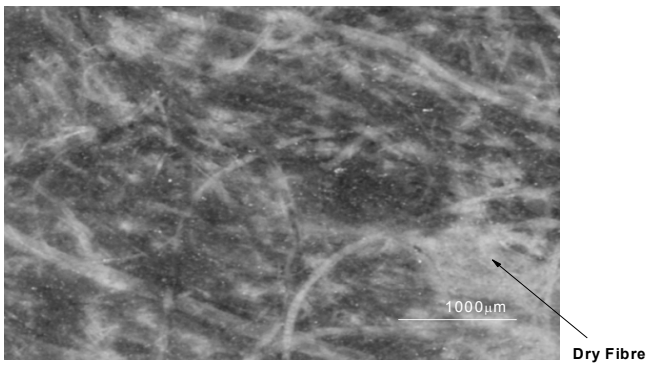

Figure 4.30 Poor wetting of fibre in ATFE composites produced by soaking for 10 minutes in the resin bath.

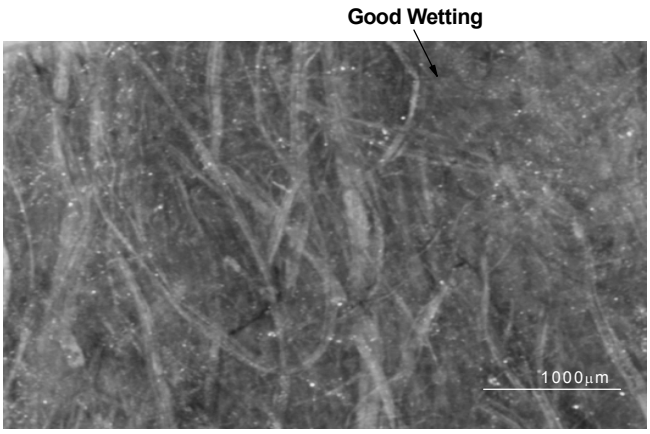

Figure 4.31 Good wetting of fibre in ATFE composites produced by soaking for 60 minutes in the resin bath.

4.3.6 Effects of Curing Temperatures on Composite Tensile Properties

Figure 4.32 shows the tensile properties of UTFE and ATFE composites produced at three different curing temperatures of 25, 70 and 120^{o}C. From the results it can be seen that TS and YM are higher at 70^{o}C than at 25^{o}C for both UTFE and ATFE composites, but decrease as the curing temperature was increased further to 120^{o}C, whereas the converse is true for FS. TS, YM and FS are consistently higher for ATFE than for UTFE composites.

The increase in curing temperature would be expected to decrease the viscosity of the epoxy resin [234], which could lead to better penetration of the resin between

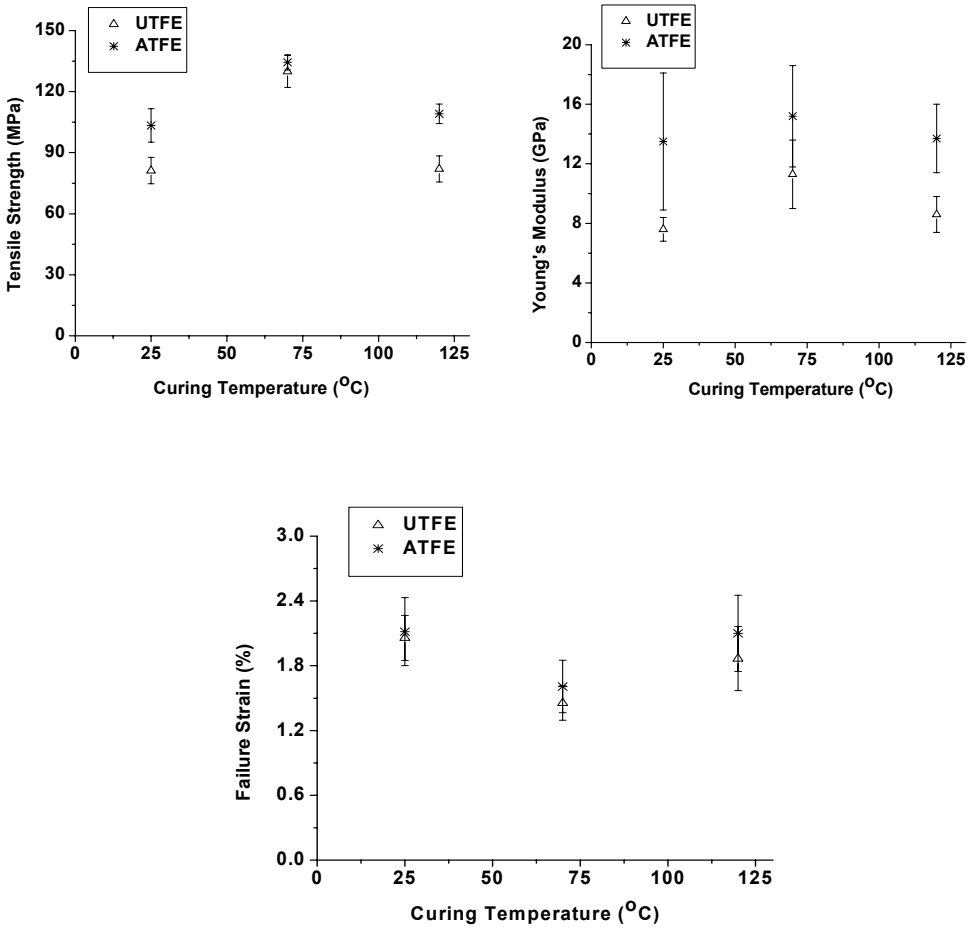

Figure 4.32 Tensile properties of UTFE and ATFE composites produced at three different curing temperatures. Error bars each corresponds to one standard deviation.

the fibres and result in an increase in fibre/resin wetting. Increased fibre/resin wetting could result in a stronger interface which could lead to an increase in TS and YM and a decrease in FS of the composites. However, a decrease in tensile properties for composites produced at 120°C, compared to those composites produced at 70°C was observed. Figures 4.33(a) and 4.33(b) show SEM

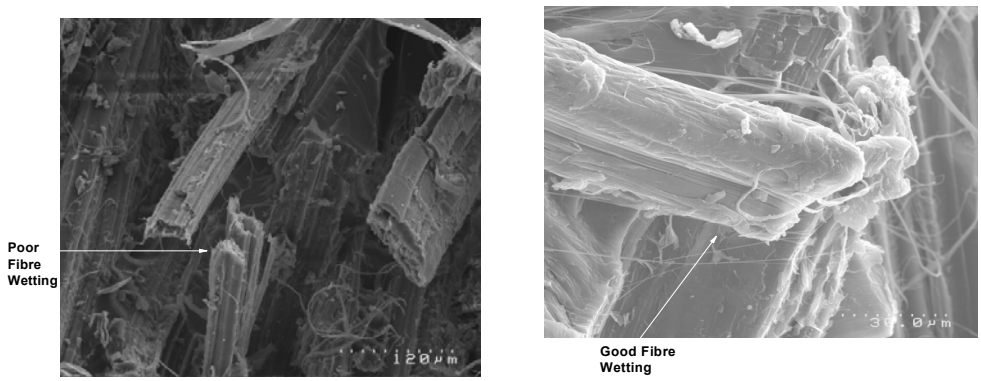

(a) (b)

Figure 4.33 SEM micrographs of fracture surfaces of tensile tested specimens with 40 wt% alkali treated fibres produced at (a) 120°C and (b) 70°C curing temperatures.

micrographs of fracture surfaces of tensile tested specimens with 40 wt% alkali treated fibres produced at 120°C and 70°C curing temperatures respectively. It can be seen from the figures that good wetting of fibre was obtained for the composites cured at 70°C and poor wetting of fibre was obtained for the composites cured at 120°C. It appears that composite production with rapid curing at 120°C might not have allowed epoxy resin to penetrate between the fibres as effectively as it did during composite production by curing at 70°C. In addition, curing at a higher temperature can also generate higher internal stresses which may have resulted in decreased tensile properties as observed by Hepworth *et al.* [203].

The increase in tensile properties for ATFE composites, compared to UTFE composites, is likely due to the increased bonding for ATFE composites as described in section 4.3.3**.**

Production of UTFE and ATFE composites by compression moulding, Figure 4.32, demonstrated much better reinforcement by the fibres compared to the composites produced by vacuum bagging, Figure 4.27, (section 4.3.4) using the same processing parameters (25°C curing temperature, 40 wt% fibre content, aligned by hand carding machine). Compression at high pressure appears to have resulted in good consolidation of the fibres in epoxy resin and reduced the level of

porosity in the composites significantly, leading to an increase in TS and YM [203].

4.3.7 Effects of Fibre Orientation (Short Fibres) on Composite Tensile Properties

Figure 4.34 shows the tensile properties of planar random (produced by hand lay-up, section 4.2.2.3) and aligned short fibre (produced by DSF, section 4.2.2.3) composites produced with untreated and alkali treated fibres. From the results it can be seen that fibre alignment along the tensile testing axis increased the tensile properties of both UTFE and ATFE composites compared to randomly oriented fibre composites. Generally, composite strength would be expected to increase with the degree of alignment along the tensile testing axis particularly with anisotropic fibres such as natural cellulosic fibres. However, perfect alignment is not possible to achieve experimentally, particularly in the case of short fibres due to processing difficulties. In this study, the increase in tensile properties of the aligned short fibre composites compared to the randomly oriented short fibre composites indicated that a reasonable extent of alignment of the short fibres were achieved by DSF. ATFE composites showed higher TS and YM compared to those for UTFE composites, which is likely to be due to better bonding of the alkali treated fibres with epoxy resin as discussed in section 4.3.3.

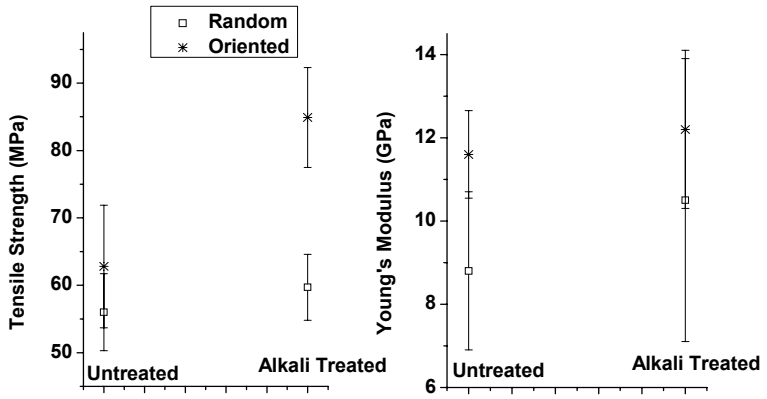

Figure 4.34 Tensile properties of random and aligned short fibre composites produced with untreated and alkali treated fibres. Error bars each corresponds to one standard deviation.

4.3.8 Effects of Fibre Loading on Composite Tensile Properties, Thermogravimetric Analysis (TGA) of the Composites, and Modelling of Tensile Strength (TS) of the Composites

4.3.8.1 Effects of Fibre Loading on Composite Tensile Properties

Long Fibre Composites

Figure 4.35 shows the tensile properties of UTLFE and ATLFE composites cured at 70°C with three different fibre contents of 40, 50, and 65 wt%. An increase in TS and YM, and a decrease in FS for both UTLFE and ATLFE composites can be seen with the increased fibre content. Similar relationships for fibre reinforced composites have been observed by other researchers [84, 235]. Increased TS and

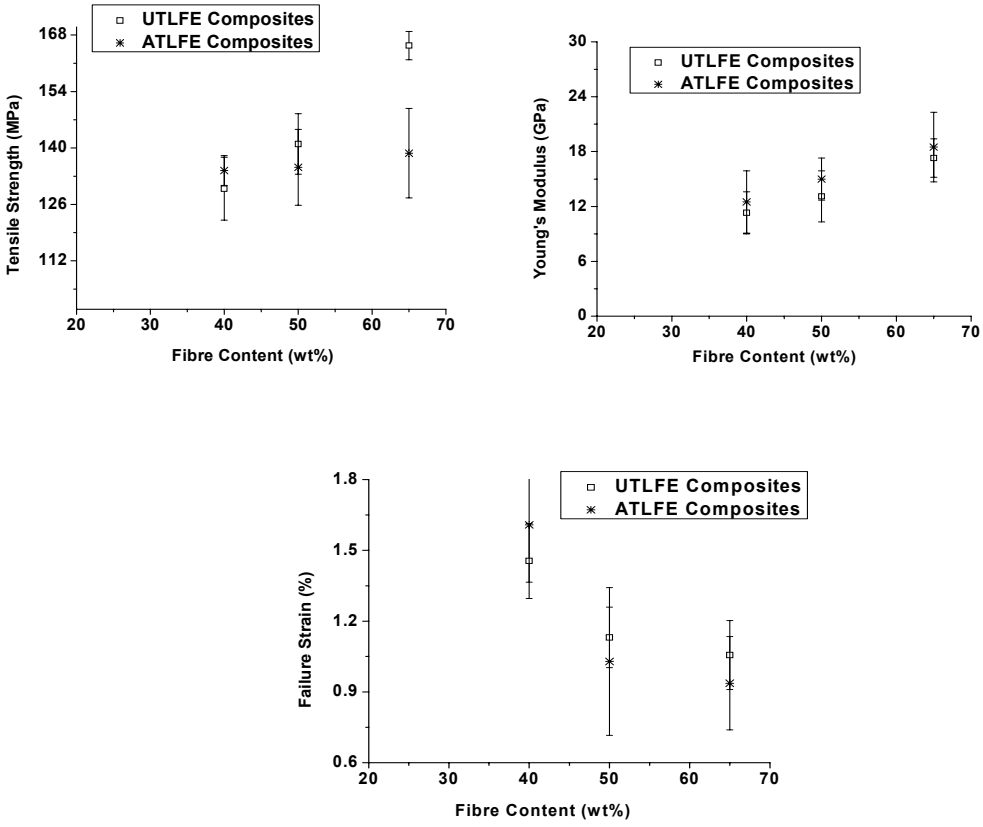

Figure 4.35 The variation in tensile properties with fibre loading for UTLFE and ATLFE composites. Error bars each corresponds to one standard deviation.

YM demonstrates effective reinforcement by the fibres of the composites which is commonly associated with a decrease in FS of the composites, probably due to increased constraint with the increased fibre content in the composites.

At 40 wt% fibre, ATLFE composites showed the most effective reinforcement, with approximate increases of TS of 4% and YM of 11% compared to UTLFE composites. However, at fibre contents of 50 and 65 wt% TS was found to decrease for ATLFE composites compared to UTLFE composites although YM was still found to increase. Alkali treatment was found to reduce fibre diameter as is supported by the results described in section 3.3.1.4. This is likely to be due to the removal of non-cellulosic materials which would also reduce the weight of individual fibres [68]. Therefore, for the same fibre content (wt%) in composites, the number of fibres would be higher for the alkali treated fibres than for untreated fibres. The increase in number of fibres at higher fibre loadings would increase fibre-fibre contact in the ATLFE composites such that inefficient stress transfer between fibres could occur and reduction in TS [217, 236]. Figures 4.36(a) and 4.36(b) show the SEM micrographs of fracture surfaces of 65 wt% UTLFE and ATLFE composites respectively. Composite fracture with longer separated fibres and holes indicative of more pull-out, Figure 4.36(b), for ATLFE composites compared to UTLFE composites, Figure 4.36(a), supports increased fibre contact occurring for ATLFE composites initiating fibre debonding. The reduction in TS of the alkali treated fibres as discussed in section 3.3.1.2 would also contribute to the reduction in TS of the composites. However, YM is

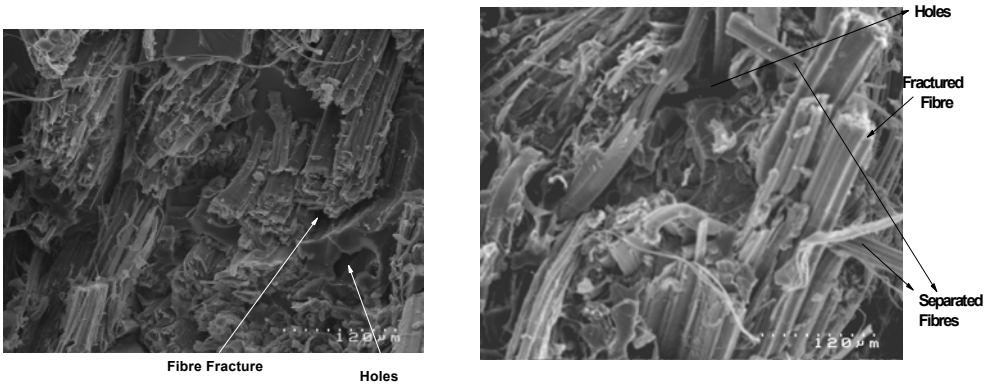

(a) (b)

Figure 4.36 SEM pictures of fracture surfaces of 65 wt% (a) UTLFE and (b) ATLFE composites.

calculated from the slope of the stress strain graphs during the initial stage of load application before the effect of stress concentration due to fibre-fibre contact becomes effective. ATLFE composites maintain higher YM than the UTLFE composites at higher fibre loadings due to higher average interfacial bonding. The reduction in FS for the ATLFE composites compared to UTLFE composites is also likely to be due to failure initiated from stress concentration caused by fibre-fibre contact in ATLFE composites.

Short Fibre Composites

Figure 4.37 shows the tensile properties of UTSFE and ATSFE composites cured at 70^{o}C and three different fibre contents of 40, 50, and 65 wt%. Similar to long fibre composites, an increase in TS and YM and a decrease in FS for both UTSFE and ATSFE composites were observed with increased fibre content.

ATSFE composites consistently had higher TS and YM with lower FS compared to UTSFE composites. The increase in TS and YM for ATSFE composites compared to UTSFE composites is likely to be due to better bonding of the alkali treated fibres with epoxy resin as described in section 4.3.3**.** Reduction in FS for the ATSFE composites compared to UTSFE composites is likely to be due to increased constraint of the alkali treated fibres compared to untreated fibres as previously discussed.

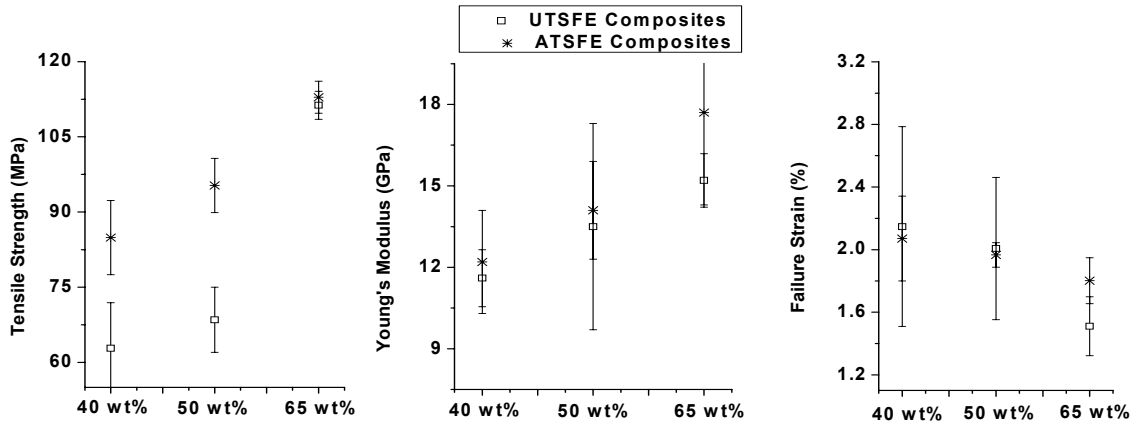

Figure 4.37 The variation in tensile properties with fibre loading for UTSFE and ATSFE composites. Error bars each corresponds to one standard deviation.

However, for 65 wt% the TSs were found to be almost similar for both UTSFE and ATSFE composites which could be due to increased fibre-fibre contact as discussed earlier for long fibre/epoxy composites. The reason for the increased FS (about 19%) for the ATSFE composites compared to UTSFE composites at 65 wt% fibre content could be due to the higher average failure strain of the alkali treated fibres from the increased number of fibres in the ATSFE composites.

Figures 4.38(a) and 4.38(b) show the SEM pictures of fracture surfaces of 65 wt% UTSFE and ATSFE composites respectively. It can be seen that fibre fracture is dominant for composites produced with 65 wt% fibre contents. Although some pull-out was seen in the form of holes for UTSFE, Figure 4.38(a), pull-out in the form of holes and long separated fibres for ATSFE composites, Figure 4.38(b), supports increased fibre-fibre contact occurring for ATSFE composites compared to UTSFE composites initiating fibre debonding as discussed earlier for long fibre/epoxy composites.

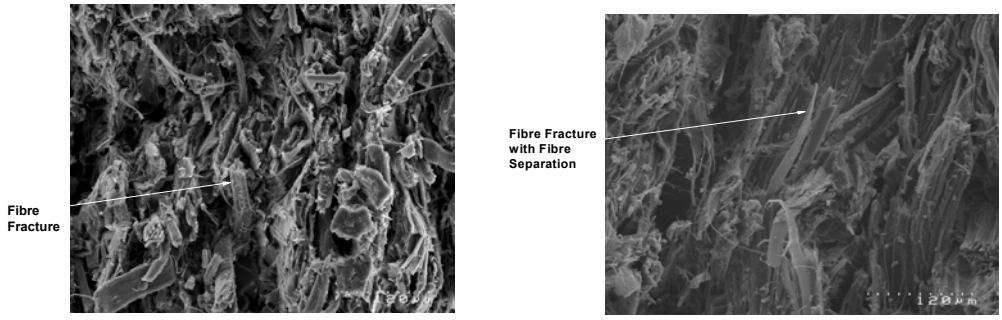

(a) (b)

Figure 4.38 SEM pictures of fracture surfaces of 65 wt% (a) UTSFE and (b) ATSFE composites.

The TS and YM of short fibre/epoxy composites compared to those of long fibre/epoxy composites were not found to be surprisingly higher at all fibre contents which would be expected due to higher reinforcement efficiency for the long fibres. However, the increase in FS for the short fibre/epoxy composites compared to the long fibre/epoxy composites may be due to less constraint from the short fibres, so the matrix can undergo greater strain before breaking.

4.3.8.2 Thermogravimetric Analysis (TGA) of the Long Fibre Composites

TGA traces for 65 wt% UTLFE and ATLFE composites are shown in Figure 4.39. It can be seen that there are three stages of weight loss of the composites. With increase of temperature, dehydration and decomposition of volatile products were observed up to about 280^{o}C, followed by rapid weight loss due to the decomposition of cellulose up to about 365^{o}C, and finally, oxidative decomposition of volatile and charred products [208, 237]. It can be seen that the weight loss was higher at the initial and final stages of thermal degradation for ATLFE composites, while it was higher at the second stage of thermal degradation for UTLFE composites. Exposure of -OH groups increase the hydrophilicity of alkali treated fibres (section 3.3.1.6) resulting in an increase in adsorbed moisture content compared to untreated fibres and therefore higher weight loss due to dehydration and decomposition of volatile products was observed for ATLFE composites. Removal of non-cellulosic components from the fibre by alkali treatment resulted in an increased cellulose content that led to lower weight loss at the second stages of thermal degradation for ATLFE composites

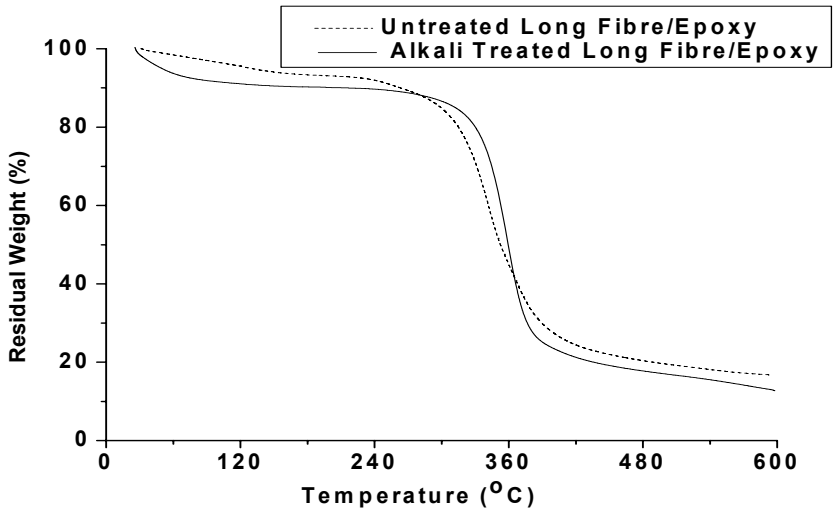

Figure 4.39 TGA traces for UTLFE and ATLFE composites.

(supported by increased cellulose crystallinity of alkali treated fibre (section 3.3.1.7)). At the third stage of thermal degradation, the presence of lignin

contribute to the formation of charred products (the weight residue was about 16% and 12% for UTLFE and ATLFE composites, respectively) that might result in a greater reduction in weight loss for UTLFE composites compared to the ATLFE composites [238].

4.3.8.3 Modelling of Tensile Strength (TS) of Composites

Figures 4.40 and 4.41 show the experimentally obtained values of TS of the untreated and alkali treated fibre/epoxy composites (long and short fibres) as a function of fibre volume fraction along with the theoretically expected TS values (the density of the hemp fibre was considered as 1.48 g/cm^3 [32]) using different models, namely: the Series, Parallel, and MROM Models, Equations (2.12) to (2.14). It can be seen that, for all the cases TS increases gradually with increasing fibre volume fraction. As discussed earlier in section 2.12, the Parallel Model (for axial TS of composite materials) can be considered to represent the upper bound and the Series Model (for transverse TS of composite materials) the lower bound of TS for continuous unidirectional composites; the experimental TS values of the composites were found to lie between the values calculated using those two models with the exception of UTSFE composites. The low TS values for UTSFE composites indicate poor reinforcement by untreated short fibres in the composites.

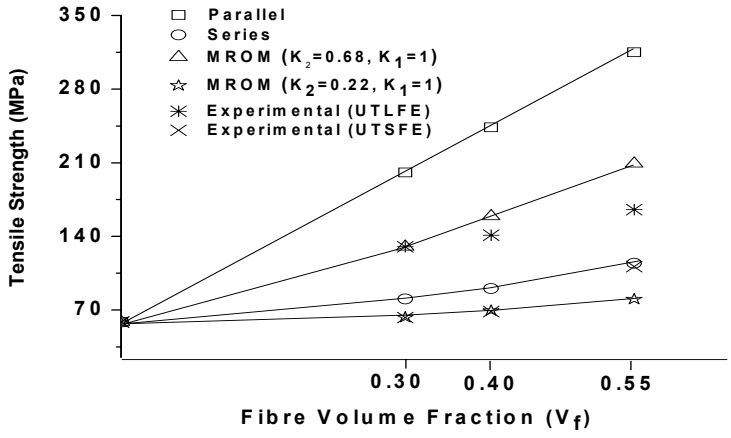

Figure 4.40 Tensile strength versus fibre volume fraction of composites (solid lines for theoretical model values and symbols for experimentally obtained values for UTLFE and UTSFE composites).

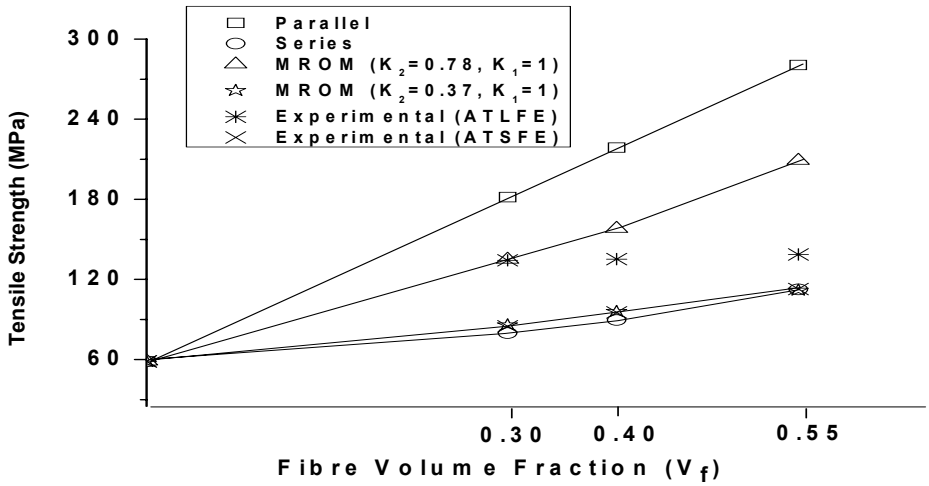

Figure 4.41 Tensile strength versus fibre volume fraction of composites (solid lines for theoretical model values and symbols for experimentally obtained values for ATLFE and ATSFE composites).

For long fibre, the factor K_2 = 0.68 and 0.78 for UTLFE and ATLFE composites respectively, in Equation (2.14) of MROM (assuming orientation factor K_1 = 1) gave the best correlation between experimental TS and the TS expected from the model at a fibre volume fraction (V_f) of 0.30. However, negative deviation from this correlation increased with the increase of the fibre content in the composites, which could be due to fibre agglomeration. According to other researchers [239] when the fibre content in the composite is low, stress is distributed more uniformly in the composite, however, at higher fibre contents fibre agglomeration predominates, causing an uneven distribution of the applied load in the composites which reduces reinforcement efficiency. Departure of experimental TS from the linearity that would be expected from the MROM model was greater at higher V_f for ATLFE than UTLFE composites, suggesting greater fibre agglomeration. As discussed in section 2.12, a three dimensional random fibre alignment yields a value of K_1 = 0.2, planar random configuration yields a value of 0.375 and an axially aligned fibre yields a value of K_1 = 1. However, as the same fibre alignment method (hand carding) was used for both UTLFE and ATLFE composites and the reinforcing efficiency of the composites can be defined as a product of K_1 and K_2, therefore, a higher value of the factor K_2 for ATLFE composites, when assuming K_1 = 1 could really indicate better fibre/matrix adhesion for ATLFE composites. Better fibre matrix adhesion of

ATLFE composites when compared to UTLFE composites can be evident from Figure 4.36(a) and (b) as shown earlier in section 4.3.8.1.

For short fibre/epoxy composites, the factor K_2 = 0.22 for UTSFE composites in Equation (2.14) of MROM (assuming orientation factor K_1 = 1) gave the best correlation between experimental TS and the TS expected from the model at V_f of 0.30 and 0.40; and positive deviation from this correlation was observed at a V_f of 0.55. However, the factor K_2 = 0.37 for ATSFE composites in Equation (2.14) of MROM (assuming orientation factor K_1 = 1) gave consistent correlation between experimental TS and the TS trend that would be expected from the model. However, as the same fibre alignment method (dynamic sheet forming) was used for both UTSFE and ATSFE composites and the reinforcing efficiency of the composites can be defined as a product of K_1 and K_2, therefore, a higher value of the factor K_2 for ATSFE composites, when assuming K_1 = 1 could again indicate better fibre/matrix adhesion for ATSFE composites. Better fibre matrix adhesion of ATSFE composites when compared to UTSFE composites can be evident from Figure 4.38(a) and (b) as shown earlier in section 4.3.8.1.

It must be remembered that the Parallel, Series, and MROM models are simplistic and do not take account of many features including agglomeration, nonuniformity, and unpredictability of fracture mechanics of the composites.

4.3.9 Flexural, Impact, and Fracture Toughness of the Composites

Long Fibre Composites

Composite Flexural Properties

Figures 4.42 and 4.43 show the flexural strength and flexural modulus respectively, of UTLFE and ATLFE composites produced with 65 wt% fibre compared to those of NE. It can be seen here that UTLFE and ATLFE composites have about 85% and 76% higher flexural strength, and about 229% and 235% higher flexural modulus respectively, compared to NE. Similar to TS, flexural strength was higher for UTLFE composites and similar to YM, flexural modulus

was higher for ATLFE composites which is likely to be due to the same reasons as described in section 4.3.8.1.

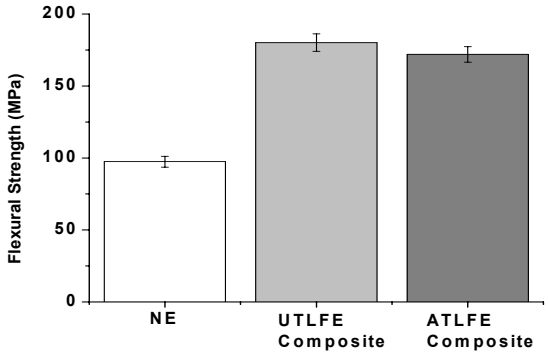

Figure 4.42 Flexural strength of UTLFE and ATLFE composites compared to NE. Error bars each corresponds to one standard deviation.

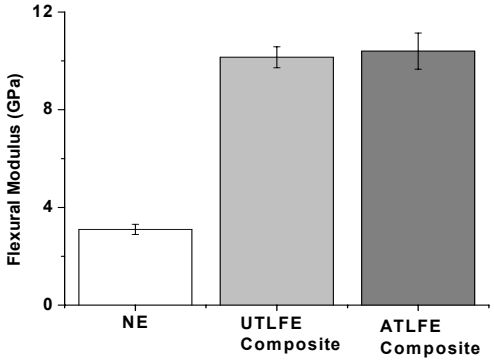

Figure 4.43 Flexural modulus of UTLFE and ATLFE composites compared to NE. Error bars each corresponds to one standard deviation.

Composite Impact Energy (IE)

Figure 4.44 shows the IE of UTLFE and ATLFE composites produced with 65 wt% fibre compared to that for NE. From the results it can be seen that the IE for composites was over six times higher than that of NE. Improvement in IE has also been observed by Acha *et al.* [240] who obtained an increase of more than three times of the IE of untreated jute fibre composites compared to the brittle unsaturated polyester matrix. Slightly higher IE was seen in the current work for ATLFE composites compared to UTLFE composites, Figure 4.44, which might be due to slightly more fibre pull-out and delamination for ATLFE composites which could bring about a difference in the fracture mode**.** As discussed in section

4.3.8.1, a reduction in fibre diameter due to treatment of the fibres with alkali increased the number of fibres for the same fibre content (in this case 65 wt%) for the ATLFE composites and would result in an increased fibre-fibre contact due to increased resin starved areas. An increased fibre-fibre contact in the composites would be expected to increase fibre pull-out in these composites and hence lead to the slight increase in IE.

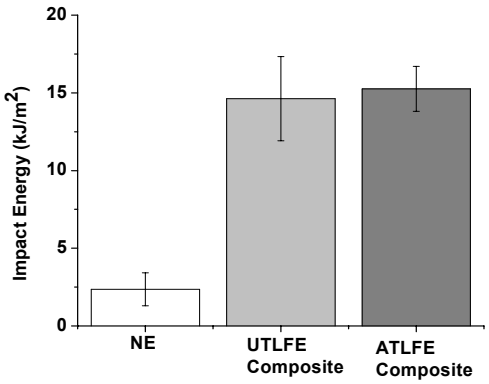

Figure 4.44 IE of UTLFE and ATLFE composites compared to NE. Error bars each corresponds to one standard deviation.

Composite Fracture Toughness (K_{Ic})

Figure 4.45 shows the K_{Ic} of UTLFE and ATLFE composites produced with 65 wt% fibre compared to that of NE. K_{Ic} was higher here for the composites than for

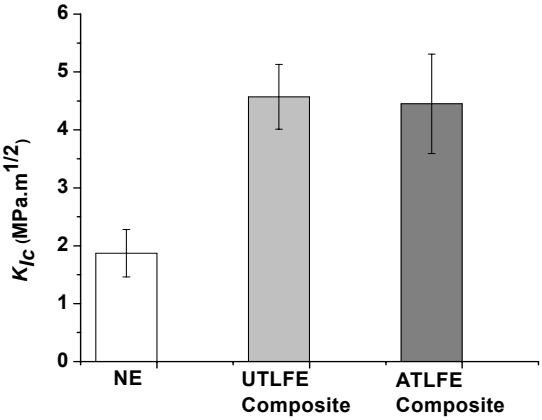

Figure 4.45 K_{Ic} of 65 wt% UTLFE and ATLFE composites compared to NE. Error bars each corresponds to one standard deviation.

NE. Other researchers have also reported higher K_{Ic} for the composites than for NE [241]. A slight decrease in K_{Ic} was seen here for ATLFE composites compared to that of UTLFE composites

This may be due to increased fibre-fibre contacts in ATLFE composites as discussed in section 4.3.8.1, which would make it comparatively easier for the alkali treated fibre to debond from the epoxy resin than for untreated fibre, Figure 4.46(a). On the other hand, less fibre-fibre contact in the UTLFE composites could lead to a stronger fibre/matrix interface, Figure 4.46(b), which would be expected to make the fibre pull-out comparatively difficult. Therefore, larger force could be required for the fibre to be debonded from the epoxy resin matrix and hence UTLFE composites have slightly higher $K_{Ic.}$

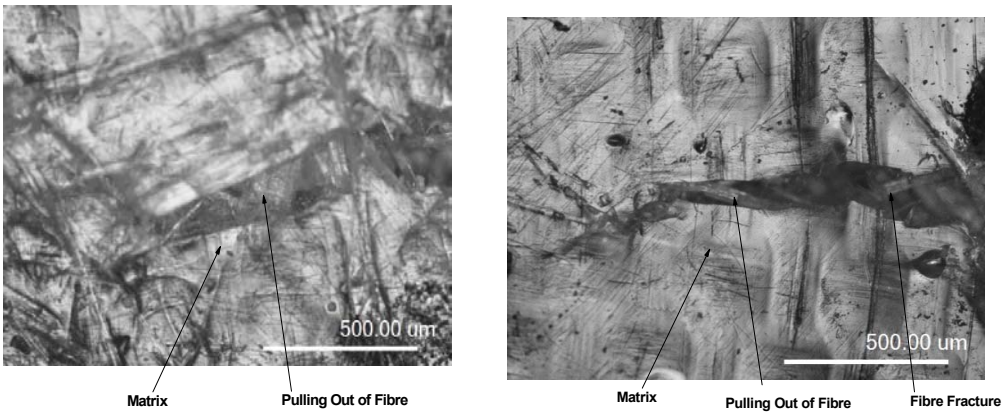

(a) (b)

Figure 4.46 Optical micrographs showing major crack of fracture toughness specimens of (a) ATLFE and (b) UTLFE composites.

Short Fibre Composites

Composite Flexural Properties

Figure 4.47 shows the flexural strength and flexural modulus of UTSFE and ATSFE composites produced with 65 wt% fibre compared to those of NE. It can be seen here that UTSFE and ATSFE composites have about 60% and 50% higher flexural strength, and about 161% and 225% higher flexural modulus respectively, compared to NE. The flexural strength and flexural modulus of short fibre/epoxy

composites were found to decrease when compared to those of long fibre/epoxy composites (section 4.3.9.1) which may be due to the lower reinforcement efficiency of the short fibre compared to that for long fibre as discussed earlier in section 4.3.8.1. As for long fibre/epoxy composites, the flexural strength was found to be higher for UTSFE composites and flexural modulus was found to be higher for ATSFE composites, which is likely to be due to similar reasons as described previously (section 4.3.9.1).

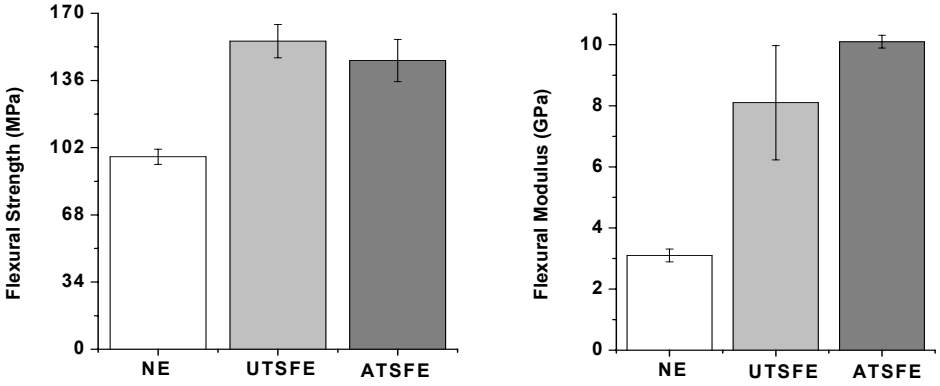

Figure 4.47 Flexural strength and flexural modulus of 65 wt% UTSFE and ATSFE composites compared to NE. Error bars each corresponds to one standard deviation.

Composite Impact energy (IE)

Figure 4.48 shows the IE of UTSFE and ATSFE composites produced with 65 wt% fibre compared to that of NE. From the results it can be seen that the IE for UTSFE and ATSFE composites was higher (about 3 and 5 times higher respectively) than the energy absorbed by NE. The IE of the short fibre/epoxy composites was found to be lower than that of long fibre/epoxy composites which may be due to less fibre pull-out in the short fibre/epoxy composites. Similar to long fibre/epoxy composites, the IE of ATSFE composites was found to be higher than that of UTSFE composites which is likely to be due to the same reasons as discussed earlier in section 4.3.9.1.

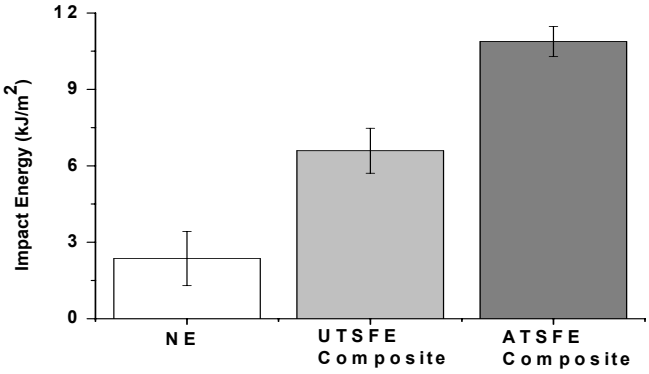

Figure 4.48 IE of UTSFE and ATSFE composites compared to NE. Error bars each corresponds to one standard deviation.

Composite Fracture Toughness (K_{Ic})

Figure 4.49 shows the K_{Ic} of UTSFE and ATSFE composites produced with 65 wt% fibre compared to that for NE. K_{Ic} was higher for the composites than for NE [241]. K_{Ic} of short fibre/epoxy composites was found to be lower than that for long fibre/epoxy composites (section 4.3.9.1) which may be due to lower fibre pull-out in short fibre/epoxy composites. Similar to long fibre/epoxy composites, a slight decrease in K_{Ic} for ATSFE composites compared to UTSFE composites (section 4.3.9.1) suggesting easier debonding of fibre from the epoxy resin matrix in ATSFE composites due to increased fibre/fibre contact.

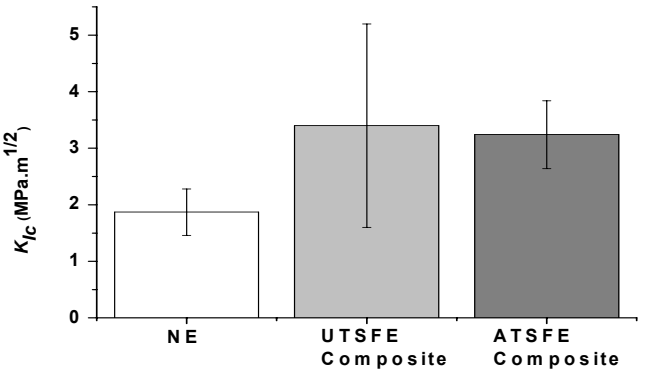

Figure 4.49 K_{Ic} of 65 wt% UTSFE and ATSFE composites compared to NE. Error bars each corresponds to one standard deviation.

4.3.10 Hygrothermal Ageing of the Composites

The immersion of samples in water for hygrothermal ageing resulted in deterioration of surface texture, in the form of matrix cracking with an associated ease of fibre visualization, which was more pronounced for UTFE composites than ATFE composites for both long and short fibre/epoxy composites. Figures 4.50(a) and 4.50(b) show the optical micrographs of the surfaces of UTLFE and ATLFE composites after hygrothermal ageing at 70^{o}C. Hygrothermal ageing resulted in an increased sample thickness which increased with temperature, Figure 4.51. ATFE composites showed less thickness swelling than that for UTFE composites supporting that they are more hygrothermally resistant. About 7% less thickness swelling was observed for the short fibre/epoxy composites compared to the long fibre/epoxy composites.

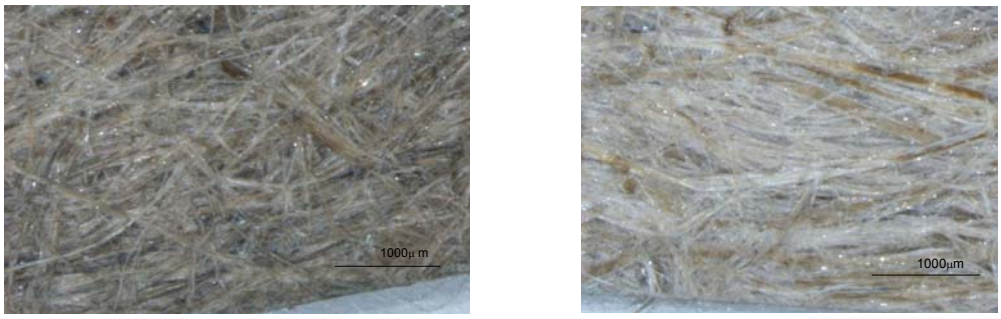

(a) (b)

Figure 4.50 Optical micrographs of (a) UTLFE and (b) ATLFE composite surfaces after hygrothermal ageing at 70^{o}C.

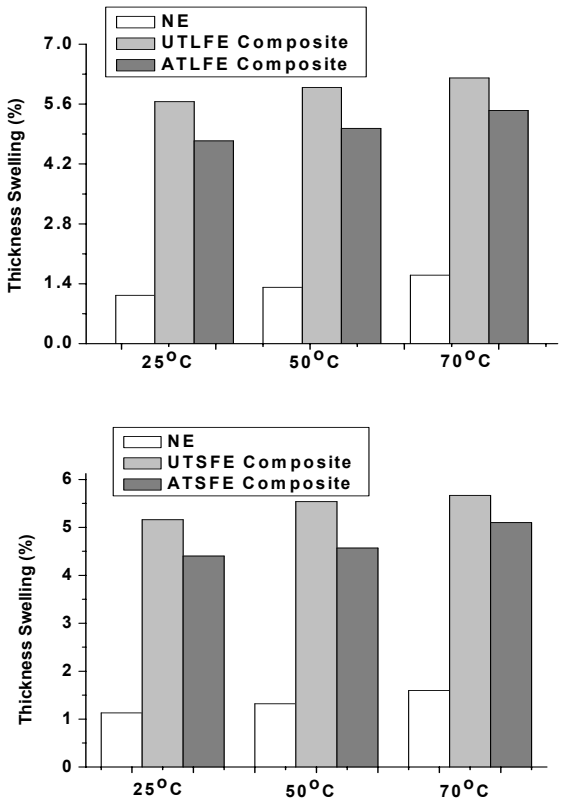

Figure 4.51 Thickness swelling of the NE and long and short fibre/epoxy composites after hygrothermal ageing.

Figures 4.52 to 4.56 show the percentage moisture content as a function of soaking time for NE, and untreated and alkali treated long and short fibre/epoxy composites. Moisture content increased with increasing time for all the samples until saturation. As it can be seen here, NE absorbed only a very small amount of moisture, Figure 4.52, compared to the composites during the immersion period, Figures 4.53 to 4.56; it seems likely that moisture penetrated composites mainly through the fibre and fibre/epoxy resin interface. It has been reported elsewhere that when exposed to moisture, the fibre/matrix interface absorbs moisture which may result in the development of shear stress at the interface leading to debonding of the fibres [7]. It has also been reported in the literature that hygrothermal ageing accelerates the debonding process that results in delamination and loss of structural integrity [242]

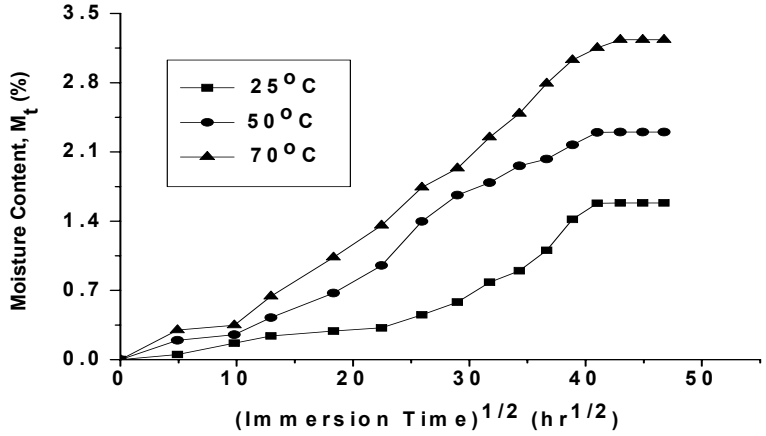

Figure 4.52 Moisture absorption behaviour of NE at 25, 50, and 70°C.

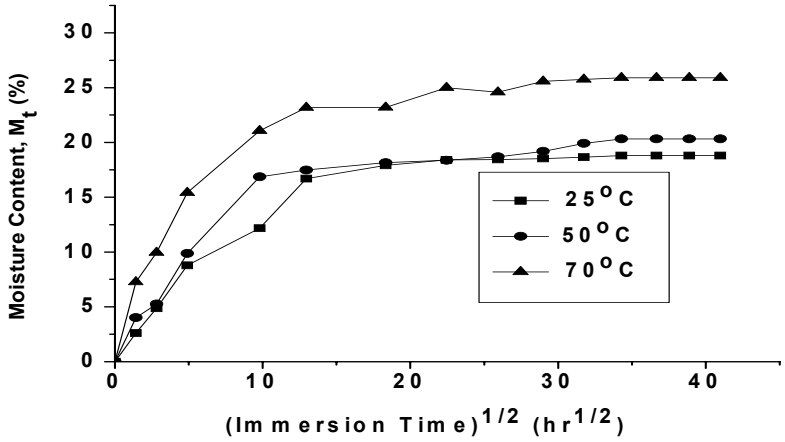

Figure 4.53 Moisture absorption behaviour of 65 wt% UTLFE composites at 25, 50, and 70°C.

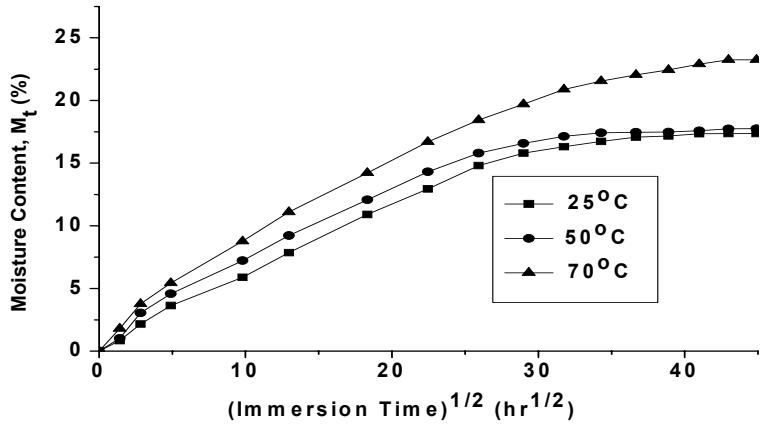

Figure 4.54 Moisture absorption behaviour of 65 wt% ATLFE composites at 25, 50, and 70°C.

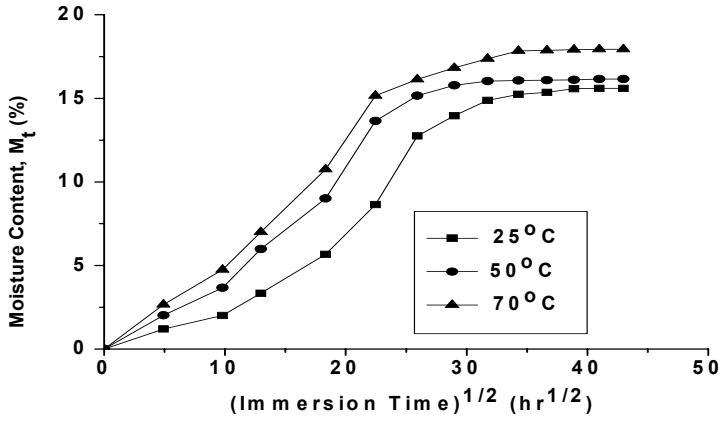

Figure 4.55 Moisture absorption behaviour of 65 wt% UTSFE composites at 25, 50, and 70°C.

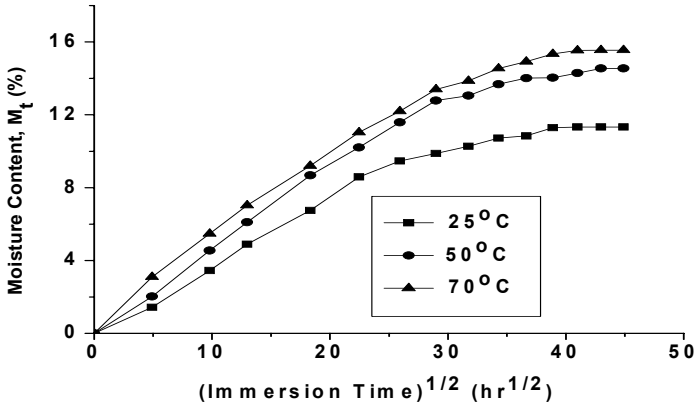

Figure 4.56 Moisture absorption behaviour of 65 wt% ATSFE composites at 25, 50, and 70°C.

The lower amount of moisture absorbed by NE is likely to be due to the hydrophobic nature of the epoxy resin and higher amount of moisture absorbed by the composites is likely to be due to the hydrophilic nature of the fibres due to the presence of polar groups such as –OH and –COOH in the fibres. Moisture absorption not being as great for ATFE composites as the UTFE composites may be due to less influence of increased fibre-fibre contacts than increased interfacial bonding in the ATFE composites, which could reduce wicking of the water molecules at the interface and increase resistance to hygrothermal ageing. Increased resistance of the ATFE composites towards hygrothermal ageing is further evident (lower loss of interfacial adhesion and matrix cracking of the ATFE composites when compared to the UTFE composites) from the SEM micrographs of Figures 4.57(a) and 4.57(b) as the optical micrographs of Figures

4.50(a) and 4.50(b) of the composite surfaces of UTFE and ATFE composites respectively, after hygrothermal ageing at 70°C. It has been seen elsewhere that the lack of interfacial interactions leads to internal strains, and porosity and increases the amount of moisture absorption [243, 244].

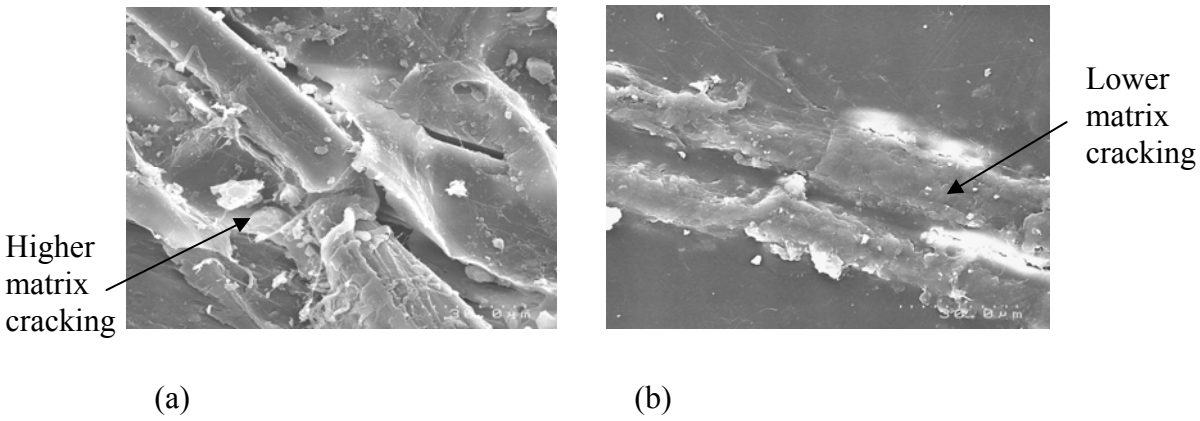

Figure 4.57 SEM micrographs of (a) UTLFE and (b) ATLFE composites surfaces after hygrothermal ageing at 70°C.

The lower absorption of water seen for the short fibre/epoxy composites compared to long fibre/epoxy composites might be due to the interrupted water channels resulting in a reduction in wicking of the water molecules at the interfaces.

Figures 4.58 and 4.59 show examples of the fitting of experimental data to Equation (2.16) for ATLFE and UTSFE composites respectively. The values of the kinetic parameter n resulting from the fitting for all samples are summarised in Table 4.7. Here, the data supports the absorption of water in HECs approaching Fickian diffusion (case I) as the values of n are less than 0.5 [7].

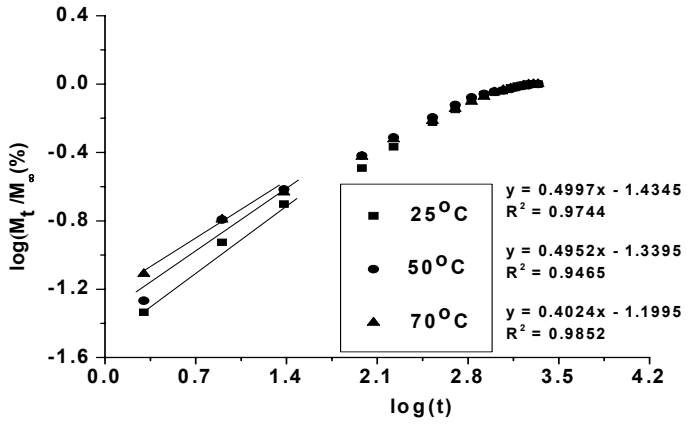

Figure 4.58 Diffusion case fitting plots for ATLFE composites at 25 and 50 and 70°C.

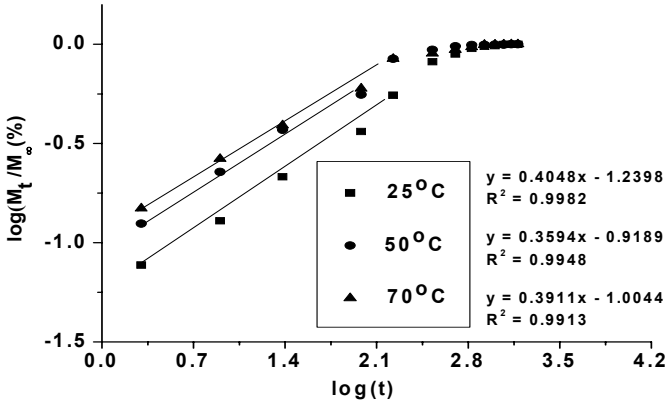

Figure 4.59 Diffusion case fitting plots for UTSFE composites at 25 and 50 and 70°C.

Table 4.7 Diffusion case selection parameter n at three different temperatures.

Sample	Temperature (°C)		
	25	50	70
NE	0.3807	0.3598	0.3583
UTLFE Composite	0.4064	0.3553	0.2996
ATLFE Composite	0.4997	0.4952	0.4024
UTSFE Composite	0.4048	0.3911	0.3594
ATSFE Composite	0.3949	0.3677	0.2771

The diffusion coefficient (D) can be obtained from Equation (2.17) using the slope of the linear part of the plot of $(M_t/M_\infty)^2$ versus tL^{-2}, Table 4.8. The diffusion coefficient (D) obtained in the current work for NE is in agreement with the results reported by other researchers [245]. The D values obtained here for composites are also in agreement with the values for sisal/PP composites obtained by other researchers [7]. The diffusion coefficient (D) increased with increasing temperature and it was found to increase for the composites. As reported

Table 4.8 Diffusion coefficients (D) for NE, UTFE and ATFE composites at three different temperatures.

Sample	D (m^2/s)×10^{13}		
	25°C	50°C	70°C
NE	1.37	4.91	5.11
UTLFE Composite	13.35	14.53	22.78
ATLFE Composite	6.53	9.09	12.03
UTSFE Composite	5.07	7.42	8.60
ATSFE Composite	3.14	5.30	8.44

elsewhere, the increase in D with the increase in temperature might be due to the increased ability of the water molecules to move among the polymer segments at higher temperatures [7]. This may be caused by the development of micro-cracks on the surface and in the bulk of the material, due to high temperature and moist

environment. The development of micro-cracks makes peeling and surface dissolution of composites possible [242]. Higher D values for composites are likely to be due to the hydrophilic fibres as discussed earlier as well as wicking of water molecules at the interfaces. The lower D values for ATFE composites compared to that for UTFE composites could be due to the reduction in wicking of water molecules at the interfaces which would be expected to be due to the influence of increased interfacial bonding in ATFE composites as discussed previously. Also, the lower D values for short fibre/epoxy composites compared to the long fibre/epoxy composites could be due to less of a continuous path for wicking of water molecules at the interfaces of short fibre/epoxy composites as discussed previously.

4.3.10.1 Effects of Hygrothermal Ageing on Mechanical Properties

Long Fibre Composites

Tensile Properties

From Figures 4.60 and 4.61, it can be seen that the TS and YM decreased with hygrothermal ageing. The reduction in YM was higher for higher immersion temperatures but remained constant for TS. Generally, there was a greater reduction in YM as the immersion temperature increased, however, reduction in

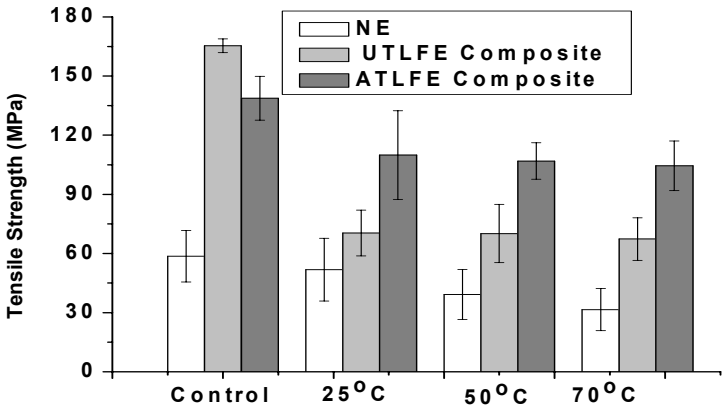

Figure 4.60 Effect of hygrothermal ageing on the TS of NE, UTLFE and ATLFE composites at three different temperatures. Error bars each corresponds to one standard deviation.

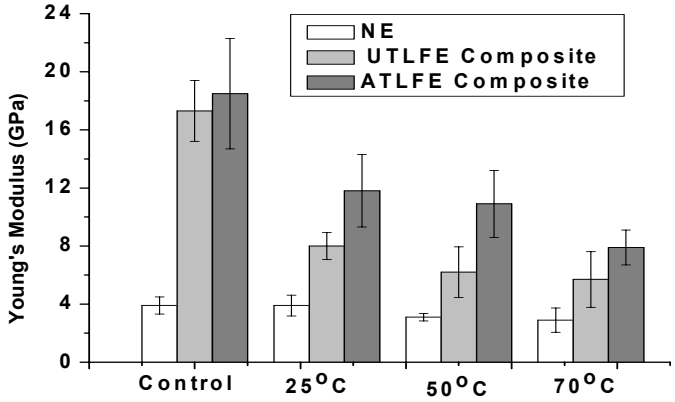

Figure 4.61 Effect of hygrothermal ageing on the YM of NE, UTLFE and ATLFE composites at three different temperatures. Error bars each corresponds to one standard deviation.

TS was similar for all immersion temperatures. The reduction in YM with hygrothermal ageing supports the fact that hygrothermal ageing accelerates the debonding process due to wicking of water molecules into the composites that resulted in delamination and loss of structural integrity as discussed previously.

Loss of fibre/matrix adhesion in hygrothermally aged samples can be visualised by the apparition of voids and loss of structural integrity as seen in Figures 4.62(a) and 4.62(b), which are not very noticeable in unaged samples (Figure 4.36(a) and 4.36(b)). With increasing temperature, more water may penetrate into the composites which would be expected to swell up the fibres causing cracks in the matrix. More water penetration into the matrix, could also lead to a reduction in fibre matrix adhesion and a reduction in TS and YM [7].

It can also be seen from the result that the reduction in TS and YM is higher for UTLFE composites than ATLFE composites. In the case of ATLFE composites, stronger interfacial bonding due to increased hydrogen and covalent bonding, and

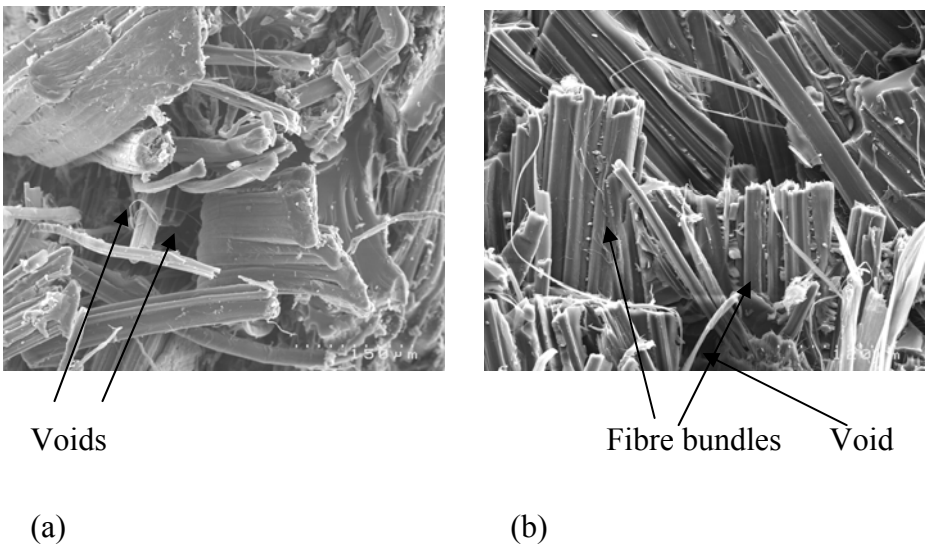

Figure 4.62 (a) UTLFE and (b) ATLFE composite fracture surfaces after hygrothermal ageing at 70^{o}C.

mechanical interlocking causing lower water absorption. As discussed above, stronger interfacial bonding formed by alkali treated fibre might outweigh the effect of point contact of the fibres in the ATLFE composites and thus give increased resistance to hygrothermal ageing compared to UTLFE composites. Lower loss in fibre/matrix adhesion is evident for ATLFE composites as higher number of fibre bundles with higher amount of fibre fracture are visisble in the ATLFE composites compared to UTLFE composites, Figures 4.62(a) and 4.62(b).

Considering the reduction in FS for NE, an increase in FS, Figure 4.63, for the composites after hygrothermal ageing might be due to increased fibre debonding from the epoxy resin due to weakening of the interface. Weakening of the interface could be caused by fibre swelling and resulting matrix cracking due to wicking of the water molecules at the interface.

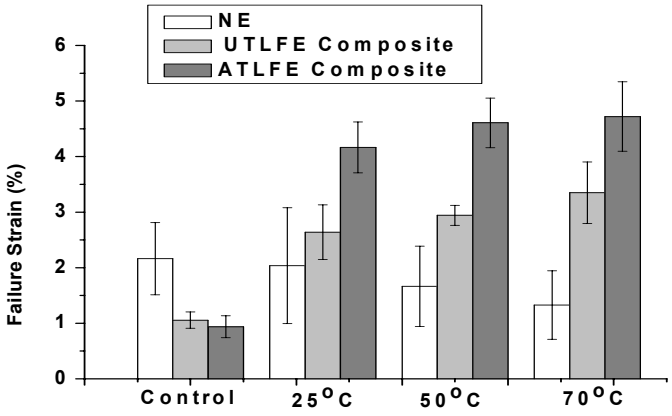

Figure 4.63 Effect of hygrothermal ageing on the FS of UTLFE and ATLFE composites compared to NE at three different temperatures. Error bars each corresponds to one standard deviation.

Flexural Properties

Flexural strength and flexural modulus were found to decrease with hygrothermal ageing for NE and composites; the extent of reduction increased with increased temperature, Figures 4.64 and 4.65. Although the flexural strain of NE was found to decrease, it was found to increase for the composites after hygrothermal ageing, Figure 4.66. It is considered that these trends are for similar reasons as for reduction in tensile properties as discussed previously.

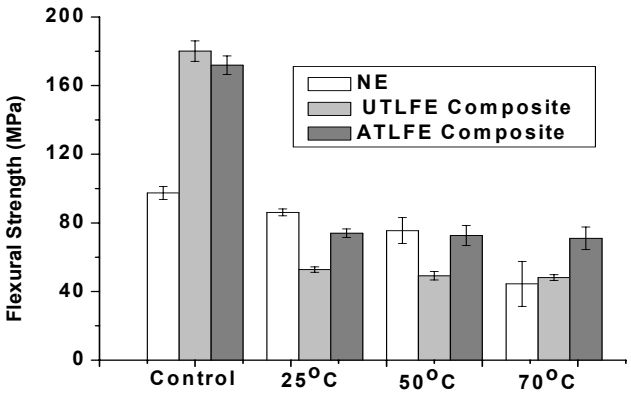

Figure 4.64 Effect of hygrothermal ageing on the flexural strength of UTLFE and ATLFE composites compared to NE at three different temperatures. Error bars each corresponds to one standard deviation.

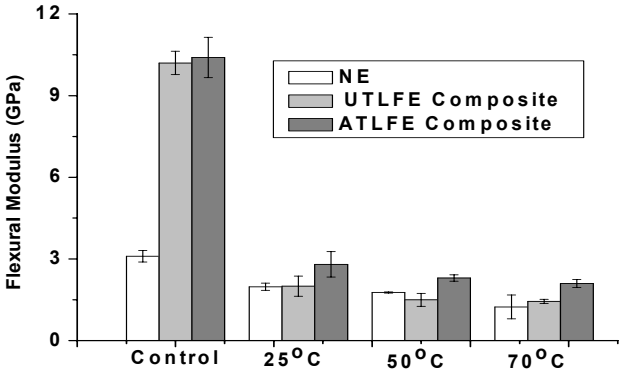

Figure 4.65 Effect of hygrothermal ageing on the flexural modulus of UTLFE and ATLFE composites compared to NE at three different temperatures. Error bars each corresponds to one standard deviation.

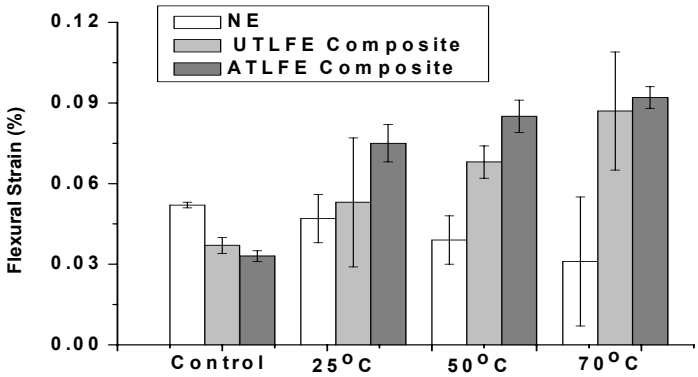

Figure 4.66 Effect of hygrothermal ageing on the flexural strain of UTLFE and ATLFE composites compared to NE at three different temperatures. Error bars each corresponds to one standard deviation.

Impact Energy (IE)

Figure 4.67 shows the effect of hygrothermal ageing on the IE of UTLFE and ATLFE composites compared to that for NE at three different temperatures. Although the IE of NE was found to be almost constant for the hygrothermally aged samples, it was found to increase for the composites; the extent of increase was found to be higher at higher temperatures. Swelling of fibre due to moisture absorption would be expected to increase with the increase of temperature, which could result in the formation of cracks in the matrix. This could weaken the fibre/matrix interface [134] which would be expected to enhance debonding of fibre from epoxy resin, leading to an increase IE. Rong *et al.* [246] reported that

IE improved with water absorption for sisal/epoxy composites as a result of interfacial debonding.

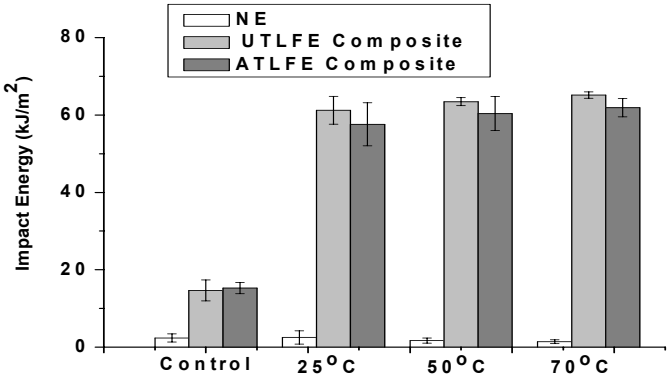

Figure 4.67 Effect of hygrothermal ageing on the IE of UTLFE and ATLFE composites compared to NE at three different temperatures. Error bars each corresponds to one standard deviation.

Fracture Toughness (K_{Ic})

Although K_{Ic} for NE increased during hygrothermal ageing at 25°C and then decreased with increasing temperature; it was found to decrease with increased hygrothermal ageing temperature for all composites, Figure 4.68. As discussed earlier in this section, with the increase of the hygrothermal ageing temperature,

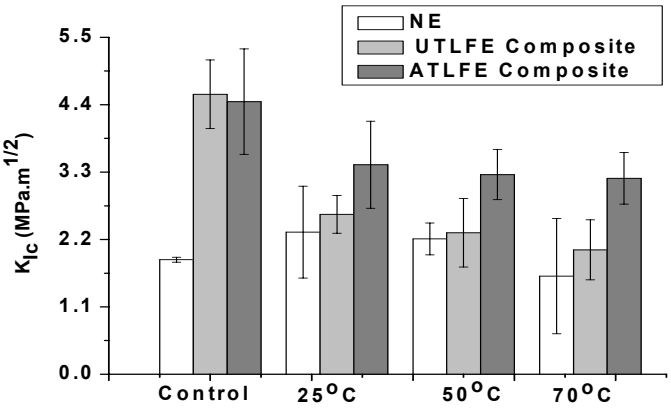

Figure 4.68 Effect of hygrothermal ageing on the K_{Ic} of UTLFE and ATLFE composites compared to NE at three different temperatures. Error bars each corresponds to one standard deviation.

the swelling of the fibre would be expected to increase, which could lead to the formation of cracks in the matrix, Figures 4.57(a) and 4.57(b). Formation of

cracks in the matrix could weaken the fibre/matrix interface and therefore requires less energy to debond the fibre from the matrix and thus, could reduce the K_{Ic} of the composites.

Thermogravimetric Analysis (TGA)

TGA traces for UTLFE and ATLFE composites after hygrothermal ageing at 70°C are shown in Figure 4.69. It can be seen that the weight loss was higher at the initial and second stage of thermal degradation for UTLFE composites, while it was higher at the third or final stage of thermal degradation for ATLFE composites. Hygrothermally aged ATLFE composites absorbed less moisture than UTLFE composites due to the influence of increased interfacial bonding of ATLFE composites as discussed previously. As the initial stage of thermal degradation is involved with dehydration, the reduced weight loss for ATLFE composites compared to UTLFE composites would be expected. As the second stage of thermal degradation is involved with decomposition of cellulose, more cellulose in the alkali treated fibres than untreated fibre might also lead to less weight loss at the second stage of thermal degradation for ATLFE composites. At the third stage of thermal degradation, the presence of lignin could contribute to the formation of charred products that might result in a reduction in weight loss for UTLFE composites compared to the ATLFE composites [238].

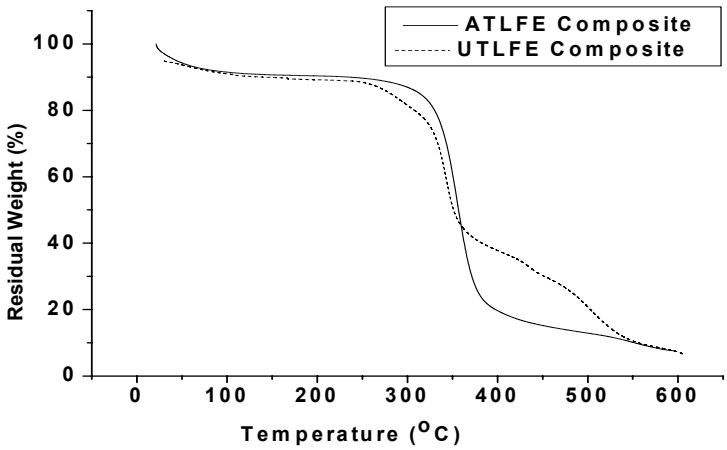

Figure 4.69 TGA traces for UTLFE and ATLFE composites after hygrothermal ageing at 70°C.

Wide Angle X-ray Diffraction (WAXRD)

Figure 4.70 shows the WAXRD pattern of UTLFE and ATLFE composites before and after hygrothermal ageing at 70°C. A reduction in intensity mainly in the peak at a 2θ angle of 22.5 (major characteristic peak for cellulose) can be observed for both the hygrothermally aged composites and the reduction is found

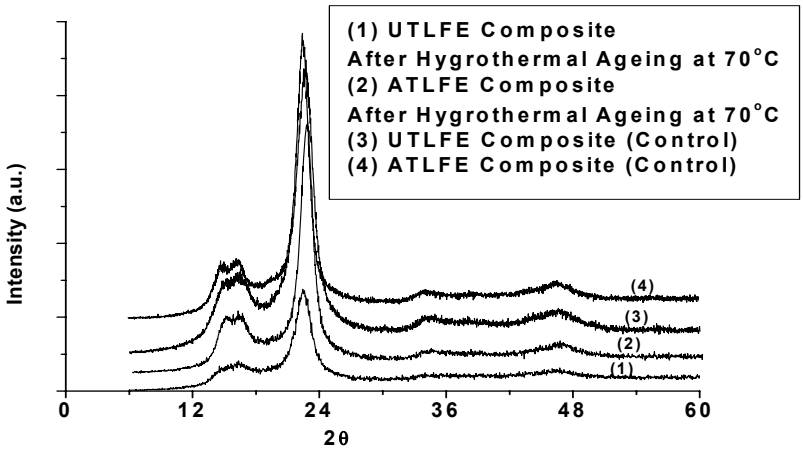

Figure 4.70 WAXRD pattern for UTLFE and ATLFE composites before and after hygrothermal ageing at 70°C.

to be greater for UTLFE composites than that of ATLFE composites. As the peak is a characteristic peak for cellulose, the reduction in intensity of this peak would be attributed to the degradation of cellulose which means greater degradation of cellulose was observed for hygrothermally aged UTLFE composites than ATLFE composites. This would be expected to be due to increased deterioration of cellulose by the increased moisture absorption by the UTLFE composites during hygrothermal ageing which is in agreement with the mechanical and thermal properties of the hygrothermally aged composites as discussed previously.

Short Fibre Composites

Tensile Properties

Similar to long fibre/epoxy composites, the TS and YM of the short fibre/epoxy composites were found to decrease with hygrothermal ageing with the extent of the decrease higher at a higher immersion temperature, Figures 4.71 and 4.72. More reduction in TS and YM (about 7% and 6% respectively, for UTSFE and

13% and 24% respectively, for ATSFE composites) was found for short fibre/epoxy composites compared to long fibre/epoxy composites with hygrothermal ageing. Also, similar to long fibre/epoxy composites, FS was found to increase for short fibre/epoxy composites with hygrothermal ageing with the extent of increase higher at a higher immersion temperature, Figure 4.73. For ease of comparison of the results of the tensile properties of hygrothermally aged short and long fibre/epoxy composites at three different temperatures are compiled in Table 4.9.

Table 4.9 Tensile properties of hygrothermally aged short and long fibre/epoxy composites at three different temperatures.

Tensile Properties	**Long Fibre**						**Short Fibre**					
	UTLFE			**ATLFE**			**UTSFE**			**ATSFE**		
	Temperature (^{o}C)			**Temperature (^{o}C)**			**Temperature (^{o}C)**			**Temperature (^{o}C)**		
	25	**50**	**70**	**25**	**50**	**70**	**25**	**50**	**70**	**25**	**50**	**70**
TS (MPa)	70.4	70.1	67.3	109.9	106.9	104.5	39.8	38.4	35.2	82.4	75.3	59.2
YM (GPa)	8	6.2	5.7	11.8	10.9	7.9	3.5	2.9	2.6	6.8	5.8	5.5
FS (%)	2.639	2.942	3.35	4.165	4.606	4.72	4.799	5.658	6.25	5.525	7.317	7.987

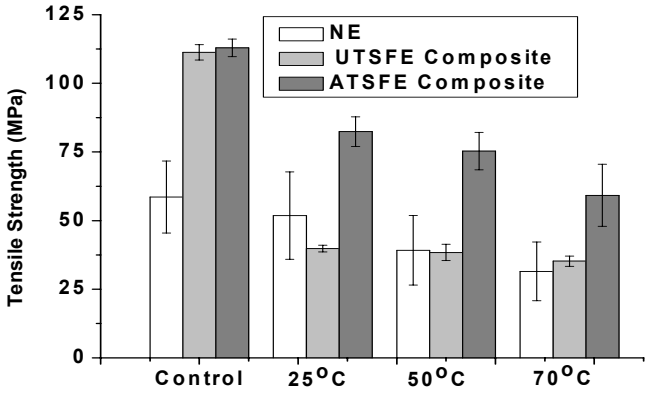

Figure 4.71 Effect of hygrothermal ageing on the TS of UTSFE and ATSFE composites compared to NE at three different temperatures. Error bars each corresponds to one standard deviation.

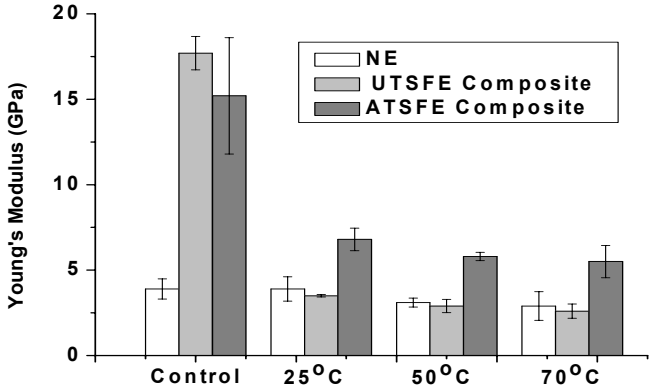

Figure 4.72 Effect of hygrothermal ageing on the YM of UTSFE and ATSFE composites compared to NE at three different temperatures. Error bars each corresponds to one standard deviation.

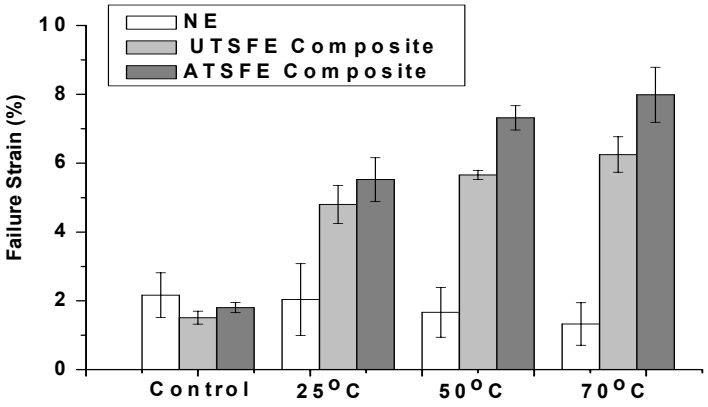

Figure 4.73 Effect of hygrothermal ageing on the FS of UTSFE and ATSFE composites compared to NE at three different temperatures. Error bars each corresponds to one standard deviation.

Flexural Properties

Similar to long fibre composites, the flexural strength and flexural modulus of the short fibre composites were found to decrease with hygrothermal ageing with the extent of decrease higher at a higher immersion temperature, Figures 4.74 and 4.75. The reduction in flexural strength and flexural modulus was found almost similar for short and long fibre/epoxy composites with hygrothermal ageing. Also, similar to long fibre composites, the flexural strain of the short fibre composites was found to increase with hygrothermal ageing with the extent of increase higher at a higher temperature, Figure 4.76.

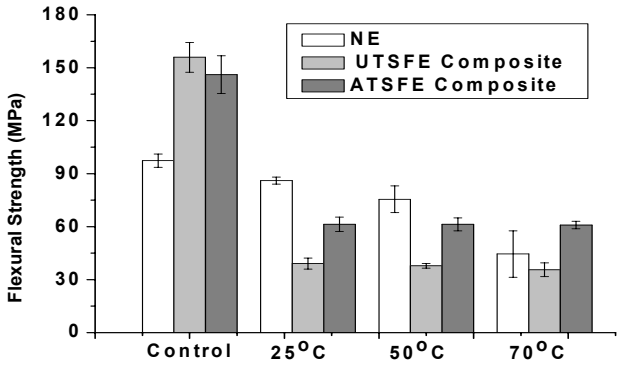

Figure 4.74 Effect of hygrothermal ageing on the flexural strength of UTSFE and ATSFE composites compared to NE at three different temperatures. Error bars each corresponds to one standard deviation.

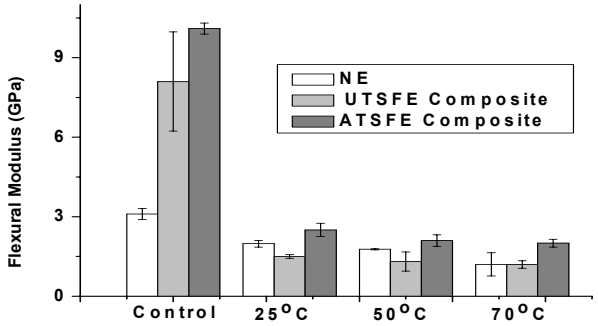

Figure 4.75 Effect of hygrothermal ageing on the flexural modulus of UTSFE and ATSFE composites compared to NE at three different temperatures. Error bars each corresponds to one standard deviation.

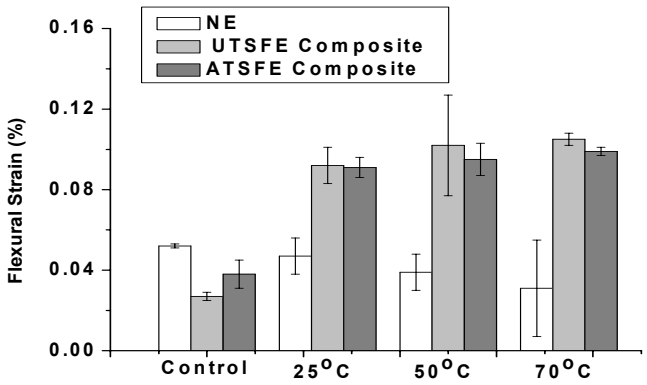

Figure 4.76 Effect of hygrothermal ageing on the flexural strain of UTSFE and ATSFE composites compared to NE at three different temperatures. Error bars each corresponds to one standard deviation.

Impact Energy (IE)

Similar to long fibre composites, the IE of the short fibre composites was found to increase after hygrothermal ageing with the extent of increase higher at a higher immersion temperature as can be seen from Figure 4.77. The increase in IE was found almost similar for UTSFE and UTLFE composites and it was found to increase about 190% more for ATLFE composites compared to that for ATSFE composites with hygrothermal ageing.

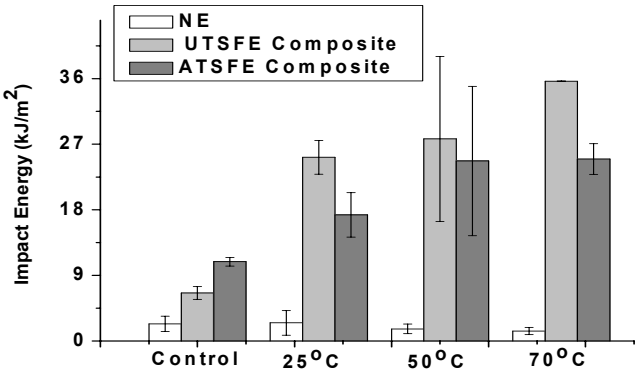

Figure 4.77 Effect of hygrothermal ageing on the IE of UTSFE and ATSFE composites compared to NE at three different temperatures. Error bars each corresponds to one standard deviation.

Fracture Toughness *(K_{Ic})*

Similar to long fibre composites, the K_{Ic} for the short fibre composites was found to decrease with hygrothermal ageing with the extent of decrease higher at a higher immersion temperature as can be seen from Figure 4.78. The reduction in K_{Ic} was found almost similar for UTSFE and UTLFE composites and it was found to reduce about 14% more for ATLFE composites compared to that for ATSFE composites with hygrothermal ageing.

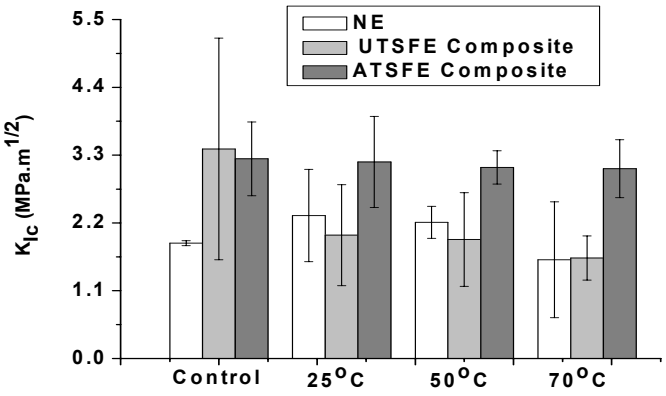

Figure 4.78 Effect of hygrothermal ageing on the K_{Ic} of UTSFE and ATSFE composites compared to NE at three different temperatures. Error bars each corresponds to one standard deviation.

4.3.11 Accelerated Ageing of the Composites

As can be seen from Figure 4.79, the exposure of samples in accelerated ageing environments slightly deteriorated the surface in the form of decolouration and

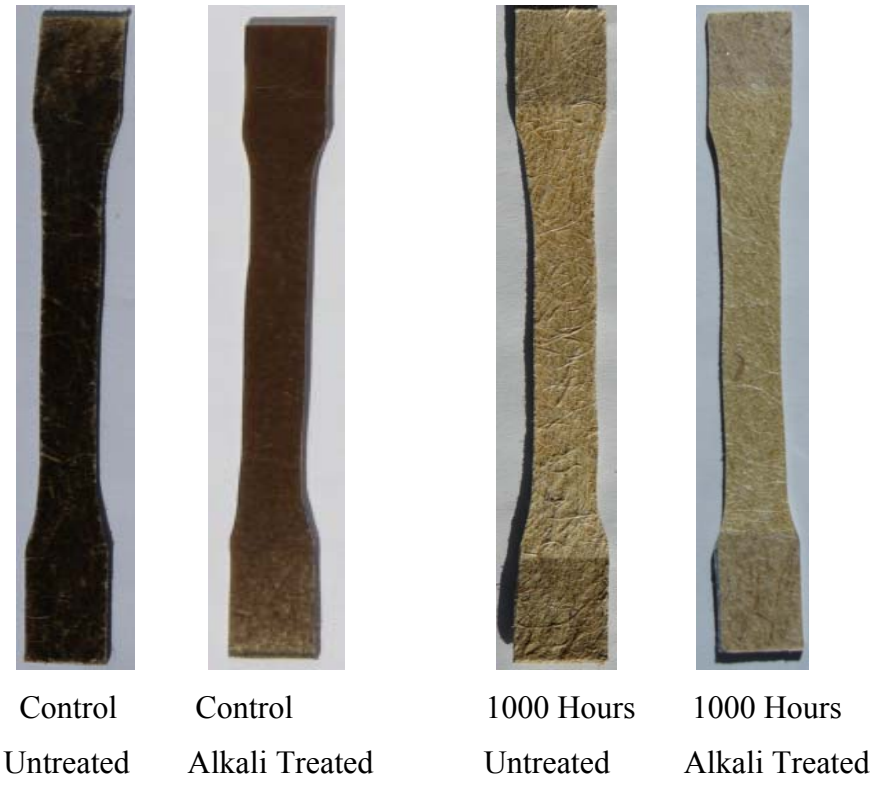

Figure 4.79 Visual change during weathering of UTLFE and ATLFE composites.

surface texture. Increasing exposure to the ageing conditions resulted in the initiation of tearing in the fibres, Figure 4.80, which could be due to degradation by UV attack as has been reported elsewhere [247]. The accelerated aged surface showed an accentuation of fibres with the erosion of epoxy resin as reported in the literature for glass/polyester composites [248]. This is attributed mainly to stress produced by differential swelling and shrinkage of the fibre/resin caused by changes in moisture content. Stresses might also build up at the interface due to a large variation in the coefficient of thermal expansion of epoxy resin and fibre leading to the failure of the fibre resin interface as reported elsewhere [249]. However, the accelerated aged samples were found to be deteriorated less when compared to the hygrothermally aged samples although higher deterioration would have been expected due to possible increase of weathering by the presence of UV-radiation. The lower deterioration of accelerated aged samples is likely due to less swelling of fibres by less moisture absorption for not immersing the samples in water during the ageing period unlike hygrothermally aged samples.

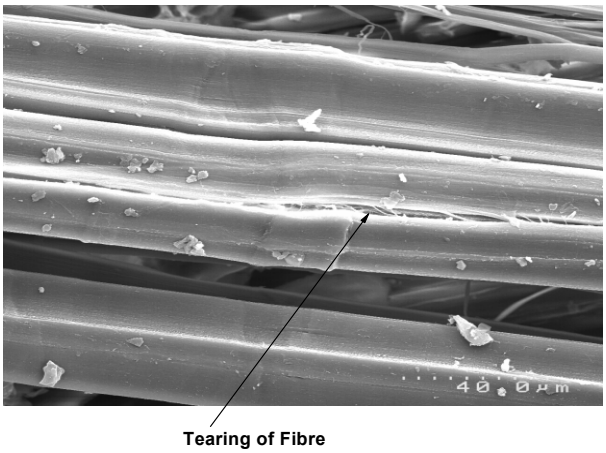

Figure 4.80 SEM of UTLFE composites showing tearing of the fibres after accelerated ageing of 1000 hours.

Progressive percentage weight gain during accelerated ageing is given in Figure 4.81. The weight gain of the samples might be caused by the absorption of water during water spray and condensation cycles. The yellowish colour of the samples, Figure 4.79, after accelerated ageing is likely due to the breakdown of the lignin to the water soluble products [151, 250].

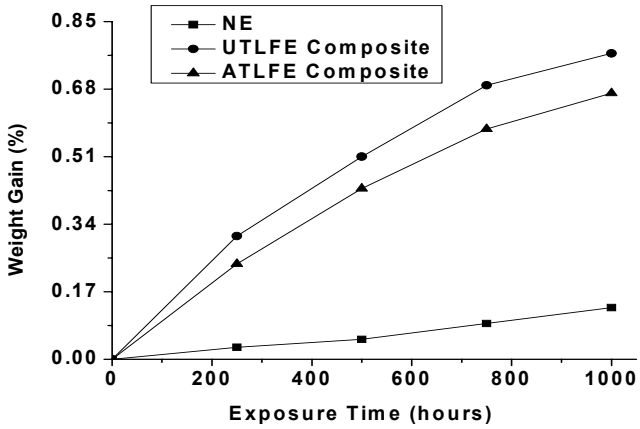

Figure 4.81 Percentage weight gain of NE, UTLFE and ATLFE composites.

The change in mechanical properties due to accelerated ageing over different time periods is presented in Figures 4.82 to 4.89. Reduction in TS, flexural strength, YM and flexural modulus for NE and composites with increased duration of ageing was observed, Figures 4.82, 4.83, 4.85, and 4.86. The highest reduction in mechanical properties was found for UTLFE composites. TS and flexural strength were found to decrease from 165.4 and 180.1 MPa to 97.9 and 56.7 MPa respectively, while YM and FM were found to decrease from 17.3 and 10.1 GPa to 3.9 and 1.3 GPa respectively, for UTLFE composites, Figures 4.82, 4.83, 4.85, and 4.86. However, the TS for both UTLFE and ATLFE composites were found to be almost constant for further ageing after 250 hours. Although FS and flexural strain were found to decrease with the increase in ageing time for NE, they were found to increase with the increase of ageing period for both UTLFE and ATLFE composites, Figures 4.84 and 4.87. Although IE was found to be similar for NE with accelerated ageing, it was found to increase dramatically for the composites, Figure 4.88. The highest increase of IE from 14.6 to 63.9 kJ/m^2 was found for UTLFE composites. K_{Ic} was found to decrease for all the samples with the increase of ageing time and the highest decrease of 4.6 to 3.3 MPa.m$^{1/2}$ was found for UTLFE composites, Figure 4.89.

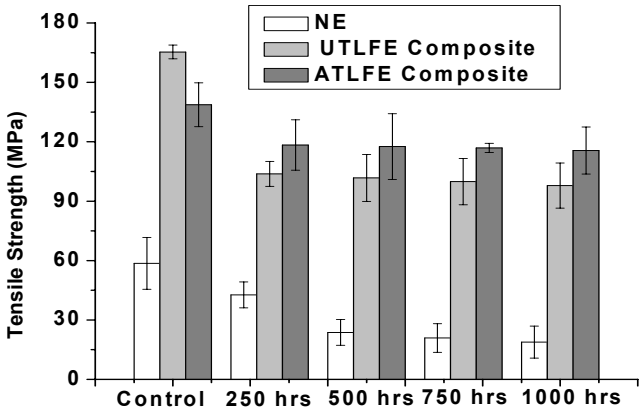

Figure 4.82 Effect of accelerated ageing on the TS of UTLFE and ATLFE composites compared to NE. Error bars each corresponds to one standard deviation.

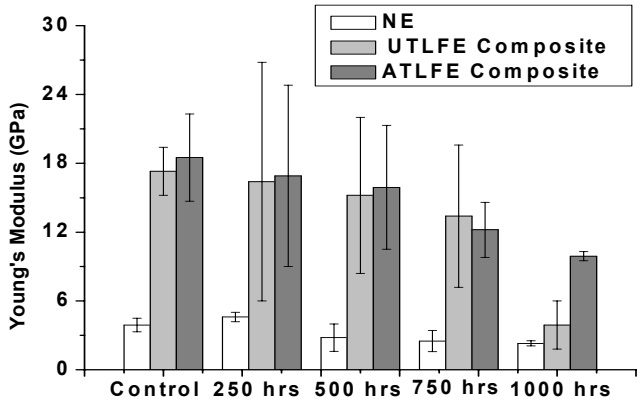

Figure 4.83 Effect of accelerated ageing on the YM of UTLFE and ATLFE composites compared to NE. Error bars each corresponds to one standard deviation.

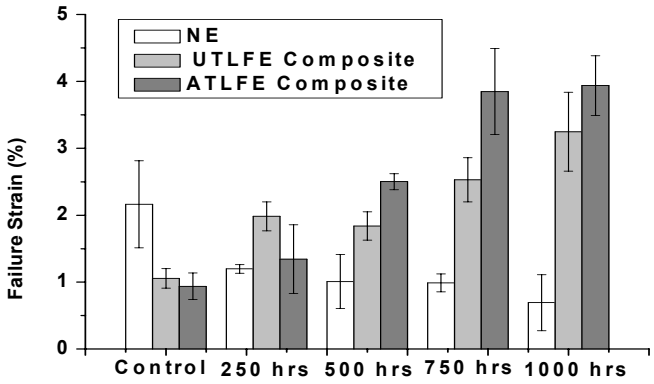

Figure 4.84 Effect of accelerated ageing on the FS of UTLFE and ATLFE composites compared to NE. Error bars each corresponds to one standard deviation.

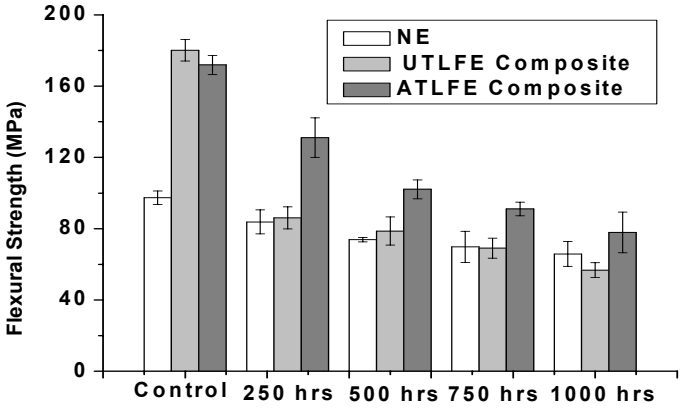

Figure 4.85 Effect of accelerated ageing on the flexural strength of UTLFE and ATLFE composites compared to NE. Error bars each corresponds to one standard deviation.

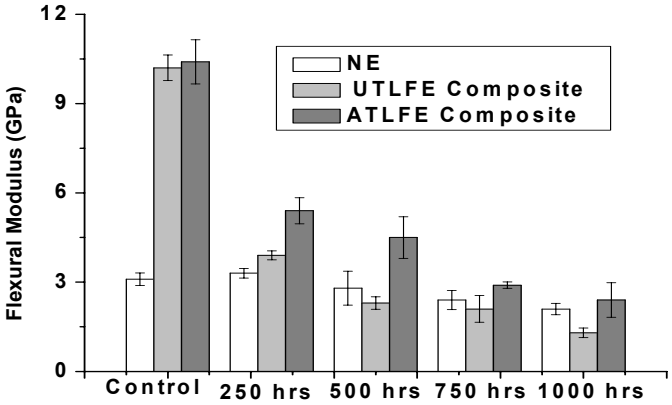

Figure 4.86 Effect of accelerated ageing on the flexural modulus of UTLFE and ATLFE composites compared to NE. Error bars each corresponds to one standard deviation.

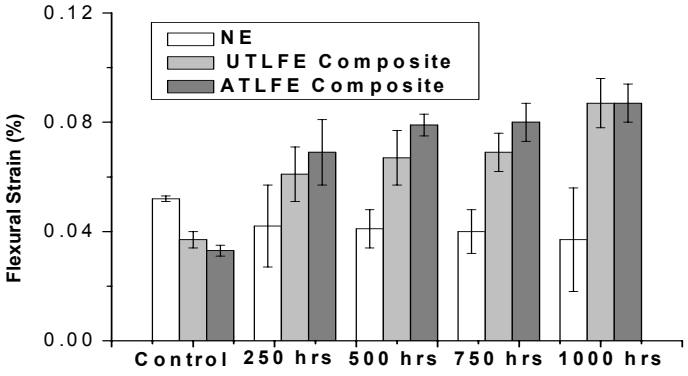

Figure 4.87 Effect of accelerated ageing on the flexural strain of UTLFE and ATLFE composites compared to NE. Error bars each corresponds to one standard deviation.

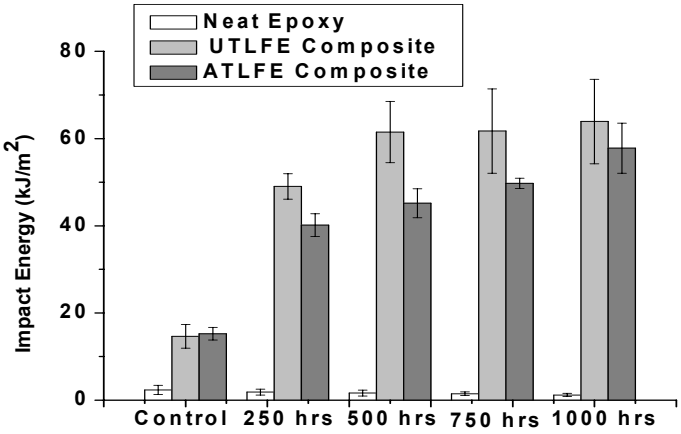

Figure 4.88 Effect of accelerated ageing on the IE of UTLFE and ATLFE composites compared to NE. Error bars each corresponds to one standard deviation.

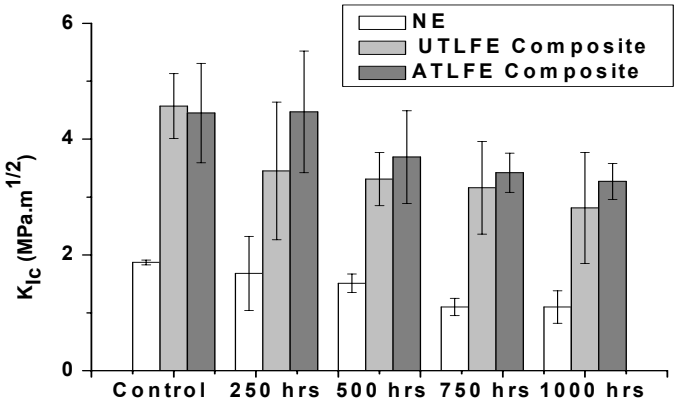

Figure 4.89 Effect of accelerated ageing on the K_{Ic} of UTLFE and ATLFE composites compared to NE. Error bars each corresponds to one standard deviation.

The reduction in TS, flexural strength, YM and flexural modulus for NE in the current work with increased duration of ageing is considered to be due to plasticisation, swelling effect [251] and photochemical degradation [7]. The reduction in TS, flexural strength, YM and flexural modulus of the aged composites in the current work is likely due to the weakening of the fibre/matrix interface by the formation of cracks in the matrix due to swelling of fibre by moisture absorption [249].

Fibrillation of the fibres in the composite fracture surface was also noticed, Figures 4.90(a) and 4.90(b), upon accelerated ageing which is likely due to degradation of lignin which acts as an adhesive holding the cellulose fibrils together. As reported elsewhere [247], after lignin degradation, the poorly bonded

cellulose fibrils could erode easily from the surface which would be expected to expose new lignin embedded cellulose fibrils for subsequent degradation reaction and thus could enhance fibre pull-out from the resin. The ageing process could cause the surface of the composites to become rough and account for significant fibre loss from the surface [247]. The constant TS of the composites on further accelerated ageing after 250 hours could be caused by lignin acting as a natural antioxidant, which is known to stabilize the fibres [252] from further degradation and an equilibrium has been reached.

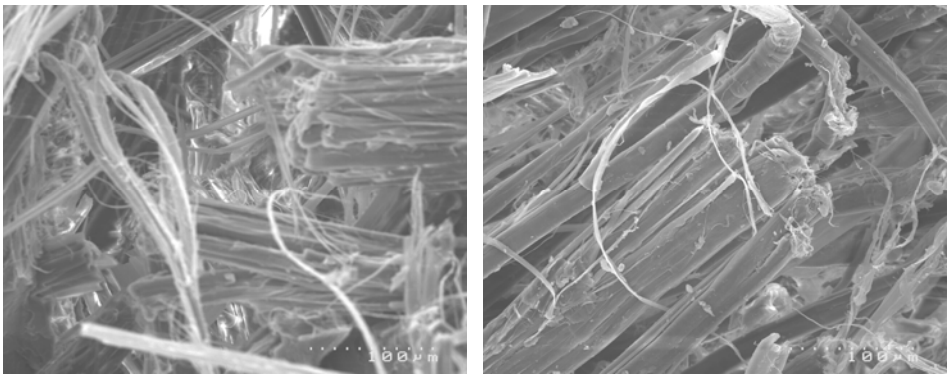

(a) (b)

Figure 4.90 (a) UTLFE and (b) ATLFE composites fracture surfaces after 1000 hours accelerated ageing.

The reduction in FS, flexural strain, IE, and K_{Ic} of NE could be due to the chain degradation and formation of surface cracks as can be seen from Figure 4.91. The increase in FS, flexural strain, and IE, and decrease in K_{Ic} for the composites in the current work is likely due to the formation of a porous structure as a result of leaching of debonded fibres by the fibrillation process upon removal of lignin [7]. As a result of the increased porosity, more water molecules were believed to be able to be trapped inside the composite structure, which might act as a plasticiser and result in an increase in FS, flexural strain, and IE, and decrease in K_{Ic} [7]. Possible matrix cracking by swelling of fibre as a result of water absorption could also weaken fibre/matrix interface and cause the fibres to be pulled-out of the resin and increase energy dissipation which in turn increased the FS, flexural strain, and IE, and decrease the K_{Ic} of the composites. ATLFE composites were found to show better resistance to accelerated weathering over UTLFE composites which could be due to the formation of stronger fibre/epoxy bonds which outweighed the effect of point contact in the fibres as discussed in section 4.3.10.

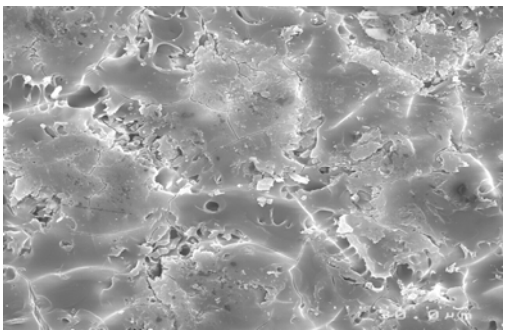

Figure 4.91 Micrograph of NE surface after weathering for 1000 hours.

4.3.11.1 Fourier Transform Infrared (FTIR) Spectra

Analysis of the FTIR spectra, Figure 4.92, showed an increase in the intensity of the C=O absorption in the 1000 hours weathered sample over control in 1734 cm^{-1} region and around 1650 cm^{-1} [253]. An increase in the carbonyl absorption indicated modification in the lignin structure. An increase in the intensity of the

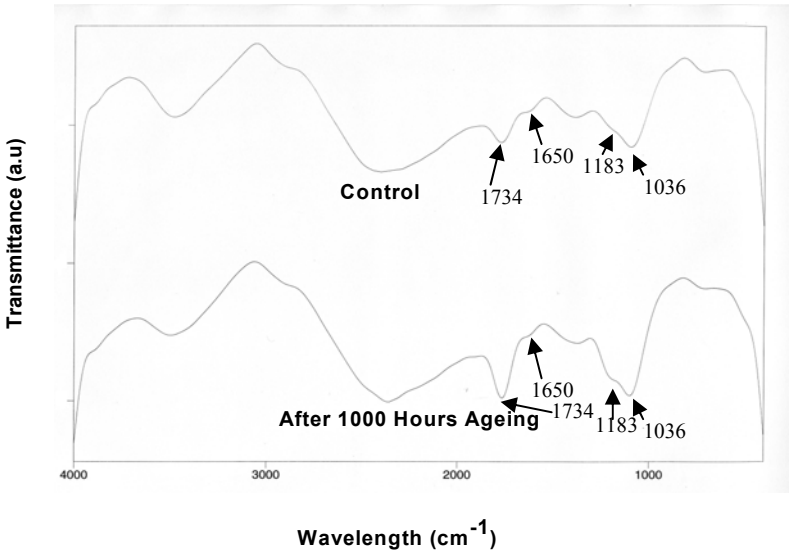

Figure 4.92 FTIR spectra of UTLFE composites of before (control) and after 1000 hours accelerated ageing.

1650 cm^{-1} band indicated quinine formation by irradiation during weathering [253]. The bands at 1734 and 1650 cm^{-1} were characteristic absorptions of carbonyl stretching vibrations of nonconjugated (in xylan) and conjugated (in lignin) esters and carboxylic acids; their concentrations were found to increase as

carbonyl groups were believed to be liberated from lignin and/or carbohydrates due to chemical degradation [253-255]. The band at 1036 cm^{-1} involves the reactivity of aromatic ether function and the band at 1183 cm^{-1} involves the cleavage of the isopropylidene group of epoxy resin according to Rivaton *et al.* [256].

4.3.11.2 Thermogravimetric Analysis (TGA)

TGA traces for UTLFE and ATLFE composites after accelerated ageing of 1000 hours are shown in Figure 4.93. Similar to hygrothermally aged composites, it can be seen that the weight loss for initial and second stage of thermal degradation was higher for UTLFE composites, while it was higher at the third or final stage of thermal degradation for ATLFE composites. It is considered that these trends are for similar reasons as for hygrothermally aged composites as discussed previously in section 4.3.10.1.

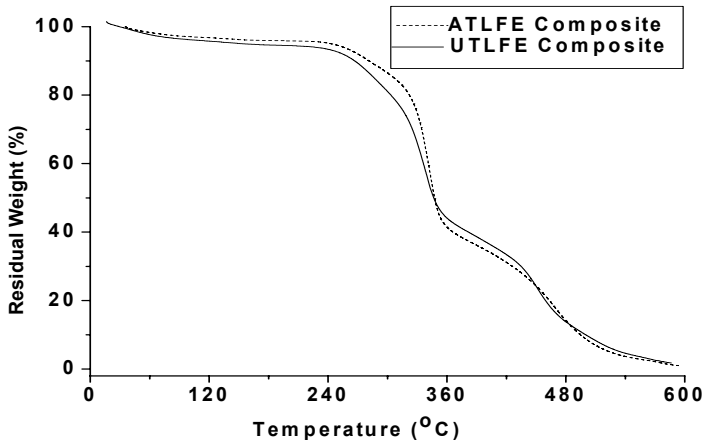

Figure 4.93 TGA of UTLFE and ATLFE composites after accelerated ageing of 1000 hours.

4.3.11.3 Wide Angle X-ray Diffraction (WAXRD)

Figure 4.94 shows the WAXRD pattern of UTLFE and ATLFE composites before and after accelerated ageing of 1000 hours. Similar to hygrothermally aged composites, a reduction in intensity mainly in the peak at a 2θ angle of 22.5 (major characteristic peak for cellulose) can be observed for both the accelerated aged composites and the reduction is found to be greater for UTLFE composites than that of ATLFE composites. It is considered that these trends are for similar

reasons as for hygrothermally aged composites as discussed previously in section 4.3.10.1.

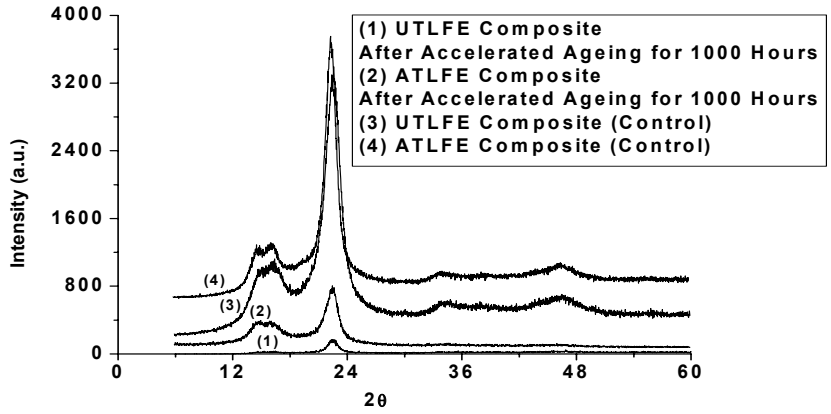

Figure 4.94 WAXRD pattern for UTLFE and ATLFE composites before and after accelerated ageing of 1000 hours.

4.4 Chapter Conclusion

A study of the curing kinetics of NE and 40 wt% UTFE composites showed that addition of fibre in NE reduced the curing time and increased the curing reaction rate which could be due to enhanced nucleophilic activity of the amine groups of the curing agent in presence of fibres. IFSS measurements of UTFE and ATFE samples revealed that samples with an epoxy to curing agent ratio of 1:1 gave the highest IFSS values than samples with other epoxy to curing agent ratios. ATFE samples had consistently higher IFSS than UTFE samples at all epoxy to curing agent ratios.

An optimised composite production method was developed with a 1:1 epoxy to curing agent ratio, 60 minutes resin soaking time and a curing temperature of 70^{o}C with aligned fibres. Composites produced with alkali treated fibres were stronger than those produced with acetylated and silane treated fibres.

Composites produced with the optimised production method at different fibre contents showed that long fibre/epoxy composites were stronger in terms of tensile properties than short fibre/epoxy composites. Flexural properties, IE and K_{Ic} were found to be higher for long fibre/epoxy composites when compared to

short fibre/epoxy composites with 65 wt% fibre content. ATFE composites were found to have greater TS at lower fibre contents while UTFE composites were found to have greater TS at higher fibre contents. Flexural strength and K_{Ic} were found to increase and IE was found to decrease for UTFE composites when compared to ATFE composites with 65 wt% fibre content.

Hygrothermal ageing of the samples indicated that the absorption of water in HECs followed Fickian diffusion (case I). The lower absorption of water seen for the short fibre/epoxy composites compared to long fibre/epoxy composites indicates interrupted water channels resulting in a reduction in wicking of the water molecules at the interfaces. Hygrothermal ageing of hemp/epoxy composites at different temperatures showed that fibre length and alkali fibre treatment had a significant effect on the mechanical properties of the composites.

Accelerated ageing of hemp/epoxy composites for different durations showed that alkali fibre treatment had a significant influence on the mechanical properties of the composites.

Chapter Five

Hemp/PLA Composites (HPCs)

5.1 Summary

This chapter describes the materials, methods, and results for the:

- determination of IFSS of untreated and alkali treated hemp fibre in polylactic acid (PLA)
- production of long and short hemp fibre preform mats
- production of untreated and alkali treated long (aligned) and short (planar random and aligned) hemp fibre/PLA composites using compression moulding
- comparison of untreated and alkali treated long aligned hemp fibre/PLA composites in terms of tensile testing and SEM analysis
- comparison of untreated and alkali treated short planar random and aligned hemp fibre/PLA composites in terms of tensile testing and SEM analysis
- comparison of film stacked 32 wt% untreated and alkali treated long aligned hemp fibre/PLA composites in terms of flexural, impact, and fracture toughness as well as SEM, WAXRD, and FTIR analysis
- hygrothermal ageing of film stacked 32 wt% untreated and alkali treated long aligned hemp fibre/PLA composites. The aged composites were assessed in terms of tensile, flexural, impact, and fracture toughness as well as SEM, TGA, WAXRD analysis

- accelerated ageing of film stacked 32 wt% untreated and alkali treated long aligned hemp fibre/PLA composites. The aged composites were assessed in terms of tensile, flexural, impact, and fracture toughness as well as SEM, TGA, WAXRD, and FTIR analysis.

5.2 Experimental Details

5.2.1 Materials

Retted hemp bast fibre was supplied by Hemcore, UK. PLA in the form of pellets, was obtained from Nature Works International, Australia. Analytical grade Na_2SO_3 and 98% NaOH pellets were used for the alkali treatment of the fibres.

5.2.2 Methods

5.2.2.1 Interfacial Shear Strength (IFSS) Measurement of Hemp Fibre/PLA Samples Using Single Fibre Pull-out Testing

For the measurement of IFSS, single-fibre pull-out test specimens were prepared according to the literature [220] by the method described in section 4.2.2. The hole at the centre of the mould was filled with PLA dissolved in dichloromethane (DCM), from which the solvent was allowed to evaporate using a vacuum oven at room temperature (20±2^{o}C) for 24 hours. The free end of the fibre that had been contained within the mould slot was glued to cardboard using PVA glue to give a gauge length of 10 mm. Five specimens were prepared at each embedded length and the average debonding force of the five specimens was measured using an Instron tensile tester at a crosshead speed of 0.5 mm/min.

5.2.2.2 Fibre Mat Production

Untreated and alkali treated fibres were dried at 80^{o}C for 24 hours.

Long Fibre Mats

Dried fibres were made into aligned long fibre mats using a hand carding machine by the method described in section 4.2.2.3.

Short Fibre Mats

Dried fibres were made into both aligned and random short fibre mats by DSF and hand lay-up respectively, as described in section 4.2.2.3.

Alkali fibre treatment method is described in section 3.2.2

5.2.2.3 PLA Sheet Production (Neat PLA):

PLA pellets were micronised into PLA powder using a microniser. PLA powder was then used to produce PLA Sheets using a hot press at 170^{o}C and 1 MPa pressure maintained for 5 minutes.

5.2.2.4 Fabrication of Composites

Impregnation of the PLA matrix into the fibre mats and the fabrication of composite samples were carried out using four different methods:

(a) Untreated Short Random Fibre Composites

A short random fibre mat weighing 30g was sandwiched between 70g of PLA powder (manually spread) in a preheated compression mould to produce a composite of 30 wt% fibre. This was pressed at a temperature of 170^{o}C and a pressure of 1.2 MPa for 15 minutes. Untreated random short fibre/PLA composites produced by this technique will be defined as 'untreated short random' in this study.

(b) Untreated and Alkali Treated Short Aligned Fibre Composites

Water was poured on a mixture of PLA powder and short fibre (308g PLA powder and 132g fibre) in a disintegrator for mixing using speeds of up to 72000 rpm. After disintegration, PLA powder was well distributed throughout the fibre, and the dynamic sheet former was then used to produce short fibre/PLA mats from the mixture. The fibre/PLA mats thus produced were dried at 100^{o}C for 24 hours, placed in a preheated compression mould and pressed at a temperature of 170^{o}C and a pressure of 1.2 MPa for 15 minutes. 30 wt% untreated and alkali treated short aligned fibre/PLA composites produced by this technique will be defined as 'untreated short aligned' and 'alkali treated short aligned' respectively,

in this study. Long fibre could not be processed by the dynamic sheet former using this methodology.

(c) Untreated Short Random and Alkali Treated Long Aligned Composites Using DCM

PLA was dissolved in DCM and the solution was poured over the fibre mat (both short and long fibre mats) and allowed to soak into the fibre mat for five minutes. The DCM was then evaporated in a vacuum oven at 120^{o}C over 24 hours, following which the mat was placed in a preheated mould and pressed at 170^{o}C and 1.5 MPa pressure for 15 minutes. 40 wt% untreated short random fibre composites produced by this technique will be defined as 'untreated short random (DCM)' and 40 wt% alkali treated long aligned fibre composites produced by this technique will be defined as 'alkali treated long aligned (DCM)' in this study.

(d) Untreated and Alkali Treated Long Aligned Fibre Film Stacked (FSt) Composites

PLA film was produced from PLA powder using the hot press at 170^{o}C and 1 MPa pressure maintained for 5 minutes. A fibre mat was sandwiched between two PLA films (commonly known as film stacking) in a preheated compression mould. This was then pressed at a temperature of 170^{o}C and a pressure of 1 MPa for 10 minutes. Untreated and alkali treated long aligned fibre composites of 32 wt% fibre were produced by this method and will be defined as 'untreated long aligned (FSt)' and 'alkali treated long aligned (FSt)' respectively, in this study.

5.2.2.5 Composite Mechanical Testing

Composites (obtained using the methods described in section 5.2.2.4) and neat PLA sheets were cut into tensile, flexural, impact, and fracture toughness test specimens using a scroll saw, to the dimensions specified by the standard test methods for each of the tests. The samples were then placed in a conditioning chamber at 23^{o}C ± 3^{o}C and 50% ± 5% relative humidity for 40 hours. The tensile, flexural, impact, and fracture toughness tests were carried out following the methods described in section 4.2.2.

5.2.2.6 Hygrothermal Ageing

Due to their better performance in tensile testing, hygrothermal ageing was only carried out for 32 wt% untreated, and alkali treated long aligned (FSt) composites (obtained by method (d) of section 5.2.2.4) and neat PLA following the method described in section 4.2.2.14.

5.2.2.7 Accelerated Ageing

As for hygrothermal ageing, accelerated ageing was only carried out for 32 wt% untreated, and alkali treated long aligned (FSt) composites (obtained by method (d) of section 5.2.2.4) and neat PLA following the method described in section 4.2.2.15.

5.2.2.8 Scanning Electron Microscopy (SEM)

The fracture surfaces of the composites were examined using SEM following the method described in section 4.2.2.10.

5.2.2.9 Differential Scanning Calorimetry (DSC) Analysis

DSC analysis of composites (obtained using the method (d) described in section 5.2.2.4) and neat PLA were carried out using a DSC 2920 differential scanning calorimeter, in an argon atmosphere with a heating rate of 5^{o}C/min. A static argon flow of 50 mL/min and an aluminum sample pan were used. Specimens of approximately 10 mg were scanned over a temperature range of 25 to 200^{o}C. The glass transition temperature (T_g), melt temperature (T_m), cold crystallisation temperature (T_c), and heat of melting (ΔH_m) were determined for both neat PLA and composites. The percentage crystallinity of each sample was calculated using the relationship

$$X_c(\%Crystallinity) = \frac{\Delta H_m}{\Delta H_m^0} \times \frac{100}{w} \tag{5.1}$$

where ΔH_m is the heat of melting, ΔH_m^o is the heat of melting for 100% crystalline PLA sample (taken as ΔH_m^o = 93 J/g) and w is the weight fraction of PLA in the sample [257, 258]. To determine the crystallinity of the sample, the heats of cold

crystallisation and pre-melt crystallisation were subtracted from heat of melting [259].

5.2.2.10 WAXRD

WAXRD analysis was carried out following the method described in section 4.2.2.12.

5.2.2.11 Fourier Transform Infrared (FTIR) Spectra

The FTIR spectra analysis of the composites was carried out following the method described in section 4.2.2.13.

5.3 Results and Discussion

5.3.1 Interfacial Shear Strength (IFSS) Measurement of Hemp Fibre/PLA Samples

Figure 5.1 shows a graph of debonding force versus embedded length for UFPLA and ATPLA samples. Linear relationships between the debonding force and embedded length were obtained for both UFPLA and ATPLA samples. A higher slope was observed for ATPLA sample compared to the UFPLA sample, suggesting increased bonding of the alkali treated fibres with the matrix PLA.

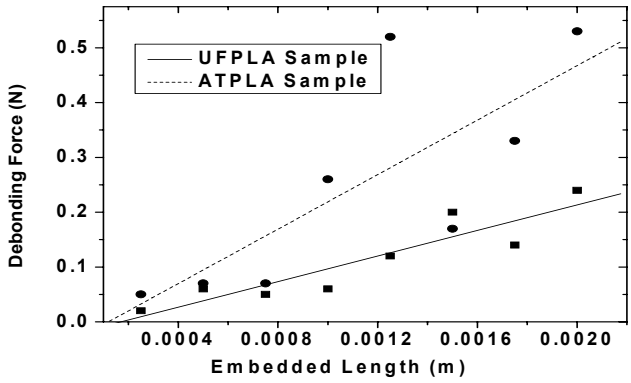

Figure 5.1 Debonding force versus embedded length for UFPLA and ATPLA samples. The solid lines indicate principal trends of data points and do not represent any data fitting.

This can be explained by the increase of available –OH groups as observed by FTIR analysis described in section 3.3.1.10 due to alkali treatment. These would be expected to occur due to removal of the non-cellulosic materials covering the cellulose –OH groups and also due to increased roughness, which would generally increase the surface area of the fibre. Increased exposure of cellulose –OH groups would provide increased potential for hydrogen bonding. In addition to increasing –OH groups for bonding, increased surface roughness would also provide for better mechanical interlocking with PLA. Strong adhesion at the fibre/PLA interface is necessary for effective stress transfer and load distribution throughout the interface.

Figure 5.2 shows the IFSS, calculated by dividing the debonding force by the interfacial area of the UFPLA and ATPLA samples, Equation (2.2), obtained from the pull-out tests [95]. The higher IFSS for the ATPLA samples when compared to that for the UFPLA samples could again be due to the increased adhesion of the alkali treated fibres to PLA. The relationship between IFSS and embedded length was found to be constant for UFPLA samples while it was found to be non-constant for ATPLA samples. A constant function of IFSS versus embedded length indicates ductile interface fracture behaviour while a non-constant function indicates a brittle interface fracture behaviour as reported by other researchers [97]. A non-constant function arises with pull-out by brittle fracture due to the requirement of a critical crack length, which, once achieved, requires no further

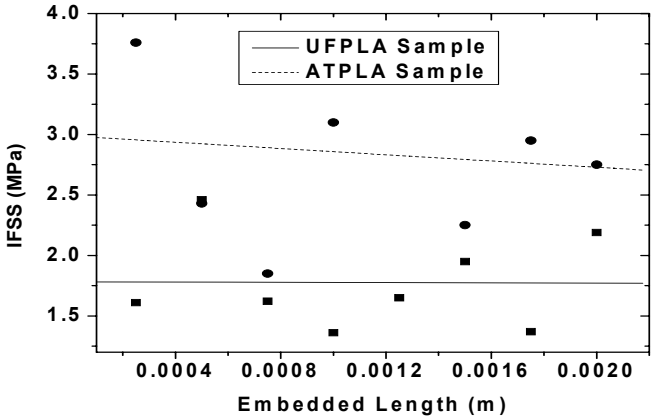

Figure 5.2 IFSS of UFPLA and ATPLA samples, obtained for eight different embedded fibre lengths. The solid lines indicate principal trends of data points and do not represent any data fitting.

increase of stress for a longer embedded fibre length. According to Meretz *et al.* [260] crystalline polymer structures cause increased bonding to the fibre, resulting in brittle fracture during the single-fibre pull-out test.

In this case, the PLA has been observed as being more crystalline in the case of ATPLA samples (section 5.3.3.1), which would therefore be anticipated to increase interfacial strength. As previously discussed, the increased access of –OH groups is also likely to be contributing to the increase in interfacial strength and therefore increased brittle behaviour of the ATPLA samples. In addition, increased crystallinity at the interface of PLA and fibre in the ATPLA samples would be expected to lead to a more brittle matrix in this region, which could also contribute to the observed brittle behaviour.

5.3.2 Mechanical Properties

5.3.2.1 Tensile Properties

Figures 5.3 and 5.4 show the TS and YM respectively, of untreated short aligned, alkali treated short aligned, and untreated short random fibre/PLA composites compared to those for neat PLA. The neat PLA has a TS of 48 MPa and a YM of 4.8 GPa. It can be seen that among the composites, only alkali treated

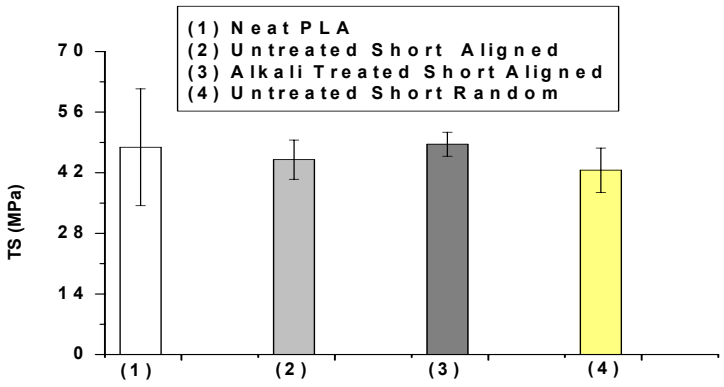

Figure 5.3 TS of untreated short aligned, alkali treated short aligned, and untreated short random composites compared to neat PLA. Error bars each corresponds to one standard deviation.

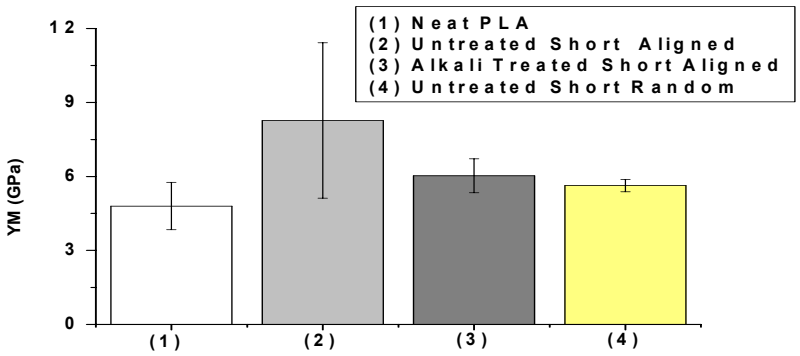

Figure 5.4 YM of untreated short aligned, alkali treated short aligned, and untreated short random composites compared to neat PLA. Error bars each corresponds to one standard deviation.

short aligned composites have similar TS (49 MPa) to neat PLA with the others having lower TS. However, the Young's moduli of the composites are all higher than that of neat PLA. Mathew *et al.* [11] reported that cellulose reinforcement increased the crystallinity of PLA. These crystalline regions would contain increased physical cross-links and therefore could be contributing to the increase in YM observed [11]. Higher YM for the untreated short aligned composites compared to that for alkali treated short aligned composites could be due to higher YM of the untreated fibres compared to alkali treated fibres as discussed in section 3.3.1.3. However, lower YM for the untreated short random composites compared to untreated and alkali treated aligned composites is likely to be due to lack of alignment for the untreated short random fibres in the composites. The addition of hemp fibres not increasing the TS, is a possible indication of poor impregnation and adhesion of PLA to the fibres. Alternatively, the increased crystallinity of PLA due to cellulose reinforcement could result in more brittle PLA and limit the TS of the composites. Higher TS for the alkali treated short aligned composites compared to those for untreated short random and aligned composites could be due to the improved adhesion of the alkali treated fibre to the PLA with increased crystallinity, potential hydrogen bonding and mechanical interlocking, achieved upon removal of non-cellulosic components from the fibres as discussed in section 5.3.1 which overrides any increased brittleness of the matrix at the interface. Also expected from pull-out tests, better impregnation of PLA into the fibres for the alkali treated short aligned composites compared to that for untreated short random and aligned composites is supported by far less

pull-out, holes and fibre free region in matrix observed in the fracture surfaces of alkali treated short aligned composites compared to untreated short fibre (random and aligned) composites, Figures 5.5(a) and 5.5(b) respectively. Almost similar TS was observed for untreated short random and aligned composites though

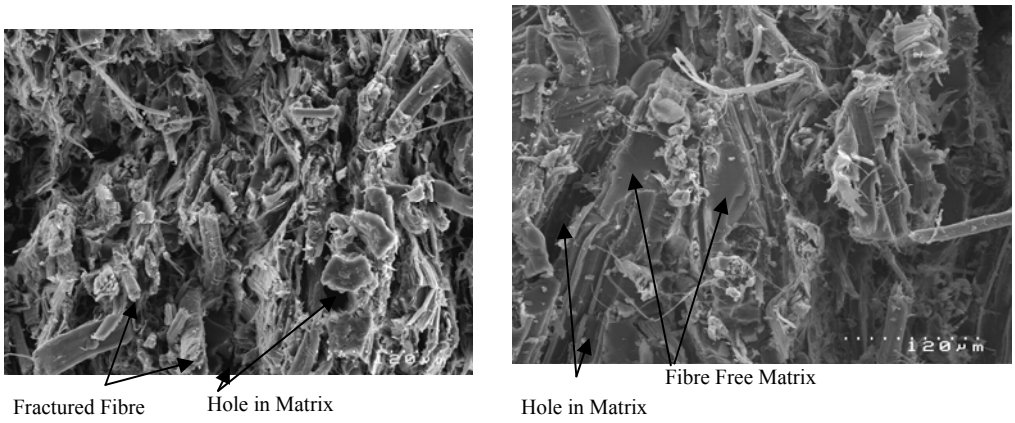

Figure 5.5 SEM pictures of the fracture surface of (a) alkali treated short aligned and (b) untreated short random composites.

it was expected to have been higher for the untreated short aligned composites due to alignment of fibre and better impregnation of PLA considered to be achieved by DSF. However, PLA absorbs moisture upon exposure to humid environments [261, 262], it might absorb water as it was processed with water in the dynamic sheet former during fibre/PLA mat formation. Absorbed moisture could cause degradation of PLA by hydrolysis during processing at higher temperature as reported by other researchers [263], resulting in a possible reduction in interfacial strength and as a consequence, composite TS [44]. This could also have limited the strength of the alkali treated short aligned fibre composites. FS was seen to increase in composites, Figure 5.6, compared to neat PLA, which could be due to some plasticising effect occurring upon addition of fibres into the PLA during composite production and is supported by the depression in glass transition, cold crystallisation, and melt temperatures for the composites compared to those for neat PLA as described in DSC analysis in section 5.3.3.1.

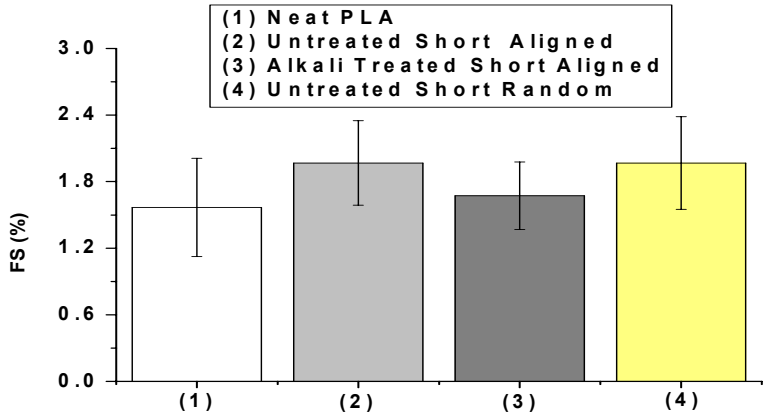

Figure 5.6 FS of untreated short aligned, alkali treated short aligned, and untreated short random composites compared to neat PLA. Error bars each corresponds to one standard deviation.

As the composites described so far did not have good mechanical properties, further effort was expended to produce composites by dissolving PLA powder in DCM (method c, section 5.2.2.4). Figure 5.7 shows the TS of composites (untreated short random (DCM) and alkali treated long aligned (DCM)) which were found to be lower than that for neat PLA. The lower TS of the composites could be explained by the presence of a large amount of pores and possible entrapped air bubbles in both alkali treated long aligned (DCM) and untreated short random (DCM) composites, Figures 5.8(a) and 5.8(b) respectively. YM was found to increase significantly in the composites, Figure 5.9 which can again be explained by the increased crystallinity of the PLA in the composites as discussed already in this section [11] and constraint of the fibres. An increase in TS and YM observed for untreated short random (DCM) composites compared to alkali treated long aligned (DCM) composites could be due to the presence of comparatively lower number of pores in the untreated short random (DCM) composites, Figures 5.8(a) and 5.8(b) respectively. The presence of pores and air bubbles in the composites was also considered to be responsible for lower composites FS, Figure 5.10 compared to those for neat PLA.

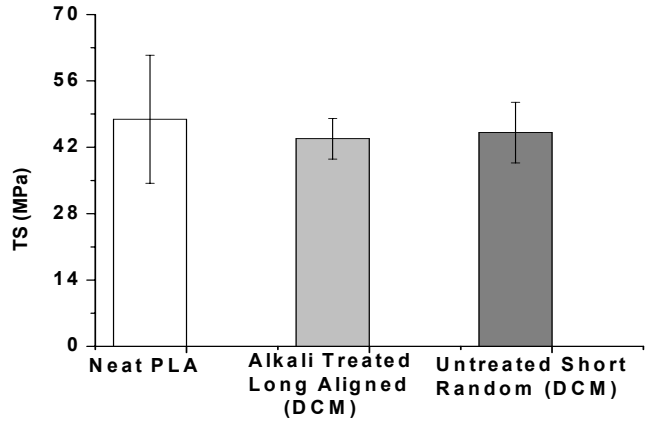

Figure 5.7 TS of alkali treated long aligned (DCM), and untreated short random (DCM) composites compared to neat PLA. Error bars each corresponds to one standard deviation.

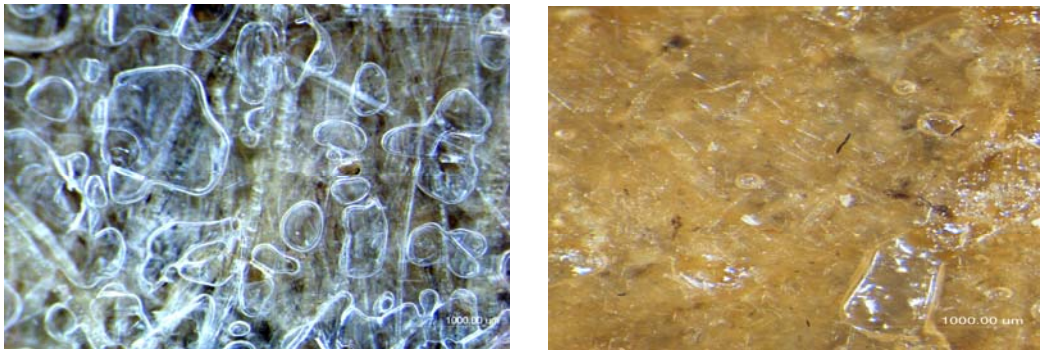

(a) (b)

Figure 5.8 Optical micrograph of the surface of (a) alkali treated long aligned (DCM) and (b) untreated short random (DCM) composites.

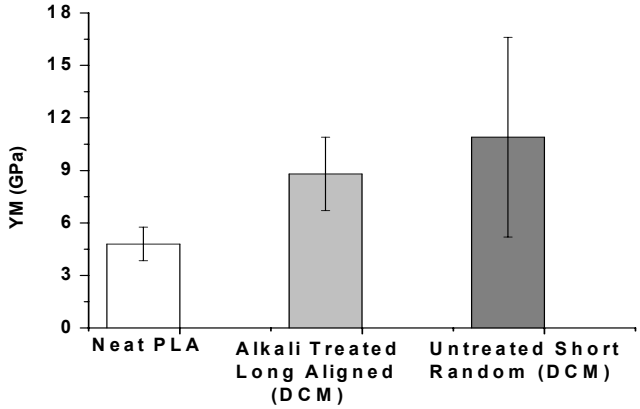

Figure 5.9 YM of alkali treated long aligned (DCM) and untreated short random (DCM) composites compared to neat PLA. Error bars each corresponds to one standard deviation.

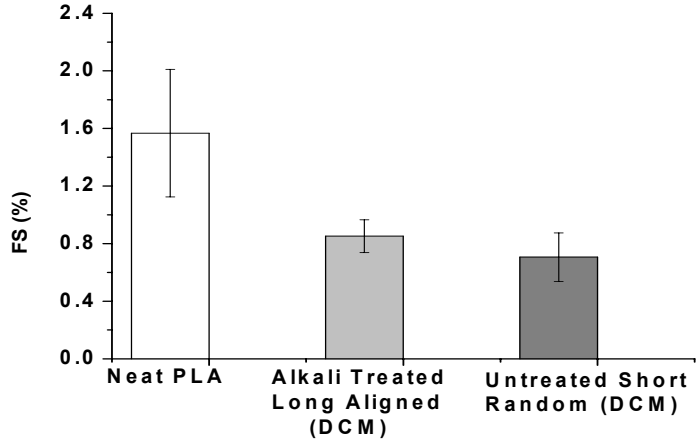

Figure 5.10 FS of alkali treated long aligned (DCM) and untreated short random (DCM) composites compared to neat PLA. Error bars each corresponds to one standard deviation.

The TS, YM and FSs of untreated long aligned (FSt) and alkali treated long aligned (FSt) composites (produced by method d, section 5.2.2.4) compared to neat PLA are shown in Figures 5.11, 5.12 and 5.13 respectively. The addition of hemp fibres increasing the TS and YM, is a possible indication of good impregnation and adhesion of PLA to the fibres. As discussed earlier, cellulose reinforcement increased the crystallinity of PLA [11]. These crystalline regions would contain increased physical cross-links and therefore could further be contributing to the increase in YM observed [11]. The increase in FS of composites compared to neat PLA is not surprising due to the higher FS of the fibres.

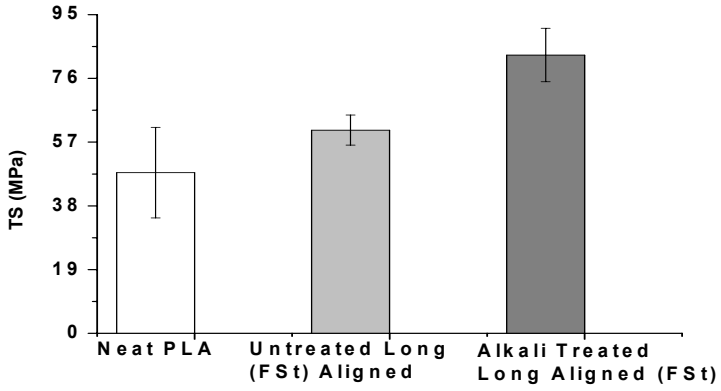

Figure 5.11 TS of untreated long aligned (FSt) and alkali treated long aligned (FSt) composites compared to neat PLA. Error bars each corresponds to one standard deviation.

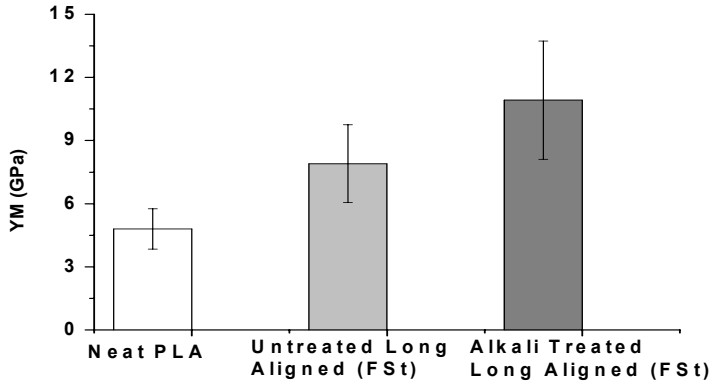

Figure 5.12 YM of untreated long aligned (FSt) and alkali treated long aligned (FSt) composites compared to neat PLA. Error bars each corresponds to one standard deviation.

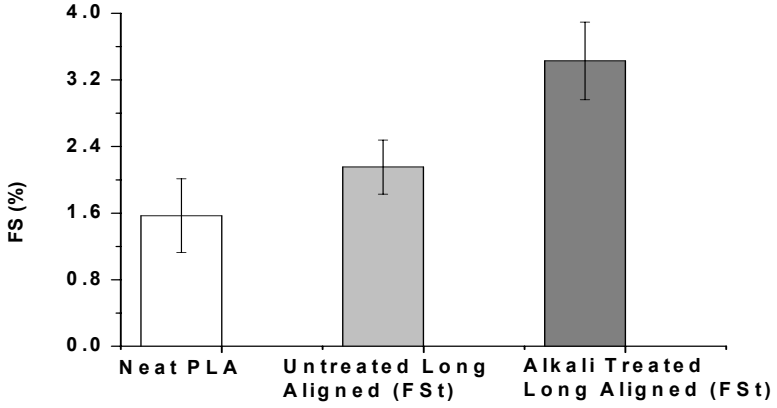

Figure 5.13 FS of untreated long aligned (FSt) and alkali treated long aligned (FSt) composites compared to neat PLA. Error bars each corresponds to one standard deviation.

However, this could also be due to a plasticising effect occurring upon the addition of fibres into the PLA during composite production, and is supported by the depression in glass transition, cold crystallisation, and melt temperatures for the composites compared to those for neat PLA as described in DSC analysis in section 5.3.3.1.

It can be seen that untreated long aligned (FSt) and alkali treated long aligned (FSt) composites have TSs of 61 and 83 MPa respectively. The higher TS of alkali treated long aligned (FSt) composites compared to that of untreated long aligned (FSt) composites can be explained due to improved adhesion of the alkali treated fibre to the PLA through potential hydrogen bonding and mechanical

interlocking, achieved upon removal of non-cellulosic components from the fibres as discussed in section 5.3.1. Increased crystallinity of PLA could also be contributing to the increased TS of the alkali treated long aligned (FSt) composites compared to that of untreated long aligned (FSt) composites. Figures 5.14(a) and 5.14(b) show SEM micrographs of the fracture surfaces of untreated long aligned (FSt) and alkali treated long aligned (FSt) composites respectively. It can be seen from the fracture surfaces that untreated long aligned (FSt)

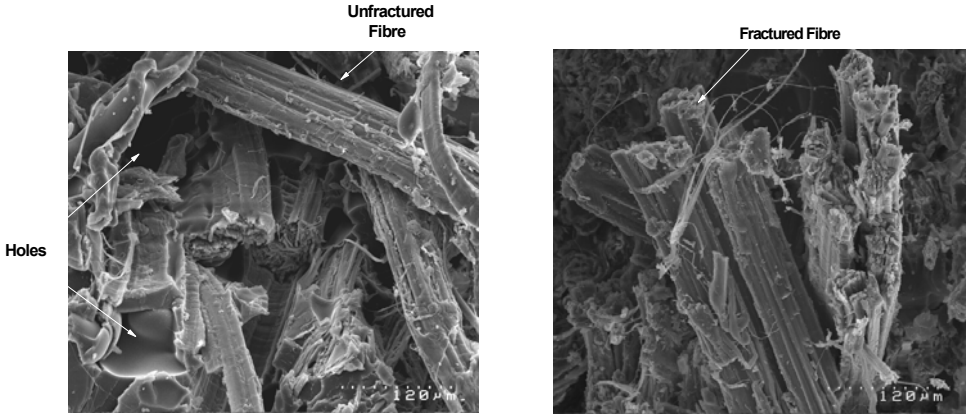

(a) (b)

Figure 5.14 SEM micrographs of fracture surfaces of (a) untreated long aligned (FSt) and (b) alkali treated long aligned (FSt) composites.

composites exhibit long unfractured fibres and holes (from which fibre/fibre bundles have been extracted), indicative of a lot of fibre pull-out. On the other hand, alkali treated long aligned (FSt) composites, show predominate fibre fracture which indicates better fibre matrix adhesion and interfacial bonding for alkali treated long aligned (FSt) composites compared to untreated long aligned (FSt) composites.

Higher YM of the alkali treated long aligned (FSt) composites than that of untreated long aligned (FSt) composites could again be due to better fibre matrix adhesion obtained in the alkali treated long aligned (FSt) composites. Moreover, increased crystallinity of the PLA in the alkali treated long aligned (FSt) composites compared to that for untreated long aligned (FSt) composites could further be contributing to the increase in YM observed for alkali treated long aligned (FSt) composites [11]. Higher FS of the alkali treated long aligned (FSt) composites compared to that for untreated long aligned (FSt) composites might

again be due to occurring of increased plasticising effect in the alkali treated long aligned (FSt) composites.

5.3.2.2 Flexural Properties

Figures 5.15 and 5.16 show the flexural strength and flexural modulus of untreated long aligned (FSt) and alkali treated long aligned (FSt) composites compared to those of neat PLA. The higher flexural properties for the composites could again indicate good impregnation and adhesion of PLA with the fibres. It can be seen that alkali treated long aligned (FSt) composites have higher flexural strength and flexural modulus of 143 MPa and 6.5 GPa respectively, when compared to those for untreated long aligned (FSt) composites (flexural strength and flexural modulus of 118 MPa and 5.5 GPa respectively). The higher flexural strength and flexural modulus for alkali treated long aligned (FSt) composites compared to untreated long aligned (FSt) composites is again an indication of the improved bondability of alkali treated fibres with PLA.

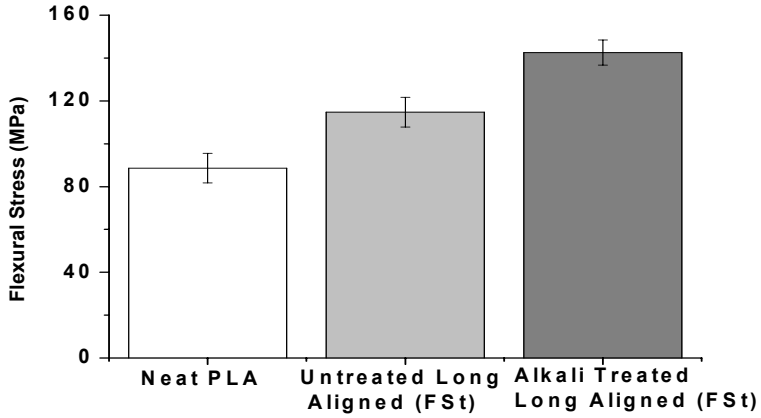

Figure 5.15 Flexural strength of untreated long aligned (FSt) and alkali treated long aligned (FSt) composites compared to neat PLA. Error bars each corresponds to one standard deviation.

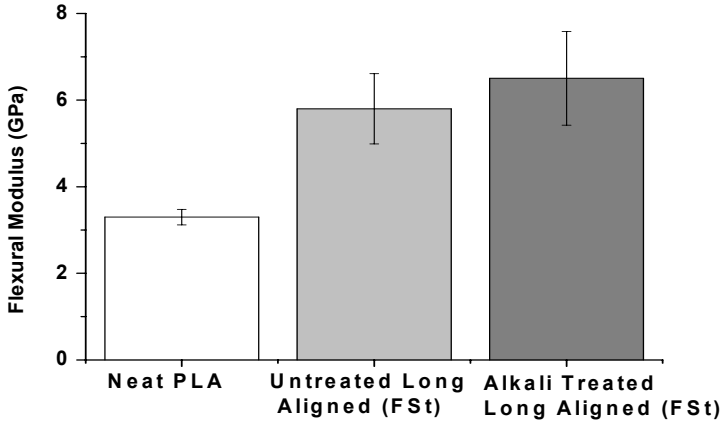

Figure 5.16 Flexural modulus of untreated long aligned (FSt) and alkali treated long aligned (FSt) composites compared to neat PLA. Error bars each corresponds to one standard deviation.

5.3.2.3 Impact Energy (IE)

Figure 5.17 shows the IE of untreated long aligned (FSt) and alkali treated long aligned (FSt) composites compared to that of neat PLA. The energy absorbed by the composites was over four times higher than the energy absorbed by neat PLA. Plasticising in the composites could contribute for their increased Impact energy. A lower IE was seen for alkali treated long aligned (FSt) composites compared

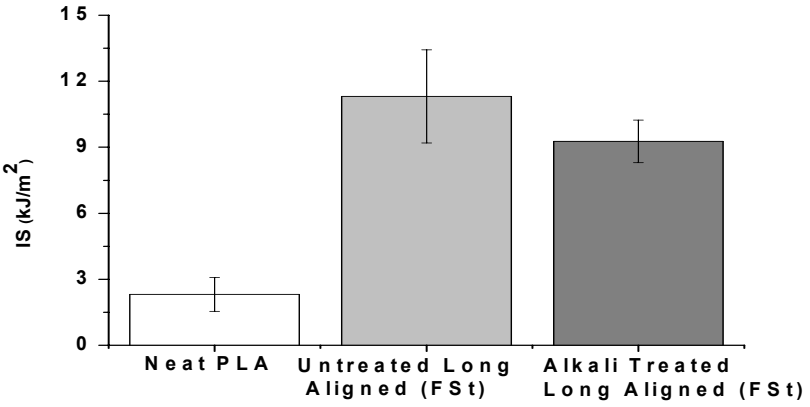

Figure 5.17 IE of untreated long aligned (FSt) and alkali treated long aligned (FSt) composites compared to neat PLA. Error bars each corresponds to one standard deviation.

to that of untreated long aligned (FSt) composites. The prime differences in the fracture modes between untreated long aligned (FSt) and alkali treated long

aligned (FSt) composites were that more fibre pull-out and delamination observed for untreated long aligned (FSt) composites. This is supported by the SEM pictures of Figures 5.14(a) and 5.14(b). As discussed so far, alkali treatment improved the interfacial bond strength (significantly reducing the occurrence of fibre pull-out and delamination in notch initiation and propagation process) and made the composite more brittle. The improved interfacial bond strength and brittle behaviour of the alkali treated long aligned (FSt) composite resulted in lower dissipation of energy and hence lower IE.

5.3.2.4 Fracture Toughness (K_{Ic})

Figure 5.18 shows the K_{Ic} of untreated long aligned (FSt) and alkali treated long aligned (FSt) composites compared to that for neat PLA. K_{Ic} was higher here for the composites than that of neat PLA [241]. An increase in K_{Ic} was seen here for alkali treated long aligned (FSt) composites compared to that for untreated long aligned (FSt) composites.

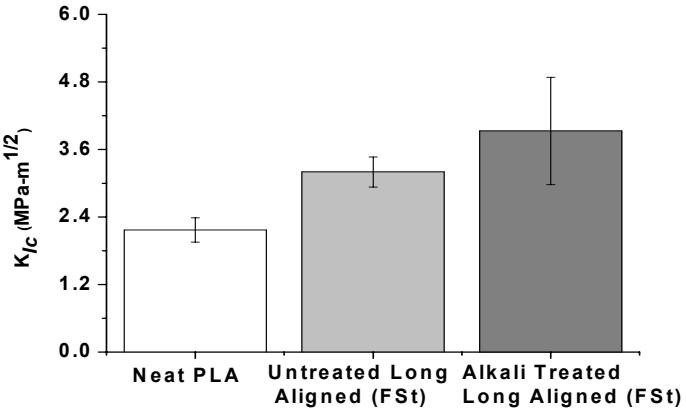

Figure 5.18 K_{Ic} of untreated long aligned (FSt) and alkali treated long aligned (FSt) composites compared to neat PLA. Error bars each corresponds to one standard deviation.

The poor interfacial bonding between the untreated fibre and PLA could make it easier for the fibre to debond from the PLA, Figure 5.19(a). For alkali treated long aligned (FSt) composites, owing to the improved interfacial bonding properties, the load used to pull-out the fibre from the matrix was high and higher fracture resistance was expected. The stronger interfacial bonding also enabled the composites to become brittle so that fewer fibres were involved in pull-out in the

alkali treated long aligned (FSt) composites, Figure 5.19(b), when compared to untreated long aligned (FSt) composites, Figure 5.19(a). Therefore, alkali treated long aligned (FSt) composites had higher K_{Ic} [241].

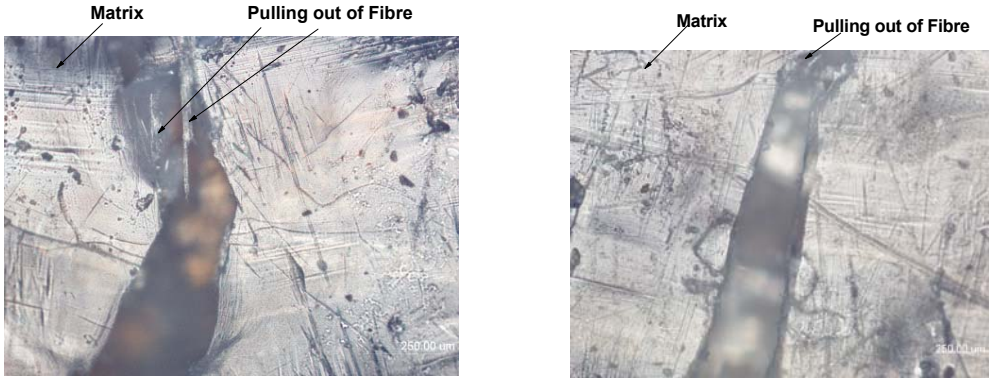

(a) (b)

Figure 5.19 Optical micrographs showing major crack of fracture toughness specimens of (a) untreated long aligned (FSt) and (b) alkali treated long aligned (FSt) composites.

5.3.3 Crystallinity

5.3.3.1 Differential Scanning Calorimetry (DSC) Analysis

Figure 5.20 shows the DSC trace displaying the heating ramp and glass transition, cold crystallisation, pre-melt crystallisation, and melting temperature for neat PLA. The details of cold crystallisation and pre-melt crystallisation can be found

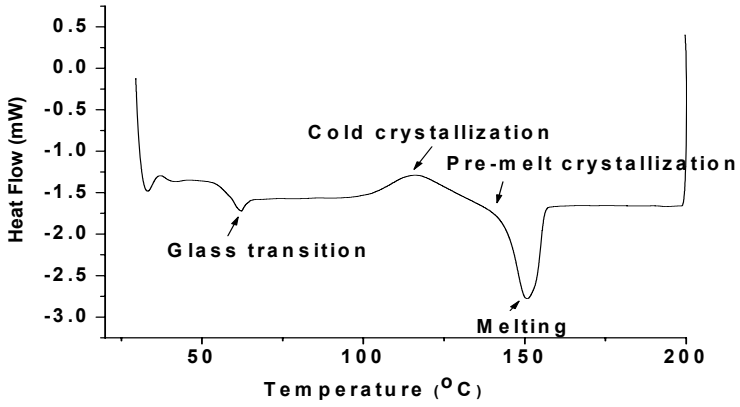

Figure 5.20 DSC trace for PLA only sample displaying the glass transition temperature, cold crystallisation, and melting.

in the literature [264, 265]. The thermal characteristics such as T_g, T_c, T_m, ΔH_m, and X_c obtained from DSC studies are summarised in Table 5.1. It can be seen that T_g, T_c, and T_m decrease with the addition of fibre to the PLA. The depression of the glass transition, cold crystallisation, and melt temperature is typical for plasticised PLA, where the plasticising effect promotes crystallinity due to enhanced chain mobility [266]. The melting endotherms, Figure 5.21, show two distinct peaks (also called a shoulder) for untreated long aligned (FSt) and alkali treated long aligned (FSt) fibre/PLA composites. It has been reported in the literature that a shoulder or a low temperature peak is formed on the melting endotherm of the original crystallites as a result of lamellar rearrangement during crystallisation of PLA [266].

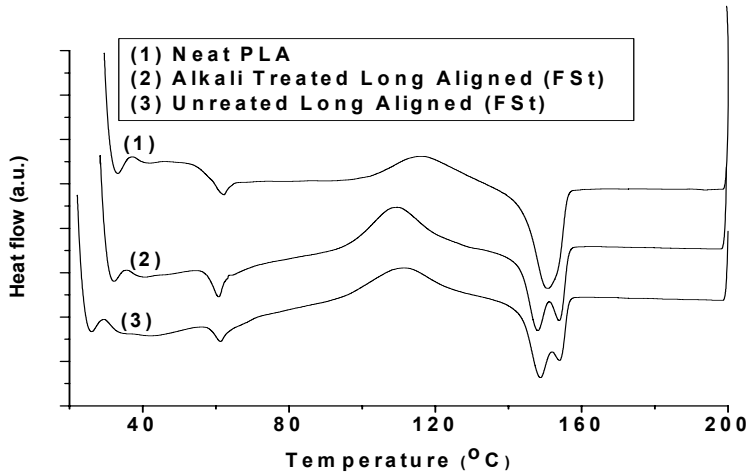

Figure 5.21 DSC thermograms of untreated long aligned (FSt) and alkali treated long aligned (FSt) composites compared to neat PLA.

It can be seen from Table 5.1 that the addition of hemp fibre to PLA results in an

Table 5.1 Thermal characteristics of PLA and its composites obtained from DSC.

Samples	T_g (°C)	T_c (°C)	T_m (°C)	ΔH_m (J/g)	Degree of Crystallinity (%)
PLA	62.20	115.92	152.85	19.99	21.4
Untreated Long Aligned (FSt) Composite	61.20	111.31	148.61	16.68	26.3
Alkali Treated Long Aligned (FSt) Composite	61.00	109.89	148.10	19.29	30.5

increase in the degree of crystallinity of the PLA matrix. This can be explained by the nucleating ability of hemp fibre allowing the crystallisation of PLA. As a result of the modification of fibre surfaces by alkali treatment, bondability between the fibre and PLA matrix improves due to increased interaction by increased potential hydrogen bonding and mechanical interlocking between them. The increased interaction of the fibre with the matrix PLA could further help the fibre surface to act as nucleation sites for the crystallisation of PLA. This promotes the growth and formation of transcrystalline regions around the fibre normal to the fibre surface [191]. Thus composites produced with alkali treated fibre (where non-cellulosic surface components such as lignin were removed from the fibres by alkali treatment) showed an increased degree of crystallinity in the matrix PLA when compared to composites produced with untreated fibre. This agrees with the belief that lignin can negatively affect the ability of the fibre to act as a nucleating agent [14].

5.3.3.2 Wide Angle X-ray Diffraction (WAXRD) Analysis

Figure 5.22 shows the WAXRD patterns for untreated, alkali treated fibres and neat PLA. It can be seen that both untreated and alkali treated fibres show a sharp peak at a 2θ angle of 22.5^{o} (the peak is sharper for alkali treated fibre than untreated fibre) which is more likely due to crystalline cellulose as discussed

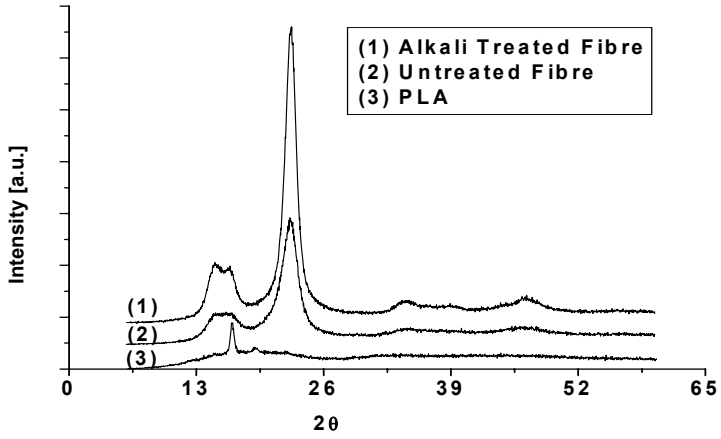

Figure 5.22 WAXRD pattern for the raw materials used.

in section 3.3.1.7**.** On the other hand, PLA shows a narrow and sharp peak at 2θ = 16.4, which could be due to the partially crystalline nature of the PLA. Except for the sharp peak at 16.4, PLA is amorphous and semicrystalline in nature. Figure 5.23 shows the WAXRD patterns for untreated long aligned (FSt) and alkali treated long aligned (FSt) composites. Both of the composites show peaks at 2θ = 15.4, 16.2, 22.5 and 34.5. The peak at 2θ = 16.4 is characteristic of crystalline PLA and the peak at 2θ = 22.5 is characteristics of crystalline cellulose. Both of these peaks are prominent and sharp for alkali treated long aligned (FSt) composites, further indicating their higher crystallinity compared to the untreated long aligned (FSt) composites [10].

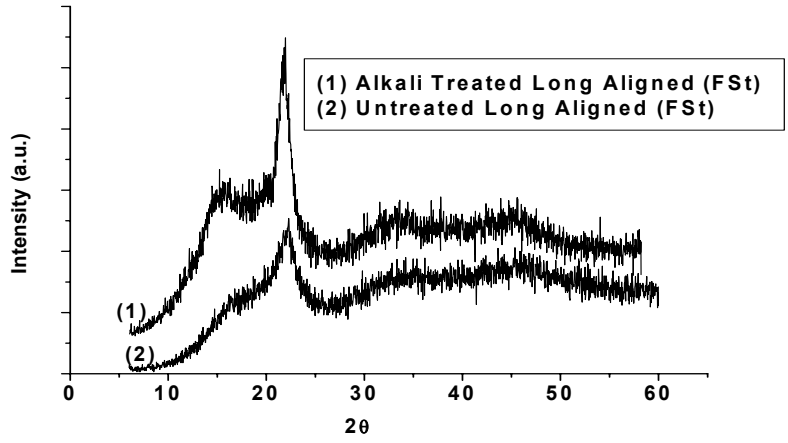

Figure 5.23 WAXRD curves for untreated long aligned (FSt) and alkali treated long aligned (FSt) composites.

5.3.4 Hygrothermal Ageing

Immersion of the samples in water for hygrothermal ageing resulted in increased visibility of the fibre and damage in the form of matrix pitting and cracking. Composites were found to be more affected than the neat PLA. Untreated long aligned (FSt) composites were found to be more affected than the alkali treated long aligned (FSt) composites, Figures 5.24(a) and 5.24(b).

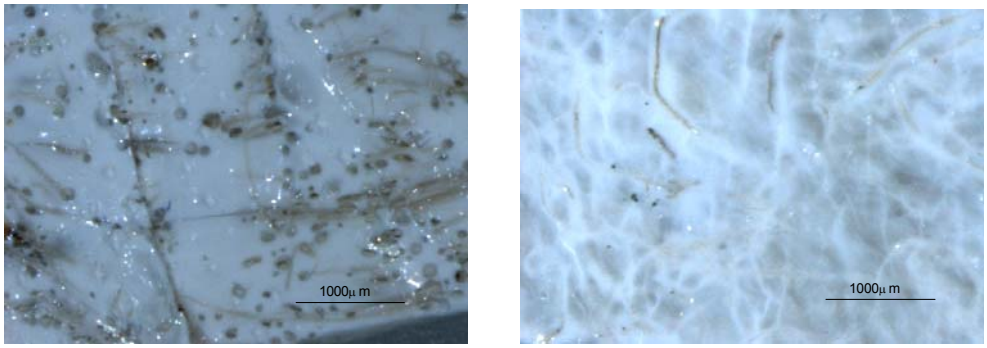

(a) (b)

Figure 5.24 (a) Untreated long aligned (FSt) and (b) alkali treated long aligned (FSt) composite surfaces after hygrothermal ageing at 50°C.

Hygrothermal ageing resulted in increased thickness of the samples with increase in temperature as can be seen from Figure 5.25. This swelling was higher for the composites compared to that for neat PLA; the untreated long aligned (FSt) composites had a higher swelling than the alkali treated long aligned (FSt) composites.

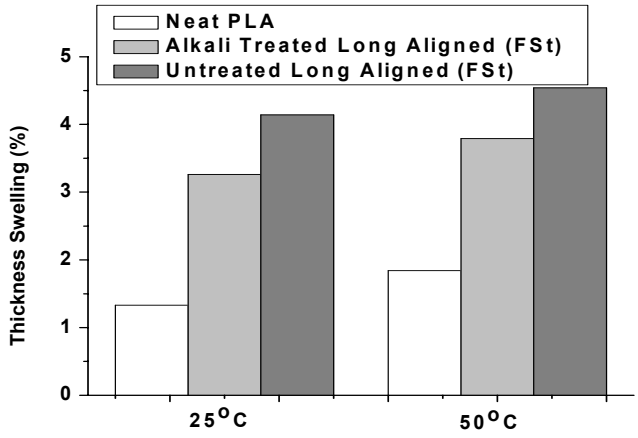

Figure 5.25 Thickness swelling of the composites compared to neat PLA after hygrothermal ageing.

The moisture contents of neat PLA and the composite samples were calculated by the weight difference between the samples exposed to water and the dried samples. Figures 5.26 to 5.28 show the percentage moisture content as a function of immersion time for neat PLA, untreated long aligned (FSt) and alkali treated

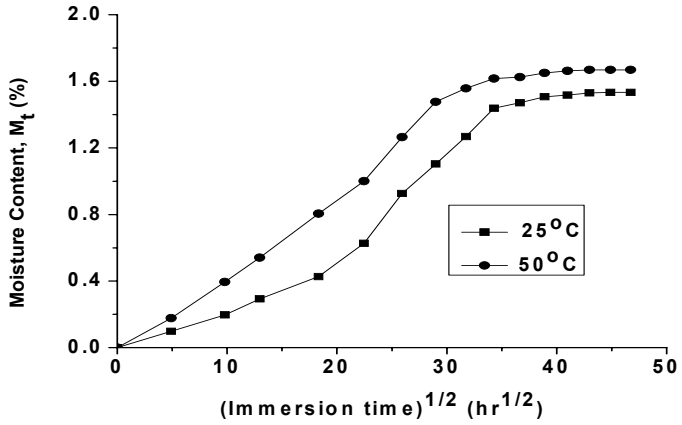

Figure 5.26 Moisture absorption behaviour of neat PLA at 25 and 50°C.

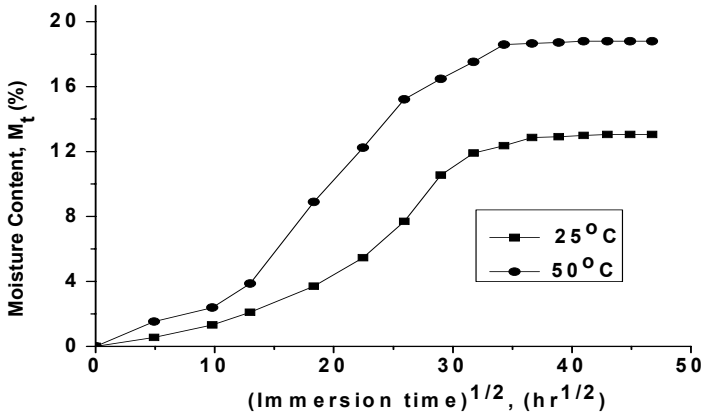

Figure 5.27 Moisture absorption behaviour of 32 wt% untreated long aligned (FSt) composites at 25 and 50°C.

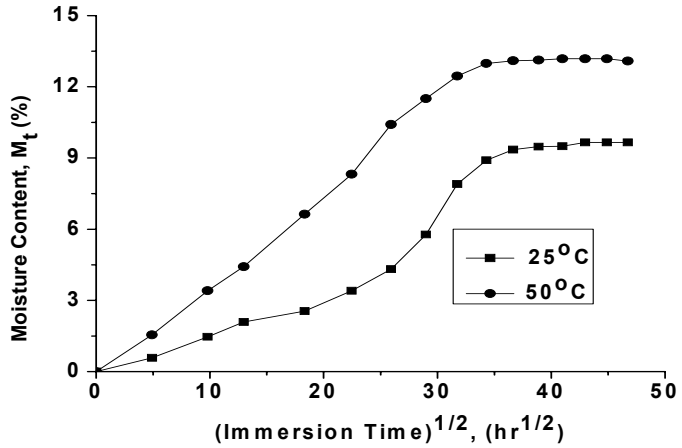

Figure 5.28 Moisture absorption behaviour of 32 wt% alkali treated long aligned (FSt) composites at 25 and 50°C.

long aligned (FSt) composites respectively. After hygrothermal ageing a plateau was observed for all the immersed samples. For neat PLA the plateau was observed after about 2.25 months, and for untreated long aligned (FSt) and alkali treated long aligned (FSt) composites it was observed after about 1.7 months. It can be seen that the temperature of the absorption process has an influence on the water absorption curves. Higher temperature generally increased the water absorption of neat PLA and composites, as well as shortening the saturation time. The low amount of moisture absorbed by neat PLA is expected due to its hydrophobic nature and the high amount of moisture absorbed by the composites is more likely to be due to the hydrophilic nature of the fibres by the presence of polar groups such as –OH and –COOH in the fibres. The reduced water absorption by alkali treated long aligned (FSt) composites compared to the untreated long aligned (FSt) composites can be explained by the stronger interface formed by improved fibre/PLA adhesion as described in section 5.3.1. Strong adhesion in the fibre/PLA interface is necessary for the reduction of interface wicking of the water molecules and increase of resistance to hygrothermal ageing. According to other researchers [243, 244], a lack of interfacial interactions leads to internal strains, porosity, and increases the amount of moisture absorption.

Figure 5.29 shows an example of the fitting of experimental data to Equation (2.16) for alkali treated long aligned (FSt) composites. The values of the kinetic parameter *n* resulting from the fitting of neat PLA, untreated long aligned (FSt) and alkali treated long aligned (FSt) composites are summarised in Table 5.2.

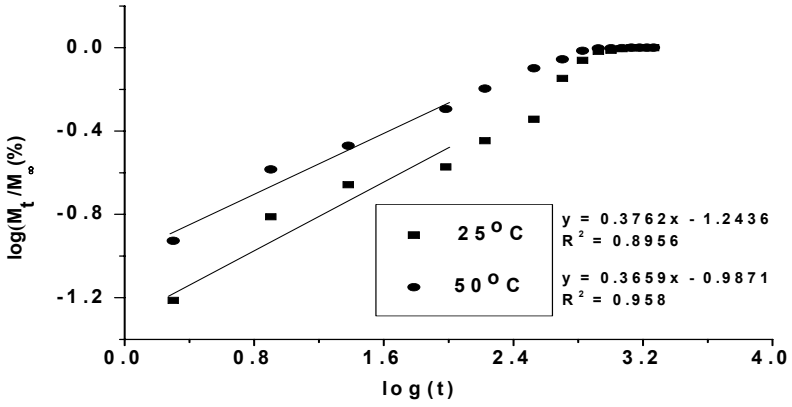

Figure 5.29 Diffusion case fitting plots for 32 wt% alkali treated long aligned (FSt) composites at 25 and 50°C.

Table 5.2 Diffusion case selection parameter n.

Sample	Temperature (°C)	
	25	50
Neat PLA	0.3922	0.3707
Untreated Long Aligned (FSt) Composite	0.4876	0.4538
Alkali Treated Long Aligned (FSt) composite	0.3762	0.3659

The data supports the absorption of water in HPCs approaching Fickian diffusion (case I) as the values are less than $n = 0.5$ [7]. Using Equation (2.17) the diffusion coefficient (D) can be obtained from the slope of the linear part of the $(M_t/M_\infty)^2$ versus tL^{-2} plot. Table 5.3 shows the values of the diffusion coefficients obtained by fitting the linear part of Equation (2.17). The results for the composite samples are similar with those obtained for sisal/PP composites by other researchers [7]. The increase in diffusion coefficient with temperature is likely due to the increased ability of the water molecules to move among the polymer segments at higher temperatures [7].

Table 5.3 Diffusion coefficients for NE, untreated long aligned (FSt) and alkali treated long aligned (FSt) composites at two different temperatures.

Sample	D (m^2/s) $\times 10^{13}$	
	25°C	50°C
Neat PLA	2.55	6.28
Untreated Long Aligned (FSt) Composite	4.12	10.99
Alkali Treated Long Aligned (FSt) composite	3.73	10.21

5.3.4.1 Effects of Hygrothermal Ageing on Mechanical Properties

Tensile Properties

From Figures 5.30 and 5.31, it can be seen that the TS and YM decreased with hygrothermal ageing for the composites such that the extent of decrease was higher for higher immersion temperatures. However, no significant reduction in TS and YM were observed for neat PLA which is not surprising considering its

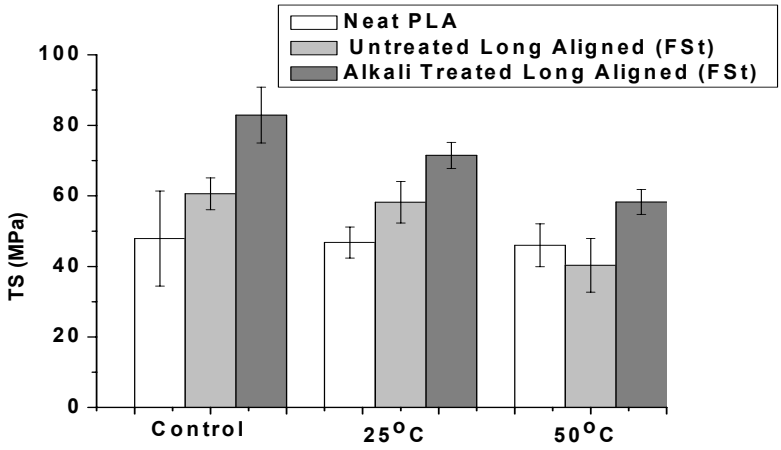

Figure 5.30 Effect of hygrothermal ageing on the TS of neat PLA, untreated long aligned (FSt) and alkali treated long aligned (FSt) composites at different temperatures. Error bars each corresponds to one standard deviation.

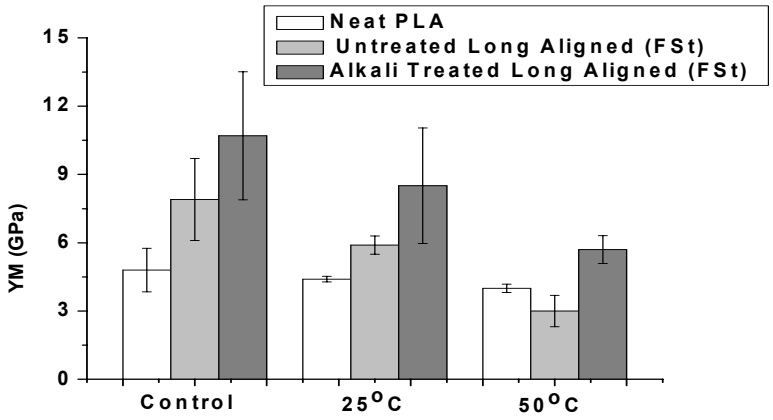

Figure 5.31 Effect of hygrothermal ageing on the YM of neat PLA, untreated long aligned (FSt) and alkali treated long aligned (FSt) composites at different temperatures. Error bars each corresponds to one standard deviation.

low moisture absorption. Generally, when natural fibre composites are immersed in water, the fibre/matrix interface absorbs moisture which results in the development of shear stress at the interface. This accelerates the debonding process, resulting in delamination, loss of structural integrity [242] and in turn reduction in TS and YM. Other researchers have also reported that the hygrothermal ageing causes water penetration into the matrix leading to a reduction in fibre matrix adhesion and a reduction in TS and YM [7].

The loss of fibre/matrix adhesion, characterised by apparition of holes with some long unfractured fibres/fibre bundles, can be seen in the SEM micrographs of the fracture surfaces, Figures 5.32(a) and 5.32(b). With the increase of temperature, more water penetrates into the composites and swells up the fibres causing cracks in the matrix.

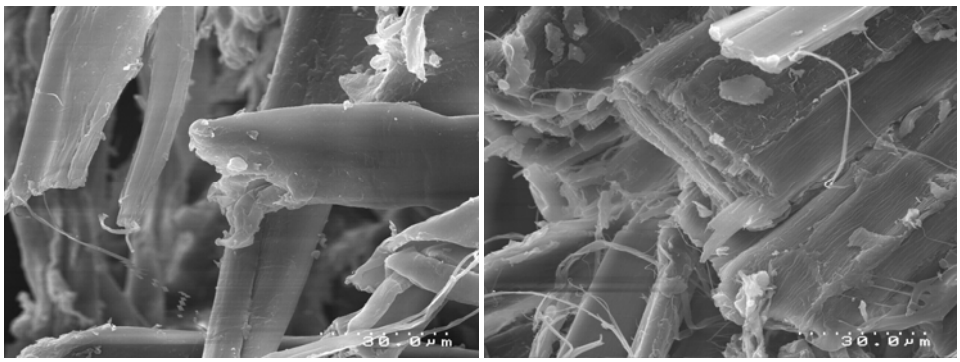

(a) (b)

Figure 5.32 (a) untreated long aligned (FSt) and (b) alkali treated long aligned (FSt) composite fracture surfaces after hygrothermal ageing at 50°C.

It can also be seen from the result that the reduction in TS and YM at higher temperature is greater for untreated long aligned (FSt) composites than for alkali treated long aligned (FSt) composites, Table 5.4. In the case of alkali treated long aligned (FSt) composites, the stronger interface formed due to increased crsytallinity of the PLA, potential hydrogen bonding and mechanical interlocking

Table 5.4 Tensile properties of untreated long aligned (FSt) and alkali treated long aligned (FSt) composites after hygrothermal ageing at two different temperatures.

Tensile Properties	**Untreated Long Aligned (FSt)**		**Alkali Treated Long Aligned (FSt)**	
	25°C	50°C	25°C	50°C
TS (MPa)	58.2	40.3	71.5	58.3
YM (GPa)	5.9	3	8.5	5.7
FS (%)	2.511	2.668	3.838	5.373

could have caused lower water absorption. Therefore, a lower loss in fibre/matrix adhesion and a higher amount of fibre fracture was noticed for the alkali treated long aligned (FSt) composites compared to untreated long aligned (FSt) composites, as can be noted from the SEM pictures, Figures 5.32(a) and 5.32(b). Low diffusion coefficient resulted from the alkali treated long aligned (FSt) composites compared to untreated long aligned (FSt) composites as summarised

in Table 5.3 further supports the stronger interfacial bonding for alkali treated long aligned (FSt) composites.

The observed increase in FS, Figure 5.33, for all the composites after hygrothermal ageing might be due to water molecules acting as a plasticising agent in the composites [7]. However, a reduction in FS for the neat PLA after hygrothermal ageing was observed, which may be due to the presence of surface cracks upon absorption of water to some extent.

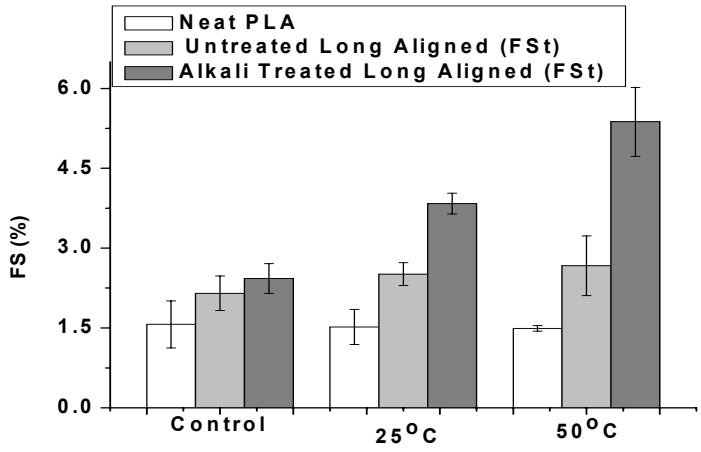

Figure 5.33 Effect of hygrothermal ageing on the FS of neat PLA, untreated long aligned (FSt) and alkali treated long aligned (FSt) composites at different temperatures. Error bars each corresponds to one standard deviation.

Flexural Properties

Flexural strength and flexural modulus were found to decrease with hygrothermal ageing, and that the extent of reduction was greater for the higher immersion temperature, Figures 5.34 and 5.35. FS was found to increase for the composites and decrease for neat PLA after hygrothermal ageing, Figure 5.36. These results are consistent with the tensile properties described previously.

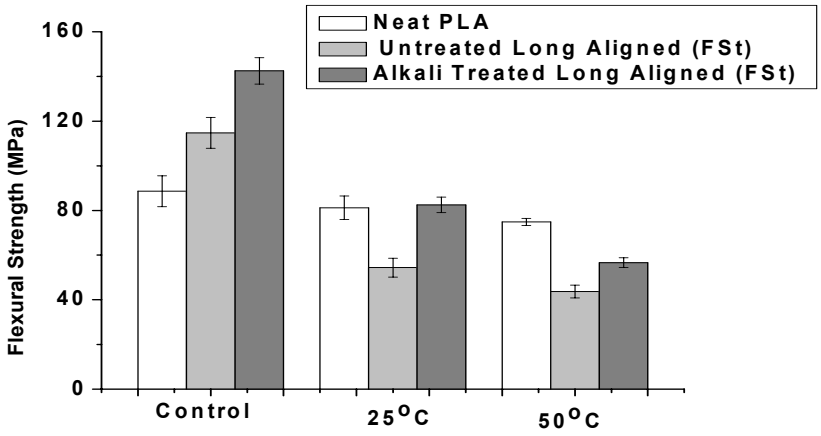

Figure 5.34 Effect of hygrothermal ageing on the flexural strength of neat PLA, untreated long aligned (FSt) and alkali treated long aligned (FSt) composites at different temperatures. Error bars each corresponds to one standard deviation.

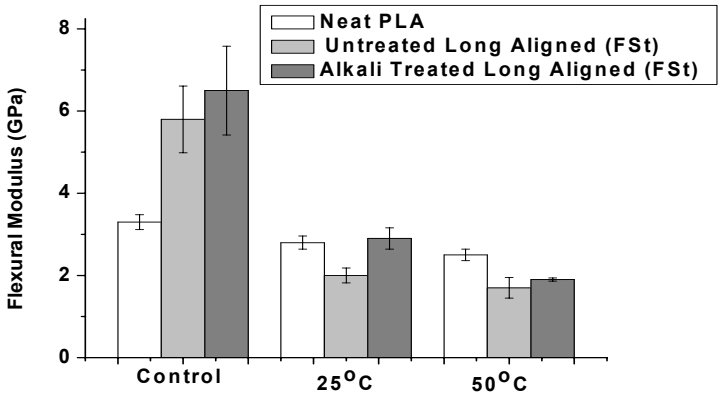

Figure 5.35 Effect of hygrothermal ageing on the flexural modulus of neat PLA, untreated long aligned (FSt) and alkali treated long aligned (FSt) composites at different temperatures. Error bars each corresponds to one standard deviation.

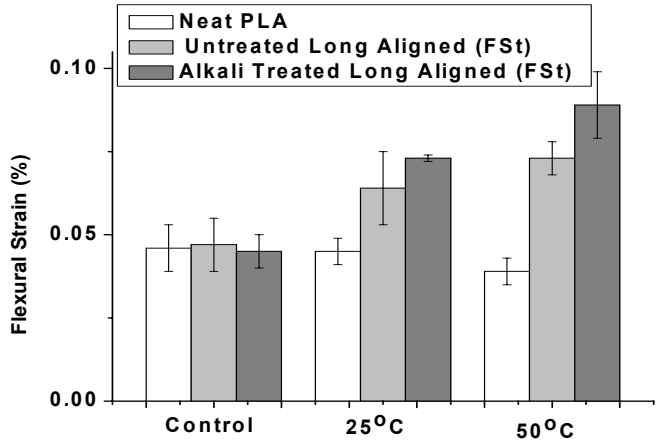

Figure 5.36 Effect of hygrothermal ageing on the flexural strain of neat PLA, untreated long aligned (FSt) and alkali treated long aligned (FSt) composites at different temperatures. Error bars each corresponds to one standard deviation.

Impact Energy (IE)

Figure 5.37 shows the effect of hygrothermal ageing on the IE of untreated long aligned (FSt), and alkali treated long aligned (FSt) composites compared to neat PLA at two different temperatures. It can be seen that the IE of the

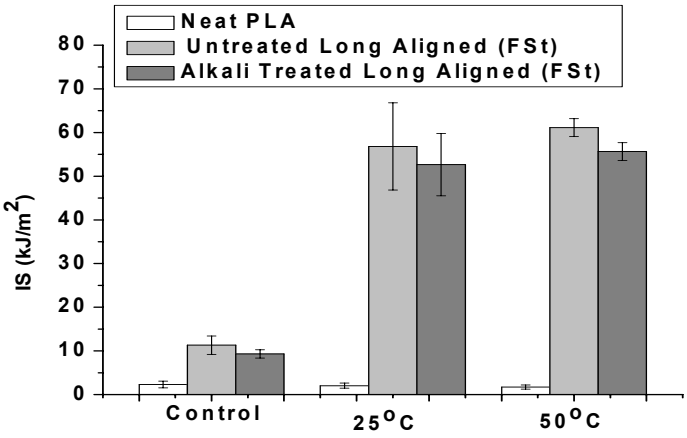

Figure 5.37 Effect of hygrothermal ageing on the IE of neat PLA, untreated long aligned (FSt) and alkali treated long aligned (FSt) composites at different temperatures. Error bars each corresponds to one standard deviation.

composites increased with hygrothermal ageing, and that the extent of increase was greater at higher temperatures. The IE is related to the plasticisation effect of the fibre/PLA interface [134], as a plasticised interface encourages the fibre pull-out mechanism. Absorption of moisture caused swelling in the fibre surface,

enhancing the frictional work of fibre pull-out from PLA matrix which increased the IE [134]. As extent of swelling was greater at higher temperatures, it leads to more frictional work of pull-out and hence the IE.

Fracture Toughness (K_{Ic})

As can be seen from Figure 5.38, K_{Ic} decreased with the increase in hygrothermal ageing temperature for all of the samples particularly for untreated long aligned (FSt) composites. With the increase in temperature, swelling of the fibre might increase which could lead to the formation of cracks in the matrix and weaken the fibre/matrix interface. Weak fibre/matrix interface could make fibre pull-out easier, resulting in a reduction in K_{Ic} of the composites.

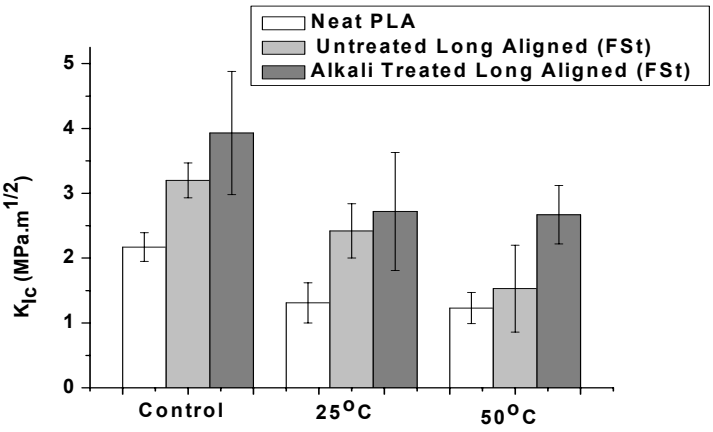

Figure 5.38 Effect of hygrothermal ageing on the K_{Ic} of neat PLA, untreated long aligned (FSt) and alkali treated long aligned (FSt) composites at different temperatures. Error bars each corresponds to one standard deviation.

5.3.4.2 Effects of Hygrothermal Ageing on Crystallinity

Differential Scanning Calorimetry (DSC) Analysis

Figure 5.39 shows the DSC traces for untreated long aligned (FSt) and alkali treated long aligned (FSt) composites after hygrothermal ageing at 50°C. The glass transition temperature was found to decrease from about 61°C, Figure 5.20, to about 50°C as well as melt temperature was found to decrease from about 148°C, Figure 5.20, to about 145°C for both untreated long aligned (FSt)

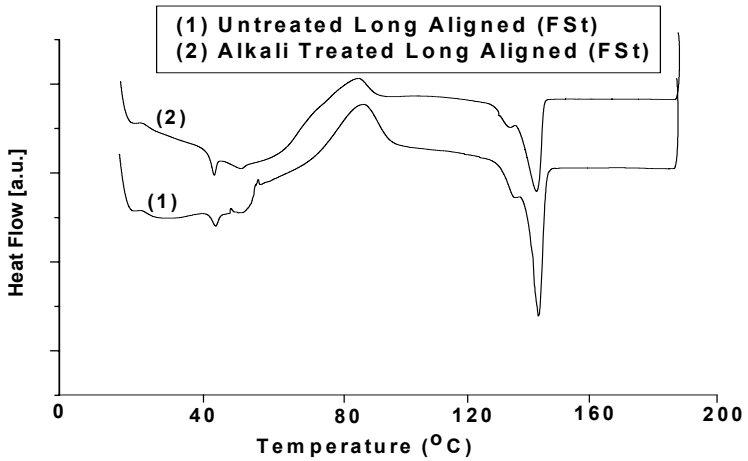

Figure 5.39 DSC traces for untreated long aligned (FSt) and alkali treated long aligned (FSt) composites after hygrothermal ageing at 50°C.

and alkali treated long aligned (FSt) composites. However, the endothermic melting peak was found to be more distinct for alkali treated long aligned (FSt) composites than for untreated long aligned (FSt) composite after hygrothermal ageing. Table 5.5 shows the thermal characteristics of hygrothermally aged PLA and its composites obtained from DSC. The degree of crystallinity was found to increase for untreated and alkali treated composites, from about 21 (Table 5.1) to 32% for untreated long aligned (FSt) composite while for alkali treated long aligned (FSt) composite it was found to increase from about 26 (Table 5.1) to 37%.

Table 5.5 Thermal characteristics of hygrothermally aged PLA and its composites obtained from DSC.

Samples	**T_g (°C)**	**T_c (°C)**	**T_m (°C)**	**ΔH_m (J/g)**	**Degree of Crystallinity (%)**
Untreated Long Aligned (FSt) Composite	48.0	85.0	145.0	20.30	32.09
Alkali Treated Long Aligned (FSt) Composite	48.0	81.0	145.0	23.64	37.38

Water is generally accepted as a plasticising agent for PLA which is supported by PLA swelling observed by Proikakis *et al.* [267]. Plasticisation could explain the lamellar rearrangement resulting in increased crystallinity. According to Zhang *et al.* [268], PLA crystallinity increases during hydrolytic degradation at a

temperature near the glass transition temperature. In addition, wicking of water at the interface would swell the fibre and result in cracks in the matrix and as a consequence loss of interfacial adhesion. Loss of interfacial adhesion and matrix crack would increase water penetration into the composites as well as PLA which could further increase plasticisation of PLA and as a consequence PLA crystallinity.

Wide Angle X-ray Diffraction (WAXRD) Analysis

Figure 5.40 shows the WAXRD patterns for untreated long aligned (FSt) and alkali treated long aligned (FSt) composites after hygrothermal ageing at 50°C. PLA shows a peak at 2θ = 16.4, which is attributed to the crystalline nature of the PLA (section 5.3.3.2). The peak intensity at 2θ = 16.4 was found to increase for the aged samples compared to the control samples, Figure 5.23, (section 5.3.3.2) showing the increase in PLA crystallinity after accelerated ageing. The sharp peak at 2θ = 22.5 is characteristic of crystalline cellulose, as shown in section 5.3.3.2, was found to decrease upon hygrothermal ageing, this could be due to degradation of cellulose and a resulted drop in crystallinity. The intensity drop for the peak at 2θ = 22.5 was found to be higher for the untreated long aligned (FSt) composites

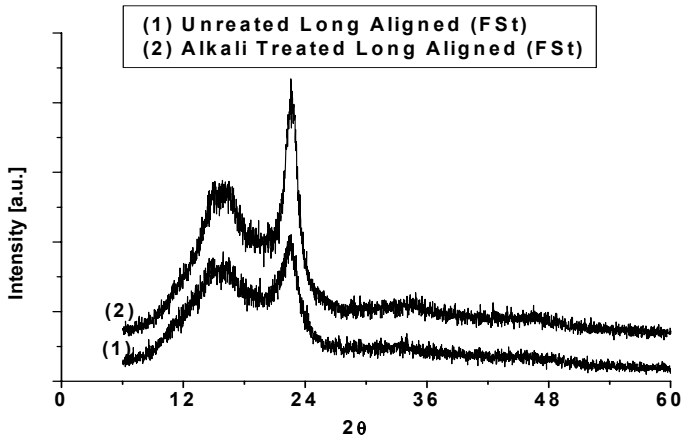

Figure 5.40 WAXRD pattern for untreated long aligned (FSt) and alkali treated long aligned (FSt) composites after hygrothermal ageing at 50°C.

than the alkali treated long aligned (FSt) composites, indicating greater degradation of cellulose for the untreated long aligned (FSt) composites upon hygrothermal ageing.

5.3.5 Accelerated Ageing

As can be seen from Figure 5.41, the exposure of the samples to accelerated ageing environments slightly deteriorated the surface texture in the form of

Control Untreated | Control Alkali Treated | 1000 Hours Untreated | 1000 Hours Alkali Treated

Figure 5.41 Visual change during ageing of untreated long aligned (FSt) and alkali treated long aligned (FSt) composites.

decoloration, appearance of a milky colour on the surface, and surface softness. The aged surface showed an accentuation of fibres with the erosion of PLA, Figures 5.42(a) and 5.42(b). The appearance of milky patches, matrix cracks, and swollen fibres are more severe for untreated long aligned (FSt) composites than that for alkali treated long aligned (FSt) composites. The deterioration of the composites is likely to be initiated by the fibre ridging followed by PLA film rupture through cracking and then fibre pop-out. This is attributed mainly to the stresses produced by differential swelling and shrinkage of the fibre/PLA caused by changes in moisture content. Stresses also built up at the fibre/matrix interface due to a large difference between the coefficients of thermal expansion for PLA matrix and hemp fibre, leading to the failure of the fibre/PLA interface [249]. Increasing exposure to the weathering conditions led to the initiation of tearing in the fibres due to degradation by UV attack.

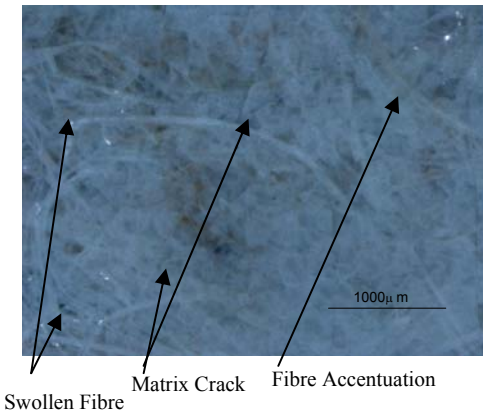

(a)

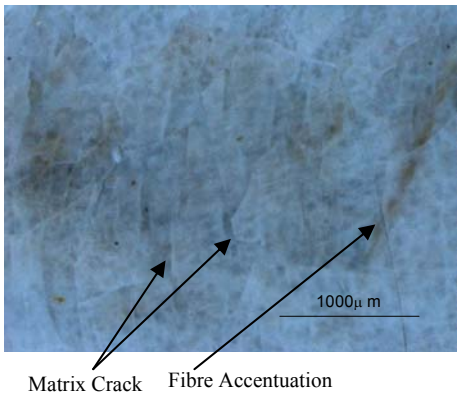

(b)

Figure 5.42 (a) Untreated long aligned (FSt) and (b) alkali treated long aligned (FSt) composite surfaces after 1000 hours accelerated ageing.

Progressive percentage weight gain in the samples during accelerated ageing is shown in Figure 5.43. The weight gain might be caused by the absorption of water during water spray and condensation cycles. The weight loss of PLA and decrease in weight gain for the composites after accelerated ageing of 1000 hours might be caused by leaching out of the PLA upon exposure to the ageing environment. The yellowish colour of the samples, Figure 5.41, after accelerated ageing might be due to the breakdown of the lignin into water soluble products [151, 250].

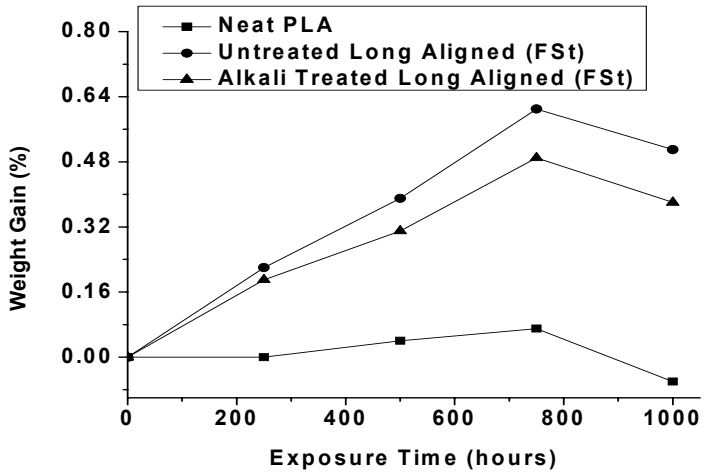

Figure 5.43 Percentage weight gain of neat PLA, untreated long aligned (FSt) and alkali treated long aligned (FSt) composites.

The change in mechanical properties due to accelerated ageing for different time periods is presented in Figures 5.44 to 5.51. A reduction in TS, flexural strength, YM, and flexural modulus for neat PLA with increased ageing duration was observed, Figures 5.44, 5.45, 5.47, and 5.48. The greatest reduction in TS, flexural strength, YM and flexural modulus was found for untreated long aligned (FSt) composites than for alkali treated long aligned (FSt) composites. Tensile and flexural strengths were found to decrease from 61 and 115 MPa to 8 and 13 MPa respectively while, YM and flexural modulus were found to decrease from 8 and 6 GPa to 1 and 2 GPa respectively for untreated long aligned (FSt) composites, Figures 5.44, 5.45, 5.47, and 5.48. FS and flexural strain were found to increase with increased weathering time up to 750 hours for both untreated long aligned (FSt) and alkali treated long aligned (FSt) composites and then decrease with further weathering, while a continuous decrease of FS and a continuous increase of flexural strain with increased weathering time were noted for neat PLA, Figures 5.46 and 5.49. IE was found to increase dramatically for all of the composites after 250 hours of weathering with a continued increase up to 750 hours and a decrease after this time. IE of neat PLA was found to decrease with increased weathering time, Figure 5.50. K_{Ic} was found to decrease for all samples with increased weathering time, with greatest decrease from 3.2 to 0.6 MPa.m$^{1/2}$ found for untreated long aligned (FSt) composites, Figure 5.51.

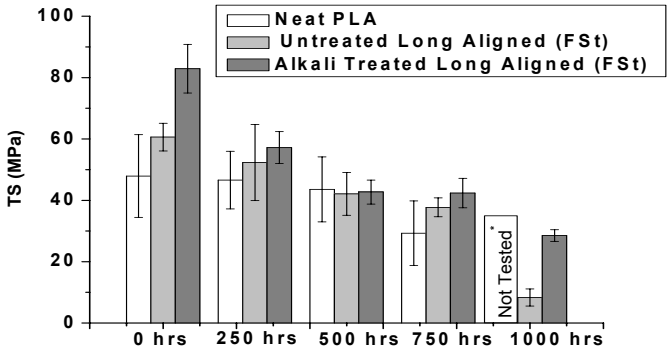

Figure 5.44 Effect of accelerated ageing on the TS of neat PLA, untreated long aligned (FSt) and alkali treated long aligned (FSt) composites. Error bars each corresponds to one standard deviation.

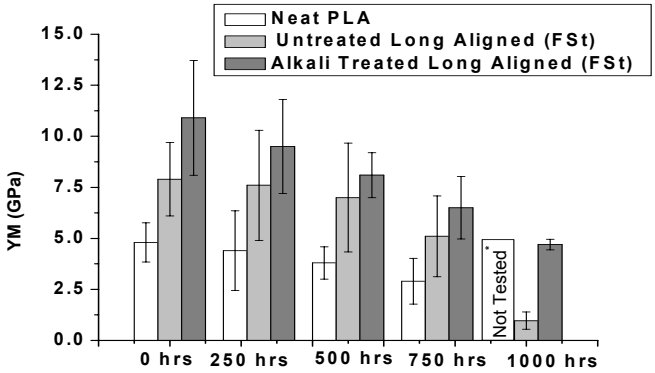

Figure 5.45 Effect of accelerated ageing on the YM of neat PLA, untreated long aligned (FSt) and alkali treated long aligned (FSt) composites. Error bars each corresponds to one standard deviation.

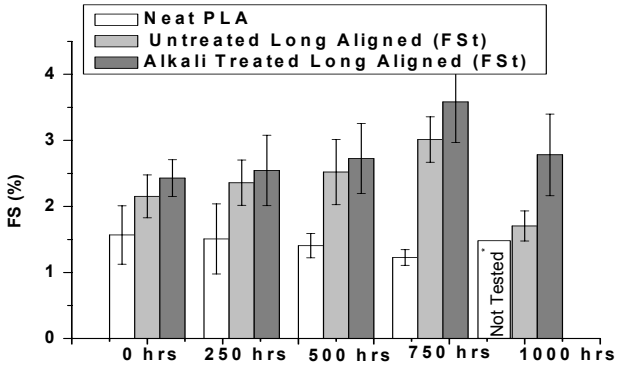

Figure 5.46 Effect of accelerated ageing on the FS of neat PLA, untreated long aligned (FSt) and alkali treated long aligned (FSt) composites. Error bars each corresponds to one standard deviation.

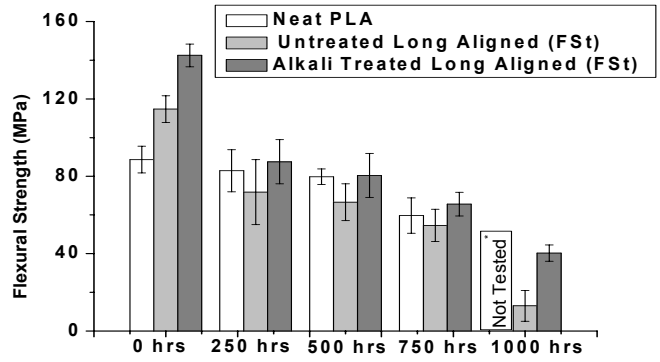

Figure 5.47 Effect of accelerated ageing on the flexural strength of neat PLA, untreated long aligned (FSt) and alkali treated long aligned (FSt) composites. Error bars each corresponds to one standard deviation.

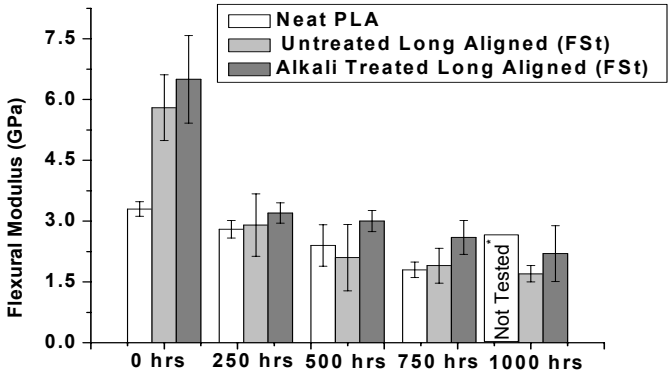

Figure 5.48 Effect of accelerated ageing on the flexural modulus of neat PLA, untreated long aligned (FSt) and alkali treated long aligned (FSt) composites. Error bars each corresponds to one standard deviation.

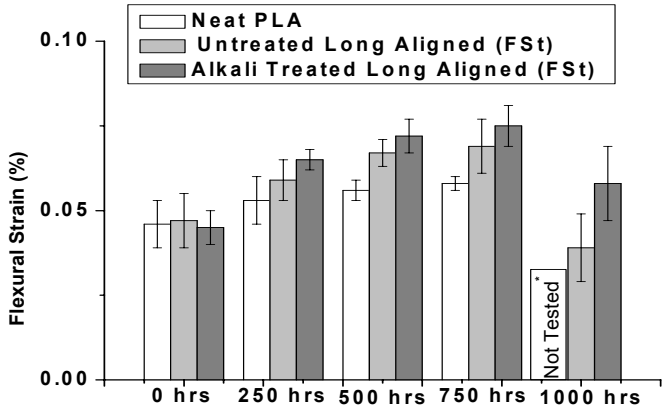

Figure 5.49 Effect of accelerated ageing on the flexural strain of neat PLA, untreated long aligned (FSt) and alkali treated long aligned (FSt) composites. Error bars each corresponds to one standard deviation.

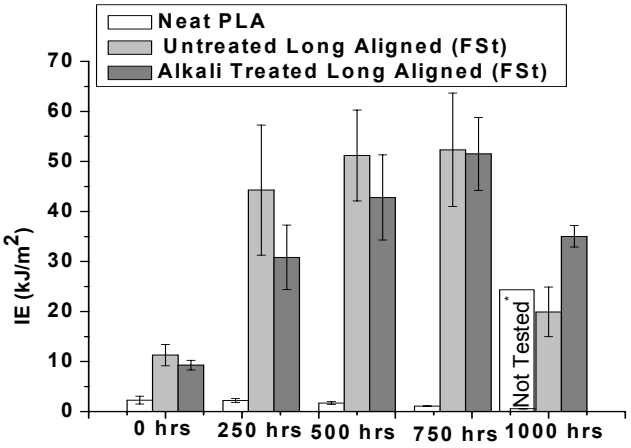

Figure 5.50 Effect of accelerated ageing on the IE of neat PLA, untreated long aligned (FSt) and alkali treated long aligned (FSt) composites. Error bars each corresponds to one standard deviation.

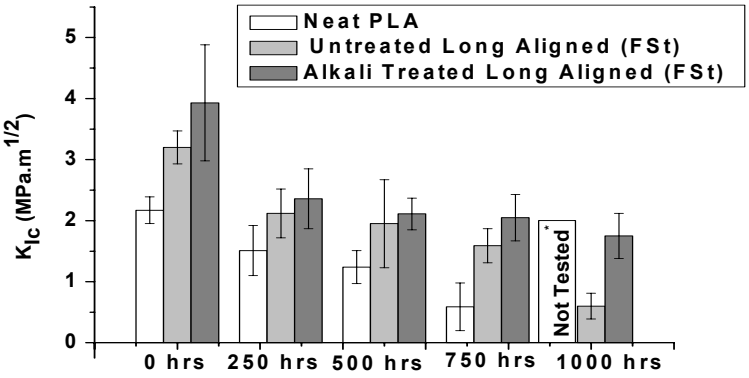

Figure 5.51 Effect of accelerated ageing on the K_{Ic} of neat PLA, untreated long aligned (FSt) and alkali treated long aligned (FSt) composites. Error bars each corresponds to one standard deviation.

The reduction in TS, flexural strength, YM, and flexural modulus for neat PLA with increased weathering duration is considered to be due to plasticisation, swelling effect [251] and photochemical degradation [7]. The reduction in TS, flexural strength, YM, and flexural modulus of the composites might be due to the development of swelling stresses, caused by the difference of expansion and contraction of fibre/PLA as a result of moisture absorption [249].

Fibrillation of the fibres in the composite fracture surfaces was also noticed, Figures 5.52(a) and 5.52(b), showing degradation of lignin which acts as an adhesive holding cellulose fibrils together. After lignin degradation, the poorly bonded cellulose fibrils could erode easily from the surface, which could expose new lignin embedded cellulose fibrils for subsequent degradation reaction and thus would be expected to enhance fibre pull-out from PLA. Thus more loss of

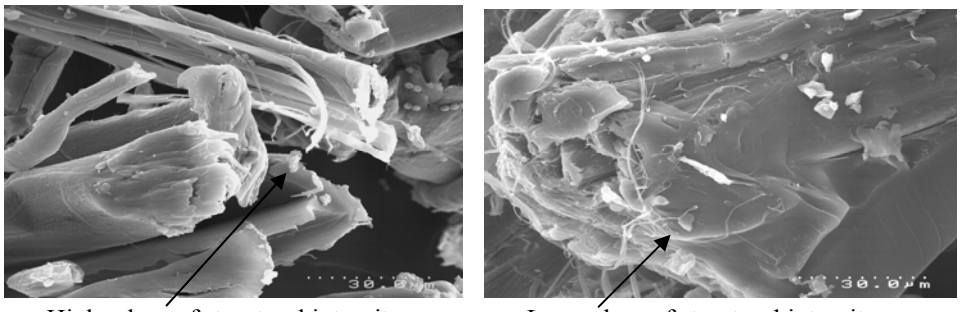

(a) (b)

Figure 5.52 (a) Untreated long aligned (FSt) and (b) alkali treated long aligned (FSt) composite fracture surfaces after 1000 hours accelerated ageing.

structural integrity can be seen for untreated long aligned (FSt) composite, Figure 5.52(a), than for alkali treated long aligned (FSt) composite, Figure 5.52(b). The ageing process could make the composite surface rougher and also could lead to significant fibre loss from the surface according to other researchers [247].

PLA is a semicrystalline polymer and the degree of crystallinity of the processed PLA (section 5.3.3.1) was found to be about 13%. As crystalline regions are impermeable to oxygen, degradation occurs predominantly in the amorphous regions by chain scission, while UV-induced cross-linking occurs in the imperfect crystalline regions. The reduction in FS, flexural strain, IE, and K_{Ic} of neat PLA with weathering of up to 750 hours could be due to PLA chain scission and formation of surface cracks, which can be seen in Figure 5.53. After weathering of 1000 hours, softening and leaching of PLA made the samples too soft to be tested. The increase in FS, flexural strain and IE, and decrease in K_{Ic}, for the composites

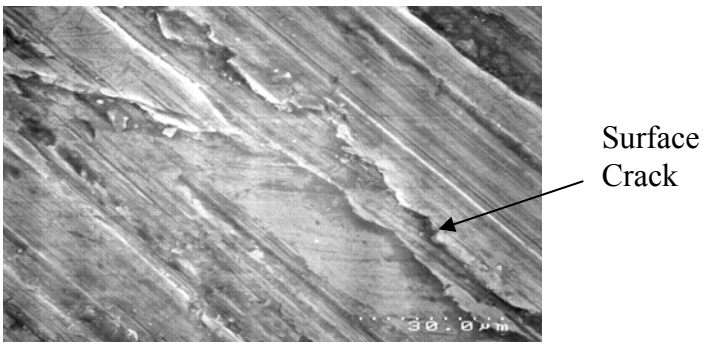

Figure 5.53 SEM micrograph of neat PLA surface after weathering for 750 hours.

may be due to the formation of porous structure as a result of leaching of debonded fibres by the fibrillation process upon removal of lignin. As a result of the increase in porosity, more water molecules would be expected to be trapped inside the composite structure, which may have a plasticising effect, resulting in the increase in FS, flexural strain and IE, and decrease in K_{Ic} [7]. Swelling of fibres as a result of water absorption also could cause the fibres to be pulled-out of the PLA matrix, increasing energy dissipation which in turn might increase the FS, flexural strain and IE, and decrease the K_{Ic} of the composites. The decrease in FS, flexural strain and IE of the composites after 1000 hours of weathering might be caused by failure of PLA by softening and leaching out. Alkali treated long aligned (FSt) composites showed better resistance to accelerated weathering due to the formation of stronger fibre/PLA bonds as discussed.

5.3.5.1 Fourier Transform Infrared (FTIR) Spectra Analysis

Analyses of the FTIR spectra, Figure 5.54, shows an increase in the intensity of the C=O absorption for the 1000 hours weathered sample over the control sample in the 1734 cm^{-1} region and also around 1650 cm^{-1}. [253]. The increase in the

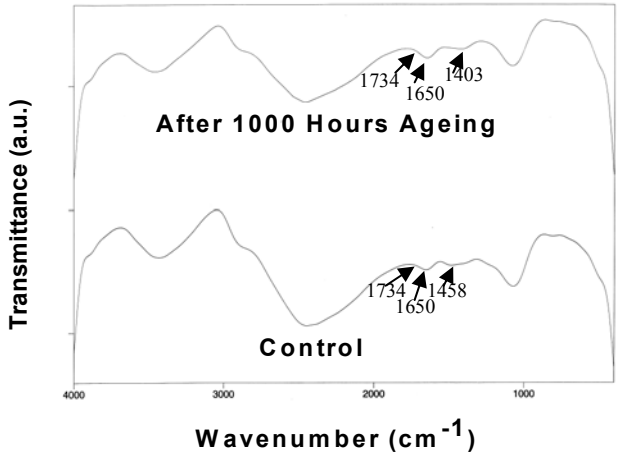

Figure 5.54 FTIR spectra of untreated long aligned (FSt) composites.

carbonyl absorption indicates modification in the lignin structure. The increase in the intensity of the 1650 cm^{-1} band indicates quinine formation by irradiation during weathering [253]. The bands at 1734 and 1650 cm^{-1} are characteristic absorptions of carbonyl stretching vibrations of non-conjugated (in xylan) and conjugated (in lignin) esters and carboxylic acids, and their concentration increases as carbonyl groups are liberated from lignin and/or carbohydrates due to chemical degradation [253-255]. Pure PLA has a C-H deformation band at 1350 to 1460 cm^{-1}, which was found to be at 1458 cm^{-1} for control sample and at 1403 cm^{-1} for 1000 hours weathered sample [155].

5.3.5.2 Wide Angle X-ray Diffraction (WAXRD) Analysis

Figure 5.55 shows the WAXRD patterns for untreated long aligned (FSt) and alkali treated long aligned (FSt) composites after 1000 hours accelerated ageing. PLA shows a narrow and sharp peak at $2\theta = 16.4$, which is attributed to the

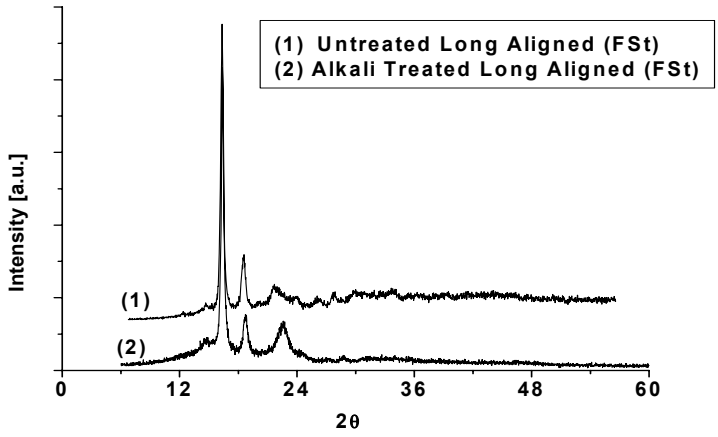

Figure 5.55 WAXRD pattern for untreated long aligned (FSt) and alkali treated long aligned (FSt) composites after accelerated ageing of 1000 hours.

crystalline nature of the PLA (as shown in section 5.3.3.2). The peak intensity increased tremendously for the accelerated aged samples showing the increase in crystallinity of PLA after accelerated ageing. The sharp peak at 2θ = 22.5 for the crystalline cellulose as shown in section 5.3.3.2, was found here to decrease significantly for the aged composites, showing a decrease in cellulose crystallinity due to the degradation of cellulose upon accelerated ageing. The intensity drop for the peak at 2θ = 22.5 was found to be greater for the untreated long aligned (FSt) composites when compared to alkali treated long aligned (FSt) composites, indicating a higher degradation of cellulose for the untreated long aligned (FSt) composites upon accelerated ageing.

5.3.5.3 Differential Scanning Calorimetry (DSC) Analysis

Figure 5.56 shows the DSC traces for untreated long aligned (FSt) and alkali treated long aligned (FSt) composites after accelerated ageing of 1000 hours. The glass transition temperature was found to decrease from about 61^{o}C, Figure 5.20, to about 42 and 45^{o}C, and melt temperature was found to decrease from about 148^{o}C, Figure 5.20, to about 140 and 144^{o}C for untreated long aligned (FSt) and alkali treated long aligned (FSt) composites respectively. The depression of the glass transition and melt temperature by photodegradation of PLA has also been

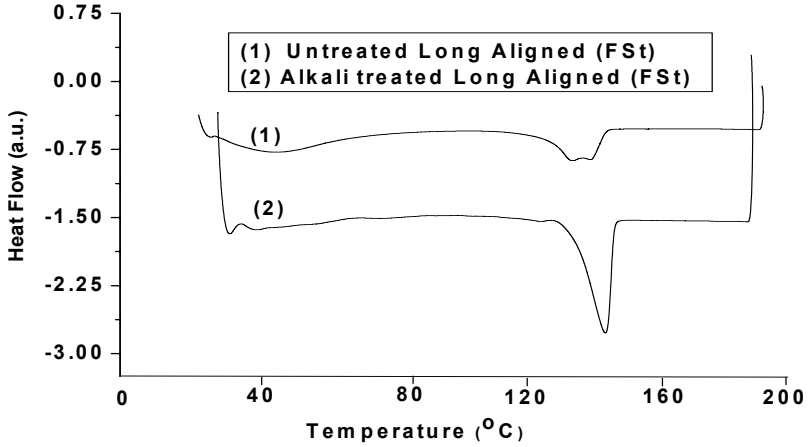

Figure 5.56 DSC traces for untreated long aligned (FSt) and alkali treated long aligned (FSt) composites after accelerated ageing of 1000 hours.

observed by other researchers [155, 269]. The shoulder in the endothermic melting peak was found to disappear for alkali treated long aligned (FSt) composite while the shoulder was found to merge for untreated long aligned (FSt) composite after accelerated aging of 1000 hours. However, the degree of crystallinity was found to increase from about 21 to 38% for untreated long aligned (FSt) composite while for alkali treated long aligned (FSt) composite it was found to increase from about 26 to 45%. The increase in crystallinity could be caused by the rearrangement of the amorphous PLA segments into crystalline phase during the degradation of PLA by chain scission. This process is known as chemicrystallisation [264]. The increase in crystallinity of PP upon UV exposure by the chemicrystallisation process and segmental mobility of the amorphous region has been reported by other researchers [7].

5.4 Chapter Conclusion

IFSS measurements showed that ATPLA samples had greater IFSS values when compared to UTPLA samples.

Composites produced with short fibres using different processing methods had poor reinforcing efficiency. Good impregnation of fibres into PLA and good reinforcing efficiency were achieved by film stacking using long fibres. Composites produced with alkali treated fibres had better properties when

compared to untreated fibres in terms of tensile properties, flexural properties, K_{Ic} and percentage crystallinity.

Hygrothermal ageing of hemp fibre/PLA composites indicated that the absorption of water in the composites followed Fickian diffusion (case I). The hygrothermal ageing at two different temperatures showed that fibre treatment with alkali had a significant influence on the mechanical properties of the composites.

Accelerated ageing of hemp/PLA composites for different durations revealed that fibre treatment with alkali had a significant influence on the mechanical properties of the composites.

Chapter Six

Conclusions

6.1 Fibre Treatment and Characterisation

Untreated hemp fibres were subjected to 16 different alkali treatments by varying four different treatment parameters (concentration of NaOH and Na_2SO_3, treatment temperature, and digestion time). A decrease in average fibre diameter was observed for all alkali treatments which appeared to increase with the severity of the alkali treatment. The parameters that most significantly influenced fibre TS and YM were the process temperature and NaOH concentration. The reduction in TS with increased temperature and NaOH concentration appeared to be due to increased degradation of structural cellulose in the fibres. The reduction in YM is believed to be due to the removal of lignin and other intra-fibrillar binders leading to degradation of cellulose and molecular relaxation of the cellulose fibre components. Upon analysis of the alkali fibre treatments by single fibre tensile testing (SFTT), SEM, zeta potential, DTA/TGA, WAXRD, lignin content and FTIR spectroscopy, the alkali treatment with 5 wt% NaOH, 2 wt% Na_2SO_3, 120^{o}C treatment temperature, and 60 minutes digestion time was found to give the best combination of:

(i) fibre TS retention (revealed by SFTT)

(ii) increased fibre roughness, fibre separation from fibre bundles, and non-cellulosic fibre component removal (revealed by SEM and lignin analysis)

(iii) increased thermal stability (revealed by DTA/TGA analysis)

(iv) increased cellulose hydroxyl group exposure (revealed by zeta potential and FTIR analysis), and

(v) increased crystalline cellulose by better packing of cellulose chains (revealed by WAXRD analysis).

The fibres obtained from the optimised alkali treatment were further treated with acetic anhydride and phenyltrimethoxy silane. Acetylation and silanation treated fibres were found to give a slight reduction of single fibre performance although an increase in crystalline cellulose was observed for acetylated fibres.

An empirical model for the TS of alkali treated fibres was obtained by a fractional factorial design using four different alkali treatment parameters as mentioned above. The TS of the alkali treated fibres could be predicted using the model within the range of experimental conditions under investigation which was verified experimentally in this study. The accuracy (at a confidence level of 95%, $\alpha = 0.05$) of the prediction of TS using the empirical model was quite satisfactory as the experimental TS of alkali treated fibre obtained was almost within the range of tolerance limit of the model. However, for better prediction (e.g. at a confidence level of 98%, $\alpha = 0.02$), full factorial design could be carried out. Such an approach, however, would require a greater number of experiments (twice the experiments required for the full factorial design compared to that for the fractional factorial design), but the accuracy of the prediction would improve very little. This empirical model for the TS of the alkali treated fibre, however, failed to give the best fibre strength which has been reported by other researchers [270], which could be due to not optimising parameters like fibre: NaOH and fibre: Na_2SO_3 solution ratios.

6.2 Hemp/Epoxy Composites (HECs)

Two dynamic models (the Kissinger and Flynn-Waal-Ozawa Models) and an isothermal model (the Autocatalytic Model) provided a good fit for the experimental data obtained from isothermal DSC scans of NE and 40 wt% UTFE composites. The activation energies for the curing of composites exhibited lower values compared to curing of NE. This indicates that the addition of fibre in epoxy resin enhanced the curing reaction between epoxy resin and amine curing agent which might be due to higher nucleophilic activity of the amine groups of the curing agent in the presence of fibres. The average activation energies obtained

from dynamic models were higher than those obtained from the isothermal model. This might be due to the wide temperature range of 25-120^{o}C used in this study. The wide temperature range might cause a decrease in the slope of the Arrhenius plot due to the large variation in the reaction constants.

The highest IFSS value (at an epoxy to curing agent ratio of 1:1 (E_1C_1)) for alkali treated fibre/epoxy (ATFE) samples was 5.2 MPa which was larger than the highest value of 2.7 for UTFE samples supporting that there was a stronger interface between alkali treated fibre and epoxy resin.

Long fibre/epoxy composites were optimised in terms of different (a) fibre treatments (b) epoxy to curing agent ratios (c) resin soaking times, and (d) curing temperatures. Of the composites produced with different treated fibres, ATFE composites were found to have a modest improvement in TS while ATFE and STFE composites were found to have modest improvements in YM compared to NE. The limited benefit of TS obtained by fibre addition might be due to poor fibre wetting leading to a weak interface (supported by SEM micrographs). The highest YM of the STFE composites compared to other composites could be attributed to excessive cross-linking of the fibre -OH groups with the highly active silane groups and active hydrogen groups of the amine curing agent (supported by brittle fracture surface obtained from an SEM image). Of the composites produced with different epoxy to curing agent ratios, the greatest increase in TS was obtained with composites produced with epoxy to curing agent ratio of 1:1 and the greatest increase in YM was obtained with an epoxy to curing agent ratio of 1:1.2. ATFE composites were found to have higher TS and YM compared to that for UTFE composites. The results were found to be consistent with the IFSS values. Tensile properties of the composites were found to increase with soaking time of 60 minutes compared to that of 10 minutes. It is likely due to increased fibre wetting during soaking by the epoxy resin leading to better interfacial strength. The increased soaking time also appears to have decreased porosity in the composites (supported by optical micrographs). Of the composites produced with different curing temperatures, TS and YM of the composites were found to be higher at 70^{o}C than at 25^{o}C for both UTFE and ATFE composites, but they were found to decrease as the curing temperature was increased further to 120^{o}C, whereas the converse is true for FS. TS, YM and FS were consistently higher for

ATFE than for UTFE composites which is likely due to increased interfacial bonding for ATFE composites.

Tensile properties of short fibre/epoxy composites produced by aligning the fibres along the tensile testing axis were found to increase compared to those of randomly oriented short fibre/epoxy composites. Fibre alignment along the tensile testing axis ATSFE composites showed higher TS and YM compared to those for UTSFE composites, which is likely due to better bonding of the alkali treated fibres with epoxy resin.

Tensile properties of long fibre/epoxy composites were found to increase when fibre was aligned by hand carding, compared to those of fibre aligned by hackling. This may be due to better separation and fibre alignment obtained by the carding process.

Long fibre/epoxy composites were found to show consistently higher tensile properties than those for short fibre/epoxy composites when produced at three different fibre contents with a 70^{o}C curing temperature. Increase in TS and YM, and a decrease in FS were observed for both long and short fibre/epoxy composites with the increased fibre content. At 40 wt% fibre, ATLFE composites showed the most effective reinforcement, compared to UTLFE composites. However, at fibre contents of 50 and 65 wt% TS was found to decrease for ATLFE composites compared to UTLFE composites although YM was still found to increase. The increase in number of fibres at higher fibre loadings would increase fibre-fibre contact in the ATLFE composites such that inefficient stress transfer between fibres could occur and result in reduction in TS. ATLFE composites maintaining higher YM than the UTLFE composites at higher fibre loadings could be due to higher average interfacial bonding. The reduction in FS for the ATLFE composites compared to UTLFE composites is also likely due to failure initiated from stress concentration caused by fibre-fibre contact for ATLFE composites. Similarly, tensile properties, flexural properties, IE and K_{Ic}, were also found to be better for long fibre/epoxy composites when compared to short fibre/epoxy composites. Flexural strength and K_{Ic} were found to increase and IE was found to decrease for UTFE composites in contrast to the trend for IFSS which is likely due to the increased stress concentration by increased fibre-fibre contact in ATFE composites.

Thus, optimum mechanical properties were obtained with a 65 wt% aligned UTLFE composite (produced by curing at 70^{o}C with an epoxy to curing agent ratio of 1:1 using compression moulding) with a TS of 165 MPa, YM of 17 GPa, flexural strength of 180 MPa, flexural modulus of 10.1 GPa, impact energy (IE) of 14.5 kJ/m^2, and fracture toughness (K_{Ic}) of 5 MPa.m$^{1/2}$.

TGA analysis of the long fibre/epoxy composites showed that the thermal stability of the ATLFE composites was better at the cellulose decomposition stage (which is far above of composite processing temperature used in the current study) than that for UTLFE composites which could be due to an increase in cellulose crystallinity by better packing of cellulose chains upon alkali treatment.

With hygrothermal ageing, equilibrium moisture content and the diffusion coefficient were found to increase with increased immersion temperature. Short fibre/epoxy composites showed lower water absorption and diffusion coefficient than that for long fibre/epoxy composites and alkali treated fibre/epoxy composites showed lower water absorption and diffusion coefficient than untreated fibre/epoxy composites. In the case of hygrothermally aged composites, TS, flexural strength, YM, flexural modulus and K_{Ic} were found to decrease and IE was found to increase which is likely due to damage in the fibre and weakening in the fibre/matrix interface by fibre swelling and resultant cracks in the matrix. Also, FS and flexural strain were found to increase which could be due to the plasticisation effect of water. These results were supported by SEM, TGA, and WAXRD analyses.

In the case of accelerated aged composites, in terms of exposure to UV-radiation and humid environments, reduction in TS, flexural strength, YM, flexural modulus and K_{Ic} and increase in FS, flexural strain and IE were observed which could be due to epoxy resin chain scission as a result of photo oxidation as well as damage in the fibres and fibre/matrix interface. These results were supported by SEM, TGA, and WAXRD analysis. FTIR analysis of accelerated aged UTFE composites showed a reduction in lignin content which could be due to the degradation of the lignin upon exposure to UV radiation.

6.3 Hemp/PLA Composites (HPCs)

The IFSS of untreated and alkali treated hemp fibres embedded in PLA was measured using single fibre pull-out testing. An improvement in the IFSS by the use of alkali treated fibre has been clearly observed, indicating a stronger fibre/matrix interface for ATPLA composites.

Short fibre reinforced PLA composites produced with both aligned (obtained by DSF) and random fibre mats, did not show any reinforcing effect which could be due to unsuccessful impregnation of PLA to fibres by various means namely, impregnation during dynamic sheet forming, manual impregnation, and impregnation using DCM as a solvent). In addition to that, for short aligned fibre composites, moisture absorption by PLA during dynamic sheet forming could cause degradation of PLA at higher processing temperatures, resulting in a possible reduction in interfacial strength and as a consequence, poor composite TS.

Film stacking was found to be most successful technique in the production of aligned long fibre/PLA composites. Alkali treatment of fibre was seen to increase the mechanical properties of aligned long fibre/PLA composites as revealed by tensile, flexural, impact, and fracture toughness tests. SEM micrographs, thermal characteristics, degree of crystallinity, and WAXRD analysis also showed that composites produced with alkali treated fibre had better performance than composites produced with untreated fibre. From the results of the long and short fibre/PLA composites produced using different processing conditions by compression moulding, it was found that a 32 wt% alkali treated long fibre/PLA composite produced by film stacking was the best, having a TS of 83 MPa, YM of 11 GPa, flexural strength of 143 MPa, flexural modulus of 6.5 GPa, IE of 9 kJ/m^2, and K_{Ic} of 3 MPa.m$^{1/2}$. Using film stacking, hemp fibre/PLA composites were limited to 32 wt% fibre. The results of the mechanical properties of the composites were consistent with the IFSS of both UFPLA and ATPLA composites.

With hygrothermal ageing of 32 wt% untreated and alkali treated long fibre/PLA composites, equilibrium moisture content and diffusion coefficient were found to

increase with increased immersion temperature. ATPLA composites showed lower water absorption and diffusion coefficient than that for UTPLA composites. In the case of hygrothermally aged composites, TS, flexural strength, YM, flexural modulus and K_{Ic} were found to decrease and IE was found to increase. Increase in moisture absorption with hygrothermal ageing is believed to weaken fibre/PLA bonding due to formation of crack in the matrix by fibre swelling which would be expected to result in interfacial failure and hence deterioration in mechanical properties of the composites as observed. Also, FS and flexural strain were found to increase which could be due to the plasticisation effect of water. These results were supported by SEM, DSC, and WAXRD analyses.

Occurrence of possible PLA chain scission as a result of photo oxidation as well as fibre swelling by moisture absorption of the accelerated aged composites are believed to result in deterioration in the mechanical properties of the composites as observed. ATPLA composites were found to be more resistant than UFPLA composites towards accelerated ageing environments as revealed by tensile, flexural, impact, and fracture toughness tests as well as SEM, DSC, WAXRD, and FTIR analyses.

Chapter Seven

Recommendations and Future Work

Brittle property of PLA has an influence on the performance of hemp/PLA composites. Therefore, plasticisers could be used in the production of hemp/PLA composites to investigate changes in the performance of the composites. The use of coupling agents and compatibilisers to improve fibre/epoxy and fibre/PLA interfacial bonding could also be investigated.

Increase of the weight fraction of fibres in the composites (especially in fibre/PLA composites) was found to be difficult in the current study. Therefore, in order to be able to increase the fibre content (volume fraction) in both hemp/epoxy and hemp/PLA composites, further development in the composite production methods is necessary.

Fibre alignment was found to be effective in composite performance improvement. Therefore, fibre alignment in the composites could be improved. This may involve the use of continuous hemp yarns to produce uniaxially aligned epoxy and PLA matrix composites by compression moulding, filament winding, and pultrusion. The DSF process could also be modified to obtain an efficient way of aligning fibres (both long and short) and in-situ impregnation of the matrices.

The single fibre pull-out test has been shown to be a potential method for obtaining the IFSS. Advanced instrumentation is required to obtain embedded fibre length with the matrices in micro scales to calculate IFSS more precisely. The influence of hygrothermal ageing on the IFSS of the composites could be studied. The possibility of using single fibre fragmentation tests in the determination of IFSS could be assessed.

Advanced modelling is required for a better understanding of the variation of composite properties with different fibre weight fractions by bringing the non-uniformity of hemp fibres and fracture mechanics of the composites into account.

Cure kinetics of the fibre/epoxy system for 40 wt% UTFE composites were assessed in the current work. Therefore, it would be interesting to assess the cure kinetics by using different fibre treatments as well as different fibre contents.

As hemp fibre absorbs moisture, reduction in mechanical properties of hemp fibre/epoxy and hemp fibre/PLA composites due to interfacial failure was observed in the current study. Therefore, silane treatment could be assessed for influence on hygrothermal ageing. The influence in the variation of fibre contents on the hygrothermal and accelerated ageing could also be assessed. Natural ageing (outdoor exposure to sun and rain) of the composites could also be carried out to correlate with the real-world performance.

References

1. S.J.Pickering, *Recycling technologies for thermoset composite materials - current status* Composites: Part A, 2005. 20: p. 1-10.
2. S.Goutianos, et al., *Development of flax fibre based textile reinforcements for composite applications.* Applied Composite Materials, 2006. 13: p. 199-215.
3. A.B.Strong, *In the beginning...The history of composites*, in *Composites Fabrication*. 1996. p. 9-10.
4. N.E.Zafeiropoulos, et al., *Engineering and characterization of the interface in flax fibre/polypropylene composite materials. Part I. Development and investigation of surface treatments.* Composites: Part A: Applied Science and Manufacturing, 2002. 33: p. 1083-1093.
5. P.K.Mallik, *Fiber-reinforced composites: materials, manufacturing, and design*. 2nd edition ed. 1993, New York: Marcel Dekker.
6. J.M.Hughes, *On mechanical properties of bast fibre reinforced thermosetting polymer matrix composites*, in *School of Agriculture and Forestry Sciences*. 2000, University of Wales.
7. P.V.Joseph, et al., *Environmental effects on the degradation behaviour of sisal fibre reinforced polypropylene composites.* Composite Science and Technology, 2002. 62: p. 1357-1372.
8. K.Joseph, et al., European Polymer Journal, 1996. 32: p. 1243-1250.
9. I.K.Varma, S.R.A. Krishnan, and S.Krishnamoorthy, *Effect of chemical treatment on mechanical properties and moisture regain of jute fibers.* Textile Research Journal, 1988. 58(9): p. 537-543.
10. Mathew, A.P., K. Oksman, and M. Sain, *Mechanical properties of biodegradable composites from poly lactic acid (PLA) and microcrystalline cellulose (MCC).* Journal of Applied Polymer Science, 2005. 97: p. 2014-2025.
11. A.P.Mathew, K.Oksman, and M.Sain, *Mechanical properties of biodegradable composites from poly lactic acid (PLA) and microcrystalline cellulose (MCC).* Journal of Applied Polymer Science, 2005. 97: p. 2014-2025.
12. K.Oksman, Wood Science and Technology, 1996. 30: p. 197.
13. M.A.Osman, et al., Polymer, 2001. 42: p. 6545.
14. S.J.Eichhorn, et al., *Review Current international research into cellulosic fibres and composites.* Journal of Materials Science, 2001. 36: p. 2107-2131.
15. T.Kasuga, et al., Biomaterials, 2001. 22: p. 19.
16. J.H.Lee, et al., Journal of Biomaterials, 2003. 24: p. 2773.
17. E.Bodros, et al., *Could biopolymers reinforced by randomly scattered flax fibre be used in structural applications?* Composites Science and Technology, 2007. 67(3-4): p. 462-470.

18. A.K.Bledzki, V.E.Sperber, and O.Faruk, *Natural and wood fibre reinforcement in polymers*. Rapra Review Reports, 2002. 13(8): p. 152.

19. M.Karus, S.Ortmann, and G.D.Vogt, *Use of natural fibres in composites in the German automotive production 1996 till 2003*. 2004, Nova-Institute.

20. P.K.Pal, Plastics Rubber Process Appl, 1984. 4: p. 215-219.

21. G.C.Ellison and R.McNaught, *The use of natural fibres in nonwoven structures for applications as automotive component substrates*, in *Research and Development report: Ministry of Agricalture Fisheries and Food. Agri – Industrial Materials*. 2000. p. 1-46.

22. R.R.Franck, *Bast and Other Plant Fibres*. 2005, Cambridge: Woodhead Publishing Limited.

23. D.Robson and J.A.Hague. *Comparison of wood and plant fibre properties*. in *Third International Conference on Woodfibre-plastic composites*. 1995. Madison, Wisconsin, USA: Forest Products Society.

24. A.K.Bledzki and J.Gassan, *Composites reinforced with cellulose based fibres.* Progress in Polymer Science, 1999. 24: p. 221-274.

25. D.Robson, et al., *Survey of natural materials for use in structural composites as reinforcement and matrices.* Woodland Publishing Ltd, Abingdon, 1996.

26. D.J.Macintosh, *A BRIEF HISTORY OF CANNABIS SATIVA L. (HEMP) in NZ!* 1997, National Organisation for the Reform of Marijuana Laws.

27. J.L.Deferne and D.W.Pate, *Hemp seed oil: A source of valuable essential fatty acids.* Journal of the International Hemp Association 1996. 3(1)(1): p. 4-7.

28. Werf, H.M.G.v.d., E.Mathijssen, and A.Haverkort, *The potential of hemp (Cannabis sativa L.) for sustainable fibre production: a crop physiological appraisal* Annals of Applied biology, 1996. 129(1): p. 109-123.

29. Vavilov, N.I., *The origin of the cultivation of "primary" crops, in particular of cultivated hemp*, in *Studies on the origin of cultivated plants*. 1926, Institute of Applied Botany and Plant Breeding: Leningrad. p. 221–233.

30. Ehrensing, D.T., *Feasibility of industrial hemp production in the United States Pacific Northwest*. 1998, Department of Crop and Soil Science, Oregon State Univ. Expt. Sta. Bul. 681. Oregon State University: Corvallis.

31. J.M.Dempsey, *Hemp*, in *Fibers Crops*. 1975, University of Florida: Gainesville. p. 46-89.

32. A.Thygesen, et al., *Comparison of composites made from fungal defibrated hemp with composites of traditional hemp yarn.* Industrial Crops and Products, 2006. xxx: p. xxx-xxx.

33. H.L.Bos, M.J.A.V.D. Oever, and O.C.J.J.Peters, *Tensile and compressive properties of flax fibres for natural fibre reinforced composites.* Journal of Materials Science, 2002. 37: p. 1683-1692.

34. *TPP Industrial Hemp Guide*, in *Health Canada*. 1998. p. 4.

35. D.G.Hepworth, et al., *The penetration of epoxy resin into plant fibre cell walls increases the stiffness of plant fibre composites.* Composites: Part A: Applied Science and Manufacturing, 2000. 31: p. 599-601.

36. R.M.Rowell, R.A.Young, and J.K.Rowell, *Chemical Composition of Fibres: Paper and Composites from Agro-based Resources*. 1997: Lewis Publishers, CRC Press. 85-91.

37. A.B.Bjerre and A.S.Schmidt, *Development of chemical and biological processes for production of bioethanol: Optimization of the wet oxidation process and characterization of products*. 1997, Riso-R-967(EN), Riso National Laboratory. p. 5-9.

38. C.Morvan, et al., Carbohydrate Polymers, 1990. 13: p. 149-163.

39. B.Madsen, *Properties of plant fibre yarn polymer composites - An experimental study*. 2004, PhD Thesis, Department of civil Engineering, Technical University of Denmark.

40. A.Sakakibara and N.Shiraishi. Wood and Cellulose Chemistry. 1991, New York: Marcel Dekker.

41. R.M.Rowell. *A new generation of composite materials from agro-based fibre*. in *The Third International Conference on Frontiers of Polymers and Advanced Materials*. 1995. Kuala Lumpur, Malaysia.

42. R.Kohler and M.Wedler, TECHTEXTIL-Symposium, 1994: p. 1.

43. R.D.Patel, R.G.Patel, and V.S.Patel, J. Therm. Anal., 1988. 34: p. 1283.

44. L.Yu, K.Dean, and L.Li, *Polymer blends and composites from renewable resources.* Prog. Polym. Sci., 2006. 31: p. 576-602.

45. B.Bax and J.Mussig, Composites Science and Technology, 2008. 68: p. 1601-1607.

46. Oksman, K., M. Skrifvars, and J.F.Selin, *Natural fibres as reinforcement in polylactic acid (PLA) composites.* Composites Science and Technology, 2003. 63: p. 1317-1324.

47. K.Meinander, et al., *Polylactides- degradable polymers for fibres and films.* Macomolecular Symp, 1997. 123: p. 147-154.

48. L.Jiang and G.Hinrichsen, *Flax and cotton fiber reinforced biodegradable polyester amide composites, 2.* Die Angewandte Makromolekulare Chemie, 1999. 268: p. 18-21.

49. U.Riedel and J.Nickel, *Natural fibre-reinforced biopolymers as construction materials - new discoveries.* Die Angewandte Makromolekulare Chemie, 1999. 272: p. 34-40.

50. A.Keller, et al., *Degradation kinetics of biodegradable fiber composites.* Journal of Polymers and the Environment, 2000. 8(2): p. 91-96.

51. K.Oksman, M.Skrifvars, and J.F.Selin, *Natural fibres as reinforcement in polylactic acid (PLA) composites.* Composites Science and Technology, 2003. 63: p. 1317-1324.

52. R.D.Leaversuch, Modern Plastics, 2000. 77(12): p. 56-60.

53. A.R.Sanadi, D.F.Caulfield, and R.E.Jacobson, *Agro-fibre thermoplastic composites; Paper and composites from agro-based resources*. 1997: Lewis Publishers. 377-401.

54. Albuquerque, A.C.D., et al., Composite Science and Technology, 2000. 60(6): p. 833-844.

55. N.A.Miller, C.D.Stirling, and V.S.M.V. Tilburg, Polymer and Polymer Composites, 1995. 3(2): p. 117-126.

56. O.A.Khondker, et al., *A novel processing technique for thermoplastic manufacturing of unidirectional composites reinforced with jute yarns.* Composites: Part A, 2006. 37: p. 2274-2284.

57. R.M.Rowell, R.A.Young, and J.K.Rowell, *Paper and composites from agro-based resources*. 1997: Lewis Publishers, CRC Press.

58. P.V.Joseph, J.Kuruvilla, and S.Thomas, Composite Science and Technology, 1999. 59(11): p. 1625-1640.

59. J.Gassan and A.K.Bledzki, Die Angew Makromolekulare Chemie, 1996. 236: p. 129-138.

60. G.B.Nando and B.R.Gupta, *Short-fibre thermoplastic elastomer composites*. Short Fibre Polymer Composites, ed. J.R.White. 1996, Cambridge: Woodland Publishing.

61. T.Nishino, K.Hirao, and M.Kotera, Composites Part A: Applied Science and Manufacturing, 2006. 37(12): p. 2269-2273.

62. S.Y.Fu, et al., Composites: Part A, 2000. 31: p. 1117-1125.

63. K.Rekab and M.Shaikh, *Statistical design of experiments with engineering applications*. Statistics: A Series of Textbooks and Monographs. 2005: Chapman & Hall/CRC, Taylor & Francis Group

64. A.B.Thomsen, et al., *Effects of chemical-physical pre-treatment processes on hemp fibres.* Bioresource Hemp (www.nova-institut.de), 2000: p. 1-6.

65. R.M.Rowell, *Performance driven composites from lignocellulosic resources",* . Proceedings of International Conference on Science and Technology of Composite Materials (COMAT 2001), 2001.

66. Gassan, J. and A.K. Bledzki, *Alkali treatment of jute fibers: relationship between structure and mechanical properties.* Journal of Applied Polymer Science, 1999. 71: p. 623-629.

67. J.Gassan and A.K.Bledzki, *Alkali treatment of jute fibers: relationship between structure and mechanical properties.* Journal of Applied Polymer Science, 1999. 71: p. 623-629.

68. J.Gassan and A.K.Bledzki, *Possibilities for improving the mechanical properties of jute/epoxy composites by alkali treatment of fibres.* Composites Science and Technology, 1999. 59: p. 1303-1309.

69. S.V.Prasad, C.Pavithran, and P.K.Rohatgi, *Alkali treatment of coir fibres for coir-polyester composites.* Journal of Material Science, 1983. 18: p. 1443-1454.

70. H.P.S.A.Khalil, et al., *The effect of various anhydride modifications on mechanical properties and water absorption of oil palm empty fruit*

bunches reinforced polyester composites. Polymer International, 2001. 50: p. 395-402.

71. A.K.Bledzki, S.Reihmane, and J.Gassan, *Properties and modification methods for vegetable fibers for natural fiber composites.* Journal of Applied Polymer Science, 1996. 59: p. 1329-1336.

72. R.N.Mukherjee, S.K.Pal, and S.K.Sanyal, Journal of Applied Polymer Science, 1983. 28: p. 3029.

73. P.Zadorecki and P.J.Flodin, Journal of Applied Polymer Science, 1985. 3: p. 3971.

74. D.Ray, et al., *Thermal behavior of vinyl ester resin matrix composites reinforced with alkali-treated jute fibers.* Journal of Applied Polymer Science, 2004. 94: p. 123-129.

75. A.K.Bledzki, H.P.Fink, and K.Specht, *Unidirectional hemp and flax EP- and PP-composites: Influence of defined fibre treatment.* Journal of Applied Polymer Science, 2004. 93: p. 2150-2156.

76. H.M.Wang and R.Postle, *Removing pectin and lignin during chemical processing of hemp for textile applications.* Textile Research Journal, 2003. 73(8): p. 664-669.

77. V.Geethamma, R.Joseph, and S.Thomas, *Short Coir-Fibre Reinforced Natural Rubber Composites: Effects of Fibre Length, Orientation and Alkali Treatment.* Journal of Applied Polymer Science, 1995. 55: p. 583-594.

78. *www.tappiphils.com/about_pulp_and_paper.asp.*

79. W.Mendenhall, *Introduction to Linear Models and the Design and Analysis of Experiments*. 1968, Belmont, California: Duxbury Press, A Division of Wadsworth Publishing Company, Inc.

80. J.C.F.Walker, *Wood chemistry and cell wall ultra structure in primary wood processing*. 1993, London: Chapman and Hall. 44-45.

81. L.Y.Mwaikambo and M.P.Ansell, *Hemp fibre reinforced cashew nut shell liquid composites.* Composites Science and Technology, 2003. 63: p. 1297-1305.

82. J.Z.Lu, Q.Wu, and H.S.McNabb, *Chemical coupling in wood fiber and polymer composites: A review of coupling agents and treatments.* Wood and Fiber Science, 2000. 32(1): p. 88-104.

83. R.M.Rowell, Wood Science 1992. 15(2): p. 172-182.

84. C.A.S.Hill and H.P.S.A. Khalil, *Effect of fiber treatments on mechanical properties of coir or oil palm fiber reinforced polyester composites.* Journal of Applied Polymer Science, 2000. 78: p. 1685-1697.

85. Rong, M.Z., et al., *The effect of fiber treatment on the mechanical properties of unidirectional sisal-reinforced epoxy composites.* Composites Science and Technology, 2001. 61: p. 1437-1447.

86. M.Z.Rong, et al., *The effect of fiber treatment on the mechanical properties of unidirectional sisal-reinforced epoxy composites.* Composites Science and Technology, 2001. 61: p. 1437-1447.

87. M.C.Matias, et al., Journal of Applied Polymer Science, 1999. 75: p. 256-266.

88. Y.Li, Y.Mai, and L.Ye, *Effects of fibre surface treatment on fracture-mechanical properties of sisal-fibre composites.* Composite Interfaces, 2005. 12(1-2): p. 141-163.

89. E.Mader and K.Gliesche. *Langfaserverstarkte Kunststoffe auf der Basis von Naturfasern*. in *7th International Techtextil-Symposium*. 1995. Frankfurt, Germany.

90. G.Desarmot and J.P.Favre, *Advances in pull-out testing and data analysis.* Composites Science and Technology, 1991. 42: p. 151-187.

91. M.R.Piggott, *Why the fibre/polymer interface can appear to be stronger than the polymer matrix.* Composites Science and Technology, 1997. 57: p. 853-857.

92. Y.Diamant, G.Marom, and L.J.Broutman, *The effect of network structure on moisture absorptionof epoxy resins* Journal of Applied Polymer Science, 1981. 26: p. 3015-3025.

93. B.Miller, P.Muri, and L.Rebenfeld, Composite Science and Technology, 1987. 28: p. 17-32.

94. M.R.Piggott and Y.X.Xiong, Composite Science and Technology, 1994. 52: p. 535.

95. A.Kelly and W.R.Tyson, J. Mech. Phys. Solids, 1965. 12: p. 329.

96. L.T.Drzal, P.J.Herrera-Franco, and H.Ho, *Fiber-Matrix Interface Tests*. Comprehensive Composite Materials, ed. A.Kelly and C.Zweben. Vol. 5. 2000, Oxford: Elsevier Science Ltd.

97. A.Stamboulis, C.Baillie, and E.Schulz, *Interfacial chracterization of flax fibre-thermoplastic polymer composites by the pull-out test.* Die Angewandte Makromolekulare Chemie, 1999. 272(4759): p. 117-120.

98. E.Schulz, G.Kalinka, and W.Auersch, J.Macromol.Sci.-Phys., 1996. B35: p. 527.

99. C.Wang, *Fracture mechanics of single-fibre pull-out test.* Journal of Materials Science, 1997. 32: p. 483-490.

100. E.Mader, *Study of fibre surface treatments for control of interphase properties in composites.* Composites Science and Technology, 1997. 57: p. 1077-1088.

101. E.Pisanova, et al., *Three techniques of interfacial bond strength estimation from direct observation of crack initiation and propagation in polymer-fibre system.* Composites: Part A, 2001. 32: p. 435-443.

102. P.J.Herrera-Franco and A.Valadez-Gonzalez, *A study of the mechanical properties of short natural-fiber reinforced composites.* Composites: Part B, 2005. 36: p. 597-608.

103. A.Arbelaiz, et al., *Flax fiber surface modifications: effect on fiber physico mechanical and flax/polypropylene interface properties.* Polymer Composites (www.interscience.wiley.com), 2005: p. 324-332.

104. R.G.C.Arridge and J.H.Speake, Polymer, 1972. 13: p. 443.

105. J.M.Charlesworth, Polymer Engineering and Science, 1988. 28: p. 221.

106. H.Stutz and J.Mertes, Journal of Polymer Science Part A: Polymer Chemistry Edition, 1993. 31: p. 2031.

107. P.Schlack, U.S.P. 2, Editor. 1938. p. 928.

108. S.Hwang and G.Lee, *Short communication: The curing and decomposition kinetics for diglycidylether of bisphenol-A/di(4-aminobenzanilide)ether system.* European Polymer Journal, 2000. 36: p. 2305-2308.

109. X.Wang and Q.Zhang, *Synthesis, chracterization, and cure properties of phosphorus-containing epoxy resins for flame retardance.* European Polymer Journal, 2004. 40: p. 385-395.

110. Y.Liang, et al., *Cure kinetics of DGEBA with hyperbranched poly(3-hydroxyphenyl) phosphate as curing agent studied by non-isothermal DSC.* Chem. Res. Chinese U., 2006. 22(1): p. 118-122.

111. A.Catalani and M.G.Bonicelli, *Kinetics of the curing reaction of a diglycidyl ether of bisphenol A with a modified polyamine.* Thermochimica Acta, 2005. 438: p. 126-129.

112. H.E.Kissinger, *Reaction kinetics in differential thermal analysis.* Analytical Chemistry, 1957. 29(11): p. 1702-1706.

113. S.Moteserrat and J.Malek, Thermochimica Acta, 1993. 228: p. 47.

114. J.H.Flynn and L.A.Wall, Journal of Applied Polymer Science, Part B, 1966. 4: p. 323.

115. O.A.Ozawa, Journal of Thermal Analysis, 1970. 2: p. 301.

116. R.B.Prime, Polymer Engineering and Science, 1973. 13: p. 365.

117. M.C.Lu and J.L.Hong, Polymer, 1994. 35: p. 2822.

118. C.D.Doyle, Nature, 1965. 207: p. 290.

119. M.R.Kamal, Polymer Engineering and Science, 1974. 14: p. 23.

120. F.Y.C.Boey and W.Qiang, *Experimental modeling of the cure kinetics of an epoxy-hexaanhydro-4-methylphthalicanhydride (MHHPA) system.* Polymer, 2000. 41: p. 2081-2094.

121. K.Horie, et al., Journal of Applied Polymer Science:Polymer Chemistry, 1970. 8: p. 1357.

122. O.A.Ozawa, Bull Chemical Society Japan, 1965. 38: p. 1881.

123. S.S.Bafna and D.G.Baird, Soc Plast Eng Tech Paper, 1991. 32: p. 255.

124. D.Hull and T.W.Clyne, *An introduction to composite materials*. 2nd ed. 1996, UK: Cambridge University Press.

125. B.D.Agarwal and L.J.Broutman, *Analysis and performance of fibre composites*. 1980, New York: John Wiley and Sons Inc.

126. K.K.Chawla, *Composite materials, science and engineering*. 1987, New York: Springer-Verlag. 177.

127. A.R.Sanadi, et al., Journal of Reinforced Plastics and Composites, 1994. 13: p. 54-67.

128. T.Peijs, et al. in *Proceedings of the European Conference on Composite Materials: Science, Technologies and Applications, ECCM-8*. 1998: Woodhead Publishing.

129. R.M.Rowell. *Research in industrial application on non-food crops, I. Plant fibres*. in *Proceedings of a seminar*. 1995. Copenhagen, Denmark.

130. J.Gassan and A.K.Bledzki, *Effect of moisture content on the properties of silanized jute-epoxy composites.* Polymer Composites, 1997. 18(2): p. 179-184.

131. H.Hatakeyema, T.Hatakeyema, and K.J.Nakamura. in *Applied Polymer Science: Applied Polymer Symposium*. 1983.

132. D.Maldas, et al., Polymer, 1988. 29: p. 1255.

133. P.Zadorecki and P.Flodin, Journal of Applied Polymer Science, 1986. 31: p. 1699.

134. C.P.L.Chow, X.S.Xing, and R.K.Y.Li, Composites Science and Technology, 2007. 67: p. 306-313.

135. M.M.Thwe and K.Liao, Composite Science and Technology, 2003. 63: p. 375-387.

136. X.Lu, et al., Composite Science and Technology, 2004. 64: p. 1301-1310.

137. C.Clemons, J Forest Prod, 2002. 52(6): p. 10-18.

138. J.Morton, J.Quarmley, and L.Rossi. *Natural and wood fiber composites in North America and Europe*. in *7th International Conference on woodfiber-plastic composites*.

139. R.M.Rowell, *Wood and Cellulose Chemistry*, ed. D.N.S.Hon and N.Shiraishi. 1991, New York: Marcel Dekker. 703-756.

140. A.G.Andreopoulos and P.A.Tarantili, Journal of Applied Polymer Science, 1988. 70: p. 747-755.

141. G.S.Springer, *Environmental effects on composite materials.* Technomic, 1981/1984/1988. 1-3.

142. Q.Lin, X.Zhou, and G.Dai, Journal of Applied Polymer Science, 2002. 85(14): p. 2824-2832.

143. J.Comyn, *Polymer Permeability*. 1985. 383.

144. A.C.Loos and G.S.Springer, *Moisture absorption of polyester to glass composites*. Environmental effects on composite materials, ed. G.S.Springer. 1981, Westport (CT): Technomic Publishing. 51-62.

145. J.J.Crank and G.S.Park, *Organic vapours above the glass transition temperature*. Diffusion in polymers. 1968, London: Academic Press. 74.

146. J.Crank, The Mathematics of Diffusion, 1956: p. 347.

147. R.Martin and R.Campion, Materials World, 1996. 4(4): p. 200-02.

148. C.W.Dence, *The determination of lignin*. Methods in lignin chemistry, ed. S.Y.Lin and C.W.Dence. 1992: Springer-Verlag. 33-62.

149. S.Harper, Composites 1982. 13: p. 123-138.

150. M.N.Anglesa, et al., Biomass and Bioenergy, 2001. 21: p. 211-224.

151. D.N.S.Hon, *Weathering and photochemistry of wood*. 2nd ed. Wood and cellulosic chemistry. 2000, New York: Marcel Dekker. 512-546.

152. W.Beckert and B.Lauke, *Critical discussion of the single-fibre pull-out test: does it measure adhesion?* Composites Science and Technology, 1997. 57: p. 1689-1706.

153. J.Schmidt, F.Kimura, and D.G.Gray, Res. Chem. Intermed, 1995. 21: p. 287-301.

154. D.S.Argyropoulus, C.Heitner, and J.A.Schmidt, Res. Chem. Intermed, 1995. 9: p. 263-274.

155. N.Nakayama and T.Hayashi, Polymer Degradation and Stability, 2007. 92: p. 1255-1264.

156. B.Mailhot, et al., Macromolecular Chemistry and Physics, 2005. 206: p. 575-584.

157. F.M.Marabella, Journal of Polymer Science, 1983. 7: p. 2403.

158. V.Bellenger and J.Verdu, Journal of Applied Polymer Science, 1983. 28: p. 2677.

159. N.M.Stark. *Changes in wood flour/HDPE composites after accelerated weathering with and without water spray*. in *2nd Wood Fibre Polymer Composites Symposium Applications and Perspectives*. March 24-25, 2005. Cite' Mondiale-Bordeaux-France.

160. N.M.Stark and L.M.Matuana, Polymer Degradation and Stability, 2004. 86: p. 1-9.

161. N.M.Stark and L.M.Matuana, Journal of Applied Polymer Science, 2003. 90(10): p. 2609-2617.

162. L.M.Matuana, D.P.Kamdem, and J.Zhang, Journal of Applied Polymer Science, 2001. 80(11): p. 1943-1950.

163. M.Kiguchi and P.D.Evans, Polymer Degradation and Stability, 1998. 61: p. 33-45.

164. L.M.Matuana and D.P.Kamdem, Polymer Engineering Science, 2002. 42(8): p. 1657-1666.

165. U.Muller, et al., Journal of Photochemistry and Photobiology B: Biology, 2003. 69: p. 97-105.

166. L.E.Alexander, *X-ray diffraction methods in polymer science*. 1969, New York: Wiley. 137-197.

167. F.J.Balta-Calleja and C.G.Vonk, *X-ray scattering of synthetic polymers*. 1989, Amsterdam: Elsevier. 175-204.

168. R.Teeaar, R.Serimaa, and T.Paakkari, Polym Bull, 1987. 17: p. 231-237.

169. S.Andersson, et al., *Crystallinity of wood and the size of cellulose crystallites in Norway spruce (Picea abies)*. Journal of Wood Science, 2003. 49: p. 531-537.

170. N.Stubicar, et al., Holzforschung, 1998. 52: p. 455-458.

171. Mwaikambo, L.Y. and M.P. Ansell, *Chemical modification of hemp, sisal, jute, and kapok fibers by alkalization.* Journal of Applied Polymer Science, 2002. 84: p. 2222-2234.

172. *www.wcaslab.com/tech/tbftir.htm*.

173. R.T.O'connor, E.F.Dupre, and E.H.McCall, Analytical Chemistry, 1957. 29: p. 908.

174. M.L.Nelson and R.T.O'connor, Journal of Applied Polymer Science, 1964. 8: p. 1311.

175. J.Blackwell, P.D.Vasko, and J.L.Koening, Journal of Applied Physics, 1970. 11: p. 4375.

176. Sahoo, P.K., et al., *Characterization and properties of chemically modified Corchorus capsularis jute fiber via pulping and grafting: Infrared, thermogravimetric analysis, differential scanning calorimetry, scanning electron microscopy, X-ray diffraction, biodegradation, and superabsorbency.* Journal of Polymer Science: Part A: Polymer Chemistry, 2003. 41: p. 2696-2703.

177. D.Ray and B.K.Sarkar, *Characterization of alkali-treated jute fibers for physical and mechanical properties.* Journal of Applied Polymer Science, 2001. 80: p. 1013-1020.

178. S.Wong, R.Shanks, and A.Hodzic, *Interfacial improvements in poly(3-hydroxybutyrate)-flax fibre composites with hydrogen bonding additives.* Composites Science and Technology, 2004. 64: p. 1321-1330.

179. R.J.Hunter, *Zeta potential in colloid science: Principles and applications*. 1981, New York: Academic Press.

180. R.J.Hunter, *Foundations of colloid science*. Vol. 1. 1986, Oxford: Clarendom Press.

181. R.J.Hunter, *Foundations of colloid science*. Vol. II. 1989, Oxford: Clarendom Press.

182. J.A.Clark, *Pulp technology and treatment for paper*. 1985, San Francisco: Miller Freeman and Publications, INC.

183. C.Werner and H.J.Jacobasch, Journal of Biomaterials Science and Polymer, 1995. 7: p. 1.

184. H.J.Jacobasch, Colloid and Polymer Science, 1988. 3: p. 263.

185. H.J.Jacobasch and I.Grosse, Textiltechnik, 1987. 37: p. 5.

186. K.Stana-Kleinschek and V.Ribitsch, *Electrokinetic properties of processed cellulose fibers.* Colloids and Surfaces A: Physicochemical and Engineering Aspects, 1998. 140: p. 127-138.

187. Aranberri-Askargorta, I., T. Lampke, and A. Bismarck, *Wetting behavior of flax fibers as reinforcement for polypropylene.* Journal of Colloid and Interface Science, 2003. 263: p. 580-589.

188. A.Bismarck, et al., *Surface characterization of flax, hemp and cellulose fibres; surface properties and the water uptake behavior.* polymer Composites, 2002. 23(5): p. 872-894.

189. L.A.Pothan and S.Thomas, *Polarity parameters and dynamic mechanical behaviour of chemically modified banana fiber reinforced polyester composites.* Composites Science and Technology, 2003. 63: p. 1231-1240.

190. H.S.Sharifah and M.P.Ansell, Composites Science and Technology, 2004. 64: p. 1219-1230.

191. P.V.Joseph, et al., *The thermal and crystallization studies of short sisal fibre reinforced polypropylene composites.* Composites: Part A: Applied Science and Manufacturing, 2003. 34: p. 253-266.

192. D.F.Arseneau. *A differential thermal analysis study of fire retardants in cellulose*. in *Wood Chem. Symp.* 1963. Toronto.

193. W.K.Tang and H.W.Eickner, *Effect of inorganic salts on pyrolysis of wood, cellulose, and lignin determined by differential thermal analysis.* U.S. For. Serv. Res. Paper FPL, 1968. 82: p. 30.

194. A.K.Rana, et al., Journal of Applied Polymer Science, 1997. 64: p. 1517-1523.

195. Mathew, A.P., K. Oksman, and M. Sain, *The effect of morphology and chemical characteristics of cellulose reinforcements on the crystallinity of polylactic acid.* Journal of Applied Polymer Science, 2006. 101: p. 300-310.

196. B.Park, et al., *Differential scanning calorimetry of phenol-formaldehyde resins cure-accelerated by carbonates.* Polymer, 1999. 40: p. 1689-1699.

197. L.Segal, et al., Textile Research Journal, 1959. 29: p. 786.

198. L.Y.Mwaikambo and M.P.Ansell, *Chemical modification of hemp, sisal, jute, and kapok fibers by alkalization.* Journal of Applied Polymer Science, 2002. 84: p. 2222-2234.

199. S.R.Schmidt and R.G.Launsby, *Understanding Industrial Designed Experiments*. Blending the best of the best Designed Experiment Technique. 1992, Colorado: Air Academy Press, Colorado.

200. S.Akhnazarova and V.Kafarov, *Experiment Optimization in Chemistry and Chemical Engineering*. 1982, Moscow and Chicago: Mir. Publishers.

201. D.C.Montgomery, *Design and Analysis of Experiments*. 2nd edition ed. Vol. 2nd edition. 1984: Wiley Interscience.

202. G.A.Milliken and D.E.Johnson, *Analysis of Messy Data*. Designed Experiments. Vol. 1. 1992: Chapman & Hall.

203. D.G.Hepworth, et al., *The manufacture and mechanical testing of thermosetting natural fibre composites.* Journal of Materials Science, 2000. 35: p. 293-298.

204. Oksman, K., et al., *Morphology and mechanical properties of unidirectional sisal-epoxy composites.* Journal of Applied Polymer Science, 2002. 84: p. 2358-2365.

205. K.S.Kleinschek and V.Ribitsch, *Electrokinetic properties of processed cellulose fibre.* Colloids and Surfaces A: Physicochemical and Engineering Aspects, 1998. 140: p. 127-138.

206. *JCPDS-International Centre for Diffraction Data.* 2003. 2.4.

207. V.Tserki, et al., *A study of the effect of acetylation and propionylation surface treatments on natural fibres.* Composites: Part A, 2005. 36: p. 1110-1118.

208. J.B.Dahiya and S.Rana, *Thermal degradation and morphological studies on cotton cellulose modified with various arylphosphorodichloridites.* Polymer International, 2004. 53: p. 995-1002.

209. D.Ray, et al., *Study of the thermal behavior of alkali-treated jute fibers.* Journal of Applied Polymer Science, 2002. 85: p. 2594-2599.

210. A.Broido, Journal of Polymer Science, 1969. A-2, 7: p. 1762.

211. B.Wielage, et al., Thermochimica Acta, 1999. 337: p. 169-177.

212. H.Stang and S.P.Shah, *Failure of fibre-reinforced composites by pull-out fracture.* Journal of Materials Science, 1986. 21: p. 953-957.

213. H.M.Chang, et al., Holzforschung, 1975. 29: p. 153.

214. W.Kemp, *Organic Spectroscopy*. 2nd ed. 1989, Hong Kong: Macmillan.

215. B.Schrader, *Infrared and Raman Spectroscopy*. 1995, Weinheim: VCH.

216. R.M.Silverstein and F.X.Webster, *Spectrometric Identification of Organic Compounds*. 6th ed. 1998, New York: Wiley.

217. M.S.Sreekala, M.G.Kumaran, and S.Thomas, *Oil palm fibres: morphology, chemical composition, surface modification, and mechanical properties.* Journal of Applied Polymer Science, 1997. 66: p. 821-835.

218. Y.Shih, Materials Science and Engineering A, 2007. 445-446: p. 289-295.

219. L.Britcher, et al., Macromolecules, 1995. 28: p. 3110-3118.

220. A.K.Patrikis, M.C.Andrews, and R.J.Young, *Analysis of the single-fibre pull-out test by the use of raman spectrocopy. Part I: Pull-out of aramid fibres from an epoxy resin.* Composites Science and Technology, 1994. 52: p. 387-396.

221. M.Naffakh, et al., Journal of Applied Polymer Science, 2005. 96: p. 660.

222. R.J.Varley, et al., Polymer, 2000. 41: p. 3425.

223. J.Lopez, et al., *Effect of poly(styrene-co-acrylonitrile) on the curing of an epoxy-amine resin.* Polymer, 2001. 42: p. 1669-1677.

224. M.Ghaemy, M.Barghamadi, and H.Behmadi, *Cure kinetics of epoxy resin and aromatic diamines.* Journal of Applied Polymer Science, 2004. 94: p. 1049-1056.

225. L.Barral, et al., *Kinetic studies of the effect of ABS on the curing of an epoxy/cycloaliphatic amine resin.* Journal of Polymer Science: Part B: Polymer Physics, 2000. 38: p. 351-361.

226. J.M.Salla and X.Ramis, Polymer Engineering and Science, 1996. 36: p. 835.

227. J.Mijovic, J.Kim, and J.Slaby, Journal of Applied Polymer Science, 1984. 29: p. 1449.

228. J.M.Kenny, Journal of Applied Polymer Science, 1994. 51: p. 761.

229. B.Francis, et al., *Cure kinetics, morphological and dynamic mechanical analysis of diglycidyl ether of bisphenol-A epoxy resin modified with hydroxyl terminated poly(ether ether ketone) containing pendent tertiary butyl groups.* Polymer, 2006. 47: p. 5411-5419.

230. K.Tanaka, et al., *Characterization of the aramid/epoxy interfacial properties by means of pull-out test and influence of water absorption.* Composites Science and Technology, 2002. 62: p. 2169-2177.

231. A.Valadez-Gonzalez, et al., *Effect of fiber surface treatment on the fiber-matrix bond strength of natural fiber reinforced composites.* Composites: Part B, 1999. 30: p. 309-320.

232. A.Kelly, *Strong Solids*. 1973, Oxford: Clarendon Press.

233. D.G.Hepworth, et al., *Short communication: The use of unretted hemp fibre in composite manufacture.* Composites: Part A, 2000. 31: p. 1279-1283.

234. A.Maffezzoli, et al., *Cardanol based matrix biocomposites reinforced with natural fibres.* Composites Science and Technology, 2004. 64: p. 839-845.

235. A.R.Sanadi, S.V.Prasad, and P.K.Rohatgi, Journal of Materials Science 1986. 21: p. 4299.

236. S.K.Pal, D.Mukhopadhyay, and S.K.Sanyal, *Studies on process variables for natural fiber composites-- Effect of polyesteramide polyol as interfacial agent.* Journal of Applied Polymer Science, 1988. 35: p. 973-985.

237. M.Gao, K.Zhu, and Y.J.Sun, Journal of Fire Sciences, 2004. 22: p. 505-515.

238. A.S.Gozdz and H.D.Weigmann, Journal of Applied Polymer Science, 1984. 29: p. 3965.

239. P.V.Joseph, et al., *Mechanical properties of short sisal fiber-reinforced polypropylene composites: comparison of experimental data with theoretical predictions.* Journal of Applied Polymer Science, 2003. 88: p. 602-611.

240. B.A.Acha, N.E.Marcovich, and M.M.Reboredo, *Physical and mechanical characterization of jute fabric composites.* Journal of Applied Polymer Science, 2005. 98: p. 639-650.

241. Yan, L., *The investigation of fracture properties of sisal textile reinforced polymers.* Acta Mechanica Solida Sinica, 2004. 17(2): p. 95-103.

242. J.Zhou and J.P.Lucas, Composite Science and Technology, 1995. 53: p. 57-64.

243. J.M.Felix and P.J.Gatenholm, Journal of Applied Polymer Science, 1991. 42: p. 609.

244. A.K.Bledzki, S.Reihmane, and J.Gassan, *Properties and modification methods for vegetable fibres for natural fibre composites.* Journal of Applied Polymer Science, 1996. 59: p. 1329-1336.

245. J.B.Enns and J.K.Gillham, *Effect of extent of cure on the modulus, glass transition, water absorption, and density of an amine-cured epoxy.* Journal of Applied Polymer Science, 1983. 28: p. 2831-2846.

246. M.Z.Rong, et al. *Effect of fibre pretreatment on the impact fracture toughness of sisal fibre reinforced polymer composites*. in *First Asian-Australian Conference on Composite Materials (ACCM-I)*. 7-9 October 1998. Osaka, Japan.

247. B.Singh, M.Gupta, and A.Verma, Composites Science and Technology, 2000. 60: p. 581-589.

248. A.Blaga and R.S.Yamasaki, Journal of Materials Science, 1973. 8: p. 654.

249. A.Devis and D.Sims, *Weathering of plastics*. 1983, UK: Applied Science Publishers.

250. C.Heitner, *Light induced yellowing of wood containing papers*. Photochemistry of lignocellulosic materials, ACS symposium series, 531. 1993: American Chemical Society. 3-25.

251. Y.Chen, et al., Composite Structures, 2007. 78: p. 101-111.

252. B.F.Abu-Sharkh and H.Hamid, Polymer Degradation and Stability, 2004. 85: p. 967-973.

253. K.K.Pandey and N.Chandrashekar, Journal of Applied Polymer Science, 2006. 99: p. 2367-2374.

254. K.K.Pandey, Journal of Applied Polymer Science, 1999. 71: p. 1969.

255. K.J.Harrington, H.G.Higgins, and A.J.Michell, Holzforschung, 1964. 18: p. 108.

256. A.Rivaton, L.Moreau, and J.L.Gardette, Polymer Degradation and Stability, 1997. 58: p. 321.

257. V.E.Reinsch and S.S.Kelley, Journal of Applied Polymer Science, 1997. 64: p. 1785.

258. R.Vasanthakumari and A.Pennings, Polymer, 1983. 24: p. 175.

259. J.Y.Nam, S.S.Ray, and M.Okamoto, Macromolecules, 2003. 36: p. 7126.

260. Meretz, S., et al., Journal of Matrials Science Letters, 1992. 11: p. 1471-1472.

261. D.Preechawong, et al., *Preparation and characterization of starch/poly(L-lactic acid) hybrid foams* Carbohydrate Polymers 2005. 59(3): p. 329-337

262. Steendam, R., et al., *Effect of molecular weight and glass transition on relaxation and release behaviour of poly(-lactic acid) tablets* Journal of Controlled Release 2001. 70(1-2): p. 71-82.

263. W.Park, J., et al., Korea Polym J, 1999. 7: p. 93.

264. M.Pyda, R.C.Bopp, and B.Wunderlich, *Heat capacity of poly(lactic acid)*. J.Chem.Thermodynamics, 2004. 36: p. 731-742.

265. N.Ljungberg and B.Wesslen, Biomacromolecules, 2005. 6: p. 1789-1796.

266. A.J.Nijenhuis, et al., 1996. 37: p. 5849.

267. C.S.Proikakis, et al., Polymer Degradation and Stability, 2006. 91: p. 614-619.

268. X.Zhang, M.Espiritu, A.Bilyk, and L.Kurniwan, *Morphological behavior of poly(lactic acid) during hydrolytic degradation.* Polymer Degradation and Stability, 2008. 93(10): p. 1964-1970.

269. A.Copinet, et al., Journal of Polymers and the Environment, 2003. 11(4): p. 169-179.

270. G.W.Beckermann, K.L.Pickering, and N.J.Foreman. *The processing, production and improvement of hemp-fibre reinforced polypropylene composite materials*. in *Proceedings of 2nd international conference on structure, processing and properties of materials (SPPM 2004)*. 2004.

Appendices

Publication List of this Work

Journal Paper

Influence of alkali treatment on the interfacial bond strength of industrial hemp fibre reinforced epoxy composites: Effect of variation from the ideal stoicheometric ratio of epoxy resin to curing agent

M.S. Islam and K.L. Pickering

Department of Materials and Process Engineering, The University of Waikato, Private Bag 3105, Hamilton, New Zealand

(Published in Advanced Materials Research Vols. 29-30 (2007) pp 319-322)

Conference Paper

(1) The Effect of Fibre Treatment Using Alkali on Industrial Hemp Fibre/Epoxy Resin Composites

M.S. Islam[1], K.L. Pickering[1], G.W. Beckermann[1] and N.J. Foreman[2]

[1]Department of Materials and Process Engineering, The University of Waikato, Private Bag 3105, Hamilton, New Zealand

[2]Managing Director, Hemptech,

PO Box 46033, Herne Bay, Auckland, New Zealand

(Published in the Proceedings of the International Conference on Mechanical Engineering 2005 (ICME2005), 28-30 December 2005, Dhaka, Bangladesh)

(2) Influence of alkali treatment on the interfacial bond strength of industrial hemp fibre reinforced epoxy composites: Effect of variation from the ideal stoicheometric ratio of epoxy resin to curing agent

M.S. Islam and K.L. Pickering

Department of Materials and Process Engineering, The University of Waikato, Private Bag 3105, Hamilton, New Zealand

(Published in the Proceedings of The 4th International Conference on Advanced Materials & Processing (ICAMP-4), December 10-13, 2006, Hamilton, New Zealand)

(3) Evaluation of IFSS and mechanical properties of hemp/PLA composites.

M. S. Islam[1], K. L. Pickering[1] and N. J. Foreman[2]

[1]Department of Materials and Process Engineering, The University of Waikato, Private Bag 3105, Hamilton, New Zealand

[2]Managing Director, Hemptech,

PO Box 46033, Herne Bay, Auckland, New Zealand

(Published in the Proceedings of International Conference on Natural Polymers, Bio-Polymers, Bio-Materials, their Composites, Blends, IPNs, and Gels: Macro to Nano Scales (ICNP - 2007), November 19-21, 2007), Kottayam, Kerala, India).

Glossary of acronyms and Symbols

Acronyms	
ANOVA	Analysis of Variance
ASTM	American Society for Testing and Materials
ATFE	Alkali Treated Fibre/Epoxy
ATLFE	Alkali Treated Long Fibe/Epoxy
ATPLA	Alkali Treated Fibre Polylactic Acid
ATSFE	Alkali Treated Sort Fibe/Epoxy
CNC	Computer Numerical Control
DCM	Dichloromethane
DGEBA	Diglycidyl Ether of Bisphenol-A
DSC	Differential Scanning Calorimetry
DSF	Dynamic Sheet Formingl
DTA	Differential Thermal Analysis
FS	Failure Strain (%)
FTIR	Fourier Transform Infrared
HEC	Hemp/Epoxy Composite
HPC	Hemp/PLA Composite
IEP	Iso-electric Point
IFSS	Interfacial Shear Strength (MPa)
IE	Impact Energy (kJ/mol)
ISO	International Standard Organization
MAPP	Maleated Polypropylene
MROM	Modified Rule of Mixtures
PHB	Polyhydroxy Butyrate

PE	Polyethylene
PLA	Polylactic Acid
PMC	Polymer Matrix Composite
PP	Polypropylene
PVA	Polyvinyl Acetate
ROM	Rule of Mixtures
SEM	Scanning Electron Microscopy
SENB	Single-Edge-Notch Bending
SFTT	Single Fibre Tensile Testing
STD	Standard Deviation
THC	Delta-9-tetrahydrocannabinol
TGA	Thermogravimetric Analysis
TS	Tensile Strength (MPa)
UFPLA	Untreated Fibre Polylactic Acid
UTFE	Untreated Fibre/Epoxy
UTLFE	Untreated Long Fibe/Epoxy
UTSFE	Untreated Short Fibe/Epoxy
UV	Ultra-violet
WAXRD	Wide Angle X-ray Diffraction
YM	Young's Modulus (GPa)

Symbols		**Units**
A	Pre-exponential Factor	
CO_2	Carbon Dioxide	
CrI	Crystallinity Index	(%)
$-COCH_3$	Acetyl	
C=O	Carbony	
-COOH	Carboxyl	
D	Diffusion Coefficient	(m^2/s)
E_a	Activation Energy	(kJ/mol)
F_{max}	Maximum Debonding Force	(N)
HCL	Hydrochloric Acid	
KBr	Potassium Bromide	

KCL	Potassium Chloride	
KOH	Potassium Hydroxide	
K_1	Orientation Factor	
K_2	Factor Dependent on the Stress Transfer Between the Matrix and the Fibres	
K_{Ic}	Fracture Toughness	(MPa.m$^{1/2)}$
L	Thickness of the Sample	(mm)
M_c	TS or YM of the Composite	(MPa) or (GPa)
M_f	TS or YM of the Fibre	(MPa) or (GPa)
M_m^*	Tensile Contribution of the Matrix at the FS of the Fibres or the YM of the Matrix	(MPa)
M_p	Mass of the Sample	g
M_t	Moisture Content at Time t;	(%)
M_∞	Moisture Content at the Equilibrium	(%)
NaOH	Sodium Hydroxide	
Na_2SO_3	Sodium Sulphite	
NFC	Natural Fibre Composite	
-OH	Hydroxyl	
R	Gas Constant	(kJ/mol.K)
T	Absolute Temperature	(K)
T_m	Exothermic Peak Temperature	(K)
V	Volume Fraction	
V_m	Volume Fraction of Matrix	
V_f	Volume Fraction of fibre	
$f(\alpha)$	Kinetic Model Function that Depends on the Conversion	
$g(\alpha)$	Integrated Form of the Conversion Dependence Function	

$k(T)$	Reaction Rate Constant	
k'	Specific Reaction Rate Constant	
l	Fibre Embedded Length	(m)
m	Reaction Order	
n	Reaction Order	
p	A Function Defined by Doyle	
q	Constant Heating Rate	(K/min)
r	Radius	(m)
t	Time	(min)
ΔH	Enthalpy of the Curing Reaction	(J/g)
(ΔH_t)	Heat Evolved at Time, t	(J/g)
ΔH_m	Heat of Melting	(J/g)
(ΔH_{tot})	Total Heat of Reaction	(J/g)
α	Degree of Conversion	
α_t	Conversion at Time, t	
φ	Rate of Heat Flow	(^oC/min)
ρ	Density	(Kg/m^3)
σ_m^*	TS of the Polymer Matrix at the FS of the Fibre	(MPa)
σ_c	TS of the Composites	(MPa)
σ_f	TS of the Fibre	(MPa)
τ	IFSS	(MPa)
ζ	Zeta Potential	